



University of Stuttgart
Institute of Nuclear Technology
and Energy Systems

Turbulence Flow Mechanisms to Cause High-Cycle Thermal Fatigue near a Horizontal T-Junction

Mi Zhou



Universität Stuttgart
Institut für Kernenergetik
und Energiesysteme

Turbulence Flow Mechanisms to Cause High-Cycle Thermal Fatigue near a Horizontal T- Junction

von der Fakultät Energie-, Verfahrens- und
Biotechnik der Universität Stuttgart zur Erlangung
der Würde eines Doktor-Ingenieurs (Dr.-Ing.)
genehmigte Abhandlung

vorgelegt von

Mi Zhou

geboren in Shiyan, China.

Hauptberichter: Prof. Dr.-Ing. habil. Eckart Laurien

Mitberichter: Prof. Dr.-Ing. Stefan. Weihe

Tag der Einreichung: 10.07.2018

Tag der mündlichen Prüfung: 06.12.2018

ISSN – 0173– 6892

天一生水

地六成成

五行德冠沛流形

洞澈玉壶冰

激浊扬清

洒净天地人

——《水赞》

Once there is water

There is the world

Best character without a certain form

So clear to see through

Let the heavy separated

Wash the sky, the ground and the people

—— Praise the water

Abstract

The mixing of cold and hot flow streams in a pipeline can create high-frequency temperature fluctuation in the mixing pipe flow, and therefore can lead to high cycle thermal fatigue (HCTF) damage of the piping material close to mixing tees, which is a potential risk for the piping system of nuclear power plants. Incidents in nuclear power plants due to thermal fatigue have been reported around the world.

According to literature review referring to previous investigations on the thermal fatigue phenomenon in thermal-mixing pipe flow, three mixing phenomena, turbulent mixing, thermal stratification and turbulent penetration can create temperature fluctuations, which can initiate thermal fatigue damage. Experimental and numerical methods to evaluate thermal fatigue damage have been developed in previous research works. However, many details of the turbulent-flow mechanisms in the mixing flow, which can cause a thermal fatigue damage in the piping material, are still unknown.

In this work, experimental and numerical investigations the thermal mixing processes at a horizontally oriented T-junction have been performed for understanding the mixing characteristics with respect to their thermal fatigue relevance. Experimental investigations have been performed with flow conditions similar to real nuclear power plants. In particular, the fluid-structure interaction between circumferential pipe weld connections and the nearby mixing flow has been investigated with different measurement methods (micro-thermocouple, Near-Wall LED Induced Fluorescence (NW-LED-IF)). Thermal fatigue damage (crack) has been initiated in the experiment applying acceleration methods of the **Artificially Induced Periodical TEmperture Changes (AIPTEC)**. Confirmed by the metallographic examination, fatigue assessment based on temperature measurements has revealed that an area close to the weld seam has the highest potential for material damage due to thermal fatigue. The results of NW-LED-IF measurements have shown that the rimmed weld root can increase the temperature fluctuation in the nearby mixing flow, and therefore can increase the possibility of the thermal fatigue occurrence.

In addition to the AIPTEC-experiments, thermal mixing experiments at the T-junction have been performed with variations of the flow boundary conditions. Results have shown that the inlet flow temperature and flow rate are decisive factors for the thermal mixing behavior and subsequently for the potential of thermal fatigue in mixing processes. Moreover, an unexpected phenomenon, the harmonic oscillation of thermal stratification in pipe-tangential direction, has been identified as a frequency maximum of about 2.6 Hz in the frequency spectra of the time-dependent temperature data, which can be found in most of the experimentally examined cases. This phenomenon can increase the potential to initiate thermal fatigue damage in the pipe wall.

For more detailed insight to the thermal-mixing pipe flow, the Large-Eddy Simulation (LES) method has been applied in the numerical work. An overview of the spatial and temporal temperature distribution in the whole mixing pipe flow can be generated from the numerical results. Locations with high temperature fluctuations can be identified in the mixing flow. Thermal stratification and turbulent penetration can also be recognized in the illustrated temperature distributions. With the temporal distribution of the temperature iso-surface in the mixing region, the harmonic oscillation of thermal stratification in pipe-tangential direction can also be reconstructed with the numerical results.

For the description of the thermal-mixing characteristics at the horizontal T-junction, a classification of flow patterns (counter-penetration jet, deflecting jet and swing jet) has been summarized from the results of the experimental and numerical investigations. Among the flow patterns, the deflecting jet shows the lowest potential for thermal fatigue. Furthermore, the flow patterns have been summarized in dependence on the inlet flow temperature and flow rate in the form of mixing envelope. The mixing envelope indicates that the thermal mixing characteristics is the property of the specific mixing tee, and

can provide an efficient method to reduce or avoid mixing flow induced thermal fatigue, by controlling the inlet flow boundary condition in the range of deflecting jet.

Zusammenfassung

Der thermische Vermischungsvorgang zwischen einer heißen und kalten Rohrströmung kann hochfrequente Temperaturfluktuationen in der Strömungsvermischungszone einer Rohrleitung generieren, die in Folge einen Schädigungsmechanismus, die sogenannte hochfrequente thermische Materialermüdung (High Cycle Thermal Fatigue – HCTF), im Rohrleitungsmaterial induzieren kann. Diese thermische Materialermüdung stellt ein potenzielles Schadensrisiko für Rohrleitungssysteme in Kernkraftwerken dar, und entsprechende Materialermüdungsereignisse sind bereits in der Vergangenheit in Kernkraftwerken eingetreten.

Gemäß der Literatur zu bisherigen Untersuchungen bezüglich der thermischen Materialermüdung bei Strömungsvermischungsvorgängen in Rohrleitungen können drei Mischungsphänomene, die turbulente Vermischung, die thermisch geschichtete Strömung und die turbulente Strömungspenetration, Temperaturfluktuation erzeugen, die die thermische Materialermüdung initiieren können. In den zurückliegenden Forschungsarbeiten wurden verschiedene experimentelle und numerische Methoden zur Bewertung der thermischen Ermüdungsschädigung entwickelt. Allerdings sind nach wie vor viele Detailfragen über die turbulenten Strömungsmechanismen bei Strömungsvermischungsvorgängen ungeklärt.

In dieser Arbeit wurden experimentelle sowie numerische Untersuchungen zu thermischen Vermischungsvorgängen in einer horizontalen Rohrleitung mit waagrecht angeordneter T-Stück-Einspeisung durchgeführt, um die Vermischungscharakteristik hinsichtlich ihre Relevanz für thermische Materialermüdung besser zu verstehen. Die Experimente erfolgten unter kraftwerkstypischen Strömungsbedingungen von Kernkraftwerken. Insbesondere wurde die Strömungs-Struktur-Wechselwirkung zwischen einer Rohrumfangsschweißnaht mit innenliegender Schweißnahtwurzel und der nahe gelegenen Vermischungsströmung mit Hilfe verschiedener Messmethoden (Mikro-Thermoelemente, Nahwand **LED**-induzierte **F**luoreszenz - **NW**-**LED**-**IF**) untersucht. Um die Initiierung der thermisch induzierte Materialschädigung (Rohranriss) zu beschleunigen, wurden in der Strömung künstlich erzeugte, periodische Temperaturschwankungen (**A**rtificially **I**nduced **P**eriodical **T**emperature **C**hanges - **AIPTEC**) generiert. Im Rahmen der Materialermüdungseinschätzung anhand von Temperaturmessungen und abgestützt durch eine metallographische Untersuchung ergibt sich, dass ein schweißnahtnaher Rohrbereich das höchste Risiko für eine thermische Materialermüdung aufweist. Die Ergebnisse aus den **NW**-**LED**-**IF** Messungen zeigen, dass die Schweißnahtwurzel die nahe gelegenen Temperaturfluktuation in der Strömungsvermischung erhöhen kann und demzufolge die Wahrscheinlichkeit des Auftretens einer thermischen Materialermüdung ebenfalls erhöht sein kann.

Zusätzlich zu den **AIPTEC**-Experimenten wurden thermische Strömungsvermischungsexperimente am T-Stück unter Variation der Strömungsrandbedingungen durchgeführt. Die Ergebnisse zeigen, dass die Strömungstemperatur und die Massenströme in den Zuläufen des T-Stücks die bestimmenden Faktoren für die Strömungsvermischungscharakteristik und folglich für das thermische Materialermüdungspotenzial darstellen. Außerdem wurde in den meisten dieser Untersuchungsfälle eine unerwartete, harmonische Oszillation der thermisch geschichteten Strömung in tangentialer Rohrrichtung identifiziert, die sich als Frequenzmaximum von ca. 2,6 Hz in den Frequenzspektrumsanalysen der zeitabhängigen Temperaturmessdaten dargestellt. Diese Tangentialschwingung kann das thermische Schädigungspotenzial für die Rohrwand erhöhen.

Um einen tieferen, detaillierten Einblick in den thermischen Vermischungsvorgang der Rohrströmung zu erhalten, wurden in den numerischen Arbeiten die Methode der turbulenten Grobstruktursimulation (**L**arge-**E**ddy **S**imulation - **LES**) angewandt. Die zeit- und ortsauflösende Temperaturverteilung der Strömungsvermischung kann aus den Simulationsergebnissen erhalten werden. Strömungsorte mit hohen Temperaturfluktuationen können identifiziert werden. Eine thermisch geschichtete Strömung

oder eine turbulente Strömungspenetration kann ebenfalls erkannt werden. Anhand der Auswertung zeitlich aufeinander folgender Temperatur-Isoflächen der thermisch geschichteten Strömung in der Vermischungzone kann die harmonische Oszillation dieser thermischen Schichtung in rohrtangentialer Richtung aus den Simulationsergebnissen rekonstruiert werden.

Zur Beschreibung der Strömungsvermischungscharakteristik wurde anhand der experimentellen und numerischen Untersuchungsergebnisse eine Klassifizierung der Strömungsmuster abgeleitet. Unter den abgeleiteten Strömungsmustern (Gegen-Penetration-Strahl, Abgelenkter Strahl und Schwing-Strahl) besitzt der „Abgelenkte Strahl“ das geringste thermische Schädigungspotenzial. Darüber hinaus wurde aus den Strömungsmustern in Abhängigkeit von der Einlaufströmungstemperatur und den Einlaufmassenströmen eine zusammenfassende Strömungsformkarte erstellt und in dieser eine Vermischungshüllkurve (Envelope) bestimmt, die charakteristisch für das spezifisch untersuchte T-Stück ist und die Strömungsrandbedingungenbereiche, der unterschiedlichen Strömungsformen angibt. Mittels der Vermischungshüllkurve ist es möglich, thermofluiddynamische Randbedingungen für das T-Stück zu ermitteln, die in einem entsprechenden Strömungsvermischungsvorgang zu einer Reduzierung oder sogar zu einer vollständigen Vermeidung der thermisch induzierten Materialermüdung führen können.

Nomenclature

Abbreviation

AIPTEC	Artificially Induced Periodical Temperature Changes
BMBF	Federal Ministry of Education and Research, Germany
BOS	Background Oriented Schlieren
BUCT	Beijing University of Chemical Technology
CCD	Couple Charged Device
CEA	Commissariat à l'énergie atomique
CFD	Computational Fluid Dynamic
CFL	Courant-Friedrichs-Lewy
CMOS	Complementary Metal-Oxide-Semiconductor
DAQ	Data Acquisition
DC	Direct Current
DNS	Direct Numerical Simulation
FSI	Fluid-Structure-Interaction
FT	Flow temperature
HCTF	High Cycle Thermal Fatigue
IAEA	International Atomic Energy Agency
IKE	Institute of Nuclear Technology and Energy Systems, University of Stuttgart
INES	International Nuclear Event Scale
INSS	Institute of Nuclear Safety Systems, Inc.
JAEA	Japan Atomic Energy Agency
LES	Large-Eddy Simulation
LDV	Laser-Doppler-Anemometry
MOTHER	Modelling T-junction Heat Transfer
MPA	Materials Testing Institute, University of Stuttgart
NTHU	National Tsinghua University
NW-LED-IF	Near-Wall LED Induced Fluorescence
PIV	Particle Image Velocimetry
PLA	Polylactic acid
PLIF	Planar Laser-Induced Fluorescence
PSD	Power Spectrum Density
PVC	Polyvinyl chloride
RANS	Reynolds-Averaged Navier-Stokes

RHR	Residual Heat Removal
RMS	Root Mean Square
SGS	Subgrid Scale
SST	Shear Stress Transport
STC	Shielded Thermocouple
TC	Thermocouple
WALE	Wall Adaptive Local Eddy Viscosity
WATLON	Water Experiment of Fluid Mixing in T-pipe with Long Cycle Fluctuation

Greek letters

Δ	Grid Size
θ	Angular position, [$^{\circ}$]
κ	Turbulent kinetic energy, [m^2/s^2]
λ	Thermal conductivity, [$\text{W}/(\text{m}\cdot\text{K})$], Taylor microscale, [mm]
μ	Dynamic viscosity, [$(\text{N}\cdot\text{s})/\text{m}^2$]
ν	Kinematic viscosity, [m^2/s]
π	Archimedes' constant
ρ	Density, [kg/m^3]
σ_{ij}	Stress tensor due to molecular viscosity, [N/m^2]
τ_{ij}	Residual stress tensor, [N/m^2]

Latin Letters

b	Branch pipe, or image distance, [m]
c_p	Thermal capacity, [$\text{J}/(\text{kg}\cdot\text{K})$]
C_w	WALE model constant
D, d	Pipe diameter, [m]
d_i	Schlieren diameter, [m]
E	Energy scale in turbulence
f	Focal length, [m], or frequency, [Hz]
g	Gravity acceleration, [m/s^2]
h	Specific enthalpy, [J/kg^2]
k	Object distance
L_R	Energy length scale
m	Main pipe

M	Flow momentum, or magnification
M_R	Momentum Ratio
\dot{M}	Flow rate, [kg/s]
n	Refractive index
N	Number of grid element
Pr	Prandtl-number
Re	Reynolds-numebr
Ri	Richardson-number
t	Time, [s]
Δt	Time step
t_{90}	Responding time of 90% temperature difference, [s]
T	Temperature, [°C], or Period length [s]
ΔT	Temperature difference, [K]
u, v	Velocity, [m/s]
X, Y, Z, x, y, z	Cartesian coordinates

CONTENTS

Abstract	I
Zusammenfassung	III
Nomenclature	V
1 Introduction	1
1.1 Motivation	1
1.2 Literature overview	2
1.3 Aim of work	21
2 Experiment facility and measurement techniques	22
2.1 Fluid-Structure-Interaction test facility	22
2.2 Dissimilar weld	25
2.3 Micro-thermocouple technique	26
2.4 Near-wall fluorescence technique	32
2.5 Particle Image Velocimetry (PIV) technique	33
2.6 Background Oriented Schlieren (BOS) technique	35
3 Numerical calculation	39
3.1 Theory and model	39
3.2 Geometry and numerical mesh	41
3.3 Boundary and initial conditions	43
3.4 Time step and time line	44
4 Results	46
4.1 Results of experimental investigations	46
4.1.1 Artificially induced fatigue damage on dissimilar weld	46
4.1.2 Fatigue assessment close to weld seam model	51
4.1.3 Reverse flow upstream the T-junction	73
4.1.4 Influence of weld root on nearby flow field	76
4.1.5 Velocity profiles in inlet flow streams	81
4.1.6 Harmonic oscillation of thermal stratification in pipe tangential direction	83
4.2 Results of numerical simulations	89
4.2.1 Maximum operation condition at FSI test facility	89
4.2.2 Flow patterns at horizontal T-junction	98
4.3 Mixing envelope	101
5 Conclusions	102
References	104
Acknowledgment	111

1 Introduction

1.1 Motivation

On May 12 1998, an incident is reported from the French nuclear power plant Civaux. In the piping system of the unit 1, a leak was found on a pipe of the Residual Heat Removal (RHR) system (see Figure 1-1), while the reactor was shut down for startup tests [1]. The leak was caused by a through-wall crack with a length of 350 mm at the inner surface. Totally 280 m³ coolant was lost through the crack in this incident. Moreover, the crack appeared after an operation time of 1500 h, which is unexpected according to the design of the piping system.

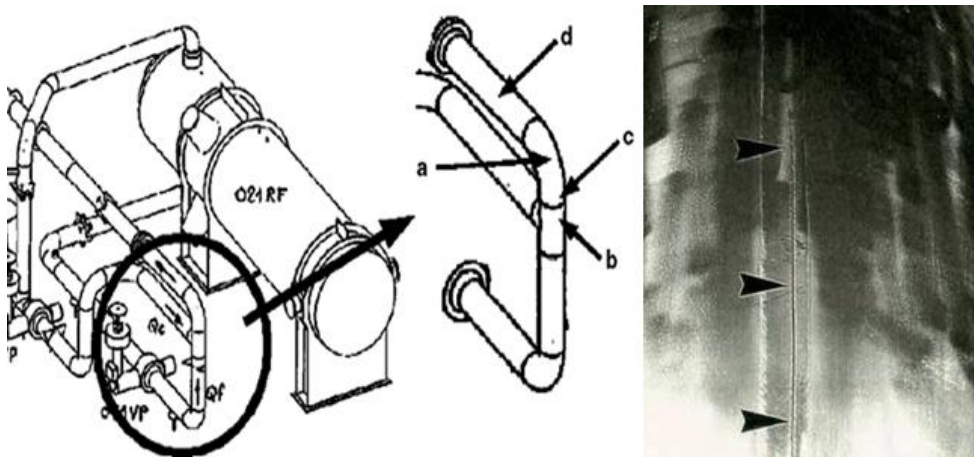


Figure 1-1: Crack on the pipe line of the RHR system in Civaux-I incident [2]

In the last 15 years, similar incidents have been reported around the world. This kind of incidents are caused by a degradation mechanism called thermal fatigue (a.k.a. thermal stripping). Damages (cracks) due to thermal fatigue in these incidents are mostly found close to mixing tees (i.e. T-junctions), where coolant flow streams with different temperatures are mixed. In the Civaux-I incident, inlet flow streams with 180 °C and 20 °C are mixed at a T-junction upstream of the position of the pipe bend [2], where the leak was found (see Figure 1-1). High frequency temperature fluctuations are created in the thermal mixing flow and can change the stress in the piping material frequently. Fatigue damages can be initiated and can develop in the pipe wall due to the stress changes in the pipe wall. Therefore, this kind of damage mechanism is also referenced as High Cycle Thermal Fatigue (HCTF).

Incidents like Civaux-I due to thermal fatigue are all categorized in the low level (level 2) in the International Nuclear Event Scale (INES) by the International Atomic Energy Agency (IAEA). However, since the Fukushima disaster, the public and the media are more critical to the safety of nuclear power plants. Even the low-level incidents can highly raise the major concerns about the nuclear safety among the public. Since thermal fatigue is a potential risk to the safety of piping system in nuclear power plants, researchers around the world are paying increasing attention on the thermal fatigue issue in the thermal-mixing pipe flow. Although great progresses have been made in the previous thermal fatigue research works, the mechanisms causing thermal fatigue damages in the mixing pipe flow are still not clear. There is still no efficient method to avoid thermal fatigue damage for the piping system in nuclear power plants, and incidents like Civaux-I are still being reported around the world. Therefore, further investigations on the thermal mixing pipe flow shall be performed particularly with the target to understanding the thermal fatigue mechanisms and to conclude a method to avoid thermal fatigue damages.

1.2 Literature overview

In recent years, several research projects have been carried out to investigate thermal fatigue in the thermal-mixing pipe flow close to T-junctions. This damage mechanism has been analyzed and discussed with different methods. And the topic of thermal fatigue in thermal mixing processes has been often discussed in the international conferences of nuclear technology or nuclear safety.

In France, the Civaux-I incident has been systematically discussed by Chapuliot et al. [3] from CEA (Commissariat à l'énergie atomique). Chapuliot's work has shown that the temperature fluctuations due to turbulent mixing processes close to the mixing tee can change the stress of the piping material. From the perspective of material science, frequency analysis has been performed with the piping materials. The frequency of the stress change in the piping material has been discussed for their relevance of thermal fatigue. Fatigue damage can be initiated due to stress changes with frequency up to 10 Hz. Moreover, CFD (Computational Fluid Dynamic) method has also been applied in investigating the thermal-mixing flow of the Civaux case, and it has shown an advantage of illustrating of the temperature and velocity distributions in the whole mixing region.

At the same time, the European THERFAT project has been launched jointly by 16 research institutions for thermal fatigue evaluation in the mixing flow of tee-pipe connections. The results of this research project have been summarized by Metzner and Wilke [4]. The research work of the European THERFAT project has been separated into three parts: thermal-hydraulic experiments, CFD simulations and structure material analyses. In the first part, thermal mixing experiments have been performed on a steel mock-up with temperature differences of 60 – 90 K (Figure 1-2, right). Four mixing tees with different geometries have been applied in the experiments. Temperature measurements have been performed with thermocouple technique in the near-wall mixing flow. For visualization of the flow field, equivalent isothermal experiments have also been conducted on a Plexiglas mock-up with mixing of different-salt water solutions (Figure 1-2, left), which can simulate a thermal mixing process with a temperature difference of about 150 K. The equivalent isothermal experiment has provided a new method for flow field visualization in the experimental investigation on thermal fatigue. In addition, this research project has also introduced the weld seam as a new topic in the scope of the thermal-fatigue research. In the piping material near the mixing tees, damages due to thermal fatigue are most likely to be initiated close to the weld connection. On one hand, the stress within the weld seam changes differently with temperature fluctuations due to material inhomogeneity. On the other hand, the rimmed weld root can increase the turbulence in the nearby flow field and therefore the temperature fluctuations in the mixing flow. With the idea of comparing different investigation methods, the European THERFAT project is one of the most representative research works on thermal fatigue in thermal-mixing processes.

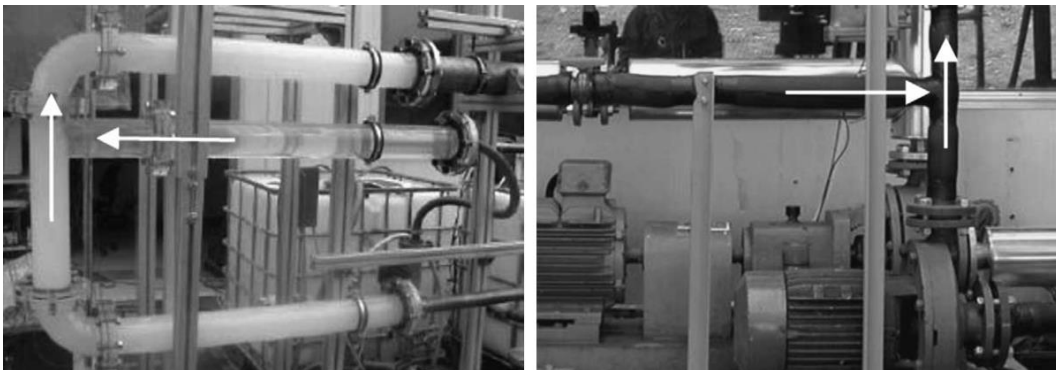


Figure 1-2: THERFAT Plexiglas mock-up (left) and steel mock-up (right) [4]

Later at CEA, T-junction experiments have been performed on the FATHER mock-up under an EDF/CEA/AREVA agreement [5]. Particularly in the FATHER mock-up, three circumferential weld

seams have been constructed in the pipeline mixing region downstream of the T-junction (see Figure 1-3) [6]. These three weld seams are denoted as S1 – S3. The weld roots of these three weld seams are handled differently [5]. The experiments on the FATHER mock-up have been performed with a temperature difference of 160 K between the hot and cold inlet flow streams. The duration of the experiments was 300 hours. Parallel with the experimental work, J.-M. Stephen [7] has performed numerical simulation based on the experiment. Distributions of temperature fluctuation at the internal wall of the mock-up has been reconstructed for the discussion on the variation of thermal stress in the piping material. After the experiment, metallographic examinations have been performed on the pipeline material of the FATHER mock-up. Cracks have been found close to all the three weld seams. Taheri et al. [8, 9] have investigated the thermal fatigue damage in the FATHER experiments from the perspective of material science. The crack depth in the weld seam is discussed with respect to influence of thermal stress changes and weld residual stress. The FATHER experiment was the first T-junction investigation with a target on thermal fatigue close to weld connections. The metallographic examinations have confirmed that thermal fatigue damages are most likely to be initiated close to the weld connections. However, the initiation of fatigue damage was the impact of the turbulent mixing flow on the piping materials. In the discussion of fluid-structure interaction, the impact of the weld seams on the nearby mixing flow has not been discussed in this work.

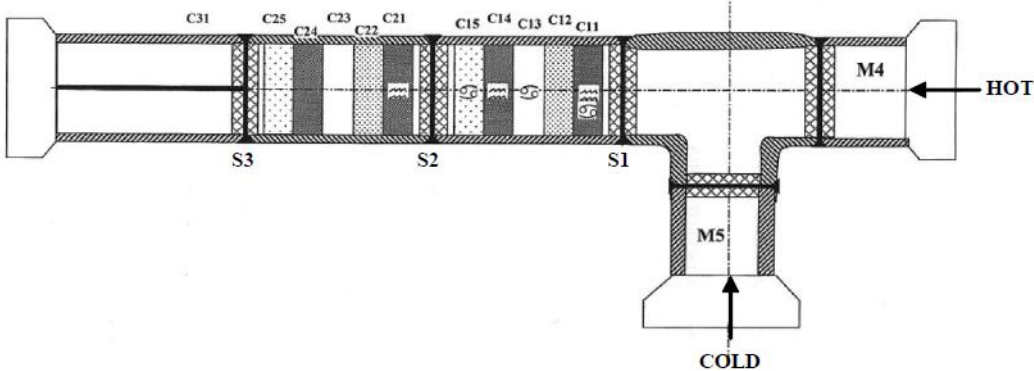


Figure 1-3: Design of the FATHER mock-up [6]

Besides the FATHER mock-up, another T-junction test facility, the FATHERINO facility, has been constructed at CEA Cadarache research center for investigating thermal-mixing pipe flow (see Figure 1-4). The first experiments at the FATHERINO test facility and parallel performed CFD simulations have been summarized by Kuhn et al. [10] in 2010. In the FATHERINO experiments, cold water at 5 °C and hot water at 80 °C are mixed at a vertical oriented T-junction, which is made of brass. Based on the experiments, Large-Eddy simulation has been performed with the Smagorinsky model. The simulation results have provided an overview on the temperature distributions on the mixing flow as well as in the pipe line, which cannot be totally captured in the experiment. The comparison between the simulation and the experiment has shown the possibility of LES to locate the maximum temperature fluctuation in the pipe wall, so that the stress distribution can be estimated for prediction of the fatigue damage in the piping materials.

After this work, the FATHERINO facility has been applied in the experimental work of the MOTHER project (**MO**delling **T**-junction **HE**at **TR**ansfe**R**), which is launched jointly by 11 partners on December 1, 2010 [11]. To distinguish from the previous work at the FATHERINO facility, the experiments in context of the MOTHER project are denoted as MOTHER experiments. Two different T-junctions (one with round corner, the other with sharp corner, see Figure 1-5) have been constructed and tested in the MOTHER experiments [12]. The T-junctions in the MOTHER experiments are made of 304L stainless steel. Particularly, the pipelines at the T-junction in this work have the same diameter of 54 mm, which is different from most of the other T-junction investigations around the world. The temperature in the hot and cold inlet flows are 30 °C and 15 °C, respectively. Temperature measurements in the MOTHER

experiments are performed with thermocouples, which are installed at different positions to capture the temperature in the fluid and piping material. In addition, an infrared camera has been used for capturing the general temperature distributions in the mixing flow. Five Plexiglas windows have been installed at different positions close to the T-junctions for the optical measurement. Laser-Doppler-Anemometry (LDV) technique has been applied in the velocity measurement.



Figure 1-4: FATHERINO facility in the lab at CEA [13]

The results of the MOTHER experiment provide a data base for the validation of CFD simulations for thermal fatigue investigations. The CFD validation study has been performed by using five different codes, namely STAR-CCM+, Code_Saturne, LESOCC2, Fluent and OpenFOAM. Seven different turbulent models were used in the CFD calculations. The simulation results have been compared with the experiments and it has been shown that Large-Eddy Simulation (LES) shows the best agreement with the experimental data [11]. The results have also shown that the designs of the T-junction has an influence on the temperature distribution in the mixing flow. In the case with round corner, the pipe wall area with high temperature fluctuation is larger than the case with sharp corner. It indicates that the heat transfer in the mixing flow is stronger downstream of the round corner than the sharp corner.

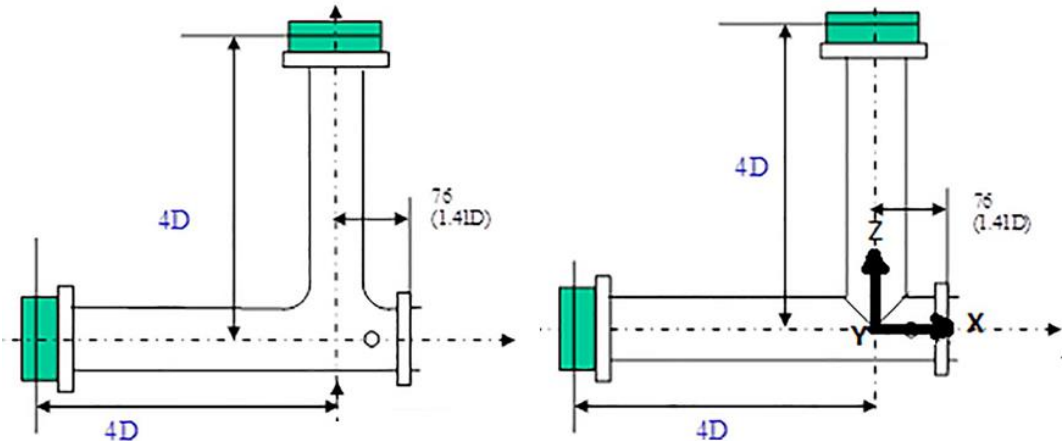


Figure 1-5: Designs of the round corner (left) and sharp corner T-junctions in the MOTHER experiments [11]

In Sweden, T-junction mixing-flow tests have been performed at the Älvkarleby Laboratory of Vattenfall Research and Development (VRD) for CFD benchmark [14, 15]. In the Vattenfall benchmark experiment, a hot water flow (36 °C) and a cold water flow (19 °C) are mixed at a horizontal oriented

T-junction (Figure 1-6). The pipeline diameters of the hot line and cold line are 100 mm and 140 mm, respectively. The T-junction test section at the test facility is made of Plexiglas for the optical investigations. The flow field visualization has been performed by using Laser Induced Fluorescence (LIF) method (Figure 1-6). The velocity measurements have been performed with LDV and PIV (Particle Image Velocimetry) techniques. Thermocouples were installed in 10 different measurement cross-sections close to the T-junction for temperature measurement. The measurement points of the thermocouples were located one millimeter from inner.

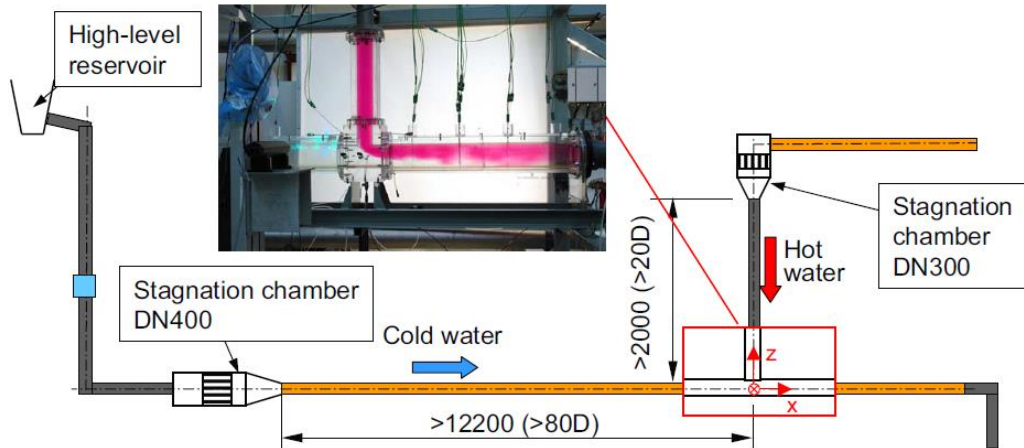


Figure 1-6: Design and side view of the Vattenfall T-junction test facility [15]

The Vattenfall benchmark experiment is one of the most well-known T-junction investigations on thermal fatigue. It provides an open data base for CFD calculations. Since then, many of numerical works have been performed for CFD validation based on Vattenfall benchmark experiments. Different codes and models have been applied in these CFD calculations. Odenmark et al. [16] have performed their numerical work with the focus on the velocity profiles in the mixing flow. The simulation results have been compared with the velocity profiles, which were captured by using PIV technique in the experiments. In addition, temperature distributions have been illustrated and compared with the visualizations in the experiments. Höhne [17, 18] has performed his simulations on the Vattenfall experiment with LES method. His work focused on the simulation of the temperature signals in the Vattenfall experiment. For identifying the regular changes in the temperature signal, frequency analysis has been performed to the temperature signals by using Fourier-transformation. Since thermal fatigue is initiated by the high frequency temperature changes in the mixing flow. Frequency peaks in the spectra of the temperature signals indicate the potential for initiating thermal-fatigue damage. As a consensus among the thermal fatigue researchers around the world, frequency analysis is one of most important analysis steps in the fatigue assessment. Similar with Höhne, Das et al. [19] have also performed simulation on the Vattenfall T-junction experiment and got a similar result. Another simulation work has been performed by Timperi [20] with LES model. In this work, the conjugate heat transfer between the mixing flow and the pipeline material has been brought in the calculation. Frequency analysis (spectrum method) has been applied and summarized in the fatigue assessment. With this method, fatigue assessment has also been performed in the simulation on the FATHER experiment [21]. Particularly, Garrido et al. [22 – 25] from Jožef Stefan Institute have launched a research project namely “Estimating the uncertainties in the thermal fatigue assessment of pipes under complex loading histories”. In this project, spectral method has been discussed for the application in the fatigue assessments in several numerical works on Vatttenfall benchmark experiment. Moreover, a very important remark has been made in their comment to the simulation work of Zhang et al. [26, 27] for the application of frequency analysis. Since the frequency analysis is a statistical method, the time interval of temperature data must be long enough for creating a significant result in the spectrum. Except the aforementioned numerical work, CFD calculations on the Vattenfall T-junction experiment have

also been performed by many other researchers e.g. Ayhan [28], Hannink et al. [29], Ndombo [30], Westin et al. [31, 32] and so on. The simulation works have helped to understand the mixing flow in the experiment. A consensus can be found from these numerical works, that the Large-Eddy simulation is most feasible method for the simulation on the thermal-mixing pipe flow, since the LES method has the advantage to present the time-dependent temperature fluctuation due to the vortex structures in the mixing flow. Moreover, a method for fatigue assessment in the mixing region can be concluded from these research works on the Vattenfall T-junction experiment. In the first step, the area with high temperature fluctuation shall be located from the temperature data in the mixing region. Then, frequency analysis shall be performed to the temperature data to check the regular changes in the temperature. Locations with high temperature fluctuation and low-frequency changes have a possibility to initiate thermal fatigue.

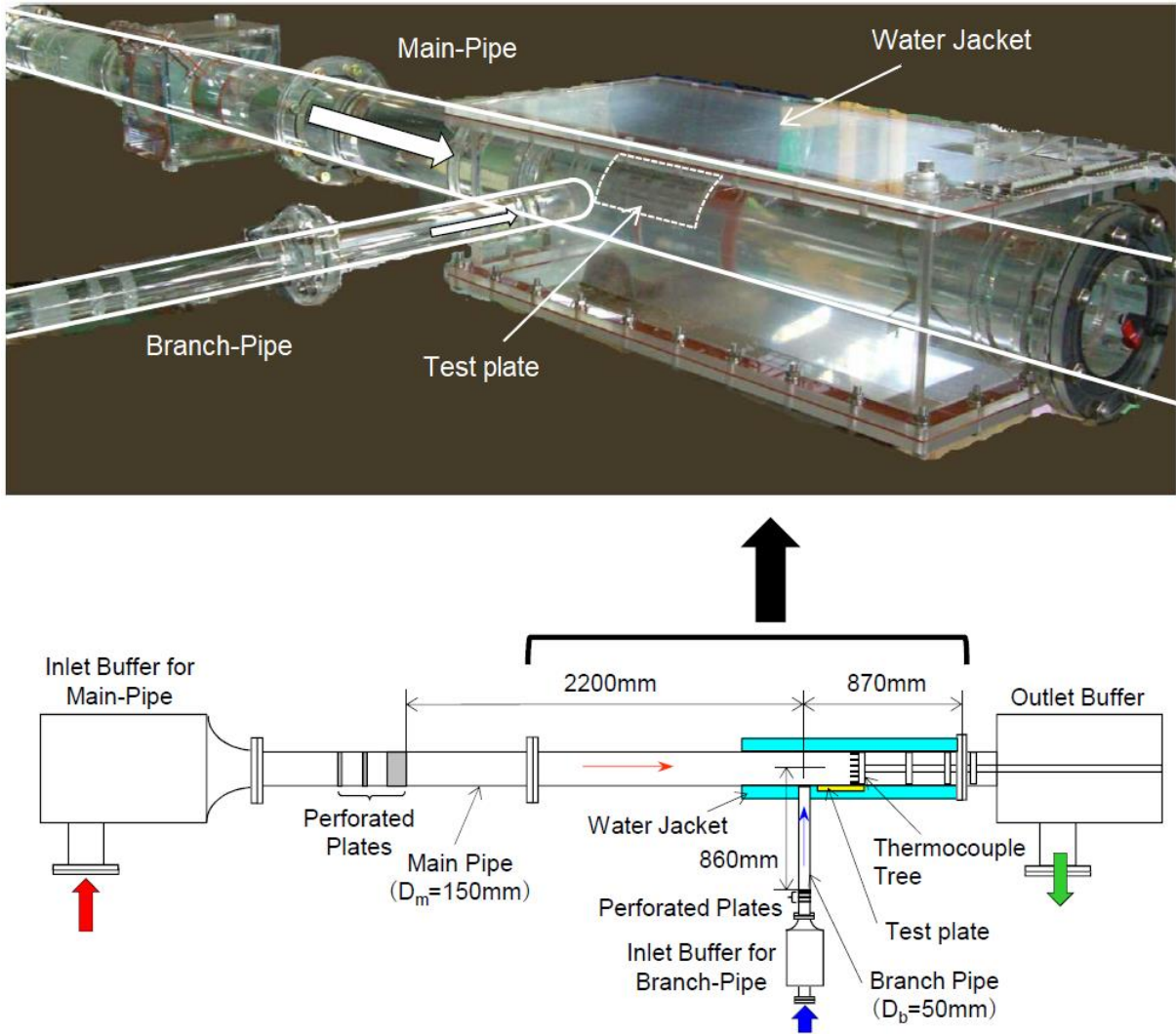


Figure 1-7: Design of the WATLON facility (below) and its T-junction test section (above) [33]

In Japan, a T-junction test facility called WATLON (WAter Experiment of Fluid Mixing in T-pipe with LONG Cycle Fluctuation) has been constructed by Japan Atomic Energy Agency (JAEA) [33]. Figure 1-7 shows the design and the T-junction test section of the WATLON test facility. The T-junction of the WATLON facility was vertical oriented, and the cold water was injected from below. The test section was made of Plexiglas (see Figure 1-7, above). The temperature in the cold inlet flow was 33 °C as well as warm inlet flow 48 °C. Temperature measurements in the WATLON experiments have been performed with two different thermocouple structures. For capturing the temperature in the pipeline inner surface, the measurements were conducted with a thermocouple test plate, in which 25

thermocouples were installed in a 5×5 matrix. The measurement points of these thermocouples were located 0.125 mm from the pipe inner wall in the pipeline. For capturing the temperature in the mixing flow downstream of the T-junction, temperature measurements were performed with a thermocouple tee (see Figure 1-8), which can rotate and can be fixed at different measurement positions in the mixing region. A water jacket was constructed to surround the pipeline close to T-junction for compensating the refraction due to the pipe-wall bend in the optical measurements. Flow field visualization has been performed with fluorescence technique. Velocity profiles have been captured by using PIV technique.

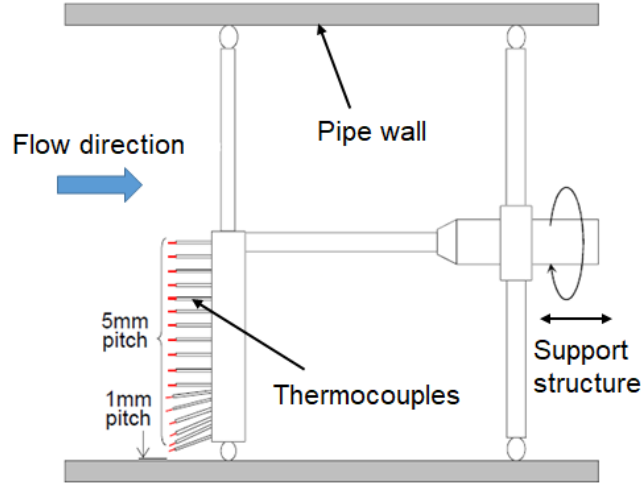


Figure 1-8: Thermocouple tree at the WATLON test facility [33]

The first experimental work on the WATLON test facility has been summarized by Kamide et al. [34] in 2009. Based on the results of flow field visualization in the experiments, the mixing characteristics close to the T-junction can be described by using flow patterns. The mixing flow has been categorized in three different kinds of flow patterns: wall jet, deflecting jet and impinging jet (see Figure 1-9). The three flow patterns can be quantitatively estimated by calculating the momentum ratio M_R , which is defined by the following equations [34].

$$M_R = \frac{M_m}{M_b} \quad (\text{E1-1})$$

$$M_m = D_m D_b \rho_m V_m^2 \quad (\text{E1-2})$$

$$M_b = \frac{\pi}{4} D_b^2 \rho_b V_b^2 \quad (\text{E1-3})$$

Table 1-1: Momentum ratio range for the flow patterns

Momentum ratio range	Flow patterns
$M_R < 0.35$	impinging jet
$0.35 < M_R < 1.35$	deflecting jet
$M_R > 1.35$	wall jet

The momentums M_m and M_b (indices m for main pipeline, b for branch pipeline) of the pipe flows at the T-junction are defined based on the projections of the flow stream in the pipeline with the pipeline diameters (D_m and D_b), velocities (V_m and V_b), and the densities (ρ_m and ρ_b) of the flow streams in the main and branch pipe, respectively [34]. According to the flow field visualization, the flow pattern and the momentum ratio have the correlation in Table 1-1.

The Kamide’s classification of the flow patterns has concluded that the mixing characteristics depends on the decisive flow factors in the inlet flow streams. Fatigue assessment in their work has shown the wall jet has the highest potential for thermal fatigue in the mixing region [34]. This classification of the flow patterns simplifies the description of the mixing characteristics and the evaluation of thermal fatigue effect in the mixing process, and has also been referenced in many of the later works of T-junction investigations on thermal fatigue [35, 36]. However, the WATLON experiment has been performed with a low temperature difference of 15 K. Therefore, the density difference between the inlet flow streams was so small, that the buoyancy effect in the mixing flow can be neglected. Also, Kamide’s definitions of the momentum is based on the projections of the flow stream in the pipe line. According to the equations E1-2 and E1-3, the flow velocity shows much more decisive than the density on the flow pattern in the WATLON experiment. Hence, the influence of the buoyancy cannot be investigated in the WATLON experiment.

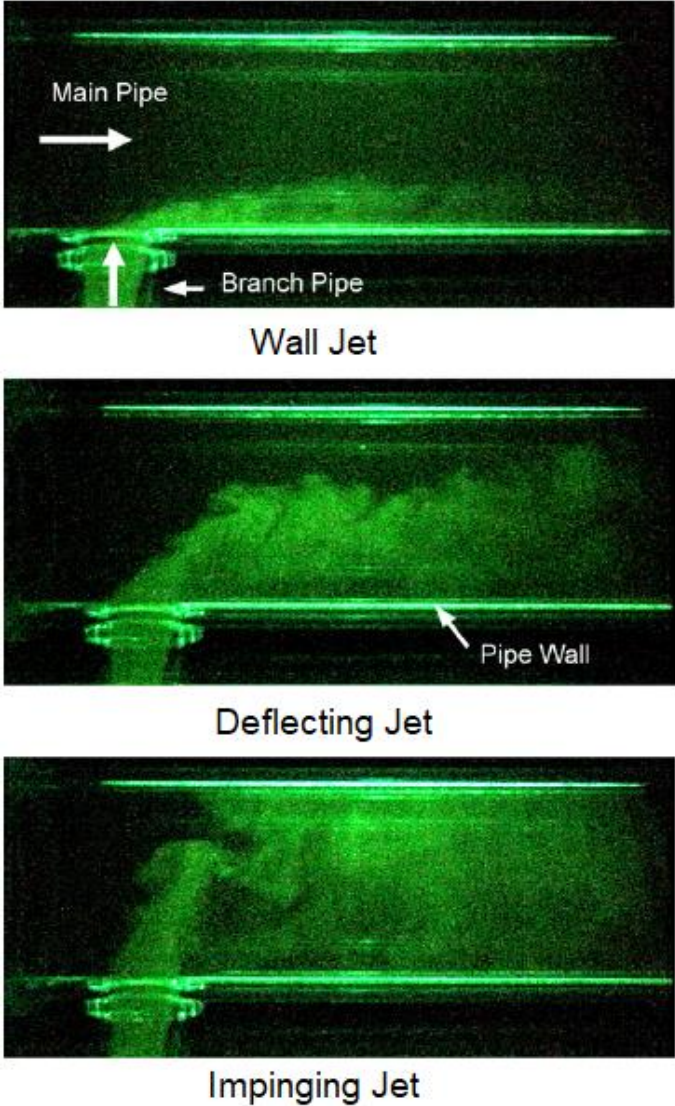


Figure 1-9: Classification of flow patterns by Kamide [34]

The experimental work on the WATLON facility has also provided a data base for validation of the numerical simulations. At JAEA, a code called “MUGTHES” has been validated with the WATLON experiments. Large-Eddy simulations have been performed with MUGTHES by Tanaka et al. [37, 38]. Some agreements have been found in the LES results in comparison with the experiment. Besides JAEA, numerical simulations on WATLON experiment have also been performed at several other institutions. Qian et al. [39] have performed their LES calculation with an open CFD software called FrontFlow/Red (FFR). Discussions in this work focused on the temperature fluctuations in the mixing flow. A frequency peak has been found in the spectrum of the near-wall temperature signal, which agrees with the results of the experiment. Nakamura et al. [40] have performed simulation on WATLON experiment with the commercial CFD code ANSYS CFX-10. Measurement cases with wall jet and impinging jet conditions have been simulated in their work. Temperature fluctuations in the mixing flow of different cases have been discussed in their work. Frequency analysis has been performed to the temperature signal and compared with the experimental results. Another LES calculation on the WATLON experiment has been performed by Utanohara et al. [41] with the CFD code Fluent. This work focused on the long-period temperature fluctuations in the mixing flow. The physical time of the simulation was 100 s. And 96 s of the temperature data has been taken for analysis. Frequency analysis has been performed to the temperature signals. Low-pass filter and window function (hamming window) have been applied in the signal analysis. Several frequency peaks have been found in the PSD (Power Spectrum Density) diagrams of the temperature data, which were in the relevance for thermal fatigue.

Based on the temperature distribution in the pipe wall obtained in the simulation by Nakamura et al., thermal stress calculations have been performed by Miyoshi et al. [42] and Kamaya et al. [43, 44], respectively. Miyoshi et al. have particularly investigated the dynamical responding properties of the shielded thermocouples and the heat transfer from the pipe inner surface to the measurement point of the thermocouples. Kamaya et al. have calculated the thermal stress distributions in the pipe wall and compared the thermal stress in axial and circumferential directions. The potential for initiation of fatigue damage has also been discussed in the pipe wall of the mixing region. Position of interest has been located on the pipe wall, where the damage factor in the piping material reached the maximum. Fatigue damage was accumulated locally and led to crack initiation.

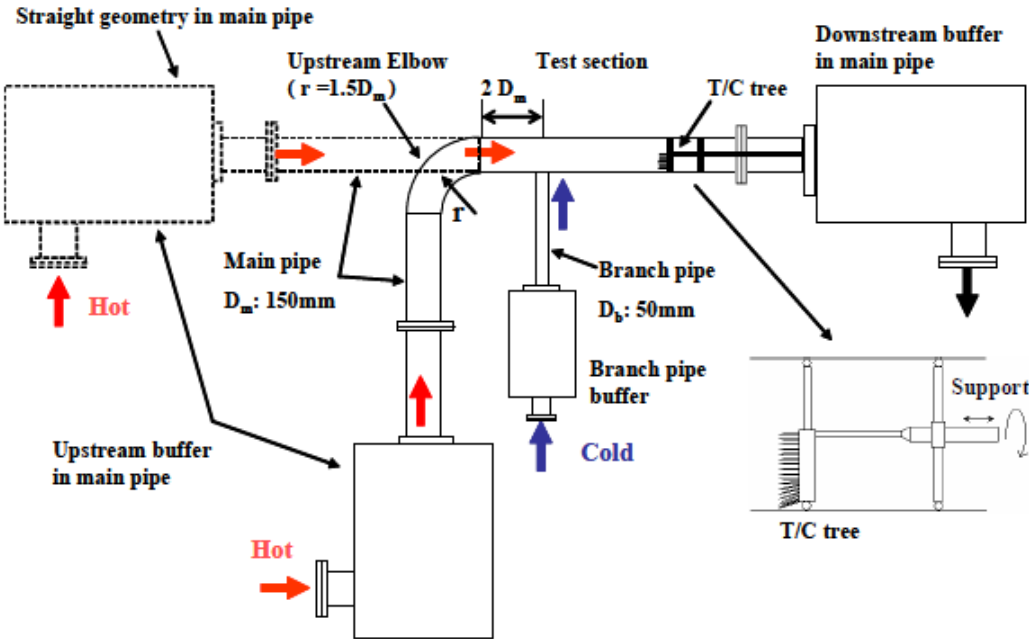


Figure 1-10: Schematic of the WATLON test section with elbow [45]

Later, the WATLON test facility has been modified for the investigation on the mixing behaviors with a upstream elbow [45, 46]. Figure 1-10 shows the WATLON test section with the upstream elbow. In the experiment, the temperature measurement has been performed with the thermocouple tee, and velocity profiles have been captured by using PIV technique. In particular, flow field visualization has been performed to compare with the previous experiments without the upstream elbow. Results have shown the ranges of the momentum ratio for the flow patterns have been changed as in the Table 1-2.

Table 1-2: Momentum ratio range for the flow patterns with upstream elbow

Momentum ratio range	Flow patterns
$M_R < 0.52$	impinging jet
$0.52 < M_R < 2.0$	deflecting jet
$M_R > 2.0$	wall jet

The shifting of the momentum ratio ranges indicated a significant influence of the upstream elbow on the mixing behavior. Moreover, the upstream elbow has also shown an influence on the temperature and velocity measurements in comparison with the experiments with straight pipeline. Based on the geometries of the WATLON test section, Coste et al. [47] have performed LES calculations on both experimental setups with straight pipeline respectively upstream elbow. With each test geometry, simulations have been performed with different flow conditions for different flow patterns. The results of the simulations have shown a good agreement with the experiments. In addition, the simulation results have shown that a secondary flow can be created by the elbow upstream the T-junction and increase the temperature fluctuation in the mixing flow.

The WATLON experiment has introduced the classification of the flow patterns for describing the mixing characteristics in the mixing flow. This idea has influenced the later investigations on the thermal mixing pipe flows. At the Tohoku University in Japan, another test facility has been constructed for investigating turbulent mixing flow at a T-junction. Different to the WATLON facility, the T-junction test section of the Tohoku facility has a vertical main pipe and a horizontal branch pipe. Hosseini et al. [48, 49] have performed PIV measurements at the T-junction. Based on the instantaneous velocity distributions at the T-junction, the mixing flows have been separated in four different flow patterns: wall jet, re-attached jet, turn jet and impinging jet. With the Kamide's calculation of the momentum ratio, the range of momentum ratio has been estimated for the different flow patterns. The Tohoku experiments have also shown that a mixing flow can be categorized with the classifications of flow patterns, which can also be applied in different mixing tees.

After the research work at JAEA and Tohoku University, investigations on thermal fatigue in thermal-mixing pipe flow have not been stopped in Japan. The latest T-junction experiments have been performed on the T-Cubic test facility at Institute of Nuclear Safety Systems (INSS), Inc.. Different to the aforementioned test facilities, the T-Cubic is one of the a few T-junction test facilities with ongoing research work at the present time. Figure 1-11 shows the pictures of the T-Cubic test facility. The branch pipeline (diameter 50 mm) is connected downwards with the main pipeline (diameter 150 mm) at a vertical T-junction. A cold flow (25.7 °C) in the branch pipeline and a hot flow (59.8 °C) in the main pipeline are mixed in the T-junction. The T-junction test section at the T-Cubic test facility has been constructed as a replaceable part (see Figure 1-11). Miyoshi et al. [50 – 52] have performed the experimental investigation on the T-Cubic test facility. In the temperature measurement, a stainless steel T-junction is installed in the test section (Figure 1-11, right). 148 thermocouple have been installed in the pipe wall. The measurement points of the thermocouples are located 0.45 mm from the pipe inner surface [50]. Moreover, temperature measurement has also been performed on the outer surface of the pipeline by using thermal camera [51]. In the optical investigations, the test section is replaced with an acrylic glass T-junction. The acrylic glass T-junction is surrounded with a water jacket to compensate

the optical refraction due to the pipe-wall bend. With this construction, velocity measurement have been performed with LDV technique.

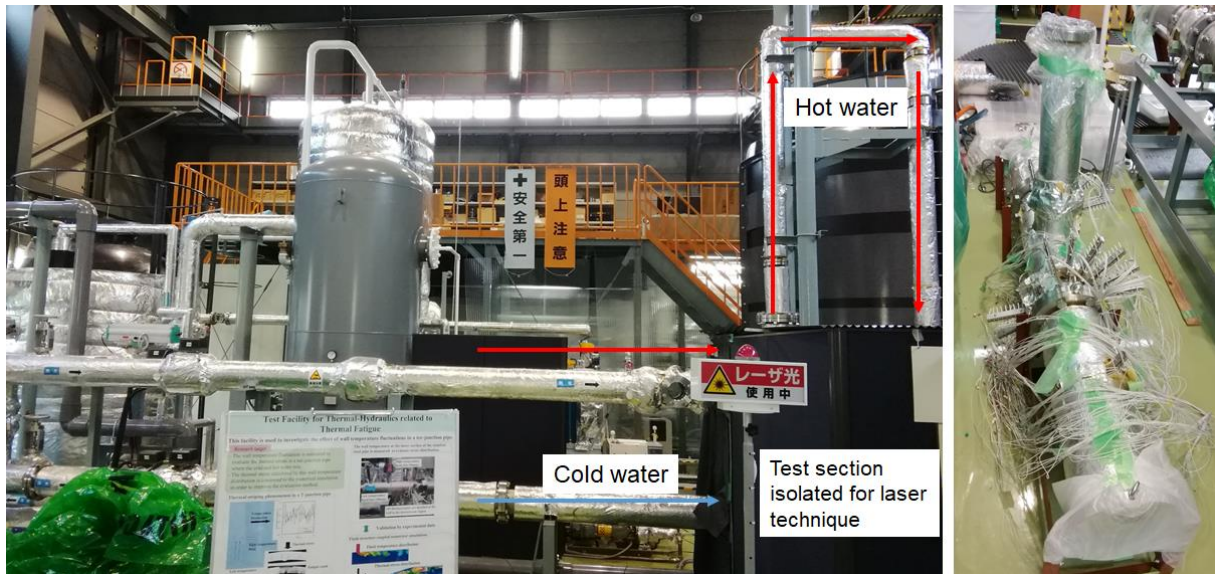


Figure 1-11: T-Cubic test facility and the stainless steel T-junction test section¹

The experimental investigations on the T-Cubic test facility focus on the distribution of temperature fluctuations in the pipe wall. Therefore, the thermocouples are installed in a measurement region near the joint position of the branch pipe to the main pipe, where the high temperature fluctuations due to turbulent mixing process are located (see Figure 1-12). With the thermocouple measurement data, the distribution of temperature fluctuation in the pipe wall have been reconstructed for further evaluation of thermal stress in the pipe wall. In addition, the experimental results have provided a data base for validation of the numerical simulations [52].

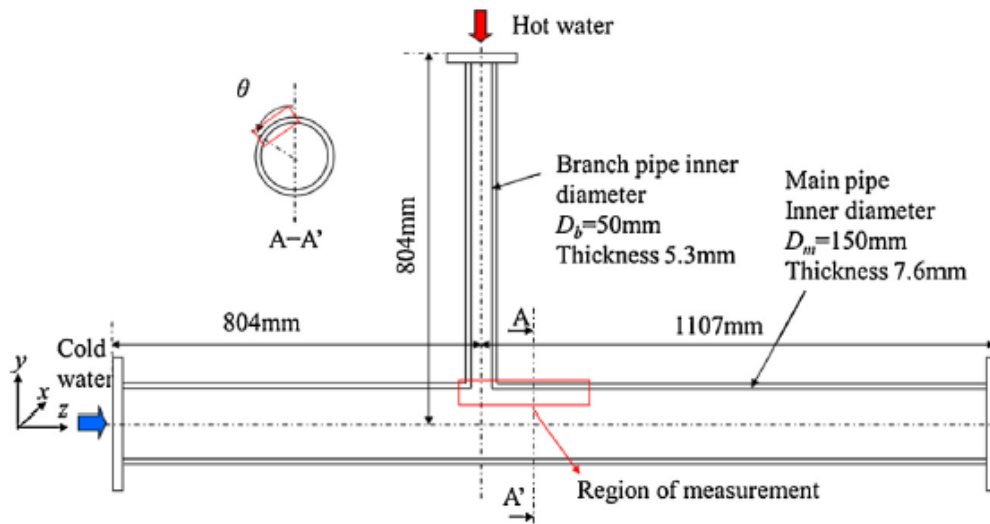


Figure 1-12: Thermocouple measurement region on the T-junction test section of the T-Cubic test facility [52]

The simulation work on the T-Cubic experiments has been performed by Utanohara et al. [53, 54]. The dynamic LES method has been applied in this simulation. Velocity and temperature distributions have

¹ Taking and using these pictures have been authorized by Dr. M. Kamaya, leader of the Thermal Hydraulics and Mechanics Group, INSS.

been reproduced with the simulation. Compared with the experiment, the velocity profiles matched well with the experimental results. The temperature fluctuations in the pipe wall inner surface in the simulation results were higher than the experimental data, which led back to the reduced heat transfer from the fluid to the pipe wall. Thermal fatigue damage assessment in the piping material in the T-Cubic experiments has been performed by Kamaya et al. [55]. The thermal stress in the pipe wall has been reconstructed with the temperature data. The fatigue life of the structure material could be predicted by elastic analysis.

The investigation on the T-Cubic test facility represents a typical research work on the thermal fatigue damage due to turbulent mixing process at T-junction. Since the temperature difference between the inlet flow streams at the T-Cubic test facility was only about 35 K. The investigation focused on the area very close to the joint position of the pipelines, where the temperature fluctuations were high enough to capture. However in the thermal-mixing pipe flow, temperature fluctuations cannot be created only with turbulent mixing process, but also with another two thermal mixing phenomena: thermal stratification and turbulent penetration (reverse flow). These two phenomena can be created by buoyancy effect in the mixing flow, and therefore request a temperature (density) difference between the inlet flow streams. In recent years, several research works have been launched to investigate thermal fatigue due to these two phenomena.

In China, a research team at National Tsinghua University (NTHU) has performed thermal-mixing pipe-flow investigations on their test facilities. The first experiment has been performed on a test facility called EXTREME test facility (see Figure 1-13) [56, 57]. On the EXTREME test facility, a cold flow at 20 °C and a hot flow at 90 °C were mixed at a vertical T-junction. And the cold flow was injected downwards into the hot flow (main pipeline) on the EXTREME test facility. Another specialty of the EXTREME test facility was the large diameter ratio between the main and branch pipelines (approximately 10), which is differed from the aforementioned experiments. Temperature measurements have been performed with thermocouple structures within the main pipe flow. Experiments have been conducted with variations of flow rates in the main and branch pipeline, respectively. In the experiments, reserve flow upstream the T-junction has been captured with the thermocouples. In addition, CFD simulations have been performed on the experiments with different turbulent models [58]. Reverse flow can also be observed in the simulation results.



Figure 1-13: the EXTREME test facility [56]

The later experimental work of this research team have been performed on another test setup, in which the pipelines are made of PVC [59, 60]. The schematics of the PVC test loop can be seen in Figure 1-14. On this test loop, the flow temperature in the cold and hot pipelines were 20 °C and 40 °C. The diameters of the hot and cold pipelines are 100 mm and 80 mm, respectively. The temperature measurements have been conducted with thermocouple structures in the main (hot) pipeline. Flow field visualization has been performed with a blue dye in the cold flow.

At first, the experiments have been performed with a 90° T-junction with two different direction of the cold flow injection. The cold flow has been injected downwards respectively upwards into the main pipe (see Figure 1-14, top) [61]. Then, a 45° mixing tee has been constructed for the test loop. The experimental investigations have been performed with the 45° mixing tee in comparison with the 90° T-junction. Moreover, the experiments have also been performed with vertical respectively horizontal setup for each mixing tee (see Figure 1-14, middle and bottom). With variations of the flow rate in the pipelines, reverse flow in the main pipe upstream of the mixing tees have been captured with the thermocouples or by flow field visualization.

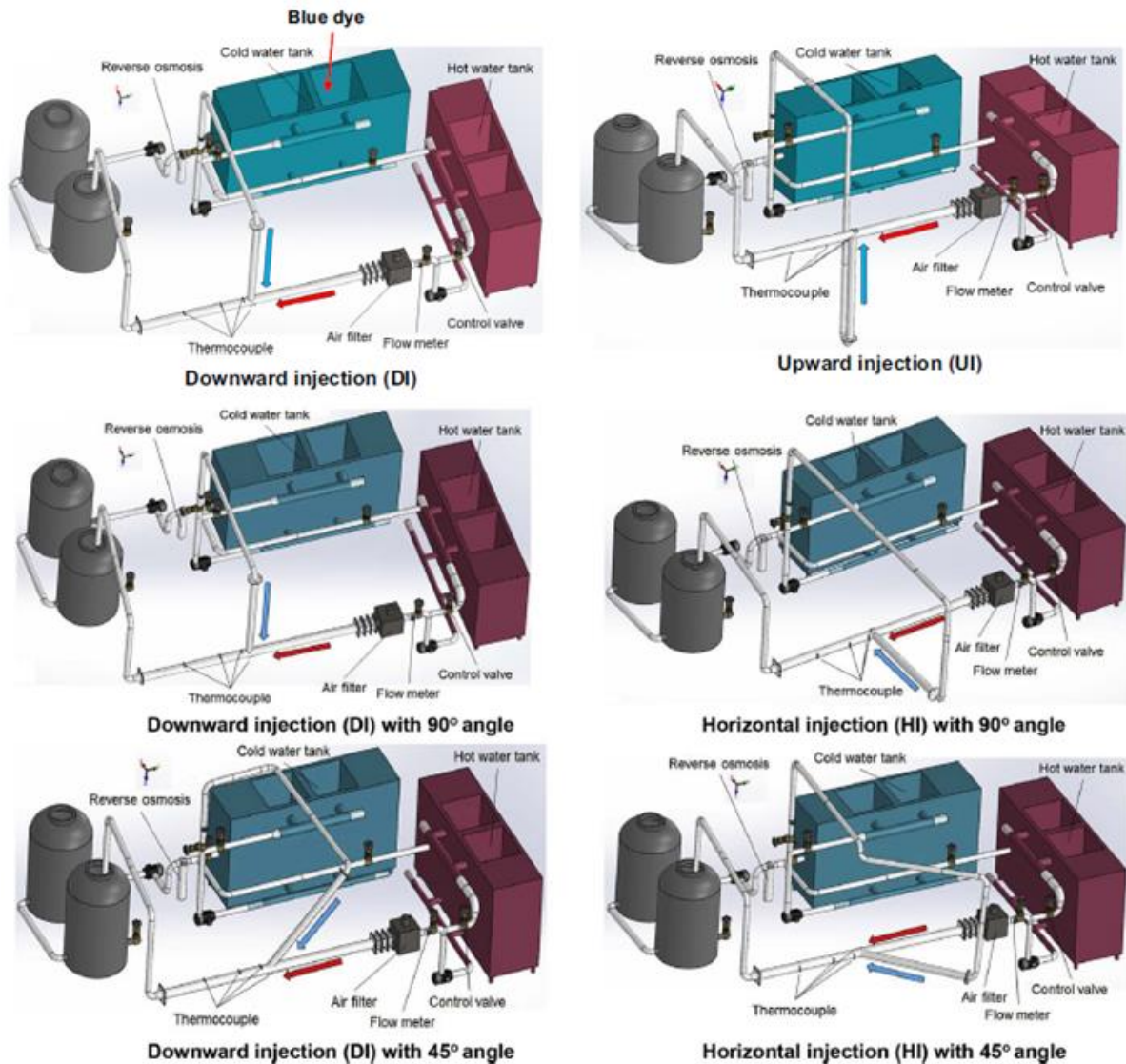


Figure 1-14: Schematics of the PVC test loop [61, 62]

This experimental work on the PVC test loop was the first investigation on the thermal-mixing pipe flow with different mixing tee configurations. The results have shown the different mixing-tee configurations have an influence on the mixing behavior. Also, the phenomenon of the reverse flow has been particularly investigated in this work. The reverse flow has been created by changing of the flow rate in the experiment. However, the reverse flow phenomenon is an effect due to density difference between the inlet flow streams. And the PVC test loop has the disadvantage of a temperature limitation. With a temperature difference of 20 K, the flow velocity ratio between the cold and hot flow streams must be very high for creating the reverse flow. In addition, the PVC test loop did not have enough thermocouple

measurement points upstream the mixing tees to capture the temperature changes in the reverse flow. Therefore, the temperature fluctuations due to the reverse flow have not been shown in this work. Anyway, this research work has introduced a novel topic in the thermal fatigue investigations.

The latest T-junction thermal fatigue research work in China has been launched jointly by Beijing University of Chemical Technology and Reach Institute of Nuclear Power Operation, which is still in progress at the present time. A T-junction test facility has been constructed and operated specially for investigating on thermal fatigue due to turbulent penetration in the mixing pipe flow. The experimental works have been performed by Guo et al. [61, 62] on this test facility.

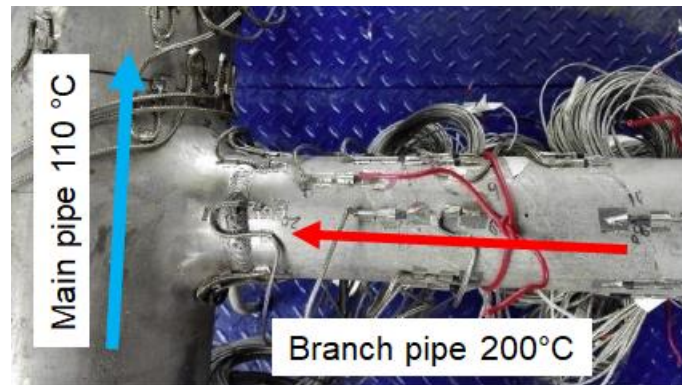


Figure 1-15: T-junction test section in the experimental setup of Guo et al. [62]

On the test facility of Guo et al., a main pipeline with inner diameter of 133 mm and a branch pipe with inner diameter of 68 mm is connected horizontally at a T-junction. The flow temperature in the main and branch pipeline are 110 °C and 200 °C in the experiments. Thermocouples have been installed on the outer surface of the pipeline close to the T-junction (see Figure 1-15). In the experiment, the cold flow in the main pipe can penetrate into the branch pipeline. Temperature drop due to the penetrated cold flow has been captured by the thermocouples in the lower part of the branch pipe. However, the thermocouple measurement points are located on the outer surface of the pipeline. The heat transfer from the pipe flow to the thermocouple has been damped due to the piping materials. Therefore, the temperature fluctuations in the mixing pipe flow as well as in the pipe wall cannot be captured for evaluation of thermal fatigue. The temperature measurement on this test facility shall be improved in the future.

The experimental work of Guo et al. has shown the turbulent penetration phenomenon in a thermal mixing process. As the boundary condition in this experiment, the flow rate in the main pipe is over 2500 times higher than it in the branch pipe. The high velocity ratio between the main and branch pipelines is similar to the experimental work of the team at NTHU. In extreme condition, the phenomenon of turbulent penetration will reach the maximum, when the flow rate in the branch pipeline is equal to zero. Such extreme condition is denoted as closed-valve or closed-branch condition. Nakamura et al. [63] have investigated penetration flow in the branch pipe with experimental and CFD methods, and divided the mixing flow in the branch pipeline into three flow regions (see Figure 1-16, left). Iguchi et al. [64] have conducted a similar experiment with closed branch pipe, and LaFleur et al. [65] have performed CFD simulations on the experiment of Iguchi to illustrate the velocity distributions along the penetration flow in the closed branch pipeline. Results have also shown the penetration distance in the branch pipeline increases lightly with the increased Reynolds-number in the main pipeline.

Recently at the University of Michigan-Ann Arbor, a T-junction investigation has been performed with focus on the flow mixing characteristics in close-valve condition. Downing et al. [66] have performed velocity measurement in the closed branch pipeline with a combination of PIV and LDV methods. The

results of the velocity measurements have shown a velocity shear in the closed branch pipe. Vortex structures can be created close to the velocity shear due to Kelvin-Helmholtz-instability. As an unexpected result, an angular shift has been found in the velocity shear in the tangential direction of the branch pipe (see Figure 1-16, right) [66].

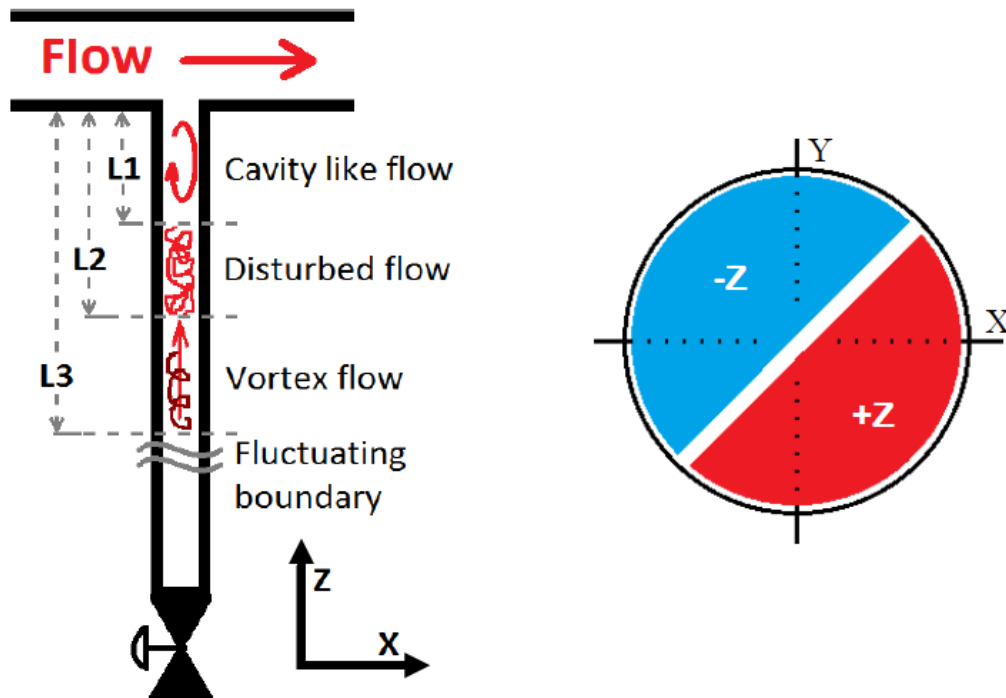


Figure 1-16: left: flow region in the closed branch pipe [63], right: the angular shift of velocity shear by Downing et al. [66]

The aforementioned investigations have shown that temperature fluctuations in the mixing pipe flow are the most important parameter for the fatigue assessment. And the temperature fluctuations can be influenced by the inlet-flow temperatures. However, these investigations have mostly been performed with a low temperature different within 100 K. It did not reach the temperature of the reality in nuclear power plants.

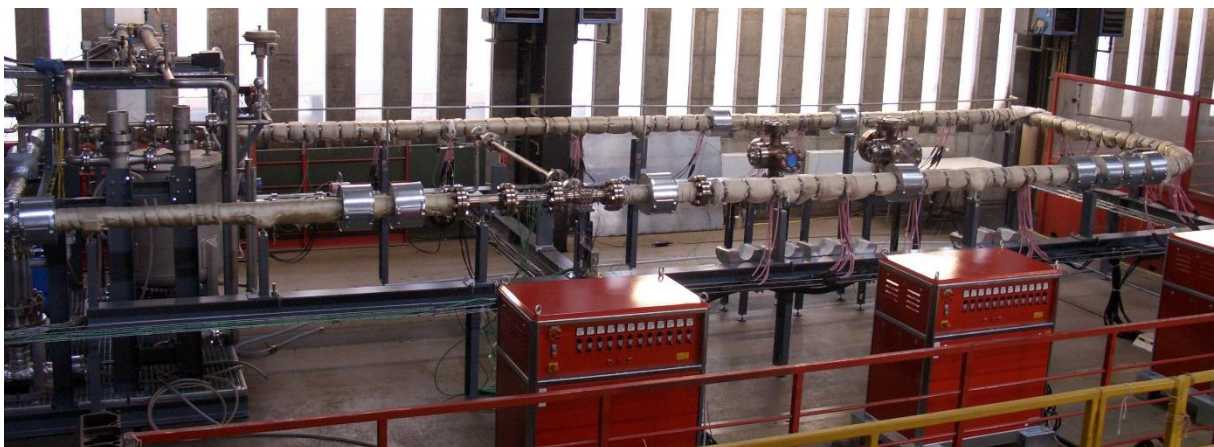


Figure 1-17: Fluid-Structure Interaction (FSI) test facility at University of Stuttgart

In 2010, founded by the German Federal Ministry of Education and Research (BMBF, Project No. 02NUK009B), a joint research project has been launched by the Institute of Nuclear Technology and Energy Systems (IKE) and Materials Testing Institute (MPA) at the University of Stuttgart. In this three-

year project, a test facility called Fluid-Structure Interaction (FSI) test facility has been constructed and operated for investigating thermal fatigue phenomenon in thermal mixing process with high temperature and high pressure at a horizontal T-junction (see Figure 1-17) [67].

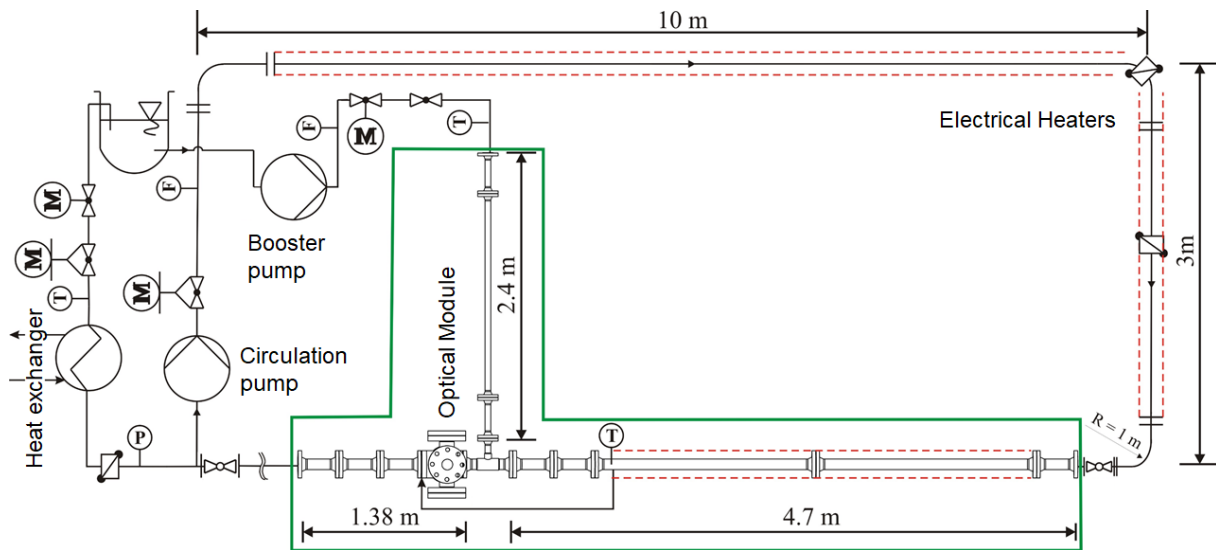


Figure 1-18: Schematics of the FSI test

The schematics of the FSI test facility is shown in Figure 1-18. As can be seen, the main pipe circuit and the branch pipeline of the FSI test facility are connected at a horizontal T-junction. In the experiments, the system pressure is charged by the booster pump, which also maintains the flow rate in the branch (cold) pipeline. The circulation pump works only for the flow rate in the main (hot) pipeline. Flowmeters and control valves are installed downstream of the pumps to ensure that the flow rates remain constant. The system pressure can reach the maximum of 75 bar in the experiments. The water flow in the main pipeline can be heated up to 280 °C. Since there is no heater for the branch pipeline, the flow temperature in the branch pipe remains constant at 20 °C. During the project, Kuschewski et al. [68] have performed experimental investigations on the FSI test facility with different measurement techniques. Thermocouples have been installed in the pipeline close to the T-junction for capturing the temperature in the near-wall fluid and pipe wall materials. Velocity measurements have also been performed on the FSI test facility with the PIV method. Especially, Kuschewski et al. [69] have developed a new technique with fluorescence dyes, the Near-Wall LED Induced Fluorescence (NW-LED-IF) method, to capture the temporal and spatial temperature in the near-wall fluid of the mixing region. For testing the optical methods, Kuschewski et al. [70] have also performed isothermal experiments at the small-scale IKE-PVC test setup, in which the temperature difference is simulated by using sugar-water solution.

Besides of the high temperature, Kuschewski [71] has performed the experiments with variation of the flow temperature respectively flow rates, so that the influence of these two decisive flow parameters on the mixing behavior can be systematically investigated. However, due to the limitations of the measurement technique and the flow parameters, no significant phenomenon of thermal fatigue has been observed in the experimental work of Kuschewski.

As project partner, Kickhofel et al. [72] from the ETH Zürich have also performed their experiments at the FSI test facility. By using their wire mesh sensor, the experimental work of Kickhofel focused on the thermal stratification in the mixing flow (see Figure 1-19). Combined with the thermocouple measurement, the results have shown a stabile thermal stratification in the mixing region downstream of the T-junction, which also matches the calculation of the Richardson-number.

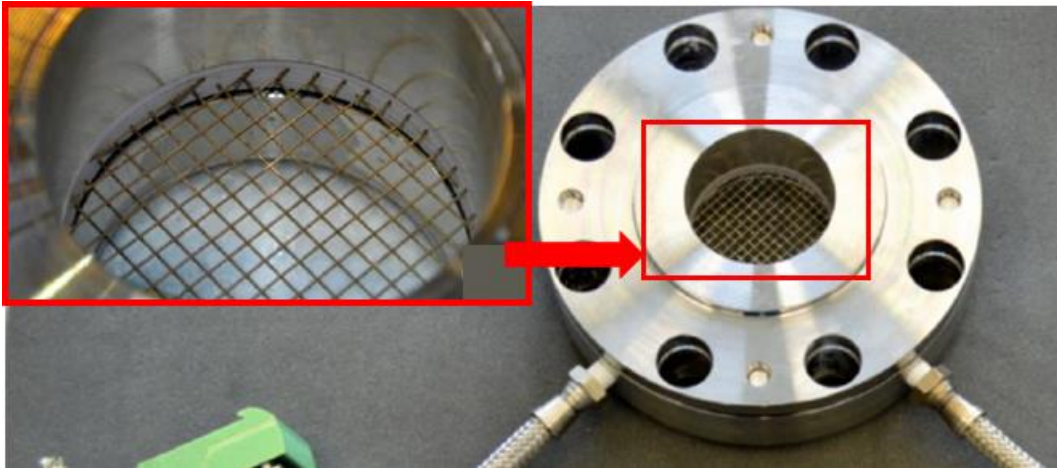


Figure 1-19: the wire mesh sensor of Kickhofel et al.

Based on the experimental work of Kuschewski, Klören et al. [73] have performed numerical simulations on thermal fatigue experiment at the FSI test facility. LES method has been applied in the simulation. The simulation has been performed with coupled heat transfer between the fluid and piping material. Temperature distributions in the mixing flow have been illustrated from the simulation results. Figure 1-20 shows the temperature distributions in the vertical cross-section of the mixing region. Thermal stratification can be identified from the vertical temperature gradient in the mixing flow. In addition, temperature fluctuations due to the turbulent mixing process can also be illustrated in the distribution of the RMS values. Moreover, the investigation have also performed to discuss the influence of the weld seam on the thermal fatigue in the mixing flow [74]. For the comparison to the NW-LED-IF measurement close to a weld seam, LES simulations have also been performed with rimmed weld root on the inner surface of the pipe wall. The stratified flow, which has been captured in the NW-LED-IF measurement, can also be found in the simulation results.

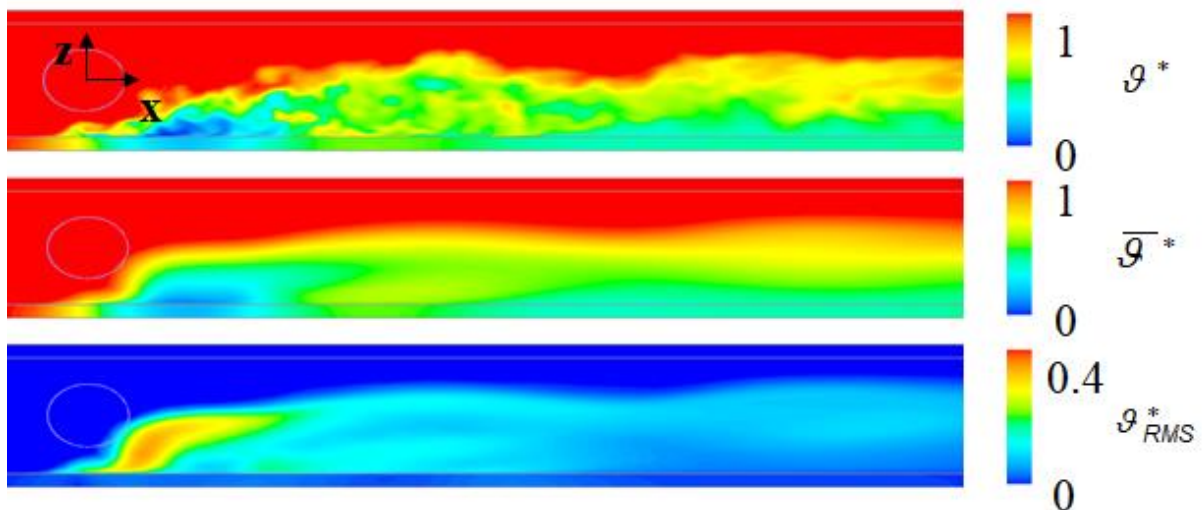


Figure 1-20: Cross-sectional view of the instantaneous Temperature (top), mean temperature (middle) and RMS temperature fluctuation (bottom) in the LES results of Klören et al. [73]

Later, P.K. Selvam [75] has taken over the investigation on the FSI test facility and focused on the CFD simulations on the thermal mixing characteristics at the horizontal T-junction. The basic numerical grid of Selvam is shown in Figure 1-21. With different modifications, this numerical grid has been applied in the simulation with different boundary conditions in the experiments. A series of LES calculations have been performed by Selvam for comparing with the experimental results.

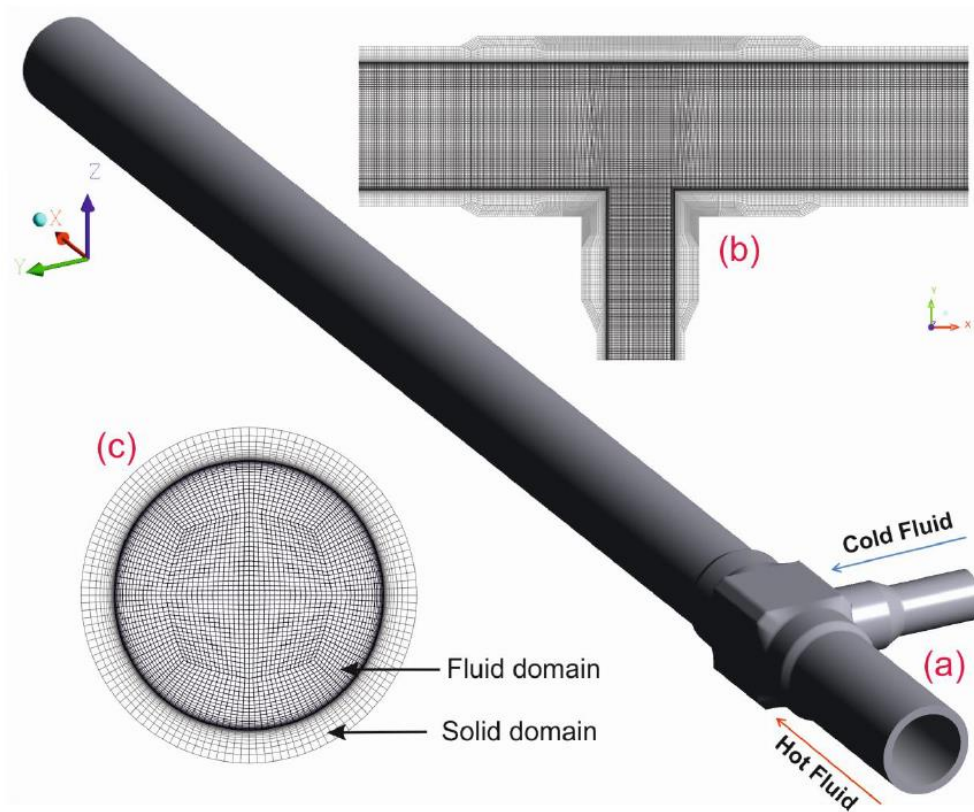


Figure 1-21: Basic numerical grid of Selvam, a) general view, b) cross-sectional view at T-junction, c) cross-sectional view of main pipe

The simulation work of Selvam et al. [76] has made a great progress for understanding the thermal mixing characteristics in the T-junction experiments with high temperature and high pressure. Thermal stratifications in the mixing flow have been illustrated from the simulation results. Temperature monitor points have been defined in the simulations for comparing with the thermocouple measurement data in the experiments. Frequency analysis has been performed to the temperature monitor data for fatigue assessment in the mixing region. In addition, the simulation work of Selvam et al. [77] has also helped to improve the experiment at the FSI test facility. In the discussion of the flow rate influence on the mixing behavior, simulations have been performed with different flow rate in the branch pipeline. The results have shown the stability of the thermal stratification in the mixing flow can be decreased with increased flow rate in the branch pipe, so that the temperature fluctuation in the mixing flow can be increased, and therefore, the potential for thermal fatigue in the mixing region can be increased. In an investigation on the boundary conditions of the experiments, a thermal stratification has been observed in the main pipe inlet flow upstream the T-junction. The vertical temperature difference in the inlet flow reached 30 K in several experiment cases. This thermal stratification was created due to the inhomogeneous heating in the main pipeline and had the ability to stabilize the turbulent mixing flow. Therefore, the temperature fluctuation in the mixing zone is much lower than expected. This inlet thermal stratification has been taken in the boundary condition in the simulation work of Gauder et al. [78]. The results have proved the influence of the inlet thermal stratification. Moreover, the LES calculations have been performed with variation of temperature difference between the inlet flow streams [79, 80]. The phenomenon of turbulent penetration in the branch pipe has been observed in the simulation results. And the inlet temperature difference has shown a clear influence on the distance of the penetrated flow. Compared with the measurement results of wire mesh sensor, thermal stratification in the mixing flow has been discussed with the inlet temperature variations. With the reconstructed temperature iso-surface in the mixing flow (see Figure 1-22), the shape of the stratified flow can provide a proof for the stability of the thermal stratification. Furthermore, the simulation results have shown an

asymmetrical spatial distribution of the flow temperature in mixing region, which was different to the thermal mixing investigations at vertical T-junctions. A spatial periodical temperature change have also been detected in the fluid-structure interface, which indicated the special mixing characteristics at the horizontal T-junction [80].

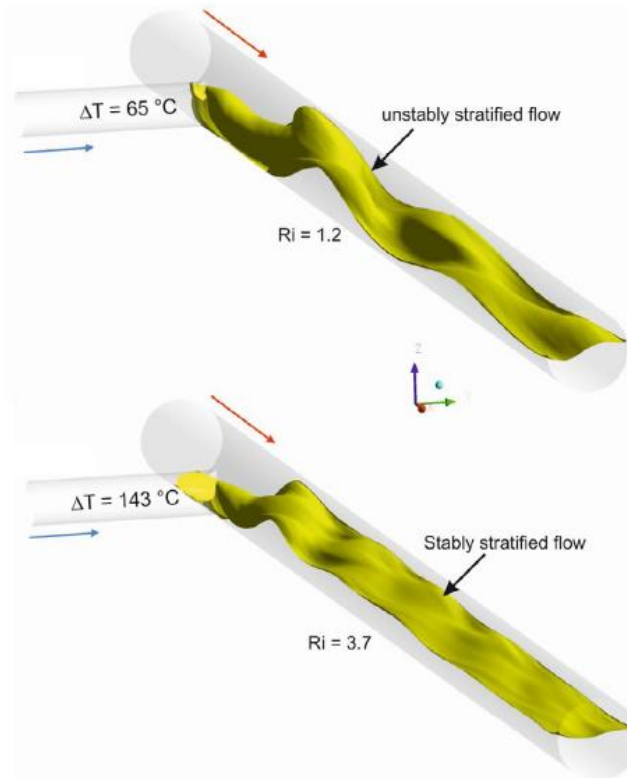


Figure 1-22: Temperature iso-surface in the mixing flow by the simulation of Selvam et al. [80]

Summarizing the previous T-junction investigations around the world, it can be understood that thermal fatigue can be initiated by temperature fluctuations due to three mixing phenomena: turbulent mixing, thermal stratification and turbulent penetration. Therefore, the thermal fatigue investigation in thermal-mixing pipe flow shall be discussed in these three areas individually. And the measurement techniques on experimental setup shall be able to capture these three mixing phenomena. For the fatigue assessments close to the T-junction, evaluation of temperature fluctuations shall be the first step. Mostly, the RMS (Root Mean Square) values of the temperature signals are calculated as the scale of the temperature fluctuations. Then, frequency analysis on the temperature signals shall be performed to estimate the regular temperature changes. In a thermal fatigue investigation on the Civaux case, Galpin et al. [81] have summarized the previous work of frequency analysis and concluded that the temperature fluctuation in the frequency range of 0.1 – 10 Hz is in the relevance for thermal fatigue. Hence, measurement areas with high temperature fluctuation and regular temperature change in this range have a potential to initiate thermal fatigue. Due to material inhomogeneity, areas close to the weld seam are mostly like to be damaged due to thermal fatigue. Piping wall areas close to the weld connections shall also be discussed in the fatigue assessments.

Since thermal fatigue is created by temperature fluctuations in the mixing process close to T-junction, the crucial factors on temperature fluctuations in the thermal-mixing pipe flow shall be investigated systematically. The aforementioned T-junction investigations have shown that the mixing characteristics can be influenced by inlet flow temperature, flow rate, mixing-tee configuration and mixing-behavior influenced pipeline segment (e.g. upstream elbow). These factors work differently on the thermal mixing characteristics and have the influence on the three thermal-fatigue related phenomena. Among these

factors, variation of inlet flow temperature and flow rate is feasible in the T-junction experiment. In particular, Lee et al. [82] have summarized the simulation works on Toshiba-/Hitachi-experiments and concluded a threshold value of 115 K for the temperature difference between the inlet flow streams. Separated with this threshold value, the penetration depth of the temperature changes into the pipe wall shows a different correlation with the frequency of the temperature changes. However, most of the T-junction experiments have been performed with a temperature difference much lower than 115 K. It is necessary to perform T-junction experiment with high temperature difference. A summary of T-junction experiments in the literatures is shown in Table 1-3 with category by inlet flow temperature.

Table 1-3: A summary of the previous T-junction experiments categorized by inlet flow temperature

		Author	Experimental setup	Inlet flow temperature
Single temperature difference	Temperature difference < 115 K	Braillard et al.	MOTHER	30 °C / 15 °C
		Smith et al.	Vattenfall	36 °C / 19 °C
		Chuang et al.	NTHU PVC	40 °C / 20 °C
		Kamide et al.	WATLON	48 °C / 33 °C
		Miyoshi et al.	T-Cube	59.8 °C / 25.7 °C
		Kimura et al.	Toshiba-experiment	60 °C / 20 °C
		Chen et al.	EXTREME	90 °C / 20 °C
		Kuhn et al.	FATHERINO	80 °C / 5 °C
		Guo et al	BUCT	200 °C / 110 °C
	Temperature difference > 115 K	Kuschewski et al.	IKE-PVC	Sugar-water, eq. $\Delta T = 106$ K
		Metzner et al.	THERFAT-Plexiglas	Salt-water, eq. $\Delta T = 150$ K
Varied temperature differences	Temperature difference < 115 K	Courtin et al.	FATHER	$\Delta T = 160$ K
		Kawamura et al.	Hitachi-experiment	$\Delta T = 31 \sim 34$ K
	Temperature difference > 115 K	Metzner et al.	THERFAT-Steel	$\Delta T = 60 \sim 90$ K
		Kuschewski et al.	FSI	$\Delta T = 25 \sim 200$ K

From the review of the literature, the following conclusions can be obtained for the previous T-junction thermal-fatigue research works.

First of all, most of the previous works on thermal-mixing pipe flow have been performed at vertical T-junctions. Insufficient details have been obtained from a few investigations for understanding the turbulent-flow mechanism at horizontal T-junction, which can cause thermal fatigue damage in the piping materials. In particular, it is unknown, what is the necessary flow boundary conditions in the thermal mixing processes to trigger thermal fatigue damage, how the flow boundary conditions work on the thermal fatigue damage, and where the thermal fatigue damage could be located.

Secondly, most of the previous T-junction thermal fatigue investigations have been performed with low temperature differences between the inlet flow streams (see Table 1-3). Hence, the buoyancy effect in the mixing flow is not significant in these works. Thermal mixing characteristics with high temperature difference is still unclear. Moreover, with a constant temperature difference, the influence of the temperature difference on the thermal mixing behavior as well as thermal fatigue damages in the mixing processes cannot be discussed in most of the previous investigations.

Thirdly, the three thermal fatigue related mixing phenomena have been concluded from the previous investigations. However, these three phenomena have been investigated individually in different research works (test facilities). The flow mechanisms to create these three phenomena at a T-junction are still unknown.

In addition, initiation of thermal fatigue damage close to weld connections in the mixing region has been investigated in the previous work. It can be concluded, that the materials close to the weld seams in the mixing region are most likely to be damaged due to thermal fatigue. However, the impact of the weld seams on the nearby mixing flow is unknown.

Furthermore, the previous investigations have concluded different methods to evaluate thermal fatigue damage in the T-junction pipe flow. No efficient method has been concluded for the operation of the piping systems to avoid thermal fatigue damages. Although monitor systems can be installed in piping system, it cannot solve the thermal fatigue issue fundamentally.

1.3 Aim of work

The aim of this work is to identify and understand the turbulent-flow mixing mechanisms, which can cause high-cycle thermal fatigue damage in the material of a nuclear power plant piping system. The flow conditions, in particular the pressure and temperature range, as well as the piping material are chosen similar to those in a real nuclear power plant. As geometric configuration, the mixing of cold and hot flow streams takes place in a horizontal 90° T-junction. In addition, a circumferential dissimilar weld seam between austenitic and ferritic stainless steel shall be constructed in the mixing region. Investigations shall also be performed for understanding the fluid-structure interaction between the weld seam and the nearby mixing flow.

To conclude an efficient data analysis procedure for fatigue assessment, fatigue damage shall be created in the mixing process in a short time. For accelerating the initiation of fatigue damage in the pipe wall, a 25° shock module is chosen in a pre-investigation in combination with an artificially induced temperature change. Results of the fatigue assessment shall be confirmed by the metallographic examination.

For understanding the influence of the flow conditions on the mixing characteristics as well as the thermal fatigue phenomenon in the mixing flow, thermal mixing experiments are performed with variations of inlet flow temperature and flow rate in the cold and hot flow streams.

For measurement and description of the mixing flow, measurement techniques are adapted for the application under these conditions. In particular, micro-thermocouples are chosen for the temperature in the near-wall fluid. PIV method is applied for capturing the velocity profiles. NW-LED-IF method is applied for capturing spatial and temporal temperature distribution in the near-wall mixing flow.

The understanding of the physical mechanisms of thermal fatigue phenomenon in the mixing pipe flow is supported by 3D numerical simulation with the Large-Eddy simulation method. The results of the simulation works shall be compared with the experiments.

2 Experiment facility and measurement techniques

2.1 Fluid-Structure-Interaction test facility

The Fluid-Structure-Interaction (FSI) test facility is a DN80 ($D = 71.8$ mm) main pipeline circuit connected with a DN40 ($d = 38.9$ mm) branch pipeline. The FSI test facility was constructed and operated jointly by IKE and MPA for investigating thermal mixing behavior of hot and cold flow at a T-junction. The alternate test conditions of the FSI test facility can be varied between room temperature and 280 °C. And the operation pressure can reach the maximum of 75 bar. The pipeline circuit is modularly constructed for application of different measurement techniques. Different to the other T-junction test facilities around the world, the FSI test facility has an advantage due to its close-system design. Therefore, the FSI test facility can be operated continuously with high temperature and high pressure for a specific long time.



Figure 2-1: FSI test facility after modification

The first aim in this work is to initiate a fatigue damage for summarizing a procedure of fatigue assessment in the thermal mixing processes. In order to generate fatigue damage in the mixing flow, the FSI test facility has been modified for this investigation. To condition an environment related to reality in nuclear power plants, a water preparation system (see Figure 2-2, right) is connected to the water tank of the FSI test facility and controls the electrical conductivity of the water in the system to stay below 0.15 $\mu\text{S}/\text{cm}$ [83]. According to the simulation work of Selvam et al. [77], the effect of thermal fatigue can be enhanced by increasing the flow rate in the branch pipeline. Therefore, the booster pump has been doubled (see Figure 2-2), so that the flow rate in the branch pipeline can reach the maximum of 200 g/s. Increasing of the cold flow rate leads to a lower temperature in the mixed flow, which requests a higher power to heat up the main pipe flow to the target temperature in the heating zone of the circuit. Therefore, a U-profile pipe section has been installed in the main pipe heating zone (see Figure 2-1), so that the temperature in the main pipe flow can be kept over 200 °C with increased branch pipe flow of 200 g/s.

In the previous work, a thermal stratification has been detected in the main pipe flow at the end of the heating zone upstream the T-junction. This thermal stratification was created by inhomogeneous heating by the electrical heater and the buoyancy effect in the hot flow. The temperature difference between top and bottom in this thermal stratification was over 30 K. This thermal stratification can stabilize the heat exchange (convection) in the mixing flow downstream the T-junction, so that the observed temperature fluctuation in the previous experiments was much lower than expected. For initiating fatigue damage in the thermal mixing process, the thermal stratification in the inlet flow must be broken up for creating high temperature fluctuation in the mixing flow. Static mixers have been applied on the FSI test facility for breaking up the thermal stratification in the hot inlet flow [84]. A static mixer is a device for continuous mixing of fluids. Static mixers are fixed in the flow cross-section and do not move with the fluid flow. The energy for the mixing comes from the pressure drop of the fluid by the static mixers.

Three different kinds of static mixers, helix mixer, propeller mixer and HiFlowRings, (see Figure 2-3) have been tested by flow field visualization and pressure drop measurement on an individual setup, in which the stratified flow is created by sugar-water solution and visualized by using fluorescence dye. In the test, the propeller mixer shows the best performance with respect to the flow mixing effect and the smallest flow pressure drop. Hence, the propeller mixer has been chosen for the application on the FSI test facility. The propeller mixer has been installed at four different positions in the heating zone of the FSI test facility. In the followed experiments, the vertical temperature difference in the inlet flow is measured below 3 K. It is possible to observe high temperature fluctuations in the mixing flow downstream the T-junction.



Figure 2-2: left: booster pump; right: water preparation system



Figure 2-3: Static mixers: left: helix mixer, middle: propeller Mixer, right: HiFlowRings

For acceleration of the fatigue damage, the branch pipeline has been modified for artificially controlling of cold-flow injection. Figure 2-4 shows the schematic sketch of the FSI test facility after the modification. A bypass has been constructed and connected to the branch pipeline with the two-way valves (COAX-I and COAX-II). Another mixing tee, the shock module (see Figure 2-5), in which the main and branch pipeline is oriented at 25° , installed in the main pipeline and connected to the branch pipeline through the two-way valve COAX-II. With this construction, the pipe module for fatigue test can be installed either downstream the T-junction (test position 1) or shock module (test position 2). By periodical switching of the two-way valves, an Artificially Induced Periodical Temperature Change (AIPTEC) can be created in the mixing flow downstream the T-junction or shock module, respectively. By controlling the durations of injection and bypass in AIPTEC, temperature in the mixing flow can be imposed to change with a specific frequency.

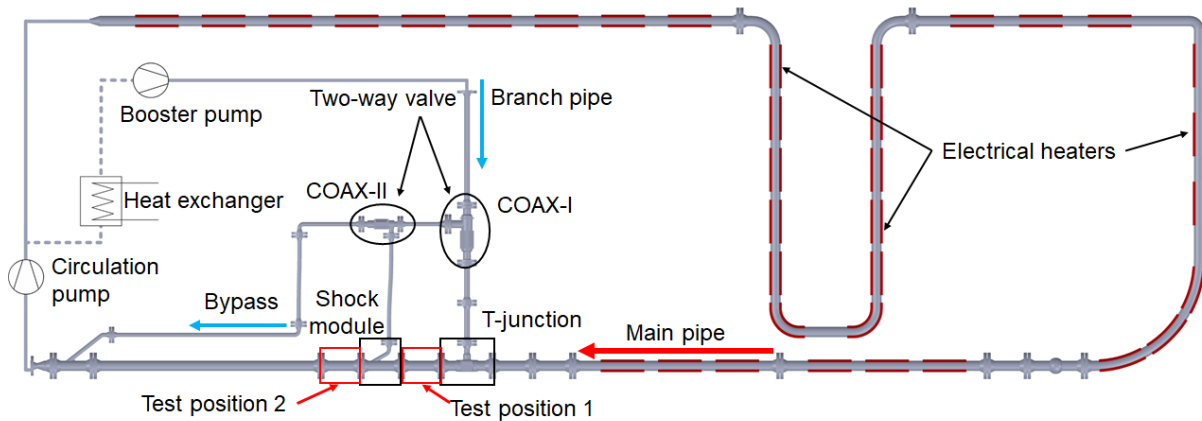


Figure 2-4: Scheme of FSI test facility after modification

The purpose for application of the shock module leads to the confirmation of the fatigue damage in the piping material. Because the angle between the main pipeline and the branch pipeline in the shock module is 25° (see Figure 2-5), the branch pipe aims at the inner wall of the test pipe module, which is installed at test position 2 downstream of the shock module. Hence, by switching of the COAX-II, high temperature fluctuations shall be created in the test pipe module, but not the shock module. After the experiment, the tested pipe module can be removed and cut open for metallographic investigation. Under scanning electron microscope, fatigue damage can be identified in the piping material.

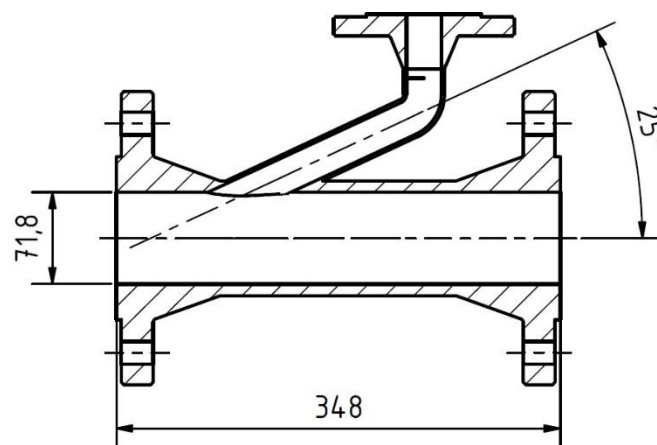


Figure 2-5: Design of the shock module

Optical measurement techniques can also be applied in the FSI test facility by using the optical modules. The optical modules have the same length with the standard pipe modules at the FSI test facility and can replace the pipe modules for optical measurement. Figure 2-6 shows the optical module for the main pipeline and its sectional view. As can be seen, the optical module consists a quartz-glass pipe and a stainless steel container with four glass windows. In the measurement, the quartz-glass pipe is connected to the pipeline circuit. The container is filled with water, so that the optical distortion due to pipe bend can be neutralized. The pressure inside and outside of the quartz glass pipe is equalized by using a tube connection to the FSI circuit. Due to the operation safety, the optical measurements are all performed with 30 bar.

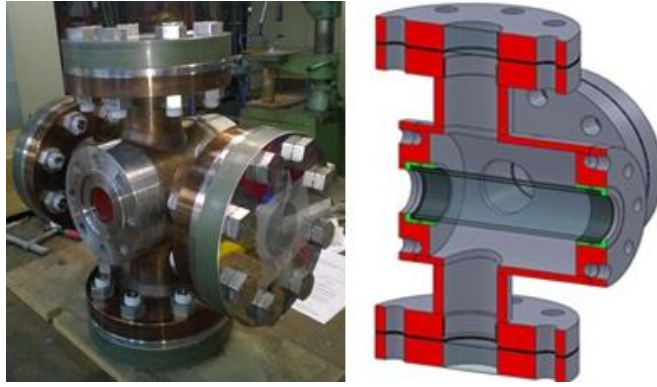


Figure 2-6: Optical module for the main pipe and its sectional view

2.2 Dissimilar weld

Cracks in piping materials of cooling systems due to thermal fatigue are mostly found close to weld seams [8, 9]. On the one hand, the weld seam represents both a geometrical and a microstructural notch, which increases the local stress in this region. On the other hand, the weld root has an influence on the flow field and increases the turbulence in the flow. For initiating a significant fatigue damage within a short time, the investigation is firstly performed on a dissimilar weld, which comprises the joint of austenitic (X6CrNiNb18-10) and ferritic (20MnMoNi5-5) steel by using of a nickel-base weld-filler material (NiCr70Nb). A sample of a dissimilar weld is shown in Figure 2-7. Within a dissimilar metal weld, different types of materials are jointed together. This results into fundamental differences in terms of thermal-mechanical loading behavior since especially thermal expansion and mechanical strength vary between the different kinds of materials. Moreover, due to the welding process a high amount of thermal energy is put into the material, changing the microstructure significantly. Also, due to the welding process, residual stresses are built up and influence the local deformation behavior. In addition to the mechanical behavior, the local chemistry is also influenced, which may change the susceptibility for corrosion fatigue phenomena.

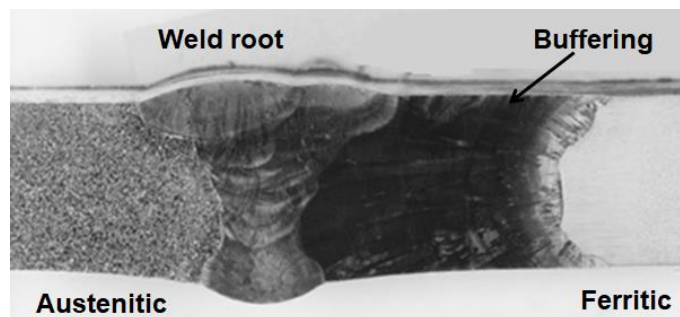


Figure 2-7: Photograph from the cross-section of a dissimilar weld sample

In order to test the dissimilar metal weld at the FSI test facility, weld seam modules are constructed and installed separately in the test position 2 downstream of the shock module. The weld seam modules are manufactured with an austenitic and a ferritic pipe segment, and consist of two dissimilar weld seams. The height of the weld root is about 1.5 mm from the inner wall. One of the weld seam modules is equipped with thermocouples to capture the temperatures in the experiments (see Figure 2-8).

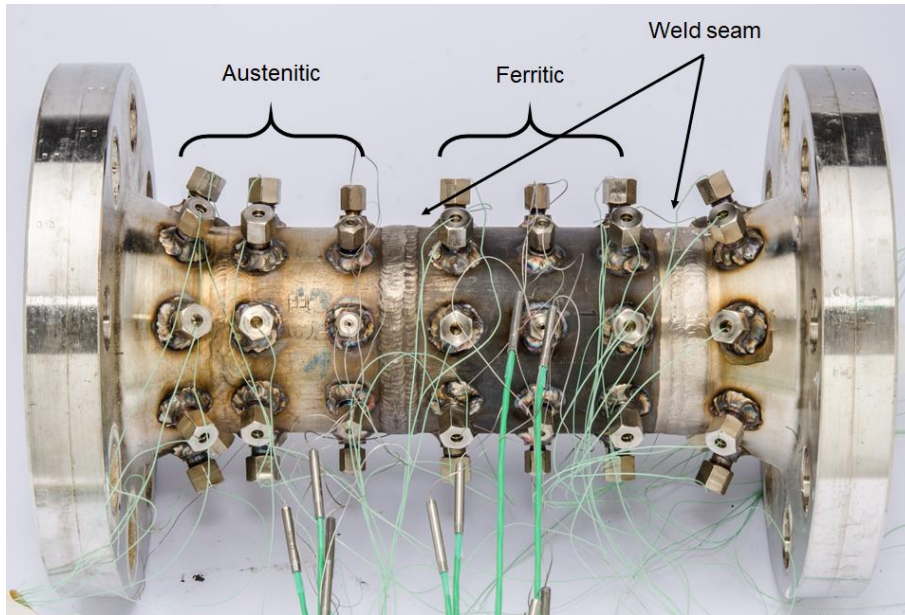


Figure 2-8: With thermocouples equipped weld seam module

2.3 Micro-thermocouple technique

In previous experiments at the FSI test facility, standard-shielded thermocouples (type K [85]) were used to capture the temperatures at different positions in the mixing zone [69]. The measurement point of these shielded thermocouples had a diameter of 0.25 mm. The measurement results of these shielded thermocouples showed much smaller temperature fluctuations than expected [71]. It indicated that the dynamical response performance of these shielded thermocouples was not fast enough to capture the high frequency temperature fluctuations. Figure 2-9 shows the design of the shielded thermocouples. As can be seen, there is MgO (magnesium oxide)-powder between the thermocouple measurement point and the protective shell. The porous MgO-powder has a low thermal conductivity and creates a thermal buffer region around the measurement point. Hence, the heat transfer to the measurement point can be delayed due to the MgO-powder, and the shielded thermocouples cannot capture the high frequency temperature changes in the mixing flow. In order to generate more accurate results, the technique for the temperature measurement must be improved.

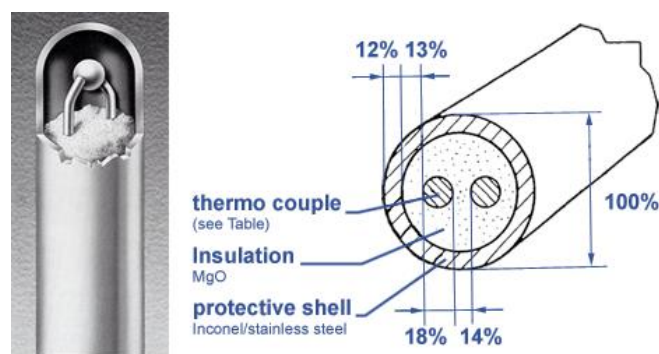


Figure 2-9: View of the shielded thermocouple [86]

For current investigations at the FSI test facility, new micro-thermocouples (diameter 0.08 mm, type K, see Figure 2-10) are chosen for the measurements of the temperature fluctuations [86]. Before application in the FSI test facility, two simple test devices were built to test the thermal performance of the thermocouples. With the first test device, the response time of the thermocouples are checked for three imposed temperature differences, which were imposed by submerging the thermocouples into oil

bath of defined temperature. Figure 2-11 shows the working principle of the test device. The DAQ system records the temperature signal of the thermocouple and the DC voltage on the device at the same time. By the time the measurement point of the thermocouple submerges into the oil bath, the electrical circuit is closed, and the DAQ system records a DC charge. The imposed temperature differences in the test were chosen for 100 K, 200 K and 250 K. Micro-thermocouples from different manufacture batches and shielded thermocouples with diameters of 0.25 mm, 0.5 mm and 1 mm are tested and compared.

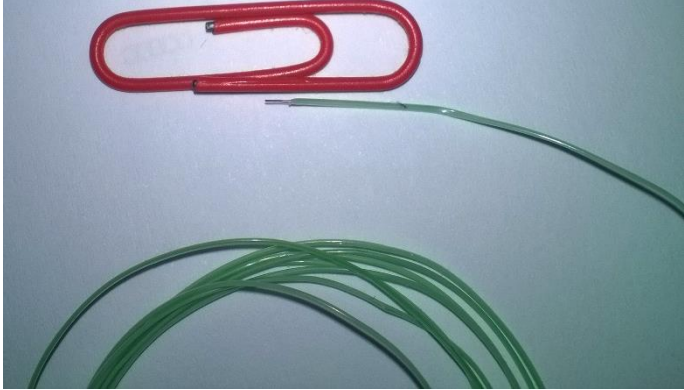


Figure 2-10: Measurement point of the micro-thermocouple in comparison with a paperclip

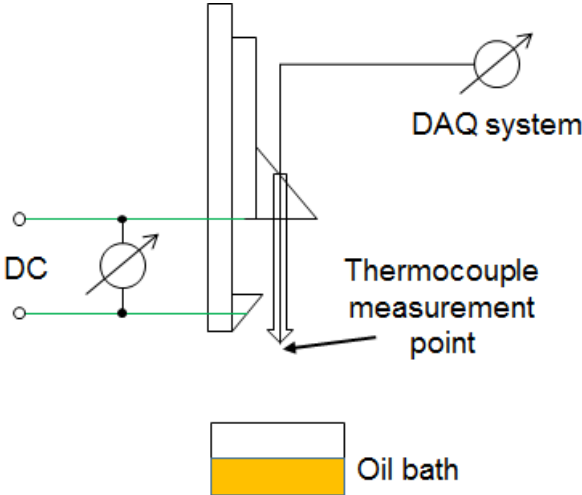


Figure 2-11: Principle of the test setup for measuring thermocouple response time

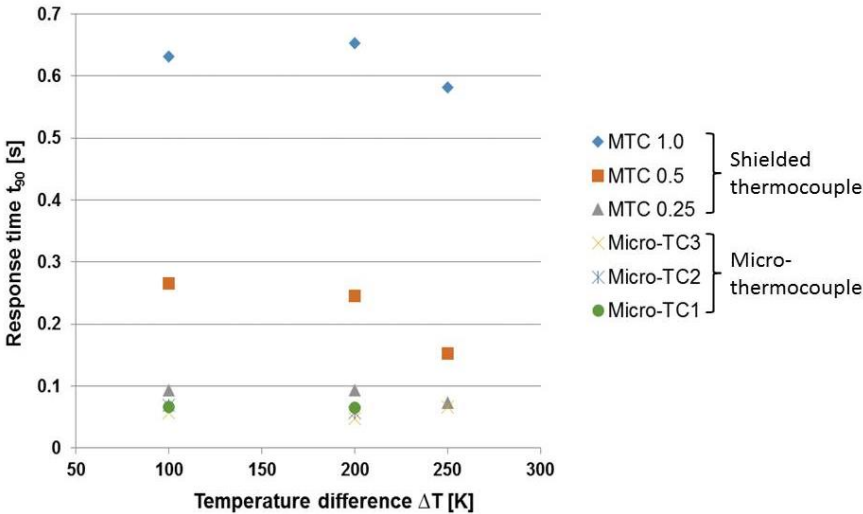


Figure 2-12: Response time of tested thermocouples

The measured response times are shown in Figure 2-12. The micro-thermocouples in different batches have shown almost the same response time t_{90} with different imposed temperature differences. The test results of the shielded thermocouples with diameter of 0.25 mm are approximately the same as the results of the micro-thermocouples. The shielded thermocouples with diameter of 0.5 mm and 1 mm respond much slower compared to the others.

In the test of the response time, the heat transfer is only in one direction from the fluid to thermocouple measurement points. However, to capture the high frequency temperature fluctuations, the thermocouples must be tested with cyclic temperature changes, since the heat-transfer direction changes with the temperature fluctuations in the fluid temperature. The amplitude damping and phase shift of the thermocouple signals at a cyclic temperature variation are examined with the second test device (see Figure 2-13). The tested thermocouple is mounted on the round head screw at the end of the holding bar, which is driven by the electrical motor and rotates in the horizontal level. In order to press the measurement point of the thermocouple into the oil bath, a cam switch, which is manufactured by a 3D printer, is installed above each oil bath. An electrical circuit is installed in the cam switch, so that the DAQ system can receive a voltage charge every time when the thermocouple is in the oil bath.

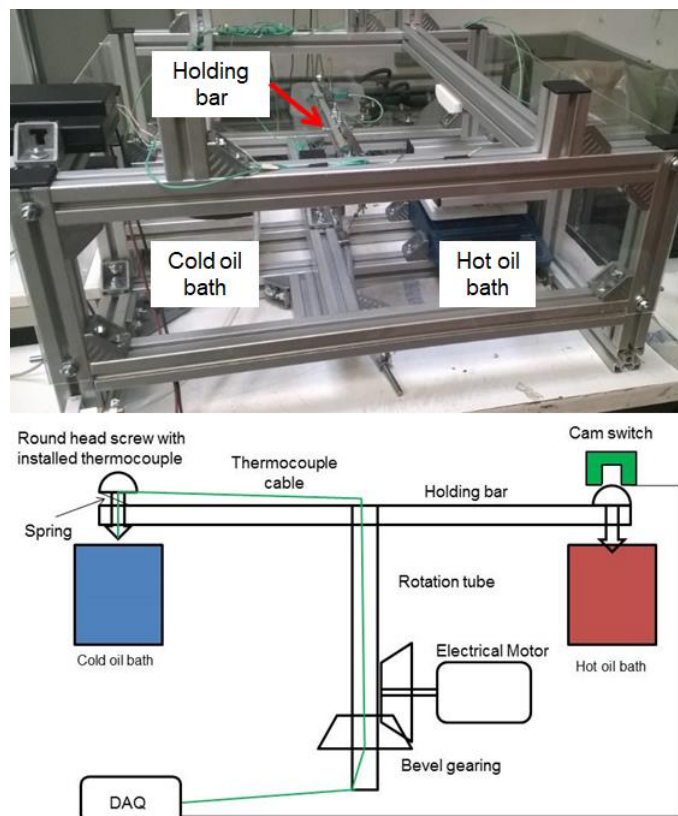


Figure 2-13: Test setup to investigate the dynamical performance of the thermocouples with periodical temperature changes (above) and its working principle (below)

With the rotation of the holding bar, the thermocouples in this test move periodically between a cold and hot temperature fluid bath. The temperature differences between the baths are set to 100 K and 200 K. The frequency of the periodical movement is approximately 1 Hz. The results of these tests are shown in Figure 2-14. Two micro-thermocouples from two different batches (Micro1 and Micro2) and one shielded thermocouple with diameter of 0.25 mm (STC) have been examined. As can be seen from Figure 2-14 the shielded thermocouple has a much higher amplitude damping and phase shift than the micro-thermocouples. The amplitude damping and phase shift of the micro-thermocouples are about 3% respectively 45% of the standard shielded thermocouples. Therefore, the micro-thermocouples are

appropriate for the measurement on high frequency temperature fluctuations. According to the results from these tests, micro-thermocouples are chosen for the temperature measurements in the flow at the FSI test facility.

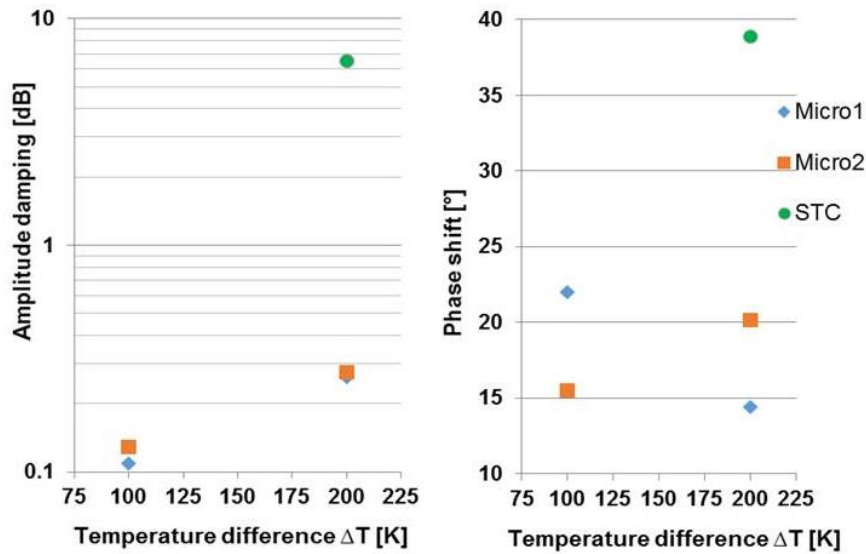


Figure 2-14: Amplitude damping (left) and phase shift (right) of tested thermocouples at 1 Hz cyclic temperature variation

Temperature measurement in T-junction experiments can be performed at different locations in the test facilities. Typical like the WATLON facility [34], the investigations focus on the temperature distribution within the flow field. Thermocouple structures (or trees) have been applied and installed inside the pipeline. Another type of facilities like T-Cubic facility [52], which concentrates on the temperature changes within the piping material, have the thermocouples installed in the pipeline. Different with these two types, the investigation on the FSI test facility focuses on the temperature fluctuations in the near-wall flow, which have the direct impact on initiation of thermal fatigue damage in the piping material.

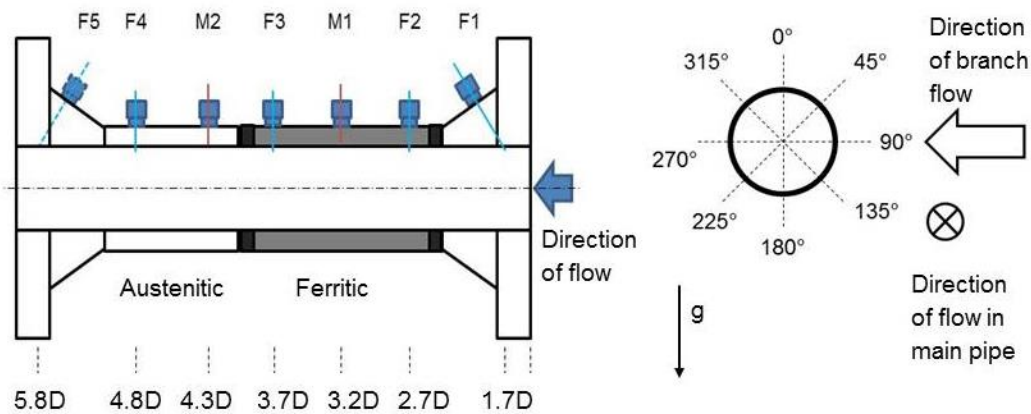


Figure 2-15: Thermocouple positions (axial position x , angular position θ) at the weld seam module

In the experiment with the weld seam module, totally 56 thermocouples measurement positions have been made on the weld seam module for temperature measurement (see figure 2-8). The thermocouples are separated in seven measurement cross-sections. In each cross-section, the thermocouples are arranged in every 45° . The locations of the measurement cross-sections and the angular positions of the thermocouples in each cross-section are shown in Figure 2-15. In the experiment, the weld seam module is installed at the test position 2 downstream of the shock module. The joint point of the main and branch

pipe axes is set as coordinate origin for the shock module. The roots of the dissimilar weld seam are located at positions of 2D and 4D downstream of the shock module. 40 micro-thermocouples (type K) have been installed on the weld seam module for capturing the temperature in the near-wall flow (F1 – F5). The measurement points of the micro-thermocouples are about 1mm from the pipe inner wall into the flow. Another 16 shielded thermocouples (type K) have been installed in the two measurement cross-sections M1 and M2 for monitoring the temperature in the piping material. Since the shielded thermocouples have been proven that their dynamical performance is much slower than the micro-thermocouples and this work focuses on the measurements in the near-wall flow, only the temperature measurements of the 40 micro-thermocouples are analyzed to discuss their relevance with thermal fatigue.



Figure 2-16: With micro-thermocouple equipped thermocouple (TC)-module

After experiment, the weld seam module has been cut open for metallographic investigation. In the following experiments at the T-junction, the thermocouple (TC-) module, which has been used in the previous of Kuschewski et al. [69], has been modified and applied for the measurements (see Figure 2-16). The shielded thermocouples, which are used in the previous work [69], have been removed from the TC-module. Four measurement cross-sections are provided for the investigations. 32 micro-thermocouples are installed on the TC-module to capture the temperature of the near-wall fluid (measurement positions of fluid temperature FT1 – FT32). The measurement points of the micro-thermocouples are 1 mm into the fluid from inner wall of the pipe.

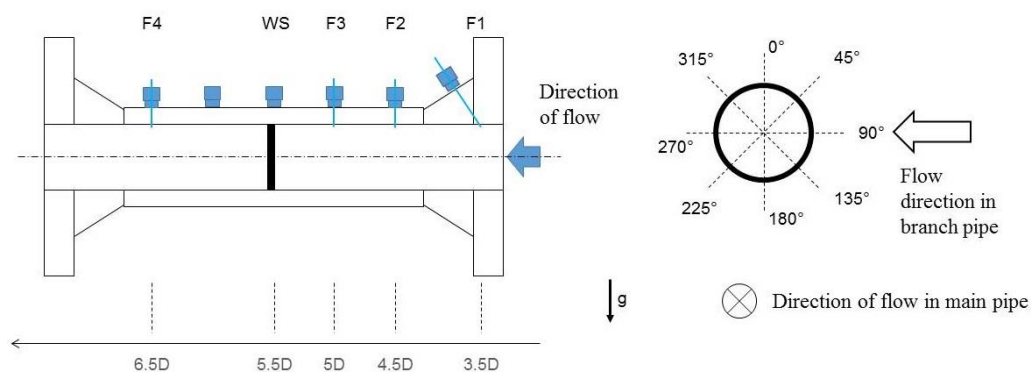


Figure 2-17: Measurement positions (axial position x , angular position θ) at the TC-module

The locations and angular positions of the micro-thermocouples at the TC-module are shown in Figure 2-17. The TC-module is installed in the test position 1 downstream of the T-junction. The crossing point of the main and the branch pipeline axes in the T-junction is defined as the coordinate origin. Due to the different manufacture configurations, thermocouples in the cross-section F3, which are installed in the drillings of the previous work, have an angular shift of 9° with the other three cross-sections in the tangential direction [75]. To simulate the effect of a rimmed weld seam root, a geometric weld seam

model has been installed in the TC-module at the position, where one of the weld roots is located in the weld seam module (5.5D downstream the T-junction, equivalent 4D downstream of the shock module, see Figure 2-15 and 2-17). The geometry of the weld seam model is shown in Figure 2-18.

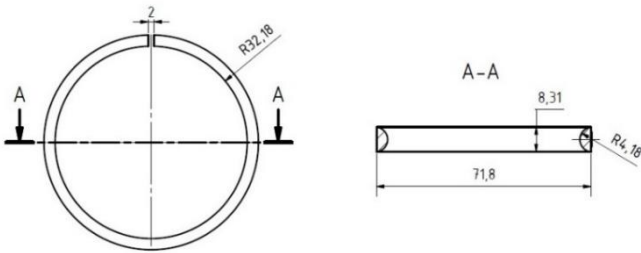


Figure 2-18: Geometry of the weld seam model

To observe the reverse flow (turbulent penetration) upstream of the T-junction, there is also a measurement cross-section with 8 micro-thermocouples at position $-4.5D$ upstream the T-junction in the main pipeline (cross-section $-F$) respectively $-7d$ in the branch pipeline (cross-section $-f$). The positions all the measurement cross-sections are shown in Figure 2-19. The angular positions of these 16 micro-thermocouples are arranged in every 45 degree intervals same with those on the TC-module.

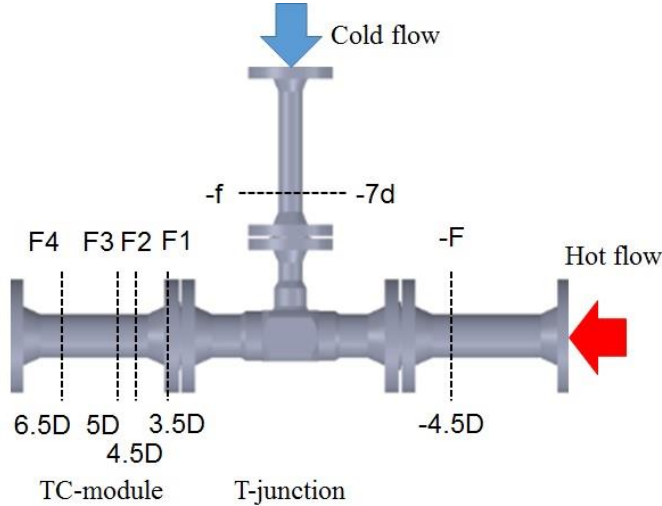


Figure 2-19: Positions of the measurement cross-sections in the mixing region

In the temperature measurements, the thermocouples are connected to the Adwin-pro II DAQ system, which records temperature signals with a frequency of 100 Hz. The experiment on the weld seam module has the aim of initiating fatigue damage. Therefore, the experiment has been performed with AIPTEC of 30 s injection and 30 s bypass, and run 24 h and seven days a week continuously for four weeks resulting in more than 10,000 injection/bypass-periods. In the four-week experiment, the FSI test facility has been operated and monitored with the three shifts of staff from IKE and MPA. In the experiment with TC-module, the investigation focuses on the thermal fatigue effect and thermal mixing characteristics at 90° T-junction. The experiments have been performed with AIPTEC and continuous cold flow injection, respectively. To generate enough data for analysis, the measurements with AIPTEC have been conducted with at least 100 periods. And the measurements with continuous cold flow injection have been performed with at least 45 min. A few additional measurements have been performed with closed branch pipe, in which the cold flow in the branch pipe flows through the bypass. The measurements with closed branch pipe have been performed for at least 30 min.

2.4 Near-wall fluorescence technique

Fluorescence dyes are widely used in fluid dynamical experiments for flow field visualization [87]. With a high sensitivity and high accuracy, fluorescence dyes can provide a noninvasive optical method to obtain the qualitative or quantitative distributions of concentration or temperature [88], which are generated with the dependence of the emission light intensity on the dye concentrations in the flow field. The fluorescence methods can be divided into two systems. Most of the fluorescence measurements are performed in so-called optical thin system, in which the concentration of the fluorescence dye is so low, that absorption of excitation light along the penetration deep can be neglected. With the optical thin systems, the fluorescence measurements are performed within the flow such as the Planar Laser-Induced Fluorescence (PLIF) method [89]. Similar method has been applied in the test on the functioning of the static mixers in chapter 2.1.

Oppositely in an optical blind system, the excitation light penetrates only a small distance into the flow and the emission light in the small depth of the flow is captured for the measurement. With the blind system, Kuschewski [71] has developed the Near-Wall LED Induced Fluorescence method (NW-LED-IF) to capture the temperature distribution in the near-wall mixing flow. In the mixing flow downstream of the T-junction, the distribution of the water density cannot be homogeneous due to the heat exchange. The refractive index of the water, which depends on the water density, is not constant in the mixing flow. Therefore, it is not possible to perform conventional optical measurement in the mixing flow. However, with the optical blind the system, only a thin layer (about) of the near-wall flow is illuminated. The optical distortion due the inhomogeneous distribution of the water refractive index can be neglected. And with the fluorescence technique, the spatial and temporal temperature distribution in the near-wall flow can be captured for fatigue assessment in the measurement area. In addition, the NW-LED-IF technique provides a possibility to capture the temperature distribution in a complete measurement area, while the thermocouples are discretely installed on the TC-Module for temperature measurement in the mixing flow. Moreover, compared to the thermocouple measurement, the NW-LED-IF has the advantage to capture the flow temperature close to the weld seam model, so that the influence of the rimmed weld root on the nearby flow can be directly observed in the measurement. So far in the research on thermal fatigue, the estimations of high potential for fatigue damage close to weld connection are concluded from the viewpoint of material science. With the NW-LED-IF method, it is possible to evaluate the fatigue potential from the viewpoint of thermal hydraulics.

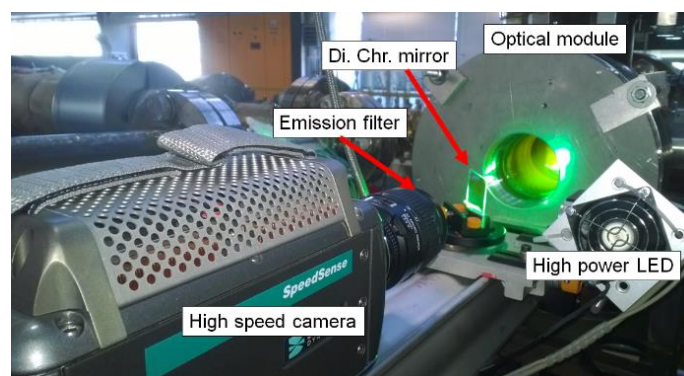


Figure 2-20: Experimental Setup of the NW-LED-IF measurement

The experimental setup of the NW-LED-IF measurement is shown in Figure 2-20. A high power LED is applied as light source and installed perpendicularly to the optical axis of the high-speed camera. With the dichroic mirror, the fluid flow in the glass pipe of the optical module is illuminated by the high power LED. In the experiments, the FSI test facility is filled with a first fluorescence dye before the measurement begins. The concentration of the first fluorescence dye is so high, that the LED light can illuminate the fluid only 1 mm from the pipe inner wall. After the first dye is homogeneously distributed

in the FSI circuit, a second fluorescence dye is injected into the T-junction with the cold flow. The second fluorescence dye will also be emitted by the LED light in the near-wall mixing flow in the measurement area. Through the emission filter in front of the camera, only the emission light of the second fluorescence dye can be captured by the high-speed camera. The distribution of the second dye is associated with the intensity of the fluorescence light in the images. The temperature distributions in the measurement area can be calculated from the fluorescence image and the calibration data. As fluorescence dyes rhodamine B and rhodamine 6G are applied in this investigation. Due to the thermal stability of these dyes, the flow temperature in the main pipeline is limited to 150 °C.

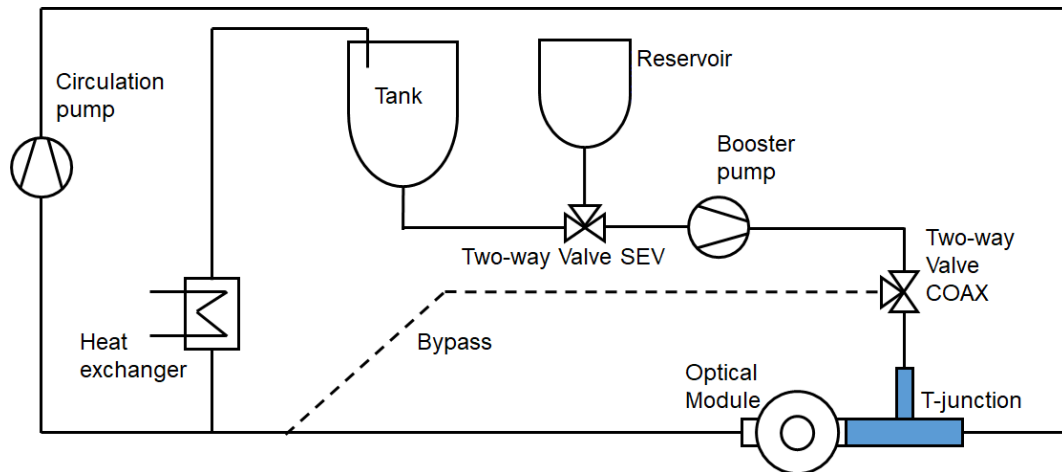


Figure 2-21: Modification on FSI test facility for NW-LED-IF measurement

In the NW-LED-IF measurement, the optical module is installed in the test position 2 downstream of T-junction. An additional reservoir is connected to the pipe line circuit upstream the booster pump (see Figure 2-21). At the beginning of the experiments, the two-way valve SEV is switched to the tank for circulation of the first fluorescence dye in the facility. After the high speed camera starts to record, the two-way valve SEV is switched to the reservoir, so that the second dye in the reservoir can be injected into the T-junction. It takes about 230 s for the fluorescence dye to circulate back to the T-junction. Therefore, the high speed camera stops recording about 230 s after switching of the two-way valve SEV. The high-speed CMOS camera Phantom Speedsense9040 V9.1 is applied in the measurement and captures the intensity images with a frequency of 100 Hz. Three minutes of the thermal mixing process within the recording time is taken for analysis. In addition, the NW-LED-IF measurements are performed with the both horizontal windows of the optical module (left and right side of the flow direction). The experiments are performed with and without the weld seam model respectively, to discuss the influence of the weld root on the nearby flow.

2.5 Particle Image Velocimetry (PIV) technique

The velocity profiles in the inlet flow streams upstream the T-junction are important boundary conditions in the experiments, and measured by using the optical measurement technique Particle Image Velocimetry (PIV). The PIV technique is one of the widely applied, noninvasive measurement method to capture the velocity profiles in fluid field. The PIV method is developed since 1980s [90]. In last 15 years, multiple progress has been made in the PIV method. With the improvements on image sensors and computer technology, firstly the stereoscopic then tomographic PIV has been developed to make 3D velocity measurement possible [91, 92]. Combined with microscope, the PIV technique has also been used in bioengineering [93]. Today, the PIV method becomes the primary technique of the velocity measurement. PIV measurements can be conducted in the optical module on the FSI test facility. Figure 2-22 shows the working principle of PIV measurement in the optical module. As can be seen, the tracing particle (seeding) is distributed in the flow stream through the quartz-glass pipe and illuminated by the

laser in vertical cross-section. Through one of the horizontal glass window, the image sensor focuses on the laser sheet in the flow field. The image sensor captures two particle images at time point t_1 and t_2 with a small time distance. The movements of the particles in the illuminated image area within the time distance can be calculated with the image processing method of cross correlation. The PIV system in this work is manufactured by Dantec, and consists a DualPower 135-15 double-pulse laser and a HiSense MKII CCD camera (resolution 1344×1024 pix). For the seeding in the flow streams, nylon particle with averaged diameter of about $20 \mu\text{m}$ is applied in the measurement. In the measurement, the time between two laser flashes is $200 \mu\text{s}$. The CCD sensor is synchronized with the laser flash and capture two images. The sample rate of the PIV system is 5 Hz, which means 10 images per second. For each measurement, the velocity profile is averaged from 2000 pairs of images.

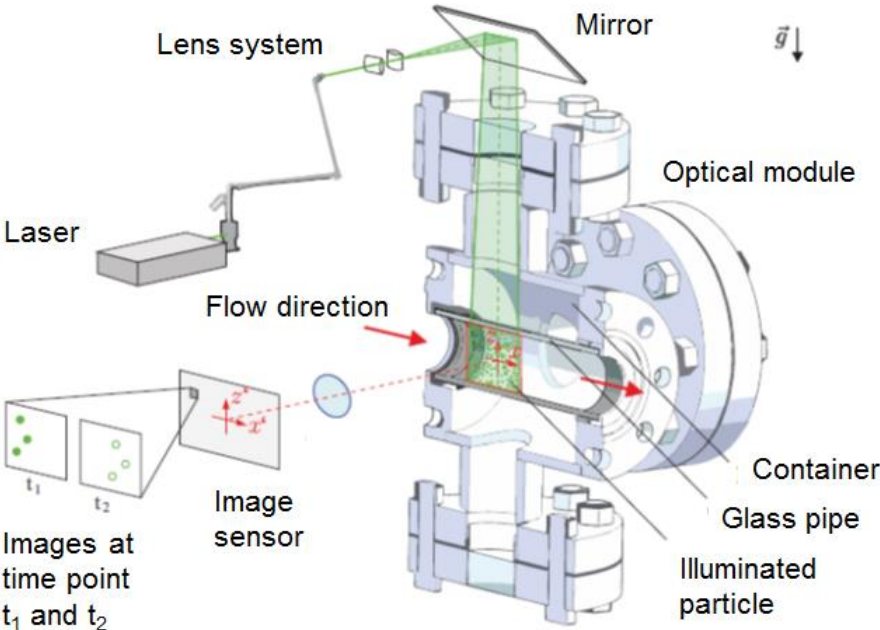


Figure 2-22: Working principle of PIV measurement in optical module [71]

In the experiments, the optical modules cannot be filled with water totally. Therefore, an air bubble remains under the glass window at the top of the modules, so that this window has not been used in the measurements. However, PIV measurements can be performed to capture the velocity profiles not only in the vertical but also the horizontal cross-sections of the pipe flow with different setups. Figure 2-23 shows the schematic sketch of the PIV setup in vertical and horizontal velocity measurement. The measurement cross-section can be changed by positioning the components of the PIV system. The optical system is calibrated for each measurement position individually.

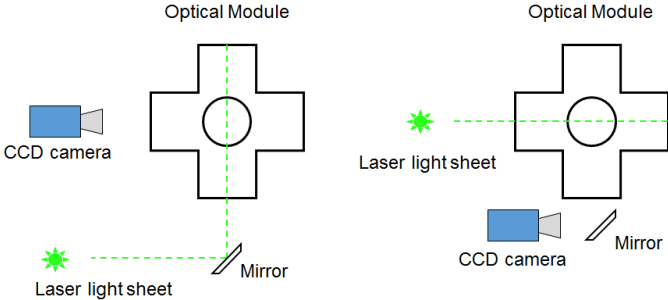


Figure 2-23: Scheme of PIV setup in vertical (left) and horizontal (right) velocity measurement

Optical modules have been manufactured for the optical measurement in the main and the branch pipeline respectively. The PIV setup for measuring the horizontal velocity profile in the branch pipeline is shown in Figure 2-24. For the operation safety with laser, the PIV setup is insulated with the red protection foil, before the measurement starts.

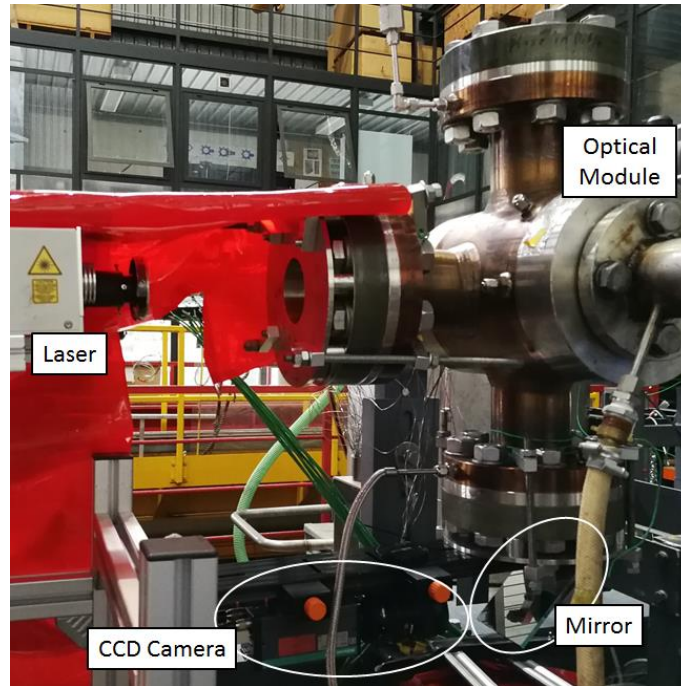


Figure 2-24: PIV setup for the horizontal velocity profile in the branch pipe

2.6 Background Oriented Schlieren (BOS) technique

Optical distortions exist in the PIV measurements in the main pipeline, in which the water are heated up. Those optical distortions lead back to two phenomena: thermal convection in the optical module and temperature gradients in the pipe flow. Both of these phenomena can create an inhomogeneous density distribution in the measurement area. Therefore, the refractive index along the optical axis of the camera is not homogenous. And the camera cannot capture clear particle image due to these phenomena.

However, optical measurement technique for measurement in inhomogeneous media has been developed since 19th century. A. Torpler [94] has developed the classical schlieren technique for flow field visualization in 1864. Since then, the schlieren technique has been widely used for illustrate the density or temperature distribution in different flow fields. Focuses a camera system on a point with diameter d , the distance between the point, lens and image can be simplified with lens equation $1/f = 1/k + 1/b$, with the focal length of the lens f and the magnification $M = b/k$. Put a medium with refractive index n in front of the camera, the image of the point defocuses to a schlieren (see Figure 2-25). The diameter of the schlieren can be calculated with following equation [95].

$$\frac{di}{d} = \frac{f(M+1) \cdot M}{f(M+1) - M \cdot \frac{n}{n+1} \cdot z_0} - M \quad (\text{E2-1})$$

In the inhomogeneous media, the light refraction can create a shift of the in the particle image. Elsinga et al. [96] have concluded this shift in two different types. Figure 2-26 shows the types of the shift in the particle image. In the position shift, the light from the solid particle is deflected towards the image

sensor. But the image illustrated the hollow marker along the straight line and cause a spatial displacement in the measurement. If the particle moves in a time interval Δt , the spatial displacement of the particle leads to a shift in velocity and create an error in the velocity measurement.

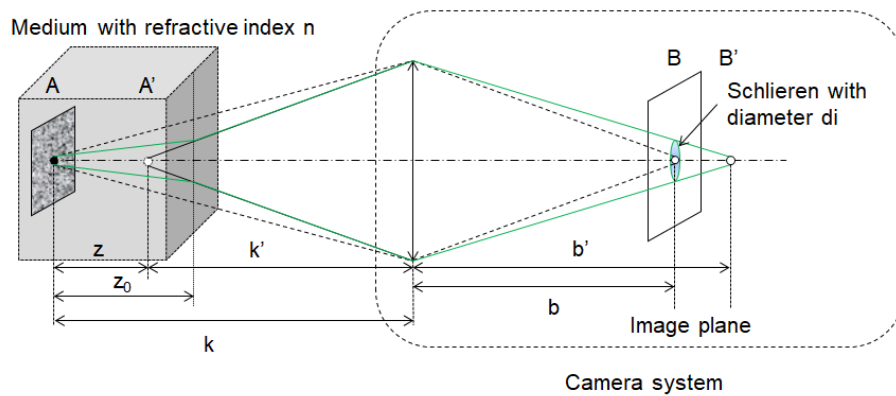


Figure 2-25: Schlieren in a defocused image

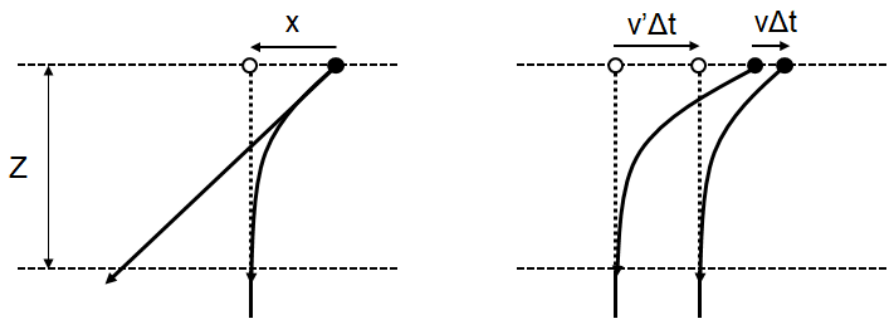


Figure 2-26: position shift (left) and velocity shift (right) in PIV measurement with optical distortion [96]

Based on schlieren photography and laser speckle photography, Richard and Raffel [97] have developed the Background Oriented Schlieren (BOS) technique to reduce the optical distortion in PIV measurement due to the inhomogeneous flow field. In their work, the BOS technique has been successfully applied in the PIV measurement on the vortex structure under helicopter rotor blade [97]. In recent years, BOS technique has been applied in some complicated cases like shock wave [96] or flame [98] to reduce the optical distortions due to inhomogeneous distribution of refractive index. In addition, the BOS technique can be individually used for investigating the density distribution in the flow field [99].

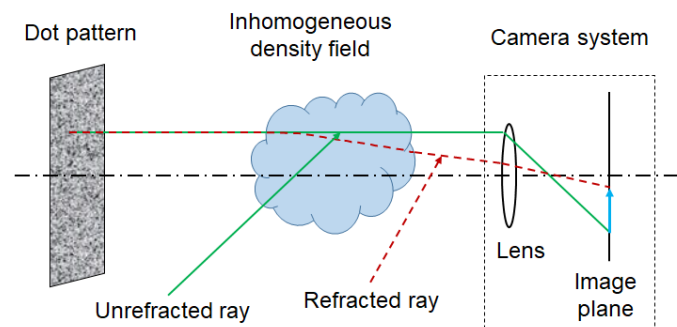


Figure 2-27: Working principle of BOS technique

The principle of BOS technique is shown in Figure 2-27. A random distributed dot pattern with high contrast (white dots on black background) is used as the background plane. The camera focuses on the

background plane, which is located at the opposite of the investigated flow field. In the BOS measurement, images of the background plane are taken firstly without optical distortion. Then, the boundary condition is changed to the PIV measurement condition (with optical distortion). The camera system takes a series of images on the background plane. The images are enhanced with digital image processing methods, and the locations of the dots on the background are identified. The shift of the dots can be found between the images with and without optical distortion can be calculated with the function of cross correlation in the PIV software. This shift is correlated to the density distribution in the flow field, and can be summarized and used for correction of PIV measurement.

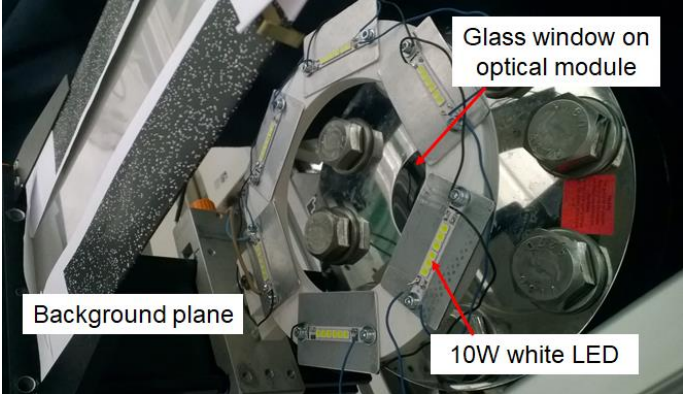


Figure 2-28: BOS setup on the optical module

The BOS setup on the optical module at FSI test facility is shown in Figure 2-28. A sheet of random distributed white dots is used as the background plane. The diameter of the dots is about 1.2 mm. A LED-ring, which is manufactured of PLA (polylactic acid) by a 3D-printer, is placed between the glass window of the optical module and background plane. Through the ring, the CCD-camera on the other side of the optical module focuses on the background plane. On the LED-ring, six high power white LED chips can illuminate the background plane in the measurement. To avoid light interference from outside, the BOS setup is covered with black curtain during the measurement.

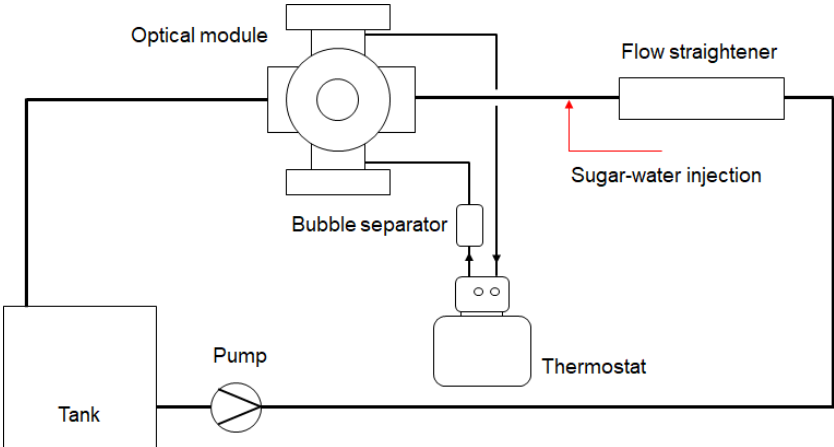


Figure 2-29: Schematic sketch of the PIV-BOS setup

At FSI test facility, the PIV measurement in branch pipe is not interfered by the optical distortion, since the flow stream and the optical modules remain cold in the measurement. Before application at the FSI test facility, the BOS method is tested in an individual PIV-BOS setup (see Figure 2-29). The aforementioned two phenomena of optical distortion are simulated with hot-water circulation in the module container and sugar-water injection into the pipe flow respectively. PIV and BOS measurements have been performed in the optical module. With current technique, optical distortion due to heat convection in the container can be reduced by BOS method. But the optical distortion due to temperature

gradient (thermal stratification) in the pipe flow cannot be reduced by current BOS technique, because the change of the refractive index in this phenomenon is so large, that the dots in the image of the background plane cannot be identified any more. Moreover, it is also impossible to conduct PIV measurement within thermal stratification, because the laser beam is refracted in the stratified flow, so that the particle in the measurement plane, on which the camera system focuses, cannot be illuminated. But since BOS method has been individually applied for density measurement [99], the thermal stratification can be detected by dot shifting in the BOS results. With the help of BOS method, the reversed cold in the main pipe can also be detected upstream the T-junction.

3 Numerical calculation

3.1 Theory and model

In turbulent mixing flow, the kinetic energy E is transferred between the eddies with different sizes f in the turbulence. The energy transfer can be illustrated in the form of the energy cascade with decreased size of the eddies in the turbulence (see Figure 3-1). The energy cascade can be divided into three regions with different sizes of the eddies. The eddies with large sizes have the most of the energy in turbulence and are located in the energy containing range. With reduced size of the eddies, the kinetic energy of the eddies decrease in the inertial range. In the double logarithmic diagram, the gradient of the decreased energy is $-5/3$. The kinetic energy in the turbulence is transferred from the large eddies to the small ones, until the size of the eddies reaches the smallest scales, which is also called Kolmogorov scales [100]. The range for the eddies with small size is denoted as dissipation range.

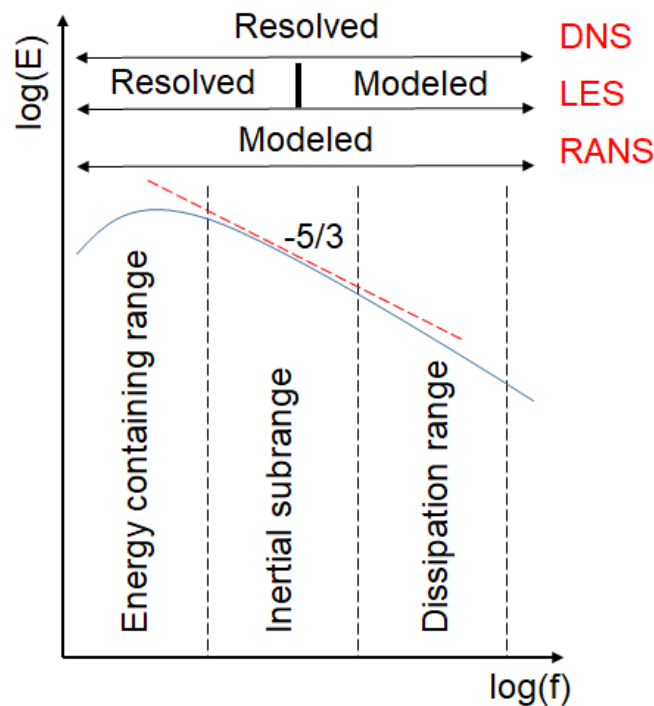


Figure 3-1: Simplified illustration of energy cascade in turbulence

For the numerical investigating the motions in the turbulent mixing flow, Direct Numerical Simulation (DNS), Large-Eddy Simulation (LES) and Reynolds-Averaged Navier-Stokes (RANS) approach are the mostly applied numerical methods. With the DNS method, the motions in the whole spectrum of the energy cascade can be resolved. Therefore, the DNS method has the advantage of high accuracy and the disadvantage, that the DNS method requests an enormous amount of computational resource. Oppositely with the RANS method, the flow motions are modeled with time-averaged parameters. The RANS does not request so much computational resource. However, the time-dependent temperature fluctuations in the mixing flow, which is one of the most important research subject, cannot be generated with RANS, since the parameters are time-averaged. With the LES method, the large eddies in the turbulence are resolved directly as well as DNS and the small eddies are modeled similar with RANS. Therefore, the LES method has the advantage of high accuracy for describing the eddies with large size and requests less computational resource than DNS.

For investigating the thermal mixing flow, the time-dependent temperature changes in the mixing flow are required. Therefore, the numerical calculations in this work are performed with Large-Eddy-Simulation (LES) method. With LES, the small flow scales, which are separated by using filtered, time-dependent Navier-Stokes equations, are considered isotropic. The filtered Navier-Stokes equations for LES calculations are as follows [101]:

$$\frac{\partial \rho}{\partial t} + \frac{\partial(\rho \bar{u}_i)}{\partial x_i} = 0 \quad (\text{E3-1})$$

$$\frac{\partial(\rho \bar{u}_i)}{\partial t} + \frac{\partial}{\partial x_j}(\rho \bar{u}_i \bar{u}_j) = -\frac{\partial \bar{p}}{\partial x_i} + \frac{\partial}{\partial x_j} \left[\mu_{eff} \left(\frac{\partial \bar{u}_i}{\partial x_j} + \frac{\partial \bar{u}_j}{\partial x_i} \right) \right] + f_i \quad (\text{E3-2})$$

$$\frac{\partial}{\partial t}(\rho \bar{h}) + \frac{\partial}{\partial x_j}(\rho \bar{u}_j \bar{h}) = \frac{\partial}{\partial x_j} \left(\lambda_{eff} \frac{\partial \bar{T}}{\partial x_j} \right) \quad (\text{E3-3})$$

with \bar{u} , \bar{p} , \bar{h} , \bar{T} as the filtered velocity, pressure, enthalpy respectively temperature. f_i represents the term of buoyancy effect, and is defined as $f_i = g(\rho - \rho_{ref})$. ρ_{ref} is the reference density which is usually the averaged density of the mixing flow. The effective thermal conductivity is defined as follows:

$$\mu_{eff} = \mu + \mu_t^{SGS}; \quad \lambda_{eff} = \lambda + \frac{\mu_t^{SGS} c_p}{Pr_t^{SGS}} \quad (\text{E3-4})$$

with λ as thermal conductivity. Pr_t is the turbulent Prandtl number with the empirical value of 0.9 [75]. The turbulent eddy viscosity μ_t is modeled by using Wall Adaptive Local Eddy Viscosity (LES WALE model) and is defined as:

$$\mu_t^{SGS} = \rho (C_W \Delta)^2 \frac{(S_{ij}^d S_{ij}^d)^{3/2}}{(\bar{S}_{ij} \bar{S}_{ij})^{5/2} + (\bar{S}_{ij} \bar{S}_{ij})^{5/4}} \quad (\text{E3-5})$$

with the WALE model constant $C_W = 0.5$. S_{ij}^d is the traceless part of the square of the velocity gradient tensor \bar{g}_{ij} [101] and defined as:

$$S_{ij}^d = \frac{1}{2}(\bar{g}_{ij}^2 + \bar{g}_{ji}^2) - \frac{1}{3} \delta_{ij} \bar{g}_{kk}^2 \quad (\text{E3-6})$$

$$\bar{g}_{ij} = \frac{\partial \bar{u}_i}{\partial x_j} \quad (\text{E3-7})$$

3.2 Geometry and numerical mesh

In the previous numerical work of Selvam [79], the reverse flow has been observed upstream the T-junction in some of the cases with high temperature difference between the inlet flow streams. The phenomenon of the reverse flow cannot be totally illustrated with a small geometry for the simulation. Hence, three different sizes of geometry has been chosen for the simulation work. Figure 3-2 shows the geometries for the simulations. They are designed based on the construction of the FSI test facility. For simulating the measurement cases without or with small reserve flow, a numerical mesh is generated with the geometry size S, which consists T-junction, one pipe module upstream and three pipe modules downstream the T-junction in the main pipeline as well as one pipe module of the branch pipe. For the cases with clear reverse flow phenomena, the numerical mesh is generated with geometry size M, which consists two pipe modules upstream and four pipe modules downstream the T-junction in the main pipeline as well as two pipe modules in the branch pipe. For the cases with a strong phenomenon of reverse flow, simulations are performed with geometry size L, which has an additional pipe segment with a length of 1.8 m. For generating the numerical mesh, the flange connections between the pipe modules have been neglected and the geometries are simplified as complete pipe lines. The outside diameters of the main and branch pipe lines are 88.9 mm and 48.3 mm according to the geometry of the FSI test facility. The coordinate system is the same as in the experiment at the T-junction. At position 5.5D downstream of the T-junction, a weld seam is constructed with the design of the weld seam model (see Figure 2-18).

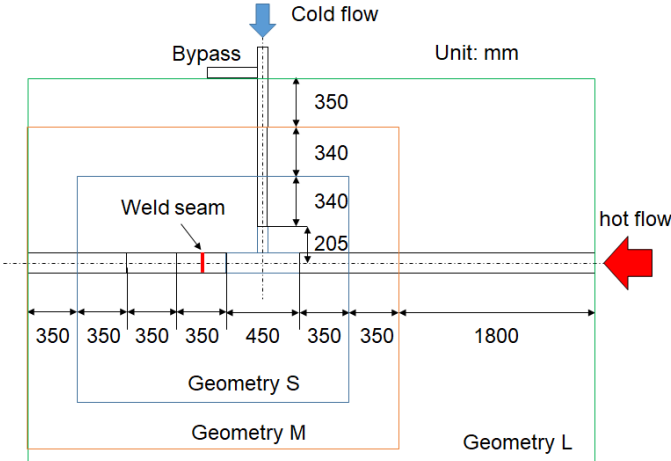


Figure 3-2: Geometries for simulation

In this work, the numerical meshes are generated with the meshing software ICEM CFD of ANSYS. For each geometry, several meshed with different numbers of nodes are generated at first. As example, the details of the mesh in the main pipe cross-section and close to the weld seam are shown in Figure 3-3. Then, the quality of the meshes are checked with the mesh quality criteria for the operation conditions of the simulated cases.

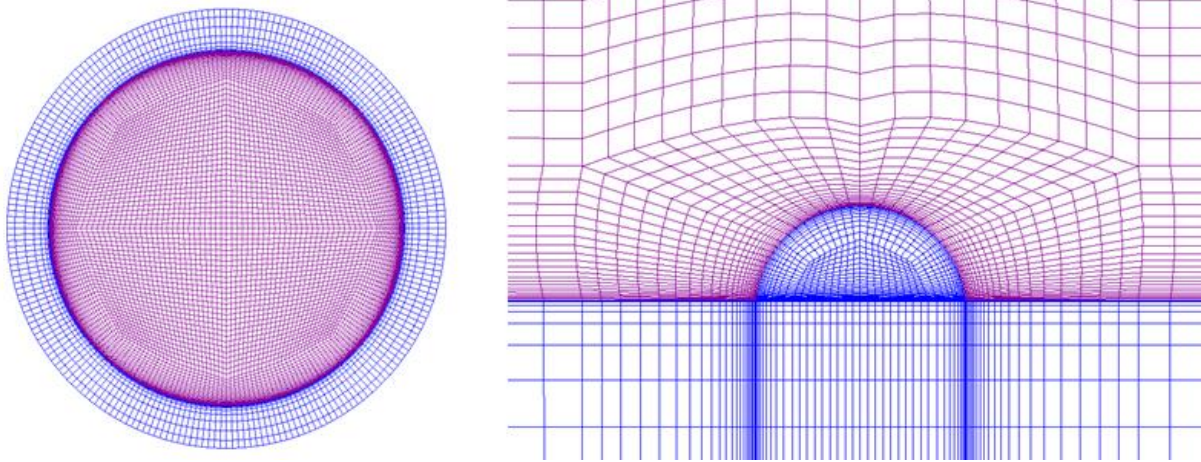


Figure 3-3: Details of the numerical mesh: main pipe cross-section (left), weld root (right)

At first, the non-dimensional grid size are estimated to check the mesh quality. Since the geometry of the pipe lines is symmetrical, the non-dimensional grid size $\Delta y^+ = \Delta z^+$. The non-dimensional grid size can be calculated according to Piomelli [102]:

$$\Delta x^+ = \frac{\Delta x \cdot u_\tau}{\nu} \quad (\text{E3-8})$$

$$\Delta z^+ = \frac{\Delta z \cdot u_\tau}{\nu} \quad (\text{E3-9})$$

Table 3-1 shows the comparison of the non-dimensional grid size in this work with the suggestion of Piomelli. According to the literature, the optimal grid size for LES calculation shall be smaller than the values of Piomelli.

Table 3-1: Non-dimensional grid size in comparison with literature

	Δx^+	$\Delta y^+ / \Delta z^+$
Present work	87 – 115	36 – 39
Piomelli	50 – 150	15 – 40

The next criterion for evaluating the mesh quality is to estimate the energy length scale (L_R) and the Taylor micro-scale (λ). This method is summarized by Addad et al. [103]. Parameters are defined as follow:

$$\lambda = \sqrt{\frac{10k\nu}{\varepsilon}} \quad (\text{E3-10})$$

$$L_R = \frac{k^{3/2}}{\varepsilon} \quad (\text{E3-11})$$

where ε is the turbulent dissipation rate, k is the turbulent kinetic energy and ν is the kinematic viscosity. These parameters are calculated from the results of the steady-state simulation with RANS method. With the calculated parameter, the condition of (E3-12) shall be satisfied with the value of the average mesh size Δ , which is defined with (E3-13).

$$\Delta = \max(\lambda, L_R/10) \quad (\text{E3-12})$$

$$\Delta = \sqrt[3]{\frac{V_{total}}{N_{total}}} \quad (\text{E3-13})$$

In this work, at least three numerical meshes have been generated for each geometry size. The quality of the meshes have been checked with the aforementioned criteria. The one, which is satisfied in these criteria, is chosen for the LES calculation for the correlated cases.

3.3 Boundary and initial conditions

The boundary conditions of the inlet flow streams consist the temperature and velocity profiles. Since the water flow in the branch pipeline is not heated up and remains constant of 20 °C, the temperature profiles for the boundary condition in the branch pipeline is set as homogeneous. In the experiments, the thermocouple measurement in the inlet flow has confirmed that the thermal stratification in the main pipe inlet flow has been broken up by using static mixers (see chapter 2.1). The temperature profiles in the inlet of the main pipeline is also set as homogeneous. The inlet velocity profiles are generated with the individual single pipe simulations. Numerical meshes have been created with a length of 100D for the main pipeline and 60d for the branch pipeline separately. Velocity profiles are captured from the fully developed turbulent flow in the simulations of the single straight pipe flow with the correlated flow temperature and flow rate. As examples, the velocity profiles for the simulation case with the maximum operation condition ($T_m = 265$ °C, $T_b = 20$ °C, $\dot{M}_m = 560$ g/s, $\dot{M}_b = 200$ g/s) are shown in Figure 3-4. In the simulation of the T-junction experiments, the velocity profiles are loaded in the simulation setup as boundary conditions.

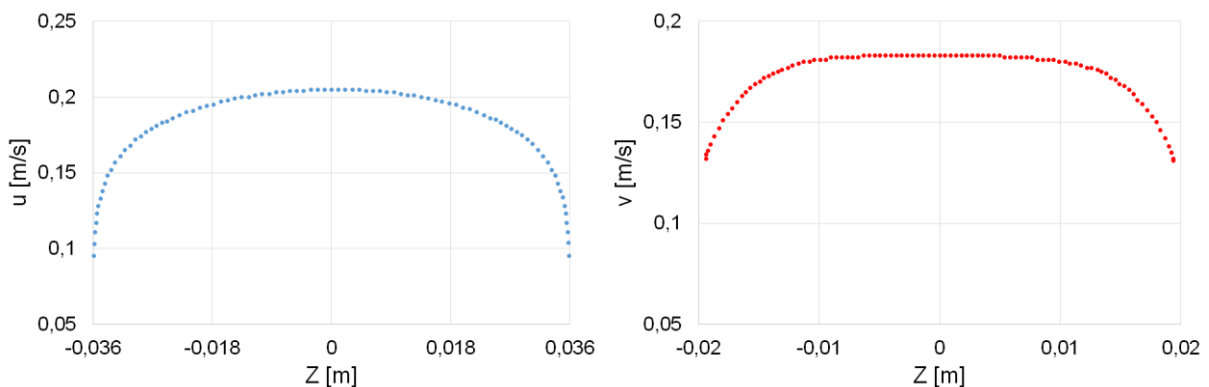


Figure 3-4: Velocity profiles for the boundary conditions in main (left) and branch (right) pipeline

The initial conditions for the LES calculations are generated by steady-state simulation with the Shear Stress Transport (SST) model and the boundary conditions of the correlated cases. The method of the steady-state simulation for initializing LES calculation is recommended by the practice guideline of ANSYS [104]. Figure 3-5 shows the procedure of the simulation in this work. The results of the steady-state simulations are applied as the initial conditions in the LES calculation. The LES calculations are conducted with the help of the high performance computer Cray40 at the University of Stuttgart. Due to

the different size of the numerical meshes, the numbers of the applied processors are chosen from 960 to 2400.

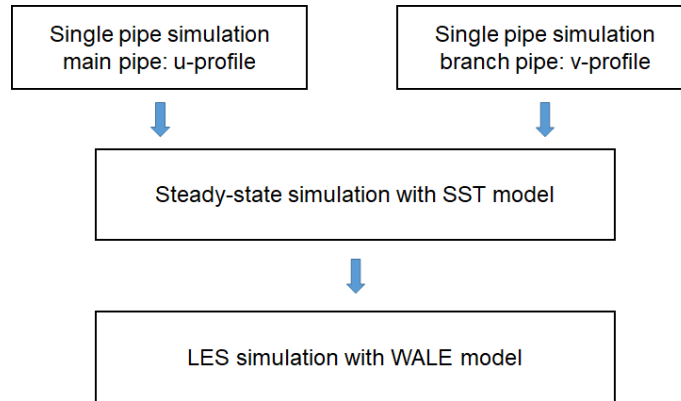


Figure 3-5: Procedure of the simulation in this work

For comparing the experimental results, temperature monitor points have been defined in the LES calculations at the positions, where micro-thermocouples have been installed in the experiments (see chapter 2.3, Figure 2-17). Temperature monitor data are analyzed and compared with the experimental results.

3.4 Time step and time line

The time steps has an influence on the stability in the LES calculations. The maximum allowed time step can be estimated with the help of the Courant-Friedrichs-Lewy (CFL) number, which is defined as follow.

$$CFL = \frac{\Delta t \cdot u}{\Delta} \quad (E3-14)$$

For estimating the time steps in the simulation, the CFL-number must be smaller than 1. Due to the calculations of the CFL-number the maximum time step is limited to 0.5 ms. To discuss the influence of the time step on the simulation, a time step study is performed separately [105]. The calculations are performed with time steps of 0.2 ms respectively 0.5 ms for physical time of 60 s. The result shows that the calculations are unstable in the first 30 s due to the high RMS-values of the variants. Moreover, the calculation with the time step of 0.2 ms shows a better convergence property at the beginning of the simulation. Considering the balance of the simulation quality and the time efficiency, the simulations in this work are performed with a combination of two different time steps.

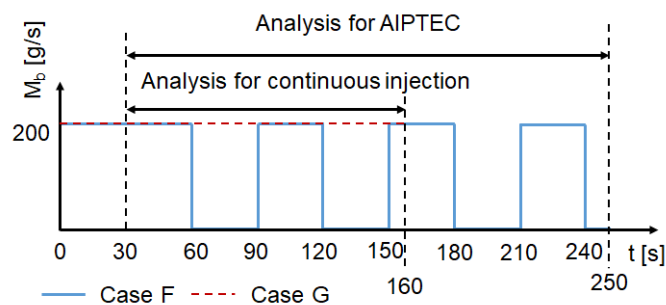


Figure 3-6: Time line of the simulations on case F and case G

Figure 3-6 shows the time line of the simulations of case F and case G as example. In the experiments, case F and case G are both performed with the maximum operation condition of the FSI test facility. Case F is conducted with AIPTEC, while case G is conducted with continuous cold flow injection. The LES calculations of both cases begin with 30 s initial simulation. The time step in this initial simulation is 0.2 ms. After the initial simulation, the calculations are conducted with the time step of 0.5 ms. Since AIPTEC consists of significant long-period temperature changes, the physical time of the simulations must be long enough for the analysis [41]. Moreover, analyses on thermal mixing flow require mainly statistical methods, and therefore sufficient data points for the analyses [27]. Hence, 220 s simulation data of case F (AIPTEC) respectively 130 s simulation data of case G have been applied for analyses on mixing characteristics. The LES calculations of the other cases are all performed with the similar combination of different time steps.

4 Results

4.1 Results of experimental investigations

4.1.1 Artificially induced fatigue damage on dissimilar weld

As the first stage in this work, fatigue damage shall be artificially created in the weld seam module, which is installed downstream of the shock module in the FSI test facility (see Figure 2-4) [83, 106, 107]. To accelerate the initiation of the fatigue damage, the experiment has been performed with AIPTEC. The durations of injection and bypass in the AIPTEC are set to 30 s. 40 micro-thermocouples have been installed on the weld seam module to capture the temperature in the near-wall flow. Figure 4-1 shows the temperature signal in the measurement cross-section F2 (2.7D) in time interval about 120 s. The experiment has been performed continuously for four weeks, which correlates to more than 10,000 injection/bypass-periods. Over 33 GB data has been collected in the experiment. In this dissertation, the results of a data length of 3.1 million rows are presented and discussed. This data length correlates to a measurement duration of 8.6 h (516 periods). For comparison with the experiments downstream of the T-junction in the whole investigation, the experiment with shock module is referenced as case S.

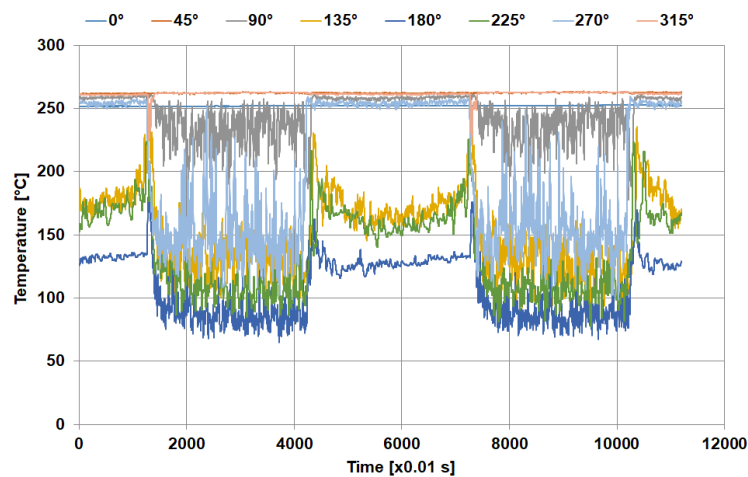


Figure 4-1: Temperature signals in measurement cross-section F2 with AIPTEC in a time interval of about 120 s

The data of the temperature measurement with the micro-thermocouples have been processed with standard data analysis procedures (see Figure 4-2). The standard data analysis procedure consists of three steps. In the first step, the circumferential distributions of the mean temperature and the RMS temperature fluctuations are reconstructed from the measurement data. The mean distribution shows the general temperature in the mixing flow during the experiment. And the area with high temperature fluctuations can be found in the distribution of RMS fluctuations. Combined with these two distributions, a qualitative estimation can be made for the thermal stratification in the mixing flow. In the second step, frequency analysis with Fourier-transformation is performed to the temperature measurement data at every measurement position. The frequency spectra of the measurements are used to check the regular temperature changes during the experiment, which are characterizing the thermal-mixing process. The regular temperature changes in the frequency range for thermal fatigue can be identified in these frequency spectra. Thus the potential for thermal fatigue at all measurement positions can be estimated. In the final step, the results of the temperature distributions and frequency analyses are summarized in the form of a spectrum pattern. Since the structure materials close to the dissimilar weld seam are most likely to be affected by thermal fatigue due the material inhomogeneity, the position of the weld seam

(or weld seam model) is also highlighted in the spectrum pattern. With the conclusions of all these factors in the spectrum pattern, the positions in the weld seam module (or in the TC-module) with high potential for material damage due to thermal fatigue can be identified.

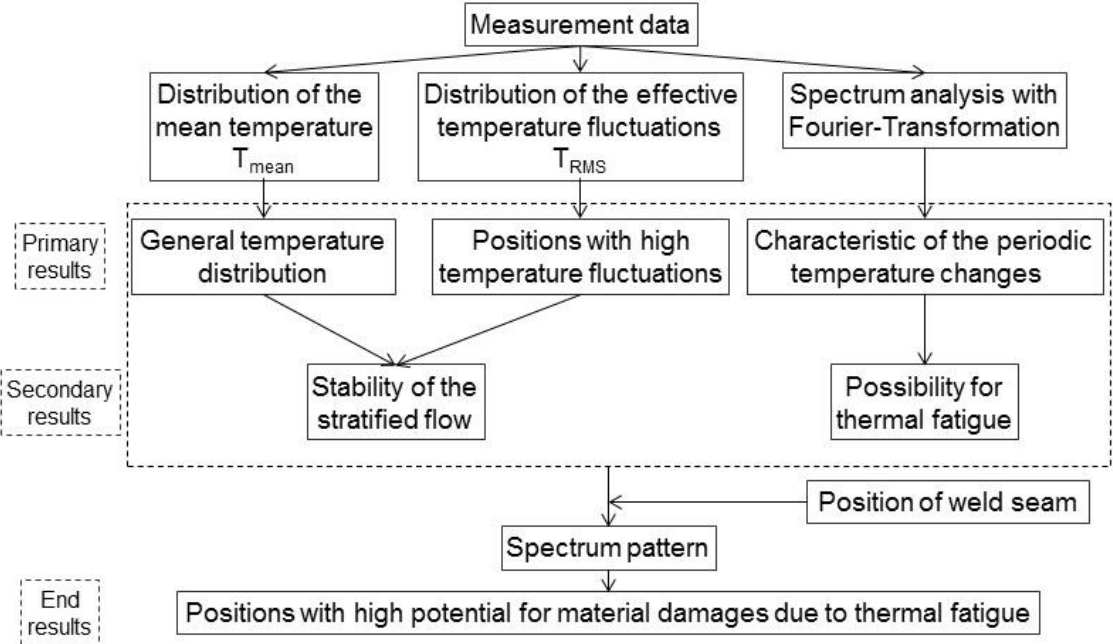


Figure 4-2: Standard data analysis procedure for thermocouple measurement

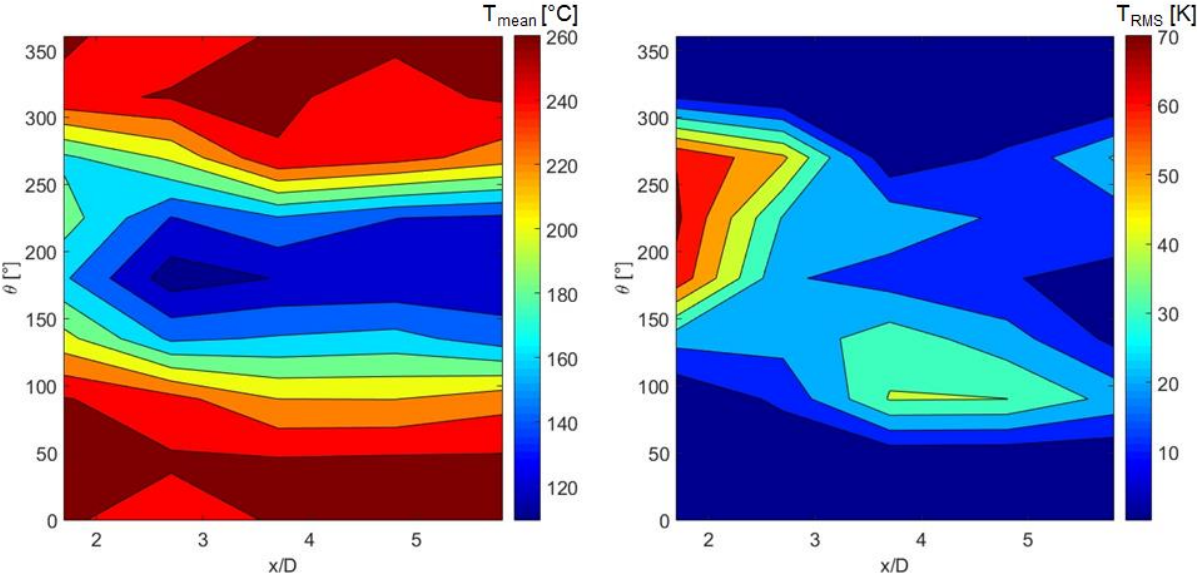


Figure 4-3: Reconstructed circumferential distributions of mean temperature (left) and RMS temperature fluctuation (right) in the thermocouple measurement on weld seam module

Figure 4-3 shows the reconstructed circumferential distributions of the mean temperature and the RMS temperature fluctuation. Generally, the mean temperature distribution shows a thermal stratification in the pipe flow due to the temperature difference in the horizontal pipe. An area with low temperature is found between the two weld seams (between 2D and 4D). In the distribution of the mean temperature, the path of the low-temperature flow through the weld seam module is not straight nor symmetrical to the middle of the pipe (see the dark yellow region along 220 °C in the mean temperature distribution). The angular location of this temperature region is about $\theta \approx 120^\circ - 300^\circ$ at cross-section F1 (1.7D), about $\theta \approx 70^\circ - 260^\circ$ at cross-section F3 (3.7D) and about $\theta \approx 90^\circ - 280^\circ$ at cross-section F5 (5.8D). This kind

of the S-shaped path indicates a specialty in the mixing flow. Compared with the distribution of the RMS-value, the positions with high temperature fluctuations are located at the turning of this path. The highest temperature fluctuation reaches the maximum of 72.0 K at position of FT6 (cross-section F1, 1.7D, angular position 225°). Since the temperature fluctuation at the edges is much higher than in the middle of the thermal interface, the thermal stratification in the mixing flow can be stable.

To understand the periodic low frequency flow oscillations and to compare the turbulence spectrum of the measurement data with numerical simulations to be performed, Fourier transformation is used for the frequency analysis. The characteristics of the long-period fluid temperature fluctuations can be found in the spectrum of the temperature data [41]. Frequency analysis has been performed to the temperature data of the thermocouple measurement at every measurement position. The temperature signals are first normalized with the correlated temperature difference, then analyzed with Fourier-Transformation. The results of the frequency analysis are summarized in the power spectrum density (PSD) diagrams. Each PSD diagram is generated with 100 data sets from original temperature data by using an averaging method [52]. As an example, the PSD diagram of the temperature measurement at the measurement position FT11 (F2, 90°) is shown in Figure 4-4. Several clear peaks can be found in the frequency spectrum of the FT11. The frequency peak at 0.0167 Hz can be derived from AIPTEC. Since the durations of injection and bypass of AIPTEC are both 30 s in this experiment (period 60 s), the basic frequency of AIPTEC can be calculated as 0.0167 Hz. In Figure 4-4, a series of frequency peaks can be seen from the basic frequency to about 1 Hz. The values of these frequencies are the N times of the basic frequency (N is integer 2, 3, 4, ...). To explain these frequencies in the spectrum, a mathematic model is necessary.

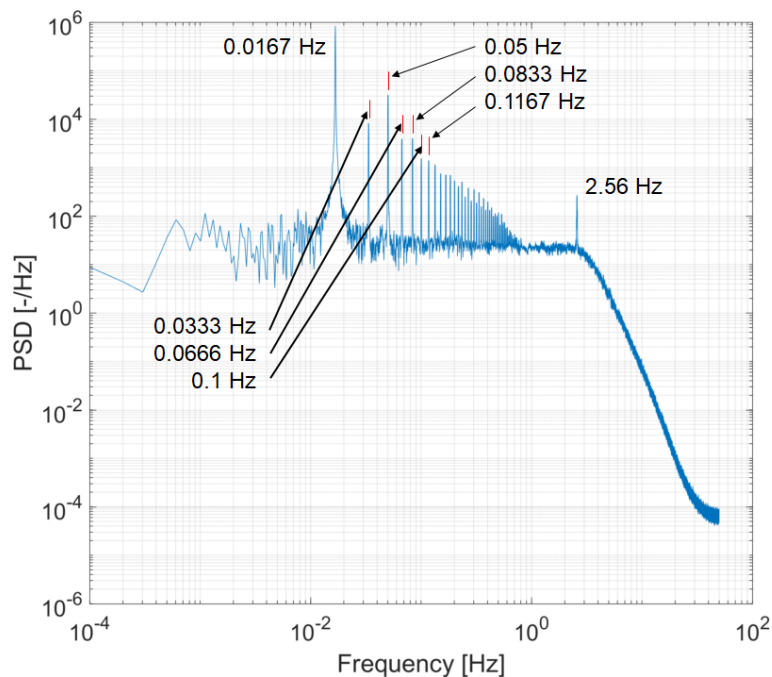


Figure 4-4: PSD diagram of the normalized temperature signal at position FT11 (F2, 90°)

Based on the switching of the two-way valve, a simulated periodic square temperature signal has been generated. The high and low temperature in this signal are set to $T_{\text{high}}=265\text{ °C}$ and $T_{\text{low}}=120\text{ °C}$. The durations of both temperature signals are set to 30 seconds (see Figure 4-5, left). Fourier-Transformation has been conducted to this temperature signal. The PSD diagram of this periodic temperature signal is shown in Figure 4-5, right. In this PSD diagram, a series of frequency peaks can be recognized. These peaks are similar to the frequency peaks in the spectrum at position FT11 in Figure 4-4.

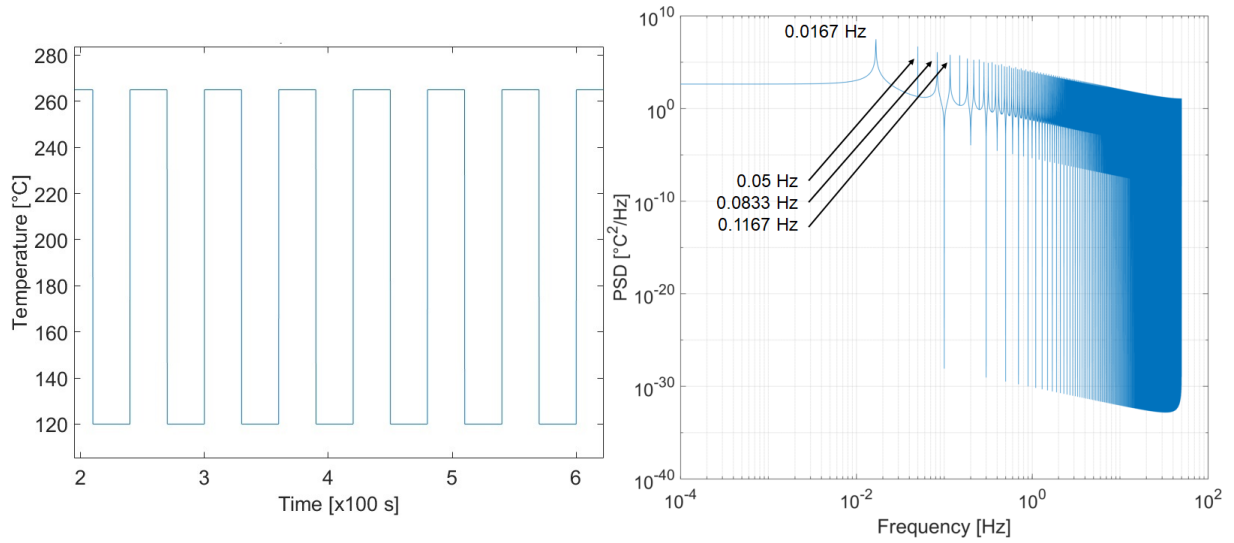


Figure 4-5: Simulated periodic square temperature signal (left), PSD diagram of the simulated periodic square temperature signal (right)

In mathematics, every periodic function can be written into the form of Fourier-series:

$$s_N(x) = \frac{A_0}{2} + \sum_{n=1}^N A_n \cdot \sin\left(\frac{2\pi nx}{P} + \phi_n\right) \quad (\text{E4-1})$$

For the periodic square signal, the Fourier-series can be written in the following form.

$$\begin{aligned} f(x) &= \sum_{n=1}^{\infty} \left(\frac{2E}{n\pi} \sin \frac{n\pi}{2} \sin(n\omega_1 t) \right) \\ &= \frac{2E}{\pi} \sin(\omega_1 t) - \frac{2\pi}{3} \sin(3\omega_1 t) + \frac{2\pi}{5} \sin(5\omega_1 t) \\ &\quad - \frac{2\pi}{7} \sin(7\omega_1 t) \dots \end{aligned} \quad (\text{E4-2})$$

With the period of 60 seconds, the basic frequency of this signal can be calculated as $f_1 = 0.0167 \text{ Hz}$. Due to the correlation in the Fourier-series, the frequencies of $3f_1$, $5f_1$, $7f_1$ and so on should also exist in the spectrum [108]. These explain the peaks in the PSD diagram of the simulated periodic square temperature signal.

Considering the harmonic oscillation in the Navier-Stokes equations, there is a quadratic correlation for the waves in incompressible media. A coupled wave can be found in incompressible medium for a simple wave. Hence, a doubled frequency must exist in the spectrum [109, 110]. The frequencies $2f_1$, $4f_1$ and $8f_1$ can be found for the basic frequency of f_1 in the measured spectrum. Furthermore, the double frequency $6f_1$ of $3f_1$ can be found. Based on these two mathematic explanations, the series of frequencies in the PSD diagram of FT11 can be identified as the effect of AIPTEC in the experiment (see Figure 4-4).

Another two kinds of frequency peaks can also be found in the frequency spectra of the temperature signals at several measurement positions. The PSD diagram of the normalized temperature signal at measurement position FT12 is shown in Figure 4-6, left. Similar with the PSD diagram of FT11, the frequency peaks can be seen in the spectrum. Moreover, an additional frequency of 2.56 Hz can also be

seen in the spectra of both positions and several other positions. This frequency cannot be explained with the result of a single experiment case. In this work it is denoted as an additional ‘low’ frequency. It is the identification of an important phenomenon in the thermal mixing process and will be systematically discussed with the experiments downstream of the T-junction in chapter 4.1.6. Another series of frequencies can be seen in the PSD diagram of FT29 (see Figure 4-6, right). This series of frequencies is defined as additional ‘high’ frequencies. The additional high frequencies are similar with a periodical signal and can be found in the frequency spectra at eight specific measurement positions. Furthermore, the additional high frequencies can also be found in the results of the following experiments downstream of the T-junction. With a cross-check experiment, the additional high frequencies are identified as a noise signal from one of the data module of the DAQ system, which has eight channels for signal input. An individual discussion has been performed for frequency analysis with low pass filter, and shown the additional high frequencies have no influence on temperature distribution. Therefore, the additional high frequencies will not be further discussed in this work.

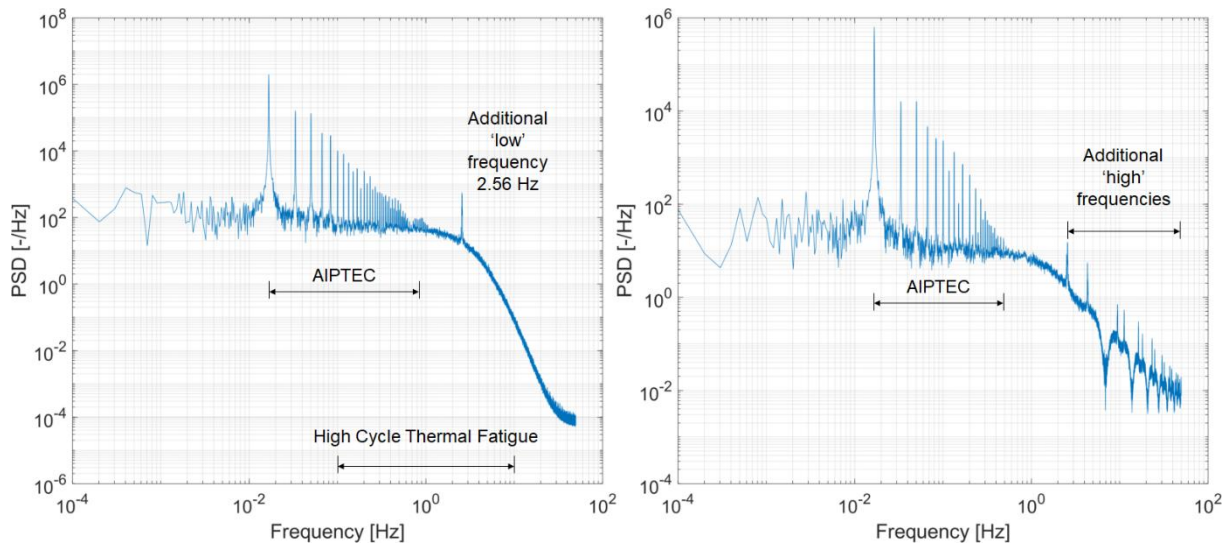


Figure 4-6: PSD diagrams of the normalized temperature signals at measurement positions FT12 (left, 2.7D, 135°) and FT29 (right, 3.7D, 180°)

		Weld seam		Weld seam		
		F1 (1.7D)	F2 (2.7D)	F3 (3.7D)	F4 (4.8D)	F5 (5.8D)
		FT1	FT9	FT25	FT41	FT49
		FT2	FT10	FT26	FT42	FT50
		FT3	FT11 ○	FT27 40.7	FT43 (40.1)	FT51 ○
➔ Direction of flow		FT4 ○	FT12 ○	FT28 35.4	FT44	FT52
		FT5 (66.8)	FT13 ○	FT29 ○	FT45 ○	FT53 ○
		FT6 (72.0)	FT14 ○	FT30 ○	FT46 ○	FT54 ○
		FT7 (69.4)	FT15 (52.1)	FT31	FT47	FT55 (30.8)
		FT8 ○	FT16	FT32	FT48	FT56

Effect of AIPTEC (strong)	Value in K	RMS temp. fluctuation
Effect of AIPTEC (weak)	○	additional low frequency

Figure 4-7: Spectrum pattern of the case S

The frequency range 0.1 – 10 Hz is of relevance for thermal fatigue in the thermal mixing process [81]. To estimate the possibility of thermal fatigue in the AIPTEC effect, the following definitions have been made to evaluate the AIPTEC. If the basic frequency can be recognized and at least two of the related AIPTEC frequencies can be found in the frequency range for thermal fatigue, the effect of AIPTEC is defined as strong. If only the basic frequency can be recognized but no related AIPTEC frequency is located in the frequency range for thermal fatigue, the AIPTEC effect is defined as weak. Without clear

peak of the basic frequency, there is ‘no effect’ of AIPTEC at this measurement position. With these definitions, the positions with strong effect of AIPTEC as well as positions with the additional low frequency have the possibility for initiation of the thermal fatigue.

In terms of this spectrum interpretation pattern, the results of the spectral analysis and the distribution of temperature fluctuations for the case S are summarized and shown in Figure 4-7. According to the spectrum pattern, two areas close to measurement positions FT5, FT6, FT7, FT15 respectively FT27, FT28 have both high temperature fluctuations and a strong effect of AIPTEC. The weld seams are located within these two areas. Therefore, these two areas have high potential for the material damage due to thermal fatigue. In addition, the temperature fluctuations in the near-wall flow close to the first weld seam (FT5, FT6 and FT7) is much higher than the second weld seam (FT27, FT28). The fatigue damage is more likely to be initiated close to the first weld seam.

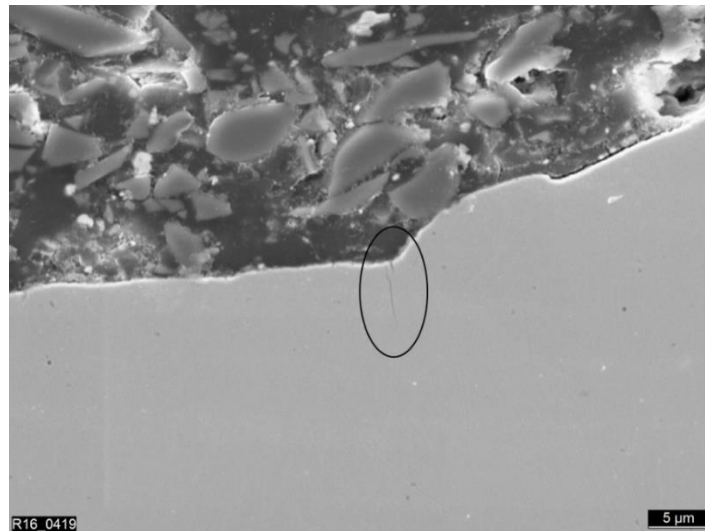


Figure 4-8: Crack in the piping material at the dissimilar weld under scanning electron microscope

After these experiments, the weld seam module has been cut open for fractographic and metallographic investigations. A crack is found in the weld seam module by scanning with an electron microscope (see Figure 4-8). This crack is located within the first weld seam (close to position 2D) in the transition of the weld filler material and the austenitic base material at an angular position of 270° [111]. Within a topographic analysis of the pipe inner wall surface, it was found that the crack from Figure 4-8 extends to at least 15 degrees in circumferential direction along the fusion line of the weld. A comparatively small crack depth of only $15\ \mu\text{m}$ at the location of the cut is related to a very early stage of fatigue crack growth. In the case of thermal cycling within pipes the resulting stress-gradients are maximum at the inner wall and decrease with increasing crack depth very quickly. Therefore, cracks are often found to arrest completely when a specific crack depth is reached and no primary load acts as driving force. The location of this crack is close to the measurement position FT7, which is in the area with high potential for material damage due to thermal fatigue. This crack confirms the expectations based on the results of the temperature measurements in the near-wall fluid. Hence, the standard data analysis procedure can be used for fatigue assessment in the following experiments downstream of the T-junction.

4.1.2 Fatigue assessment close to weld seam model

4.1.2.1 General

The primary target of this work is to investigate the thermal fatigue effect and thermal mixing characteristics in the thermal mixing process at 90° T-junction, which is the most applied mixing-tee

configuration in the piping system in the nuclear power plants. Since the weld seam module has been cut open for the metallographical investigation, the TC-module is installed at the test position 1 (see Figure 2-4) downstream of the T-junction. The weld seam model is installed in the TC-module to simulate the rimmed weld root of real weld seam. With the micro-thermocouples on the TC-module and inlet modules close to the T-junction, temperature signals in the near-wall flow are captured for the analysis on thermal mixing behaviors. Considering the influence of the different boundary conditions on the experimental results, the experiments are divided into four phases.

- Phase I: varied durations of AIPTEC [112];
- Phase II: varied temperature in the inlet flow streams [113, 114];
- Phase III: varied flow rate in the inlet flow streams [115];
- Phase IV: reduced boundary conditions with combination of multiple measurement techniques [116].

The variations of the boundary conditions in the experiments have been chosen with considerations of the limitations of the FSI test facility. In phase I, the experiments are conducted with the maximum flow temperature of the FSI test facility. The injection/bypass-durations of AIPTEC are changed in the measurements. As reference in the comparison, the measurement is also conducted with continuous cold flow injection. In phase II, only the flow temperature in the main pipeline are changed, since the flow stream in the branch pipeline cannot be heated up and remains 20 °C. In phase III, the flow rate in the main and branch pipe has been changed individually. And the flow temperature in the main pipeline remains constant at 200 °C. The system pressure in phase I – III is 75 bar. Due to the limitations of the optical measurement techniques, the system pressure is reduced to 30 bar in phase IV. And the maximum temperature in phase IV is 150 °C. The boundary conditions in the experiments downstream of the T-junction are shown in Table 4-1.

Table 4-1: Overview of the experiments downstream of the T-junction

Phase No.	Case No.	Pressure [bar]	T_m [°C]	\dot{M}_m [g/s]	Re_m [-]	\dot{M}_b [g/s]	Re_b [-]	Injection [s]	Bypass [s]
I	A	75	265	560	99018	200	6555	20	10
	B	75	265	560	99018	200	6555	20	20
	C	75	265	560	99108	200	6555	20	40
	D	75	265	560	99018	200	6555	20	60
	E	75	265	560	99018	200	6555	10	10
	F	75	265	560	99018	200	6555	30	30
	G	75	265	560	99018	200	6555	continuous	-
II	1	75	160	600	61899	200	6555	-	-
	2*	75	200	600	78384	200	6555	-	-
	3	75	240	600	95067	200	6555	-	-
III	4	75	200	600	78384	100	3277	-	-
	5	75	200	500	65320	200	6555	-	-
	6	75	200	400	52256	200	6555	-	-
	7	75	200	300	39192	200	6555	-	-
IV	8	30	90	600	33758	200	6543	-	-
	9	30	120	600	45706	200	6543	-	-
	10	30	150	600	58109	200	6543	-	-

* Case 2 is also a part of phase III as reference of flow-rate variations.

To discuss the influence of the boundary-condition variations in the measurement with AIPTEC, the experiments in phase II – IV are also performed with AIPTEC and continuous cold flow injection, respectively. The measurement cases with AIPTEC are referenced with a, and the cases with continuous cold flow injection are referenced with b. Figure 4-9 shows segments of temperature signals in the measurements with AIPTEC (case 1a) and continuous cold flow injection (case 1b). With the flow parameters of case 10, an individual measurement is conducted with closed branch condition and PIV technique. This individual measurement is referenced as case 10c.

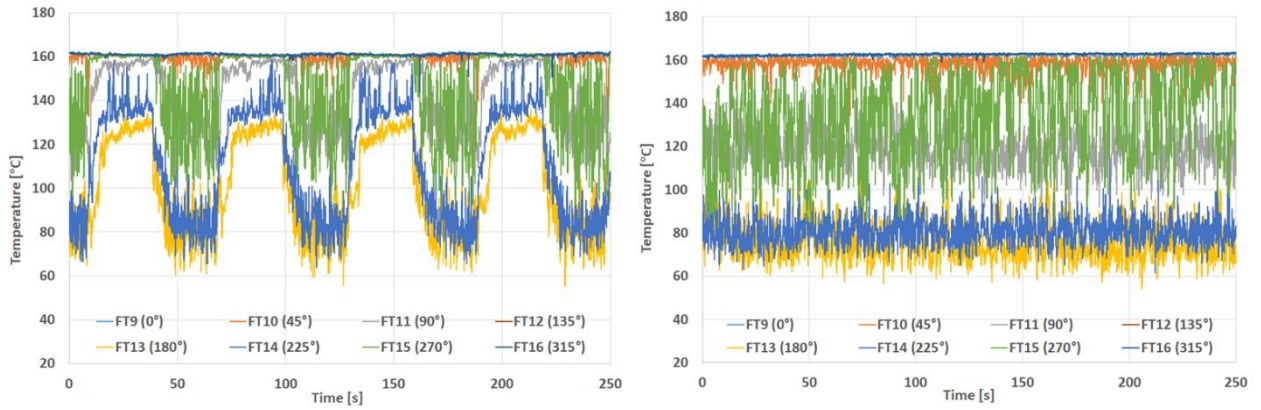
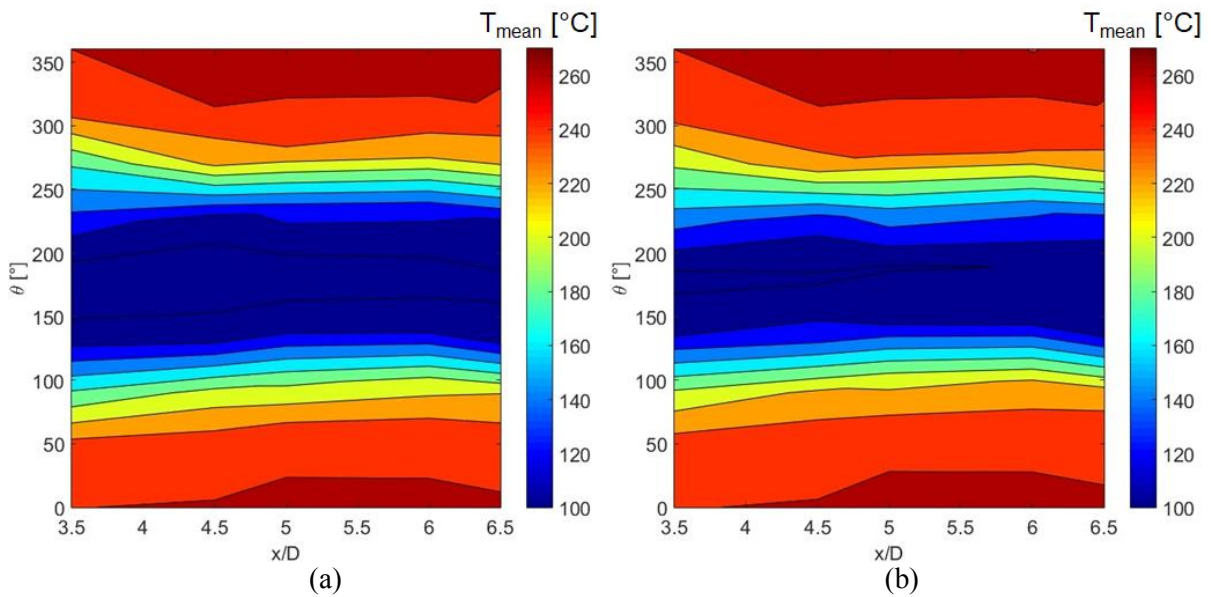


Figure 4-9: Temperature signals in the measurement cross-section F2 with AIPTEC (case 1a, left) and continuous cold flow injection (case 1b, right)

4.1.2.2 Phase I: varied duration of AIPTEC

AIPTEC is a new concept in this work. Whether the durations of AIPTEC have influence on the thermal mixing behavior is investigated in the first phase of the experiments. In the first step, four measurement cases (A – D) are performed with different ratios of the injection/bypass-durations in the AIPTEC. In these four cases, the durations of the cold flow injection are all set to 20 seconds. The durations of bypass flow varies with 10, 20, 40 and 60 seconds (0.5, 1, 2 and 3 times of the injection duration).



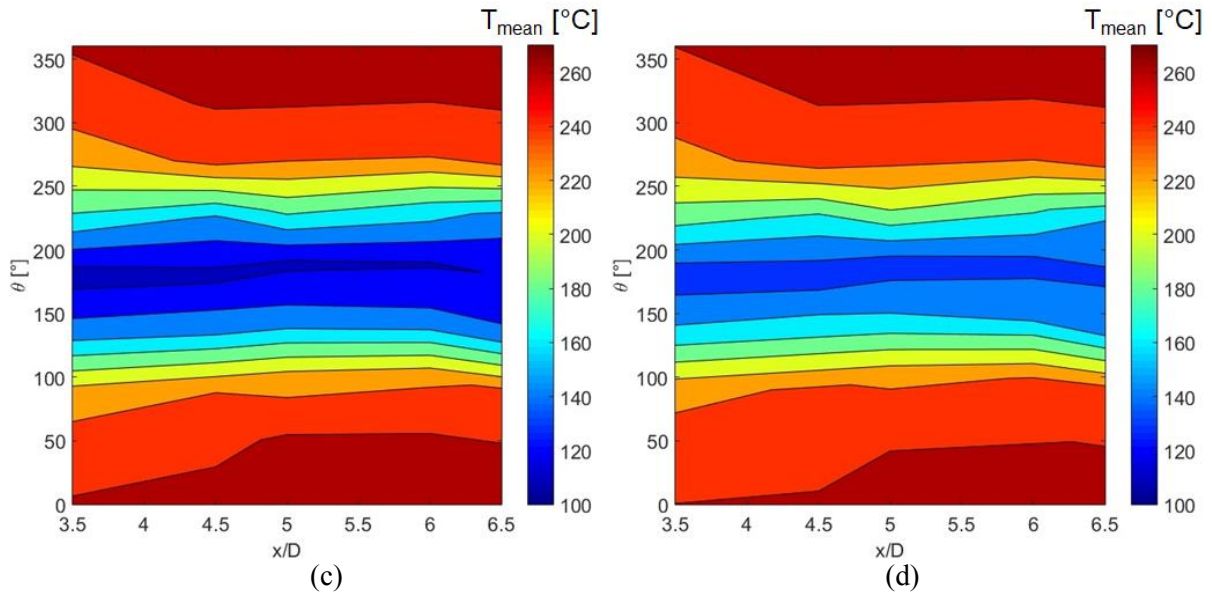
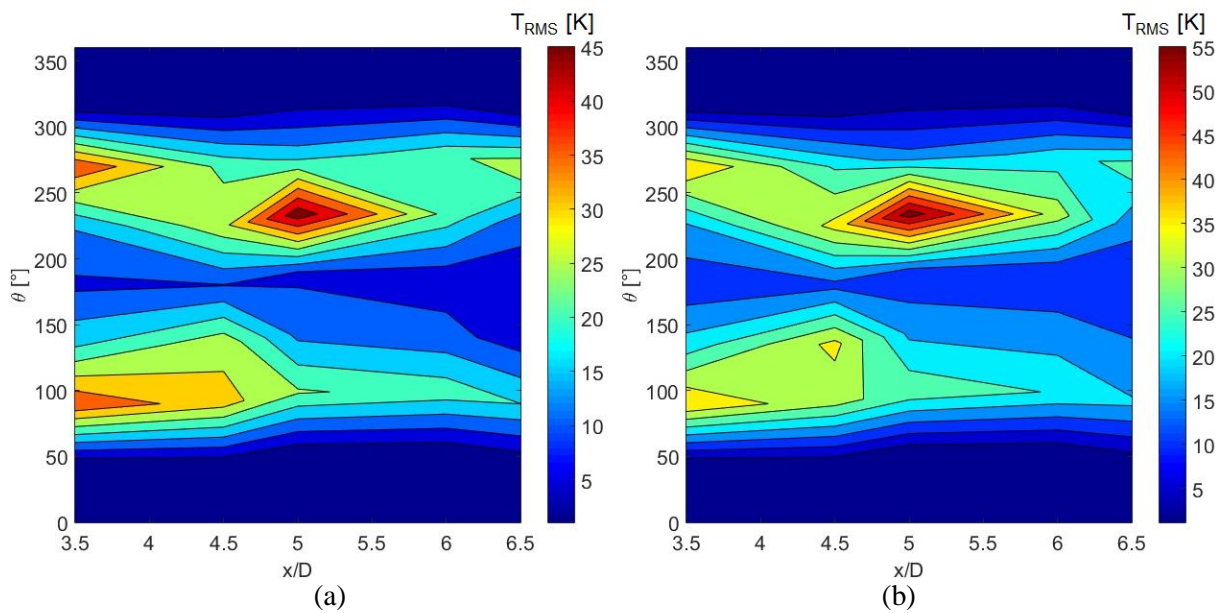


Figure 4-10: Reconstructed circumferential distributions of mean temperature in the mixing flow in the measurement cases A (a), B (b), C (c) and D (d)

The temperature measurement data have been analyzed with the standard data analysis procedure. The reconstructed circumferential mean temperature distributions of these four cases are shown in Figure 4-10. The general temperature distributions show almost the same shape and indicate thermal stratifications due to the temperature difference in the mixing flow through the TC-module. However, the mean temperature in the lower part of the mixing flow ($\theta \approx 180^\circ$) of measurement case A is lower than 100°C , in case D is approximately 140°C . The mean temperature in the lower part of the mixing flow increases from case A – D. While the duration of the bypass flow is increasing, there is more time for the hot flow in the main pipeline to warm up the TC-module in every period. Therefore, the mean temperature in the lower part of the mixing flow increases with the increased duration of the bypass flow.



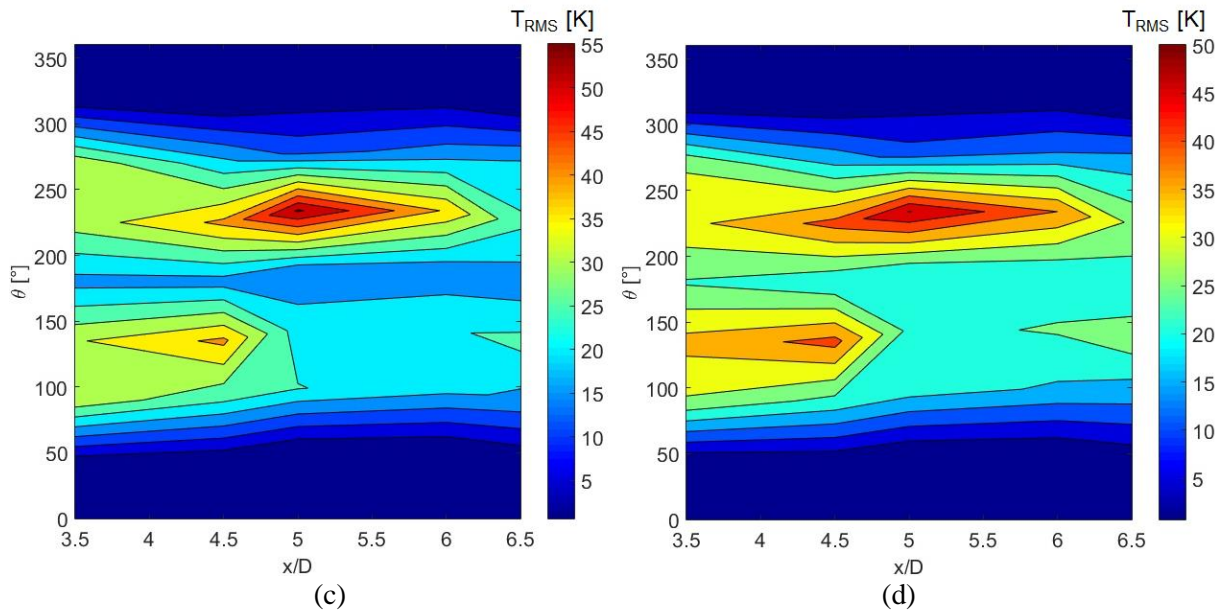


Figure 4-11: Reconstructed circumferential distributions of effective temperature fluctuations (RMS-value) in the mixing flow for measurement cases A (a), B (b), C (c) and D (d)

The reconstructed circumferential distributions of RMS temperature fluctuations in the mixing flow of measurement cases A – D are shown in Figure 4-11. The maximum temperature fluctuations in these four cases are located at the same measurement position of FT22 ($5D$, $\theta = 234^\circ$), the exact values are shown in Table 4-2. Since the maximum temperature fluctuation in these cases are all about 50 K and do not have a difference larger than 10 K with each other, area around FT22 has a high possibility for thermal fatigue in all of these cases. However, the measurement case B, in which the AIPTEC has the same duration of 20 s for injection and bypass, shows the highest maximum temperature fluctuation of 57.7 K. The possibility for thermal fatigue in the measurement case B is little higher than the other cases in comparison.

Table 4-2: Maximum temperature fluctuation in measurement cases A - D

Case	A	B	C	D
Max. T_{RMS} [K]	48.3	57.7	55.7	50.2

The thermal stratification in the mixing flow can be estimated comparing the distributions of mean temperature and temperature fluctuation. The flow path of the cold fluid can be recognized in the circumferential distribution of mean temperature (see Figure 4-10). In the comparison between the distributions of mean temperature and temperature fluctuation, the temperature fluctuations at the both edges of the cold flow are higher than the fluctuations in the middle of the cold flow path (see Figure 4-11). This indicates that the temperature fluctuation in the lower part of the mixing flow does not change so much during mixing, and the temperature changes are mostly located at the thermal interface in the stratified flow. The thermal stratification with low temperature change in the lower part of the flow is stable. However, the temperature fluctuation in the lower part of the mixing flow in the measurement case A is about 5 K (see Figure 4-10, a), and is increasing from case A to D with induced extended duration of the bypass flow. In measurement case D, the temperature fluctuation in the lower part of the mixing flow is about 20 K. This indicates the stability of the thermal stratification in the mixing flow is decreased in the cases A – D.

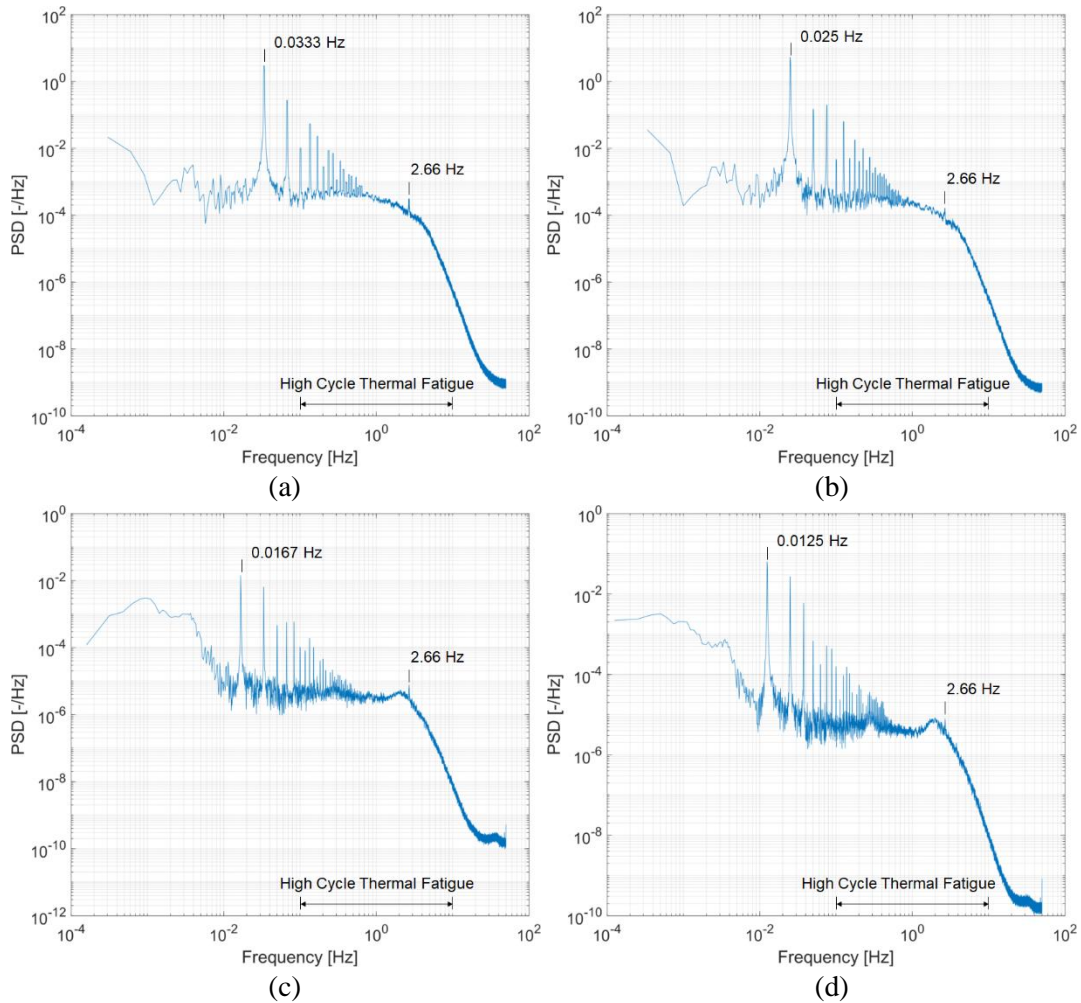


Figure 4-12: PSD diagrams of the normalized temperature signals at FT23 (F3, 279°) in case A (a), FT23 in case B (b), FT10 (F2 45°) in case C (c) and FT10 in case D (d)

Frequency analysis has been performed to the temperature measurement data at every thermocouple measurement position. Figure 4-12 shows the PSD diagrams of the normalized temperature signal at one measurement position in each case as example. As can be seen, frequency peaks of AIPTEC can be clearly recognized in the frequency spectrum of the temperature signals. Due to the variations of the AIPTEC periods, the values of the basic frequencies are different in these four cases (the basic frequency in case A: 0.0333 Hz, case B: 0.025 Hz, case C: 0.0167 Hz, case D: 0.0125 Hz). The temperature fluctuation distribution and the results of spectrum analysis are summarized in the spectrum pattern. With the same principle for the definition of AIPTEC effect, no matter how much the basic frequency changes in the measurement cases, this definition of strong AIPTEC effect is also applied in the discussion of results. Therefore, a strong AIPTEC effect indicates a possibility to initiate thermal fatigue at the measurement position.

Weld seam model (5.5D)					Weld seam model (5.5D)				
θ	F1 (3.5D)	F2 (4.5D)	F3 (5D)	F4 (6.5D)	θ	F1 (3.5D)	F2 (4.5D)	F3 (5D)	F4 (6.5D)
0	FT1	FT9	FT17	FT25	0	FT1	FT9	FT17	FT25
45	FT2	FT10	FT18	FT26	45	FT2	FT10	FT18	FT26
90	FT3 39.4	FT11	FT19	FT27	90	FT3	FT11	FT19	FT27
135	FT4	FT12	FT20	FT28	135	FT4	FT12	FT20	FT28
180	FT5	FT13	FT21	FT29	180	FT5	FT13	FT21	FT29
225	FT6	FT14	FT22 48.3	FT30	225	FT6	FT14	FT22 57.7	FT30
270	FT7	FT15	FT23	FT31	270	FT7	FT15	FT23	FT31
315	FT8	FT16	FT24	FT32	315	FT8	FT16	FT24	FT32

(a)

(b)

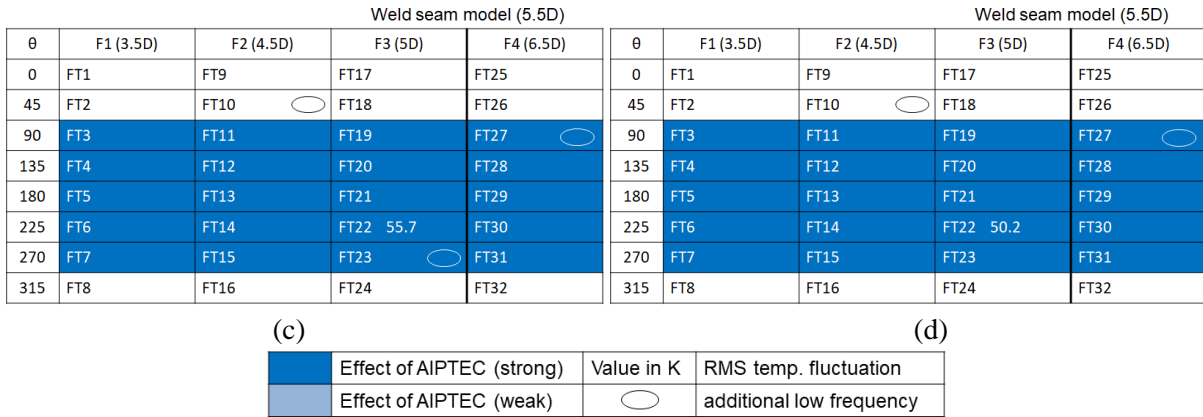


Figure 4-13: Spectrum pattern maps of the measurement cases A (a), B (b), C (c) and D (d)

The spectrum pattern maps of the measurement cases A – D are shown in Figure 4-13. To find the position with high potential for material damage due to thermal fatigue in the spectrum pattern, there are three important factors: high temperature fluctuations, temperature changes in the frequency range for thermal fatigue and properties of the structure materials in the pipeline (weld seam). The AIPTEC effects in measurement cases A – D are all strong in the lower part of the TC-module (90° - 270°). It is possible to initiate thermal fatigue at all measurement positions with AIPTEC effect. The weld seam model in the TC-module simulates the weld root of a real weld seam module, which was used in the previous experiment case S. Due to the material inhomogeneity, the area close to the weld seam is most likely to be damaged due to thermal fatigue. The maximum temperature fluctuations in investigated four cases A – D are all located at position FT22 (5D, $\theta = 234^\circ$), which is close to the weld seam model (5.5D). For a real dissimilar weld, this area around FT22 has the highest potential for material damage due to thermal fatigue. The value of the maximum temperature fluctuation should be the decisive factor to describe the possibility for material damage. Among all four measurement cases, case B with the same duration of injection and bypass has the highest temperature fluctuation of 57.7 K among these four cases and therefore the highest potential for material damage due to thermal fatigue.

The results of measurement cases A – D show that the AIPTEC with the same duration of injection and bypass (case B) has the highest potential for material damage due to thermal fatigue. With this finding, experiments have been conducted to discuss the influence of the periodic time with equal duration of injection and bypass. In measurement cases E and F, the durations of injection and bypass are both set to 10 seconds respectively 30 seconds. The results of these two cases will be discussed together with case B in this section.

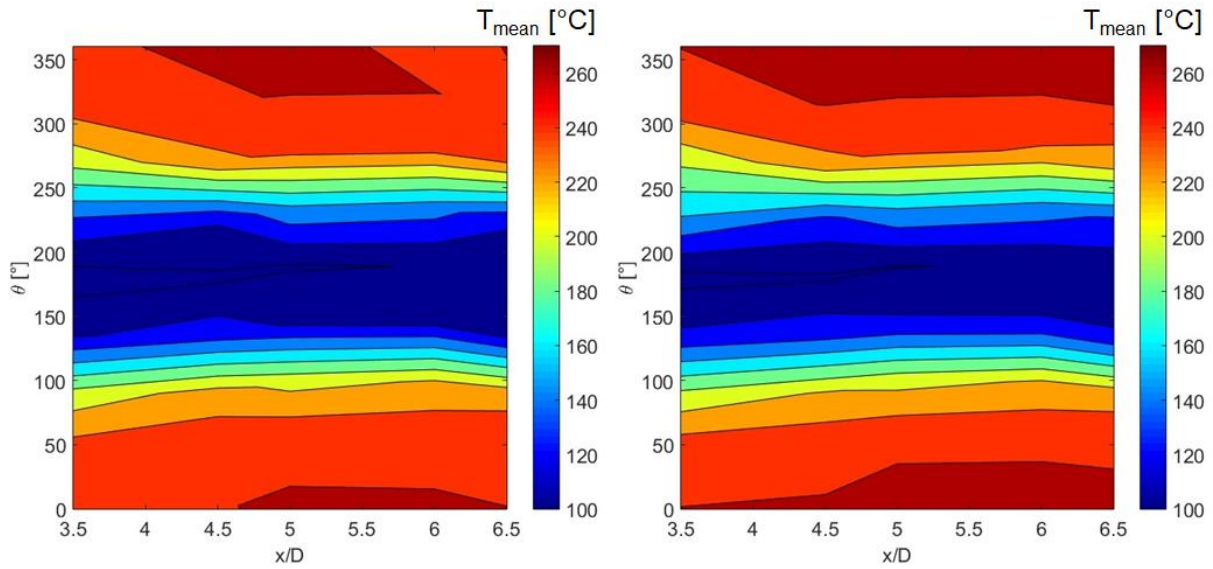


Figure 4-14: Reconstructed circumferential distributions of mean temperature in the mixing flow for measurement cases E (left) and F (right)

The reconstructed circumferential distributions of the mean temperature in the mixing flow of measurement cases E and F are shown in Figure 4-14. Compared to measurement case B (see Figure 4-10, b), the mean temperature distribution in the mixing flow through the TC-module in these three cases are almost the same, not only the shape of the cold flow, but also the values of the temperature (about $100\text{ }^{\circ}\text{C}$ at $\theta \approx 180^{\circ}$). They indicate a thermal stratification with the same temperature gradient due to the temperature difference in the mixing flow.

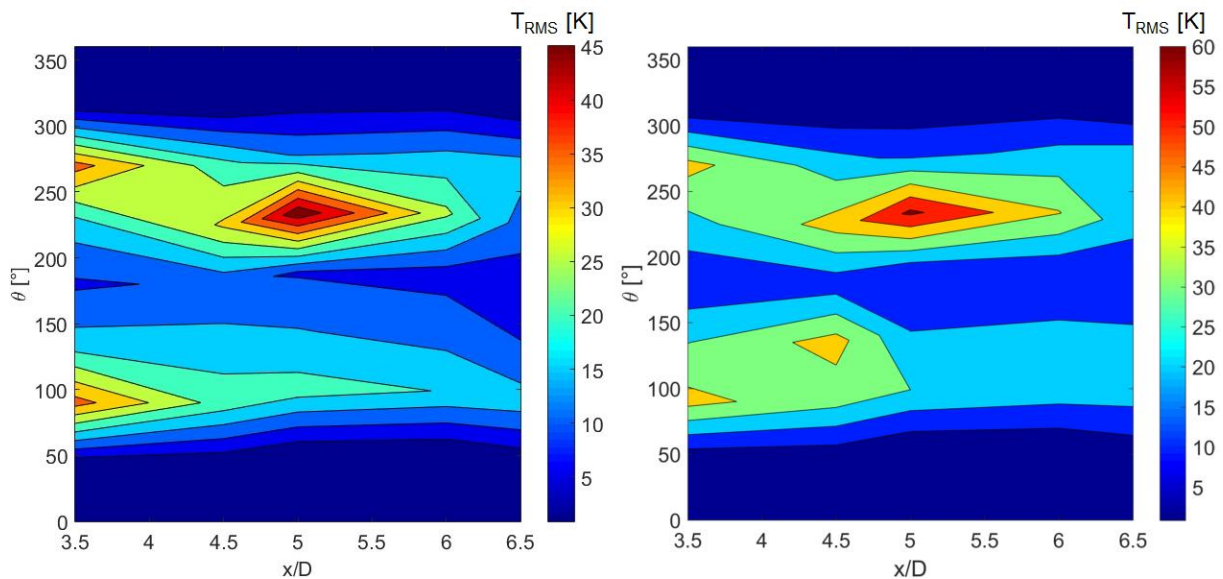


Figure 4-15: Reconstructed circumferential distributions of RMS temperature fluctuation in the mixing flow for measurement cases E (left) and F (right)

The reconstructed circumferential distributions of the RMS temperature fluctuations in the mixing flow of measurement cases E and F are shown in Figure 4-15. Compared with the distribution of temperature fluctuation of case B (see Figure 4-11, b), the general distributions of the temperature fluctuation in these three cases are also similar. A significant similarity is that the maximum temperature fluctuation is located at the same measurement position (FT22, $5D$, $\theta = 234^{\circ}$) in each individual case. However, the values of the maximum temperature fluctuation are different. The temperature fluctuation reaches the maximum of 48.6 K in case E and 62.0 K in case F. Furthermore, in the lower part of the mixing flow

the temperature fluctuations are similar (about 10 K at $\theta \approx 180^\circ$). Since the shape of the stratified flow through the TC-module in cases B, E and F are almost the same (see Figure 4-10 (b) and Figure 4-14) and the high temperature fluctuations are located at the both edges of the cold flow path, the stratified flows in these three cases are all nearly similar stable.

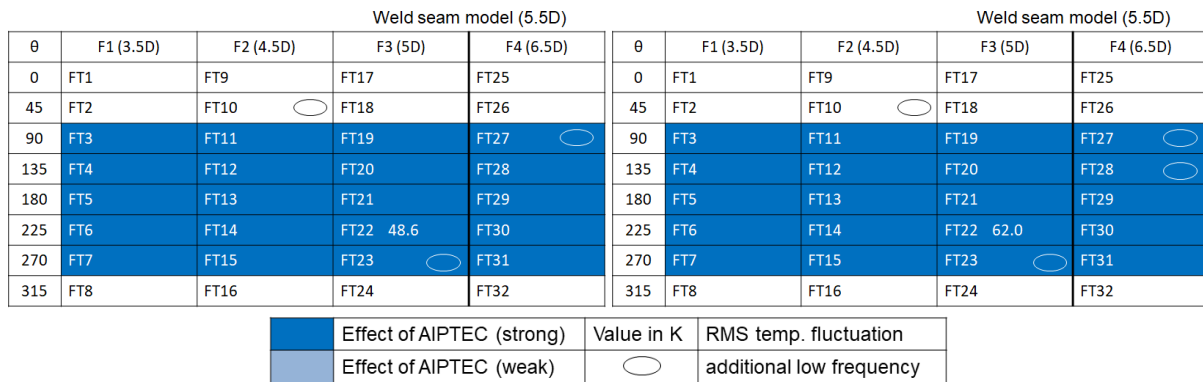


Figure 4-16: Spectrum patterns of measurement cases E (left) and F (right)

Frequency analysis has been performed to the temperature measurement data in these two cases. Examples for the PSD diagrams of the temperature data can be found in appendix A1. Figure 4-16 shows the spectrum patterns of the measurement cases E and F. The basic frequencies are 0.05 Hz respectively 0.0167 Hz. Compared with the result of case B (see Figure 4-13, b), the AIPTEC effect can also be seen in the lower part of the mixing flow. Furthermore, the AIPTEC effects in these three cases are equally strong. The maximum temperature fluctuations are all located at the measurement position FT22. It increases with the induced duration of the AIPTEC period and reaches the maximum of 62.0 K in case F, in which the durations of injection/bypass are both set to 30 seconds. Thus, case F has the highest potential for material damage due to thermal fatigue in the area close to FT22. Considering the all cases A – F, a clear statement can be drawn that the change of durations in AIPTEC does not have influence to the mixing behavior in the thermal mixing process. Moreover, the area with high potential for material damage due to thermal fatigue cannot be changed with investigated different periods of AIPTEC. Operating time is the only decisive factor for the initiation of material damage due to thermal fatigue under discussed mixing conditions.

These results can be compared with experiments at the weld seam module downstream of the 25° shock module in the previous measurement case S. With the same flow parameters and boundary conditions, the previous work downstream the shock module shows a different mixing behavior in comparison to the present experiments downstream the 90° T-junction. In contrast to the current experiments, the cold flow in the experiments downstream the shock module shows a clear S-shaped flow path (see Figure 4-3). The highest temperature fluctuations are located at the turning of the S-shaped flow path. In addition, additional low frequency with the value of about 2.66 Hz can be found in several measurement positions in these cases. It is a little different with the value of additional low frequency in the previous case S (2.56 Hz). Among these cases with varied period durations in AIPTEC, the value of the addition low frequency remains the same.

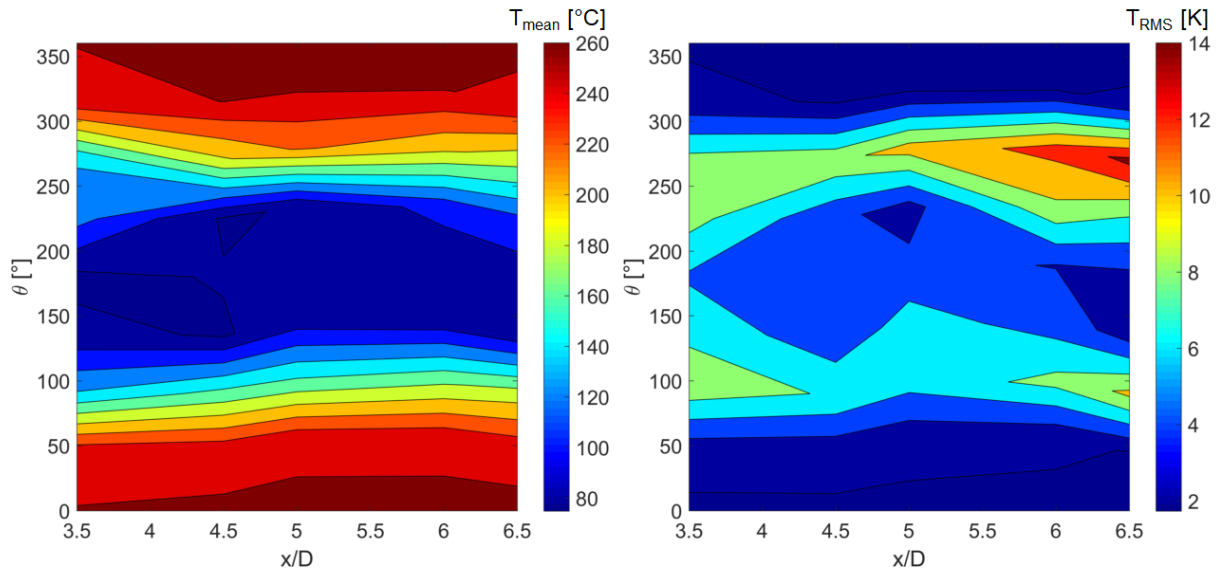


Figure 4-17: Reconstructed circumferential distributions of mean temperature (left) and RMS temperature fluctuation (right) in the mixing flow for measurement case G

The mixing processes with AIPTEC do not represent the reality in piping systems of nuclear power plants. Therefore, the experiment is also performed with realistic continuous cold flow injection (case G). Figure 4-17 shows the reconstructed circumferential distributions of the mean temperature and RMS temperature fluctuation in the mixing flow in case G. The mean temperature distribution indicates a thermal stratification in the mixing flow. Compared with the AIPTEC cases (case A – F), the path of the cold flow in the lower part of the TC-module is not so straight as those with AIPTEC. The temperature in the lower part of the stratified flow is about 80 °C and is lower than the AIPTEC cases. The maximum temperature fluctuation is 16.3 K at measurement position FT31 (6.5D, $\theta = 270^\circ$). The temperature fluctuation in the lower part of the mixing flow is about 4 K and at the both edges of the cold flow path is over 10 K. This indicates that the stratified flow in the mixing zone is stable. For the mixing process with continuous cold flow injection, the stability of the thermal stratification can be proved by the non-dimensional flow parameter Richardson (Ri) -number, which can be calculated with following equation [72].

$$Ri = \frac{(\rho_b - \rho_m) \cdot g D_m}{\rho_b \cdot u_{mix}^2} \quad (E4-3)$$

The Ri-number in case G is calculated as 1.31. Since the Richardson-number is defined as the ratio of the potential energy (buoyancy) to the kinetic energy (impulse) in the pipe flow [117], with $Ri > 1$, the thermal stratification in the mixing flow is stable in case G.

The spectrum pattern of case G is shown in Figure 4-18. Example for the frequency spectrum of the temperature data in this case can be found in appendix A1. No more AIPTEC effect can be seen in the spectrum pattern. However, the additional low frequency can still be found at several measurement positions. Compared the cases A – F, it can be understood that the additional low frequency is an important property of thermal mixing characteristics. And the value of the additional low frequency does not change with the varied durations of AIPTEC. Although the temperature fluctuation reaches the maximum at the position of FT31, there is no low frequency temperature change at that measurement position. The measurement position FT23 (5D, $\theta = 279^\circ$) has both high temperature fluctuation ($T_{RMS} = 11.1$ K) and low frequency temperature change (special low frequency 2.66 Hz). It is also located near the position of the weld seam model. Therefore, the area close to FT23 has the highest potential for material damage due to thermal fatigue. However, the temperature fluctuation at the position FT23 is

quite low in comparison with the cases A – F. The operating time shall be very long until the material damage is initiated in the thermal mixing process with the flow condition of case G.

Weld seam model (5.5D)

θ	F1 (3.5D)	F2 (4.5D)	F3 (5D)	F4 (6.5D)
0	FT1	FT9	FT17	FT25
45	FT2	FT10 ○	FT18 ○	FT26
90	FT3	FT11	FT19	FT27
135	FT4	FT12	FT20	FT28
180	FT5	FT13	FT21	FT29
225	FT6	FT14	FT22	FT30
270	FT7	FT15	FT23 11.1 ○	FT31 16.3
315	FT8	FT16	FT24	FT32

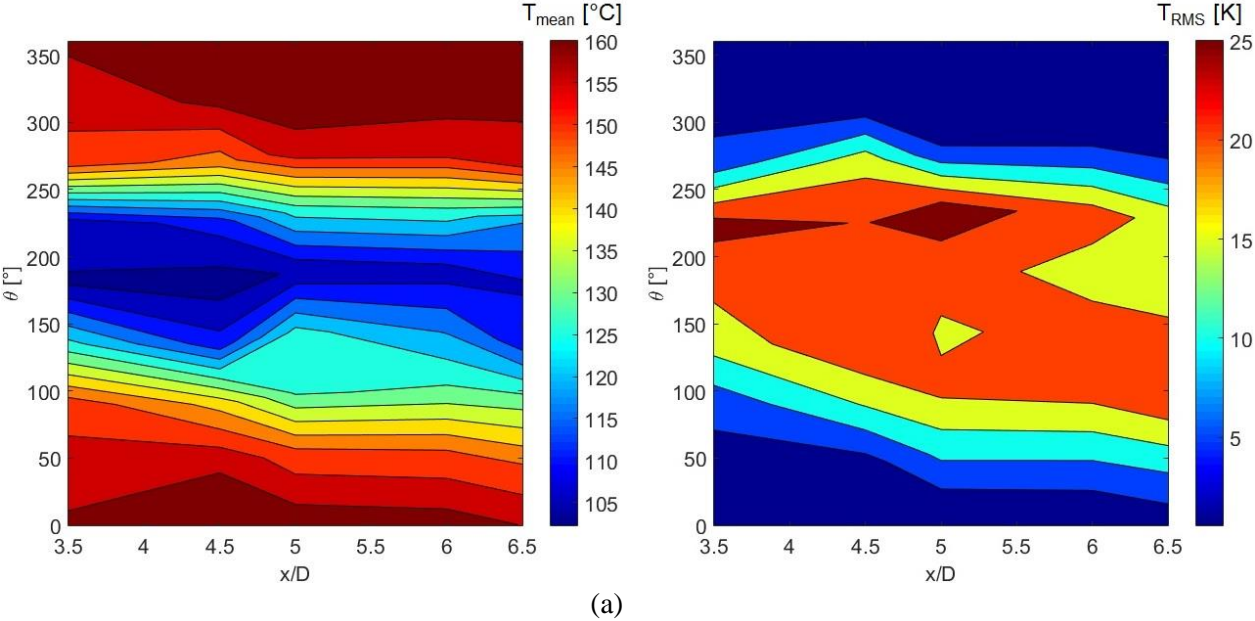
Effect of AIPTEC (strong)	Value in K	RMS temp. fluctuation
Effect of AIPTEC (weak)	○	additional low frequency

Figure 4-18: Spectrum pattern of measurement case G

Based on the results in these seven cases, the influence of AIPTEC durations in the thermal mixing flow can be summarized. Varied injection/bypass-durations in AIPTEC cannot change the thermal mixing behavior (e.g. additional low frequency) in the mixing processes. But it can increase the possibility of material damage due to thermal fatigue in the mixing region.

4.1.2.3 Varied temperature

The summary of the literature in chapter 1.2 shows that the temperature difference between the inlet flow streams is one of the decisive parameter to the thermal mixing processes. Therefore, the influence of the temperature difference in the inlet flow is investigated in the experiment phase II. Since the water flow in the branch pipeline cannot be heated, the flow temperature in the main pipeline is chosen for 160 °C, 200 °C and 240 °C, so that the temperature difference in these three cases are all above the threshold value of 115 K. The experiments are conducted with AIPTEC (case 1a – 3a) and continuous cold flow injection (1b – 3b). According to the results in phase I, the injection/bypass-durations of AIPTEC are both set 30 s.



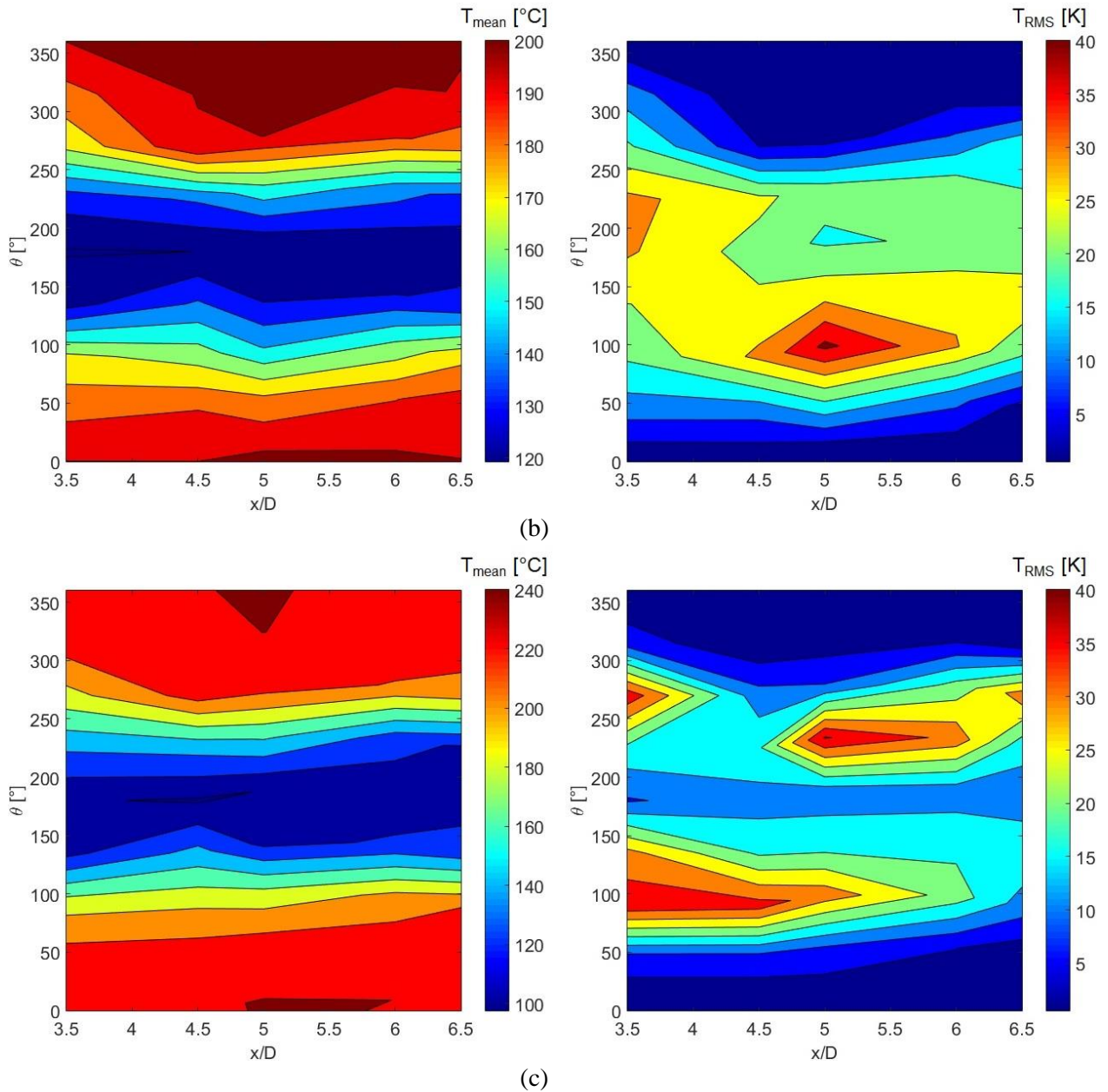


Figure 4-19: Reconstructed circumferential distributions of mean temperature (left) and RMS temperature fluctuations (right) in the investigations cases 1a (a), 2a (b) and 3a (c)

The measurements with AIPTEC are discussed at first. The circumferential distributions of the mean temperature and the RMS temperature fluctuations in the measurement cases 1a – 3a have been reconstructed and shown in Figure 4-19. In the mean temperature distribution of these cases, a stratified flow due to the temperature difference in the mixing region can be identified. The flow paths of the cold fluid ($\theta \approx 100^\circ - 250^\circ$) in these three cases do not show any clear turning compared to case S. The shapes of the cold flow in the cases 2a and 3a are almost the same. The shape of the cold flow in the case 1a is similar to those in the other two cases. The only difference exists in the cross-sections F2 (4.5D) and F3 (5D) at angular position $\theta = 135^\circ$. The RMS temperature fluctuations in these three cases are differently distributed in the near-wall fluid. In case 1a, a large area with temperature fluctuations exists at about 20 K. In case 2a, temperature fluctuations of above 20 K exists almost at 75% of the circumferential area. In case 3a, all temperature fluctuations higher than 15 K are located at the edges of the thermal interface in the thermal stratification. The locations of the maximum temperature fluctuation in these three measurement cases are shown in the Table 4-3.

Table 4-3: Maximum temperature fluctuation in measurement cases of phase II with AIPTEC

Case No.	1a	2a	3a
Measurement point	FT22	FT19	FT22
Max. T_{RMS} [K]	28.4	43.6	40.4
Location	5D, 234°	5D, 99°	5D, 234°

In the cases with AIPTEC, the stabilities of the thermal stratification can be qualitatively estimated with comparison of the distributions of mean temperature and temperature fluctuations. The location of thermal interface in the stratified flow can be identified from the circumferential distribution of the mean temperature. The locations of high temperature fluctuations in the mixing region are shown in the circumferential distribution of the RMS-values. If the temperature fluctuations in the middle of the cold flow in the same level with those at the edges of the thermal interface, it indicates that the mixing process is still taking place in the cold fluid, and therefore, the thermal stratifications is unstable. If the temperature fluctuations at the edge of the thermal interface much higher than those in the middle of the cold flow, the mixing process only takes place near the thermal interface, and the thermal stratification is stable. In the cases 1a and 2a, the temperature fluctuations in the middle of cold flow are almost the same with the edge of the thermal interface. The stratified mixing flow these two cases are both unstable. In case 3a, the temperature fluctuation at the edge of the thermal interface is higher than in the middle of the cold flow. That means, the stratified mixing flow in this case is stable.

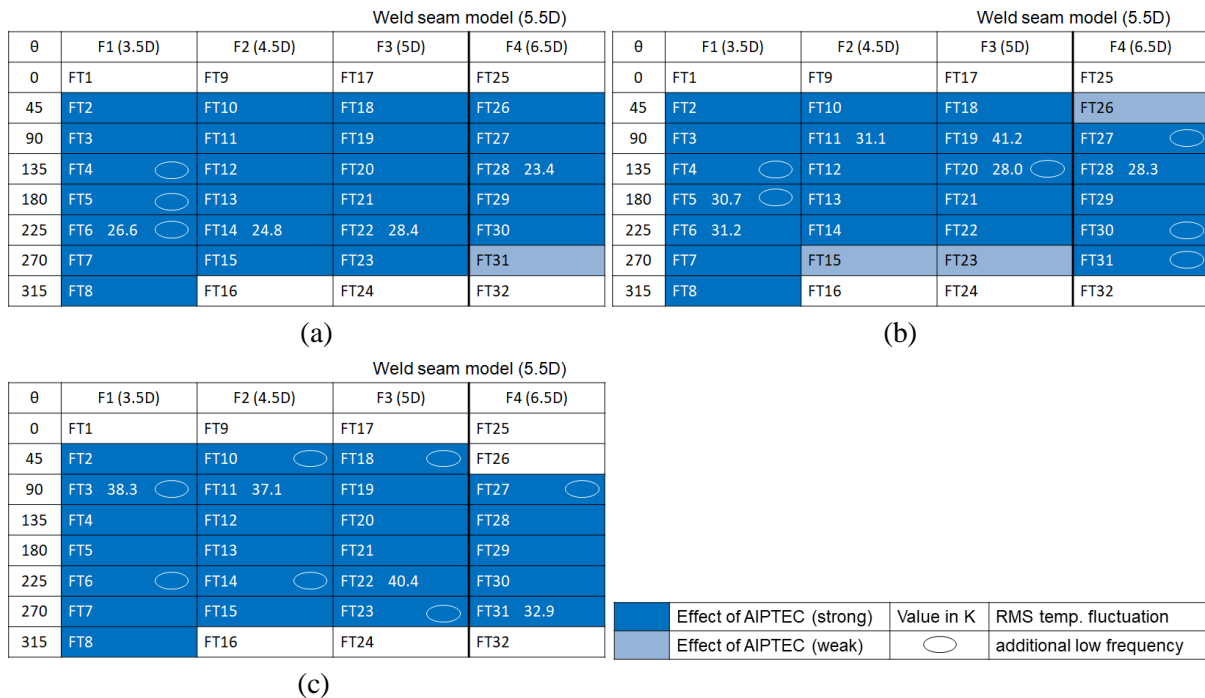
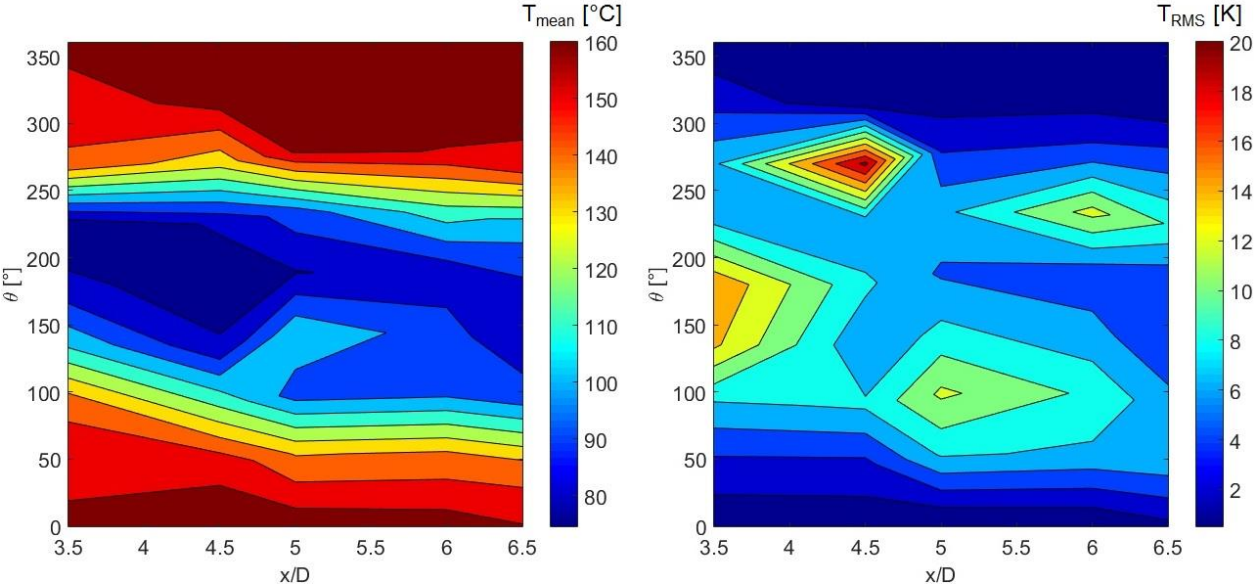


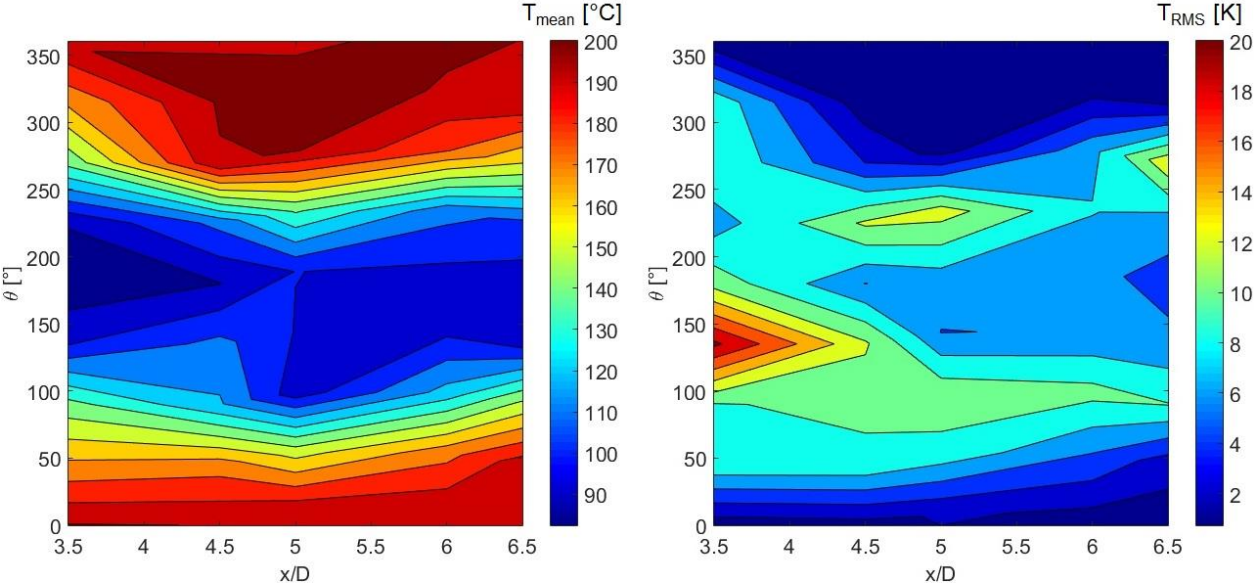
Figure 4-20: Spectrum pattern of the investigation cases 1a (a), 2a (b) and 3a (c)

The spectrum patterns of the investigation cases 1a – 3a are shown in Figure 4-20. Examples for the frequency spectrum of the temperature measurement in these cases can be found in appendix. For prediction of thermal fatigue in the thermal mixing processes, three factors must be considered: high temperature fluctuations, temperature change in the relevant frequency range and the properties of the piping materials (weld seam) [77]. In these three cases, a strong effect of AIPTEC is expected at most of the measurement positions, which indicates a high potential for thermal fatigue. Among these three cases, the temperature fluctuations in the cases 2a and 3a are higher than case 1a. Material damages are more likely to be initiated in these two cases. In the reality with a dissimilar weld, thermal fatigue is most likely to be initiated in the piping materials close to the weld seam due to the material

inhomogeneity. For this investigation, the area close to the weld seam model simulates the rimmed weld root. The measurement position FT19 ($5D, \theta = 99^\circ$) in case 2a and FT22 ($5D, \theta = 234^\circ$) in case 3a are located in the cross-section F3 ($5D$), which is close to the position of the weld seam model ($5.5D$). Both positions have a temperature fluctuation over 40 K, and therefore a high potential for material damage due to thermal fatigue in the correlated cases. Even in the case 1a, the temperature fluctuation reaches the maximum of 28.4 K at measurement position FT22. It is also possible to initiate thermal fatigue in the piping material close to this measurement position in this case. However, by increasing of temperature difference in the inlet flows, the initiation of such material damages can be accelerated with these experiment conditions (AIPTEC).



(a)



(b)

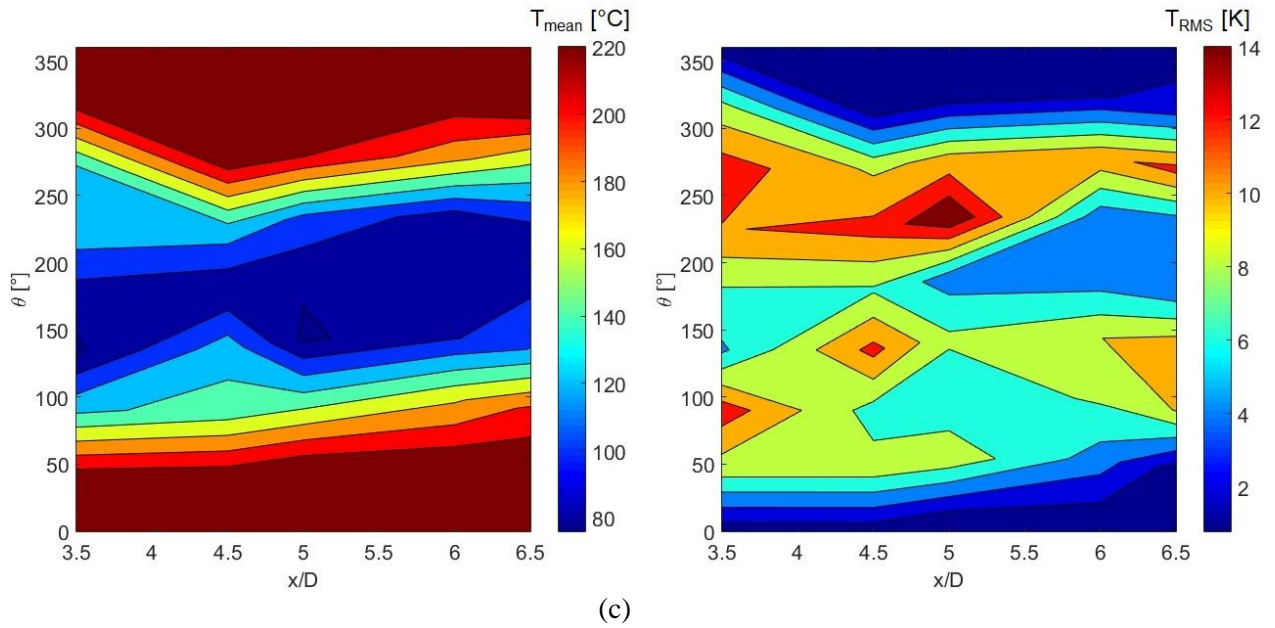


Figure 4-21: Reconstructed circumferential distributions of mean temperature (left) and effective temperature fluctuations (right) in the investigations cases 1b (a), 2b (b) and 3b (c)

To investigate thermal fatigue in a real mixing condition in nuclear power plants, experiments are also performed with continuous cold flow injection. The reconstructed circumferential distribution of mean temperature and RMS temperature fluctuations in the investigation cases 1b – 3b are shown in Figure 4-21. The mean temperature distributions indicate thermal stratification in the mixing region in these three cases. However, the shape of the stratified flow in these three cases are different. Generally, the temperature fluctuation in these three cases decreases with increased temperature difference. The maximum temperature fluctuations are much lower than those in the experiments with AIPTEC. The values and the locations of the maximum temperature fluctuation in these three cases are presented in Table 4-4.

Table 4-4: Maximum temperature fluctuation in measurement cases of phase II with continuous cold flow injection

Case No.	1b	2b	3b
Measurement point	FT15	FT4	FT22
Max. T_{RMS} [K]	20.5	20.4	15.9
Location	4D, 270°	3.5D, 135°	5D, 234°

In the cases with continuous mixing processes, the stability of the stratified mixing flow can be quantitatively estimated by calculation of the Richardson-number with equation (E4-3). The Richardson-numbers of the stratified mixing flow in these three cases are shown in Table 4-5.

Table 4-5: Richardson-number in the mixing flow in the cases of phase II with continuous cold flow injection

Case No.	1b	2b	3b
Ri [-]	0.58	0.81	1.06

The Richardson-numbers of the mixing flow in these three cases show that the stability of the stratified mixing flow increases with the increased temperature difference. For the pipe flow with $Ri > 1$, the

stratified mixing flow in the case 2b is stable. The thermal stratification in the cases 1b and 2b are unstable. In the thermal mixing flow, a stable thermal stratification can stabilize the heat exchange and reduce the temperature fluctuation in the mixing region. Therefore, the potential for thermal fatigue is reduced with the increased the stability of the stratified mixing flow.

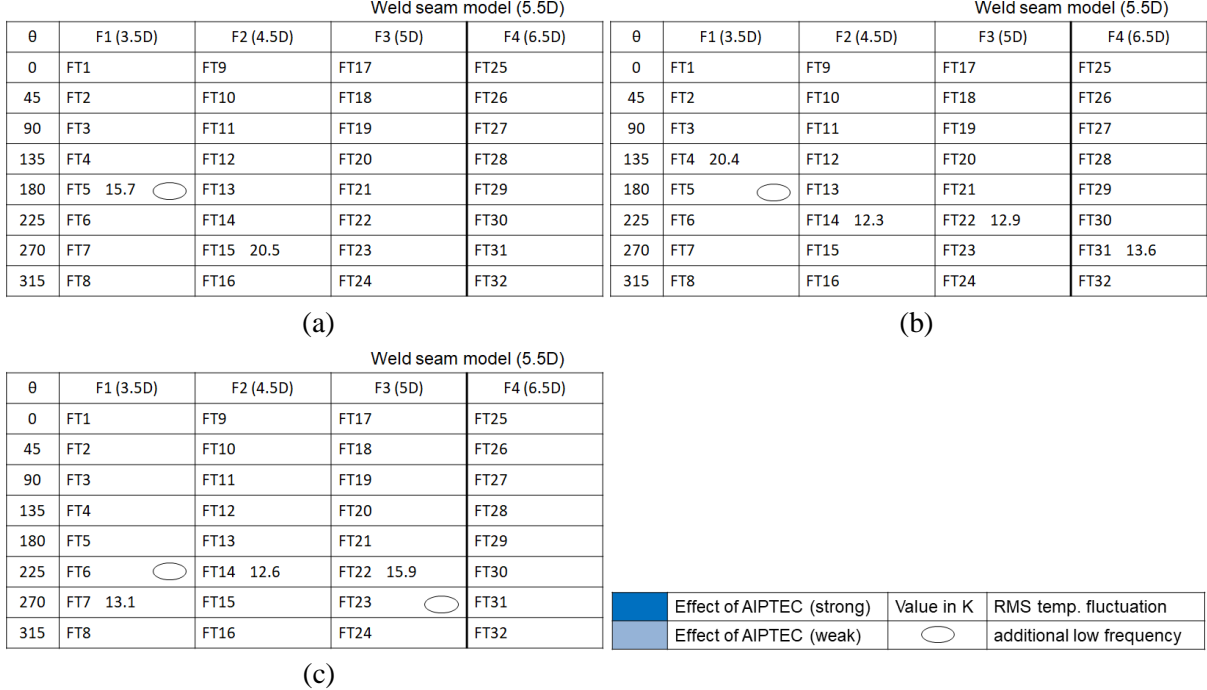


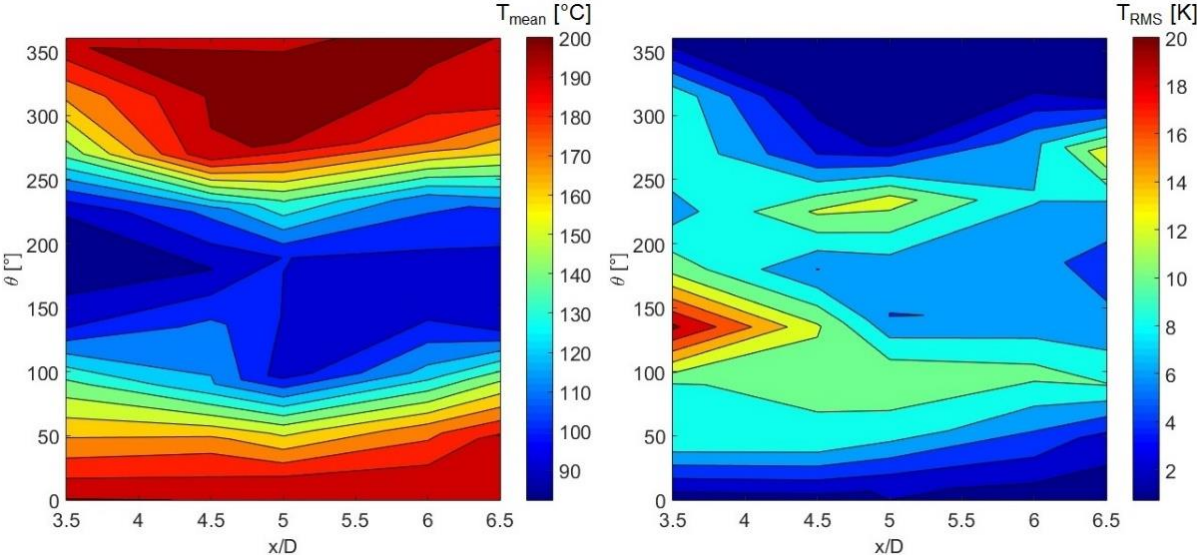
Figure 4-22: Spectrum pattern of the investigation cases 1b (a), 2b (b) and 3b (c)

The results of the frequency analysis (examples can be found in appendix) and temperature distributions of these three cases are summarized in the spectrum pattern and shown in Figure 4-22. With continuous cold flow injection, there is no effect of AIPTEC as can be seen in the spectrum patterns. Only the measurement positions with the additional low frequency have the possibility for material damages due to thermal fatigue. Moreover, not all of these measurement positions with additional low frequency exhibit a high temperature fluctuation. Compared to the experiments with AIPTEC, the possibility for thermal fatigue in the mixing processes with continuous cold flow injection is much lower. It can take a long operation time to initiate damage in the piping materials for the mixing process with continuous cold flow injection. Results of these cases also suggest that the effect of thermal fatigue can be reduced with increased stability of the stratified mixing flow, which can be created with increased temperature difference between the inlet flows.

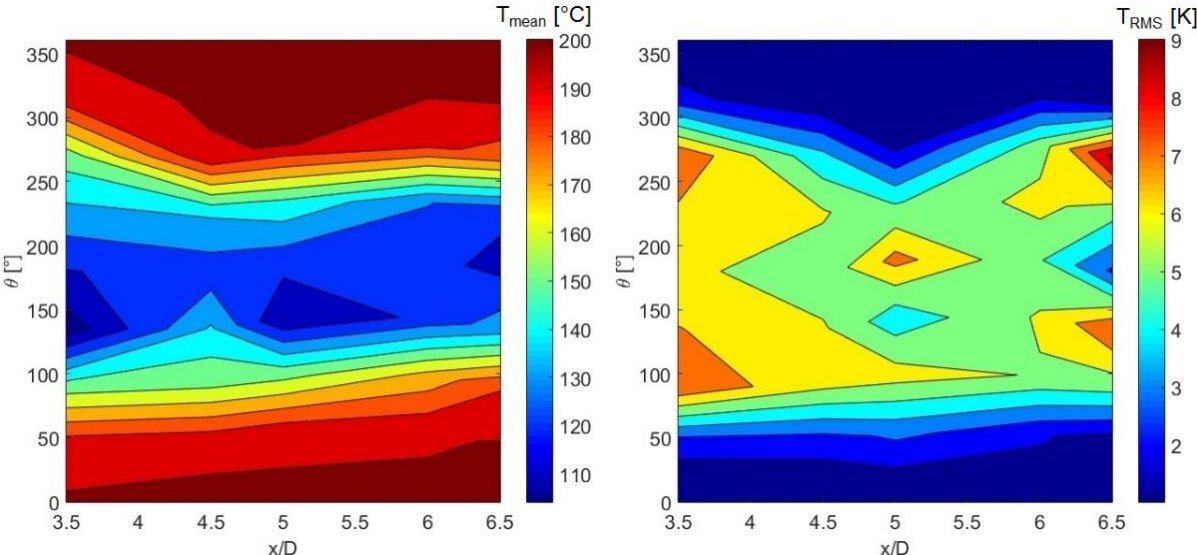
4.1.2.4 Varied flow rate

Flow rate is also an important flow parameter. The influence of the flow rate on the thermal mixing processes is investigated in phase III. As a reference case, case 2, which is already presented in the last section, has to be presented again with the measurement cases in phase III (cases 4 – 7). The results of these five cases are compared for the discussion of the flow rate influence. The experiments have been performed with AIPTEC (30 s injection / 30 s bypass) and continuous cold flow injection respectively. The results of measurements with continuous cold flow injection, which are more like the reality in the nuclear power plants, are presented in this section. The results of the cases with AIPTEC can be found in appendix A2.

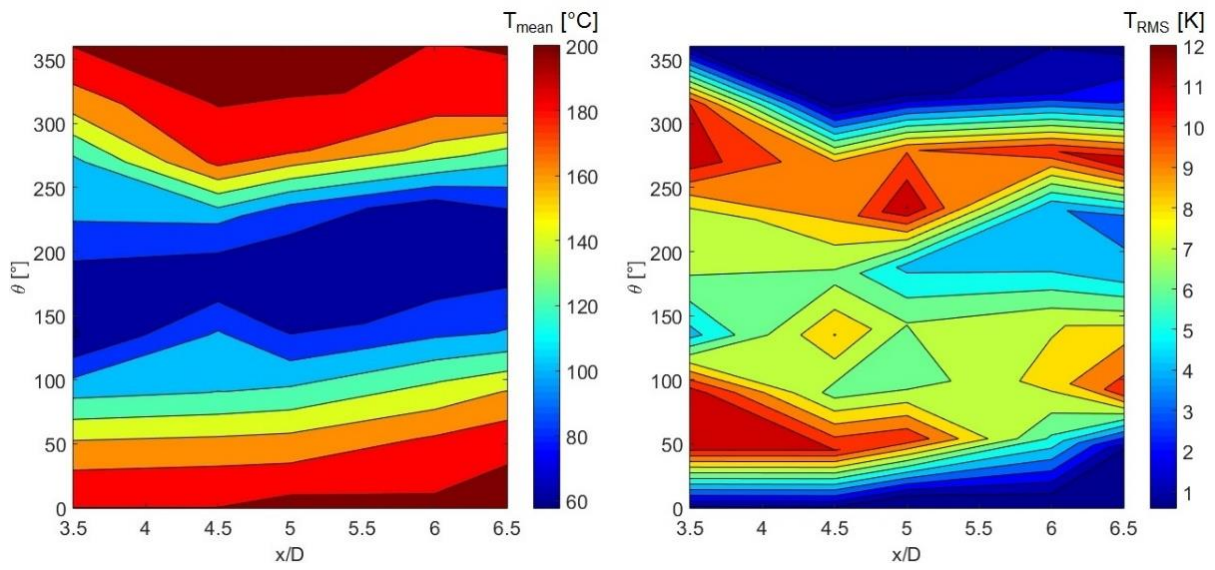
The reconstructed circumferential distributions of mean temperature and RMS temperature fluctuations in the investigation cases with continuous cold flow injection are shown in Figure 4-23. Firstly, the shapes of the cold flow path are different among these cases. In the measurement case 2b, the flow path of the cold flow has a turning at the cross-section of F3 (5D). The angular position of the cold flow path is at F1 (3.5D) about 180°, at F3 (5D) about 150° and at F4 (6.5D) about 170°. It is similar with the S-shaped flow path in the previous work with the shock module (see Figure 4-3). According to the comparison between case 2b and case 4b, this S-shaped flow path should be created by a high flow velocity in the branch pipeline. The shape of the cold flow path changes with decreasing flow rate in the main pipeline. The shape of the cold flow path of case 6b and case 7b are almost the same, but different to the other cases. The path of the cold flow in case 2b shows a clear turning, in case 5b a weak turning. For case 6b and case 7b, there is almost no turning in the path of the cold flow. The mean temperature in the lower part of the flow reduces with decreasing flow rate in the main pipeline.



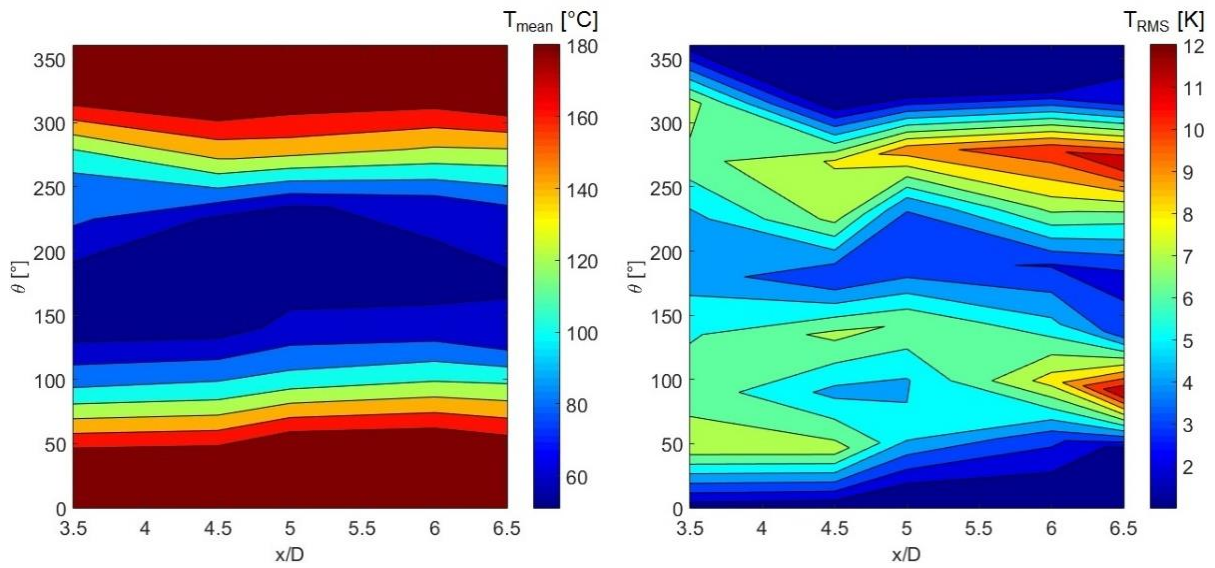
(a)



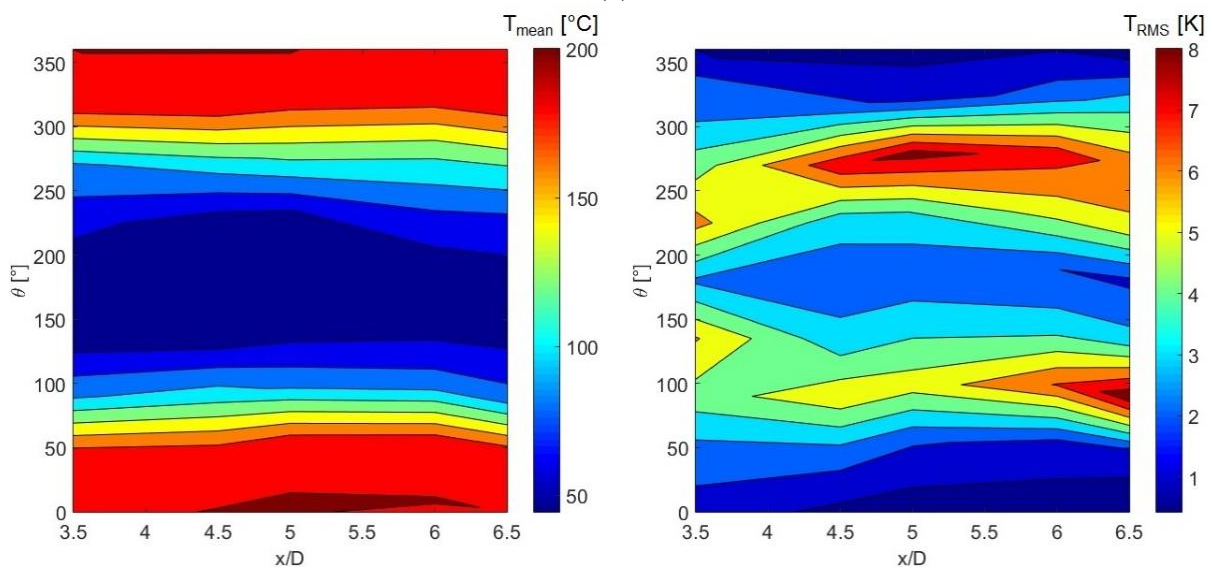
(b)



(c)



(d)



(e)

Figure 4-23: Reconstructed circumferential distribution of mean temperature (left), investigations cases 2b (a), 4b (b), 5b (c), 6b (d) and 7b (e), and corresponding circumferential distribution of effective temperature fluctuations (right)

The temperature fluctuations in the case 2b is generally higher than case 4b. The major temperature fluctuation in case 4b is very low (2 K – 9 K). The maximum temperature fluctuation is $T_{RMS} = 9.3$ K at position FT31 (6.5D, $\theta = 270^\circ$). In case 2b, a large area has temperature fluctuations higher than 6 K. The maximal temperature fluctuation is $T_{RMS} = 20.4$ K at position FT4 (3.5D, 135°). With the decreased flow rate in the main pipeline, the temperature fluctuation decreases in the cases 5b – 7b. With the decreased flow rate in the main pipeline, the temperature fluctuation decreases in the cases 5b – 7b. The values and locations of the maximum temperature fluctuation in the cases with continuous cold flow injection are shown in Table 4-6.


Table 4-6: Values and locations of the maximum temperature fluctuation in the measurements in phase III with continuous cold flow injection

Case No.	2b	4b	5b	6b	7b
Measurement point	FT4	FT31	FT22	FT27	FT27
Max. T_{RMS} [K]	20.4	9.3	12.0	12.0	8.7
Location	3.5D, 135°	6.5D, 270°	5D, 234°	6.5D, 90°	6.5D, 90°

The Richardson-numbers for the five investigation cases with continuous cold flow injection are given in Table 4-5. With Richardson-number of 1.43, the stratified flow of case 4b can be categorized as stable. In comparison with case 2b, the stability of the thermal stratification is reduced with the increasing flow rate in the branch pipe. Compared the case 2b with the cases 5b – 7b, the Richardson-number is increasing with the decreased flow rate in the main pipeline. That indicates the increasing of the stability in the stratified mixing flow.

Table 4-7: Richardson-number for the investigation cases in phase III with continuous cold flow injection

Case No.	2b	4b	5b	6b	7b
Ri	0.81	1.43	0.96	1.17	1.45

Weld seam model (5.5D)					Weld seam model (5.5D)				
θ	F1 (3.5D)	F2 (4.5D)	F3 (5D)	F4 (6.5D)	θ	F1 (3.5D)	F2 (4.5D)	F3 (5D)	F4 (6.5D)
0	FT1	FT9	FT17	FT25	0	FT1	FT9	FT17	FT25
45	FT2	FT10	FT18	FT26	45	FT2	FT10	FT18	FT26
90	FT3	FT11	FT19	FT27	90	FT3 7.9	FT11	FT19	FT27
135	FT4 20.4	FT12	FT20	FT28	135	FT4	FT12	FT20	FT28 7.9
180	FT5 	FT13	FT21	FT29	180	FT5	FT13	FT21 7.4	FT29
225	FT6	FT14 12.3	FT22 12.9	FT30	225	FT6	FT14	FT22	FT30
270	FT7	FT15	FT23	FT31 13.6	270	FT7	FT15	FT23	FT31 9.3
315	FT8	FT16	FT24	FT32	315	FT8	FT16	FT24	FT32

(a)

(b)

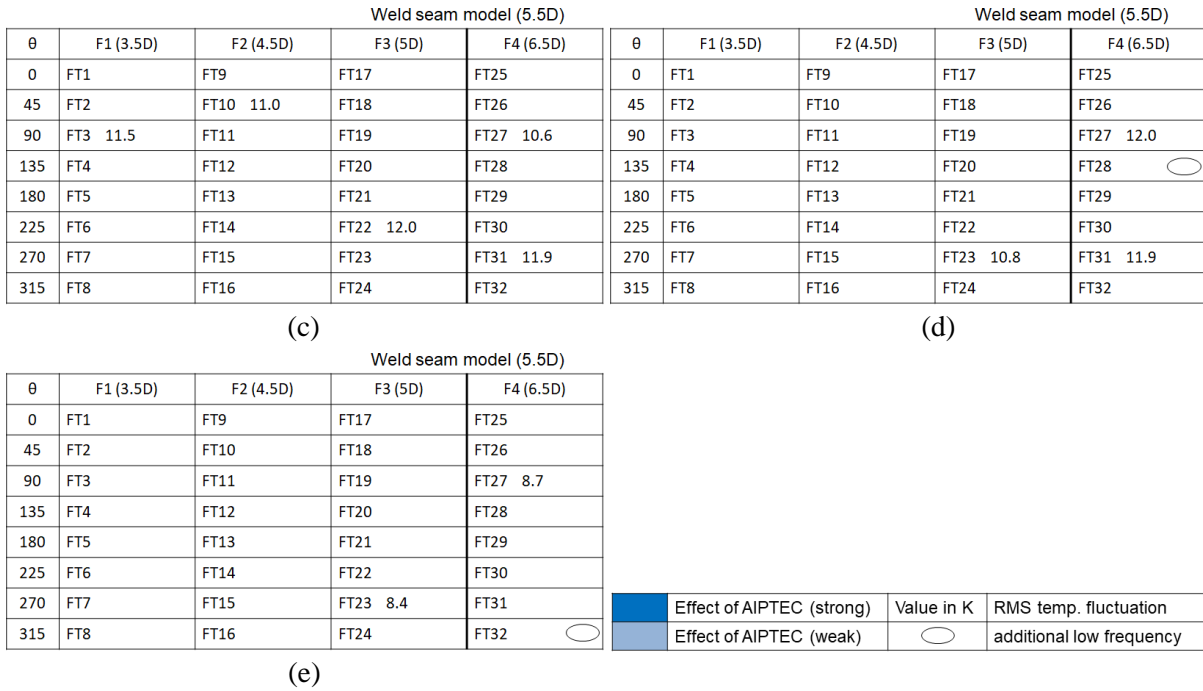


Figure 4-24: Spectrum patterns of investigation case 2b (a), case 4b (b), case 5b (c), case 6b (d) and case 7b (e)

The results of these five cases are summarized in the spectrum patterns (see Figure 4-24). Examples of the PSD diagrams in these five cases can be seen in appendix. In the experiments with continuous cold flow injection, of course no more effect of AIPTEC is visible. However, the additional low frequency can also be found at several positions in most of the cases except case 4. Moreover, the values of the additional low frequencies in these cases 5 – 7 have a small deviation to each other. This small deviation is not created by any kind of contingency. It is summarized with the results of the other cases and discussed in the chapter 4.1.6. The temperature fluctuations in the mixing flow of these case are quite low (much lower than the measurements with AIPTEC, see appendix), and most of the positions with the high temperature fluctuations have no temperature changes in the low frequency range. Considering the three factors for material damages due to thermal fatigue, the potential for material damage in these five cases are very low (much lower than the AIPTEC cases). In addition, the increased stability of the thermal stratification can stabilize the heat exchange the mixing flow, so that the temperature fluctuations are decreased. Generally, the possibility for thermal fatigue in the mixing process with continuous cold flow injection is increased with increased flow rate in the branch pipeline and decreased with decreased flow rate in the main pipeline.

4.1.2.5 Reduced operation conditions

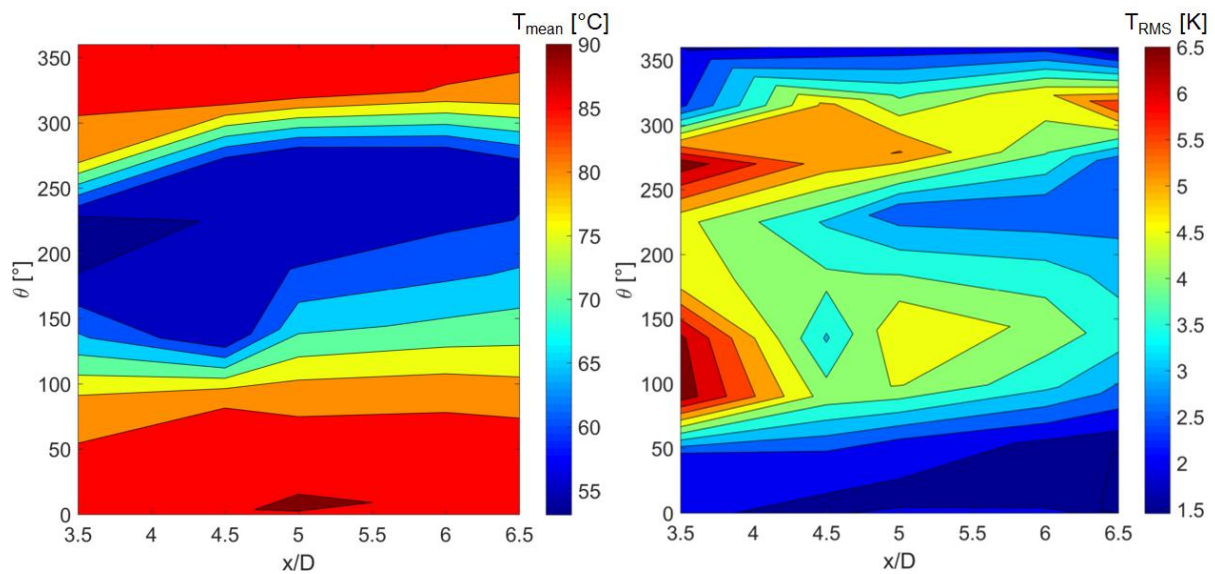
The purpose of the experiments in phase IV is to perform the experiments with combined measurement techniques. The experiments are conducted with both AIPTEC and continuous cold flow injection. Since the optical measurements are conducted with continuous cold flow injection, the results of the cases with continuous cold flow injection (cases 8b – 10b) are presented in this section. The results of AIPTEC measurements (8a – 10a) can be seen in appendix A3.

The reconstructed circumferential distributions of mean temperature and RMS temperature fluctuations in the cases with continuous cold flow injection are shown in Figure 4-25. Stratified mixing flow can be recognized in the mixing region. The shapes of the stratified flow in these three cases are also different with each other. Generally, the temperature fluctuations in these three cases is increased with increased

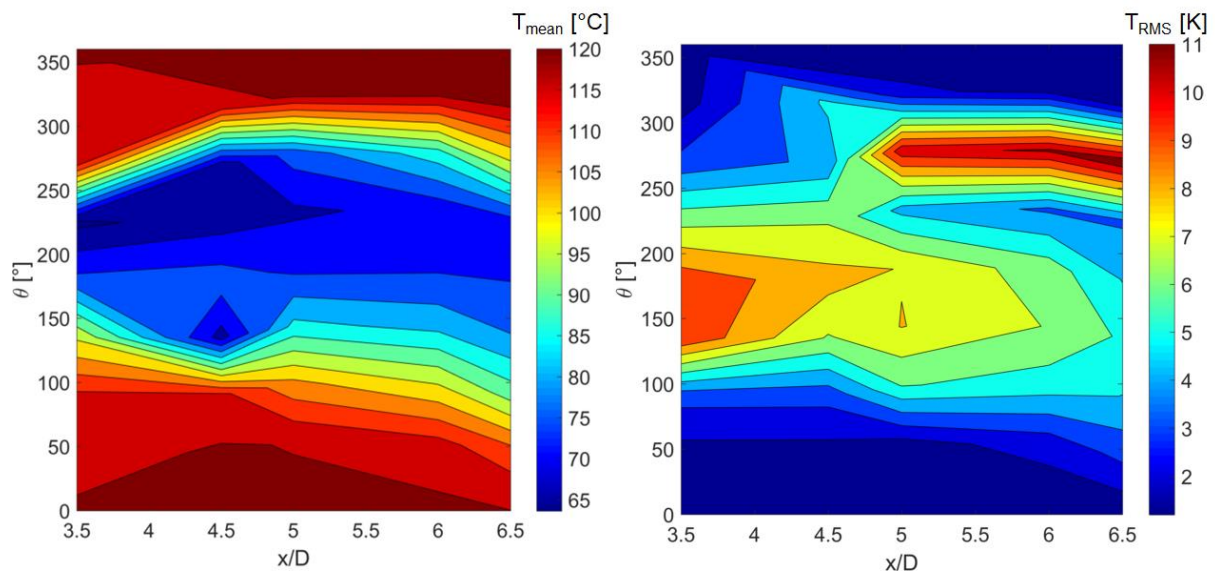
flow temperature in the main pipeline. The values and locations of the maximum temperature fluctuation in these cases are shown in the Table 4-8.

Table 4-8: Maximum temperature fluctuation in measurement cases of phase IV with continuous cold flow injection

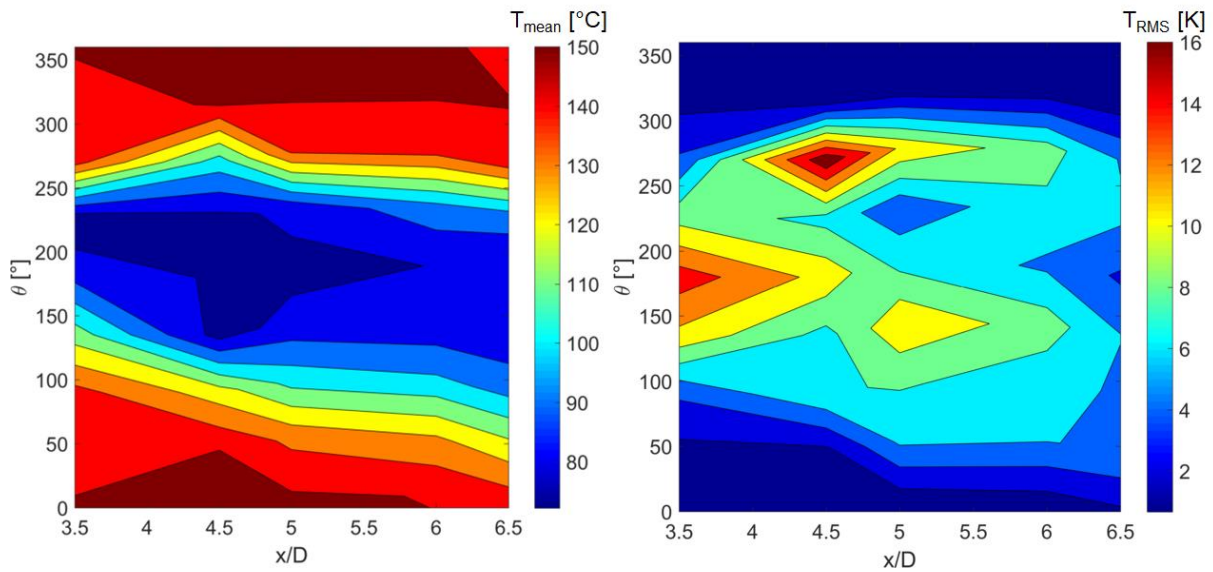
Case No.	8b	9b	10b
Measurement point	FT3	FT31	FT15
Max. T_{RMS} [K]	6.8	11.7	17.5
Location	3.5D, 90°	6.5D, 270°	4.5D, 270°



(a)



(b)



(c)

Figure 4-25: Reconstructed circumferential distributions of mean temperature (left) and effective temperature fluctuations (right) in case 8b (a), case 9b (b) and case 10b (c)

For the measurements with continuous cold flow injection, the stability of the thermal stratifications in the mixing flow can be quantitatively estimated by the calculation of the Ri-number with equation (E4-3). The calculated Ri-number in these three cases are shown in Table 4-9. According to the values of the Ri-number, the stratified flow in the mixing region in these three cases are all unstable.

Table 4-9: Richardson-number for the investigation cases in phase IV with continuous cold flow injection

Case No.	8b	9b	10b
Ri	0.22	0.37	0.53

Frequency analysis has been performed to the temperature measurement data. Examples for the frequency spectra can be found in appendix. The spectrum patterns of the three cases with continuous cold flow injection are shown in Figure 4-26. As can be seen, no AIPTEC effect nor additional low frequency can be found in the mixing flow. Moreover, the additional low frequency cannot be found at any of the measurement position in the cases with AIPTEC (see appendix). In addition, in these three cases, the temperature fluctuations are quite low. Summing up the results, the potential for material damage due to thermal fatigue in these three cases are very low.

Weld seam model (5.5D)					Weld seam model (5.5D)				
θ	F1 (3.5D)	F2 (4.5D)	F3 (5D)	F4 (6.5D)	θ	F1 (3.5D)	F2 (4.5D)	F3 (5D)	F4 (6.5D)
0	FT1	FT9	FT17	FT25	0	FT1	FT9	FT17	FT25
45	FT2	FT10	FT18	FT26	45	FT2	FT10	FT18	FT26
90	FT3 6.8	FT11	FT19	FT27	90	FT3	FT11	FT19	FT27
135	FT4 6.6	FT12	FT20	FT28	135	FT4 9.9	FT12	FT20	FT28
180	FT5	FT13	FT21	FT29	180	FT5 9.6	FT13	FT21	FT29
225	FT6 6.8	FT14	FT22	FT30	225	FT6	FT14	FT22	FT30
270	FT7	FT15	FT23	FT31	270	FT7	FT15	FT23 10.6	FT31 11.7
315	FT8	FT16	FT24	FT32 5.9	315	FT8	FT16	FT24	FT32

(a)

(b)

θ	F1 (3.5D)	F2 (4.5D)	F3 (5D)	F4 (6.5D)
0	FT1	FT9	FT17	FT25
45	FT2	FT10	FT18	FT26
90	FT3	FT11	FT19	FT27
135	FT4 11.4	FT12	FT20 11.7	FT28
180	FT5 15.1	FT13	FT21	FT29
225	FT6	FT14	FT22	FT30
270	FT7	FT15 17.5	FT23	FT31
315	FT8	FT16	FT24	FT32

	Effect of AIPTEC (strong)	Value in K	RMS temp. fluctuation
	Effect of AIPTEC (weak)	○	additional low frequency

(c)

Figure 4-26: Spectrum patterns of the case 8b (a), case 9b (b) and case 10b (c)

4.1.3 Reverse flow upstream the T-junction

Reverse flow is also one of the important mixing phenomena in thermal mixing processes. This phenomenon in the turbulent mixing processes is in some literatures also called turbulent penetration. The reverse-flow phenomenon in the thermal mixing processes has been investigated in several similar research projects around the world [57, 58, 61, 79]. In this work, the measurement cross-sections $-F$ (-4.5D) and $-f$ (-7d) are used to capture the flow temperature upstream of the T-junction in the main respectively branch pipeline. Although only one measurement cross-section cannot measure the reverse distance of the reverse flow upstream the T-junction, it can still be understood qualitatively in the comparison among the cases.

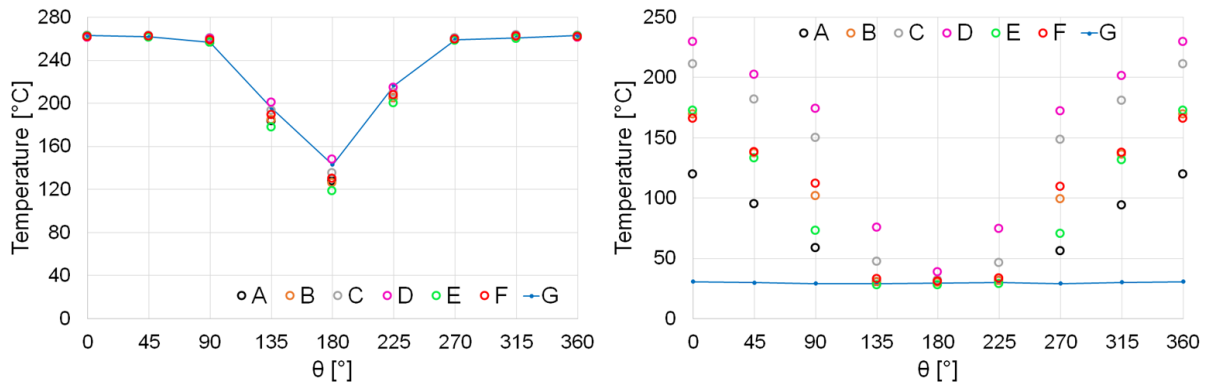


Figure 4-27: Mean temperature at the measurement cross-section $-F$ in main pipeline (left) and $-f$ in branch pipeline (right) upstream the T-junction of the measurement cases in phase I

The mean temperature in the inlet cross-section $-F$ and $-f$ in investigation phase I is shown in Figure 2-27. All the cases in phase I have the same flow parameter, but have been performed with different durations of AIPTEC (or continuous cold flow injection). In the main pipeline, temperature drop at angular position 180° indicates reverse cold flow upstream the T-junction. The decreased temperature at this position indicates a higher distance of the cold flow. Among the cases, case E shows the lowest temperature at this position, and therefore has the strongest reverse flow upstream the T-junction. In the branch pipeline, no reverse hot flow can be observed in case G, which is performed with continuous cold flow injection. In the cases with AIPTEC, the increased temperature at angular position $0^\circ/360^\circ$ indicates the turbulent penetration of the hot flow in the branch pipeline. Among the cases, case D, which has the longest bypass duration (60 s), shows the highest temperature at these position, and therefore the strongest phenomenon of reversed hot flow.

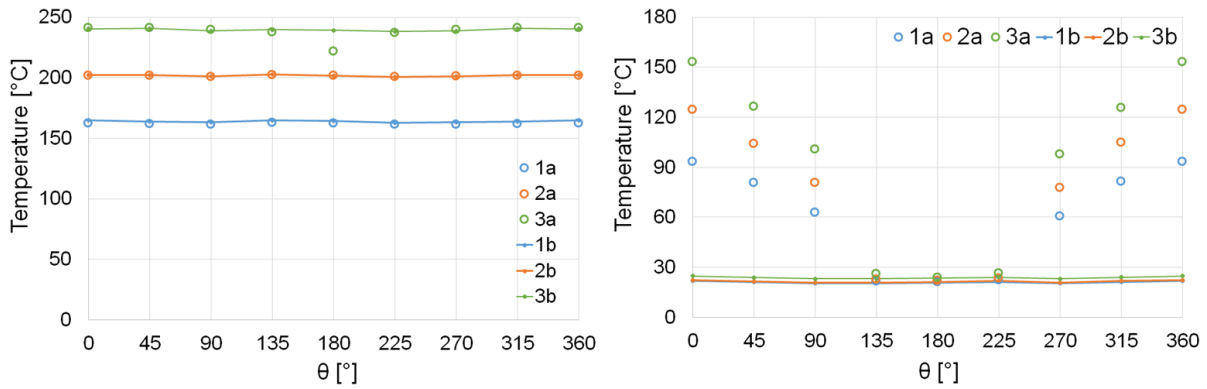


Figure 4-28: Mean temperature at the measurement cross-section –F in main pipeline (left) and –f in branch pipeline (right) upstream the T-junction of the measurement cases in phase II

The mean temperature at the measurement cross-sections upstream the T-junction in the investigation phase II is shown in Figure 4-28. The measurements in phase II have been performed with varied temperature difference between the inlet flow streams. In the cases with continuous cold flow injection, temperature do not change within the cross-sections. It indicates that either reverse flow does not exist or the reverse flow do not reach the measurement cross-section. In the experiments with AIPTEC, the influence of temperature differences between the inlet flow on the phenomenon of reverse flow can be recognized from the measurement results. In case 1a and 2a, the thermocouples in cross-section –F (main pipe) do not capture any temperature change due to reverse flow. In case 3a, a temperature drop can be found at angular position 180° (see Figure 4-28, left). It indicates that the reversing cold flow has reached this measurement cross-section. At the cross-section –f in the branch pipe, the mean temperature in upper part of the flow increases with the increased temperature differences between the inlet flow (see Figure 4-28, right). Summing up the results, the reverse-flow phenomenon is increased with increased temperature difference between the inlet flow.

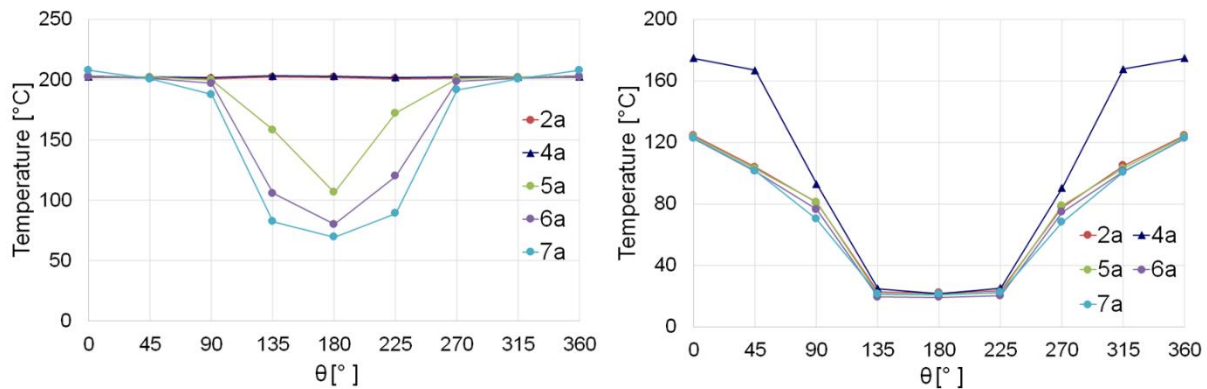


Figure 4-29: Mean temperature at the inlet cross-section in main pipe –F (left) and branch pipe –f (right) of the measurement cases in phase III with AIPTEC

Figure 4-29 shows the mean temperature at the inlet cross-sections in the cases with AIPTEC of phase III. In the main pipeline measurement cross-section, no temperature drop can be seen in cases 2a and 4a. The influence of flow rate in branch pipeline cannot be told from this diagram. Compared case 2a with the cases 5a – 7a, the temperature at angular of position 180° decreases significantly. It indicates that the reversed cold flow can reach a further distance upstream the T-junction with decreased flow rate in main pipeline. Oppositely in the branch pipeline, the influence of flow rate in main pipeline on the reversed hot flow cannot be told in the diagram, because the mean temperature at the cross-section –f in the cases 2a and 5a – 7a are almost the same. However, the influence of flow rate in the branch pipe can be seen in the comparison between case 2a and 4a. A higher temperature at angular position of 0° indicates the hot flow from main pipe can reach a further distance into the branch pipe.

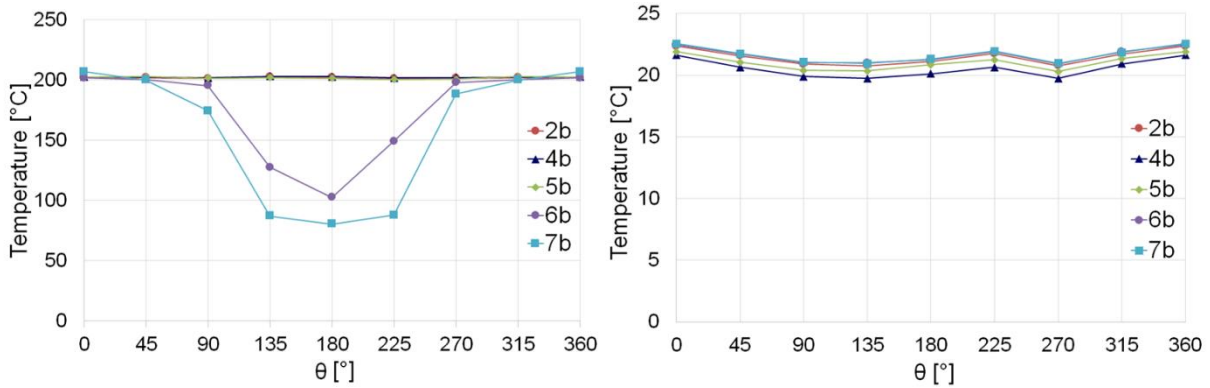


Figure 4-30: Mean temperature at inlet cross-section of main pipe –F (left) and branch pipe –f (right) of measurement cases in phase III with continuous cold flow injection

Figure 4-30 shows the mean temperature at inlet positions –F and –f in the cases with continuous cold flow injection in phase III. In the main pipeline, the temperature at angular position of 180° has a clear reduction with the decreased flow rate. Compared with the AIPTEC cases, the reversed cold flow can reach the cross-section –F in case 5a but not 5b (compared with Figure 4-29, left). It means AIPTEC can increase the reverse flow in the main pipeline. Similar with the AIPTEC cases, the reduced flow rate in the main pipeline can increase the reverse distance of the cold flow upstream the T-junction. The mean temperature at the cross-section –f shows a different result AIPTEC cases. The hot flow does not reach the cross-section –f in any of the cases with continuous cold flow injection (see Figure 4-30, right).

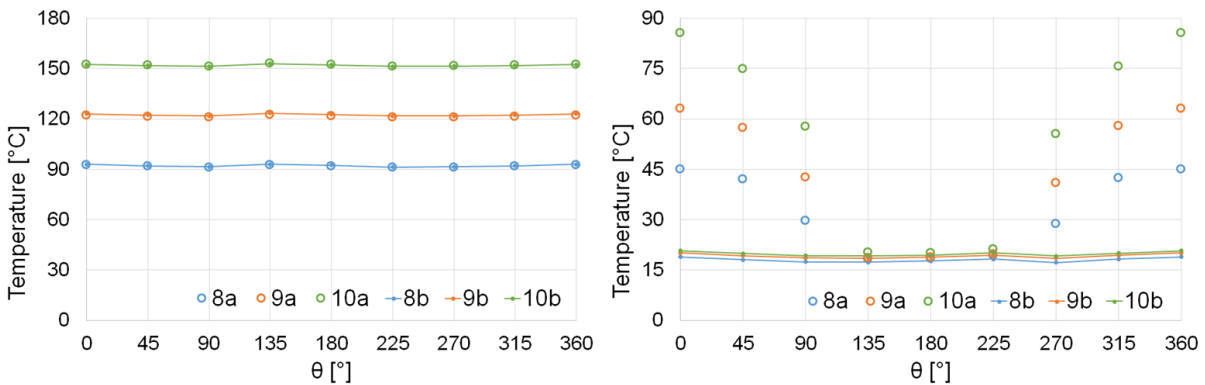


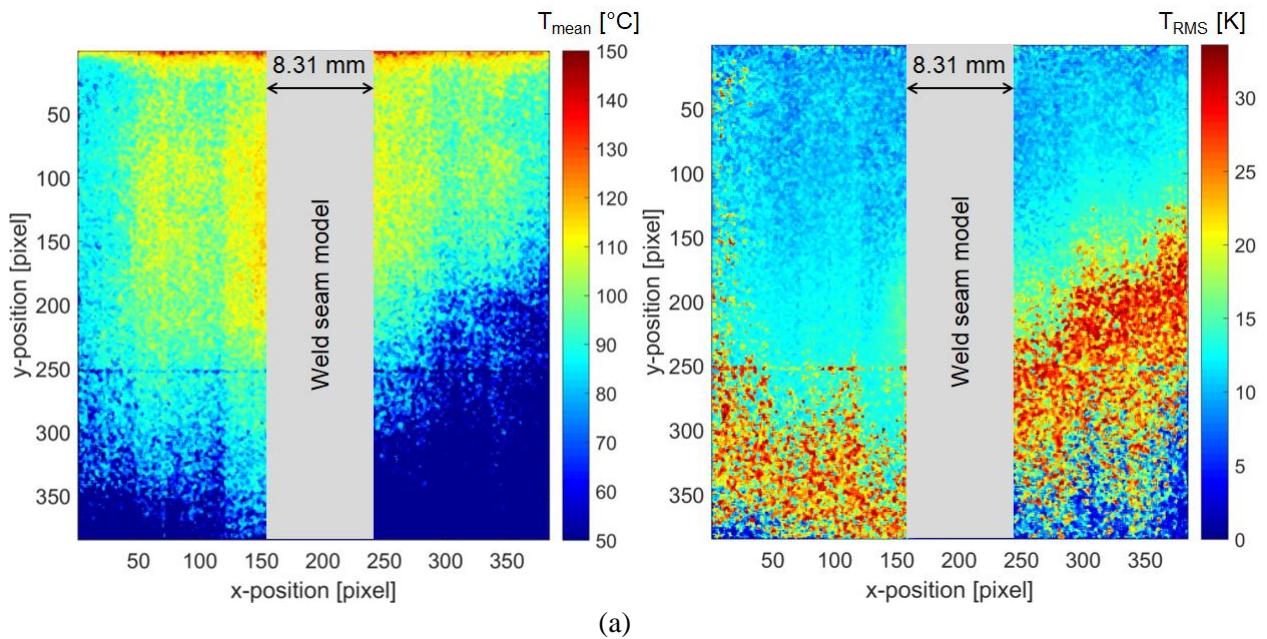
Figure 4-31: Mean temperature in the inlet measurement cross-section –F in main pipeline (left) and –f in branch pipeline (right) upstream the T-junction in the phase IV

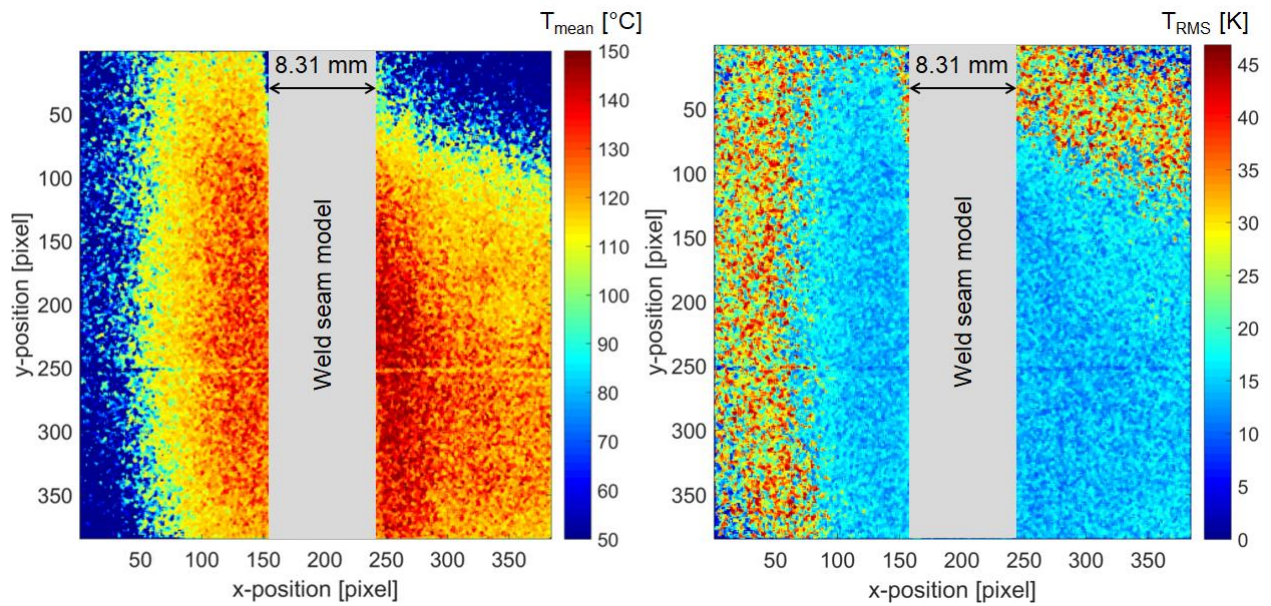
Figure 4-31 shows the mean temperature in the inlet measurement cross-sections in the investigation phase IV. In the measurements with continuous cold flow injection, there no temperature change within these two measurement cross-sections. It indicates that the reverse flow phenomenon in these three cases is very weak, so that the reversed flow cannot reach the measurement cross-section. Even in the cases with AIPTEC, no temperature drop can be at angular position of 0° at measurement position in the main pipe. In the branch pipe, there is a temperature rise in the upper part of the cross-section –f in the AIPTEC cases. It means, AIPTEC can enhance the effect of reverse flow. The temperature in cross-section –f is increased with increased flow temperature in the main pipeline. Considering the results in the phase II, it can be understood the reverse-flow phenomenon (turbulent penetration) is increased with increased temperature difference between the inlet flow.

4.1.4 Influence of weld root on nearby flow field

The influence of the weld root on initiation of thermal fatigue is one of the investigation targets in this work. However, the temperature measurement with micro-thermocouples can only provide a general view of the temperature distribution in the mixing region. Since no thermocouple is installed close to the weld seam (or weld seam model), the influence of the weld root cannot be told from the results of the thermocouple measurement. The NW-LED-IF technique provides a possibility to capture the temporal and spatial temperature distribution in the near-wall flow. And the weld root can be simulated with the weld seam model in the optical module. Therefore, optical measurements with the NW-LED-IF technique have been conducted to investigate the influence of the weld root.

In the NW-LED-IF measurements, the high-speed camera captures the fluorescence intensity in the measurement area with a frequency of 100 Hz, and saves the images with 12 bit. The images have a resolution of 386×386 pixel, which is correlated to an area of 40.1×40.1 mm². With calibration data, images of fluorescence intensity are transferred into temperature distributions. Time averaged temperature and RMS temperature fluctuation are calculated from 180 s measurement. Since the optical module has two horizontal optical window for the measurement, the NW-LED-IF measurements have been performed through both horizontal optical windows. The measurement cases, which are performed at the right side of the flow direction, are referenced with R. For measurement at the left side of flow direction, the cases are referenced with L.





(b)

Figure 4-32: Distributions of mean temperature (left) and RMS temperature fluctuations (right) in the near-wall flow close to the weld seam in case 10L (a) and case 10R (b), flow direction in the image: left to right

Figure 4-32 shows the distributions of the mean temperature and RMS temperature fluctuation in the NW-LED-IF measurement of cases 10R and 10L. As can be seen, the shapes of mean temperature distributions are different to each other, temperature in the mixing flow downstream of the T-junction is not symmetrical. Moreover, the temperature fluctuations in the right side is about 10 K higher than the left side. The NW-LED-IF measurements have also been performed with the boundary condition of case 8 and 9. The results of case 8R and 9R with weld seam model can be found in the Appendix A4.

Figure 4-33 shows the NW-LED-IF measurement results compared with their correlated areas in the thermocouple measurements. With a high spatial resolution, NW-LED-IF measurement can provide much more details of flow temperature close to the weld seam model. In Figure 4-33a, mean temperature of left side shows a similar temperature gradient, but the right side shows a different temperature distribution compared to the thermocouple measurement. In Figure 4-33b, the temperature fluctuations show also a difference. The values of the temperature fluctuation in the NW-LED-IF measurement are higher than the thermocouple measurement. Due to the absence of thermocouple in this area, this high temperature fluctuation cannot be seen in the results of thermocouple measurements.

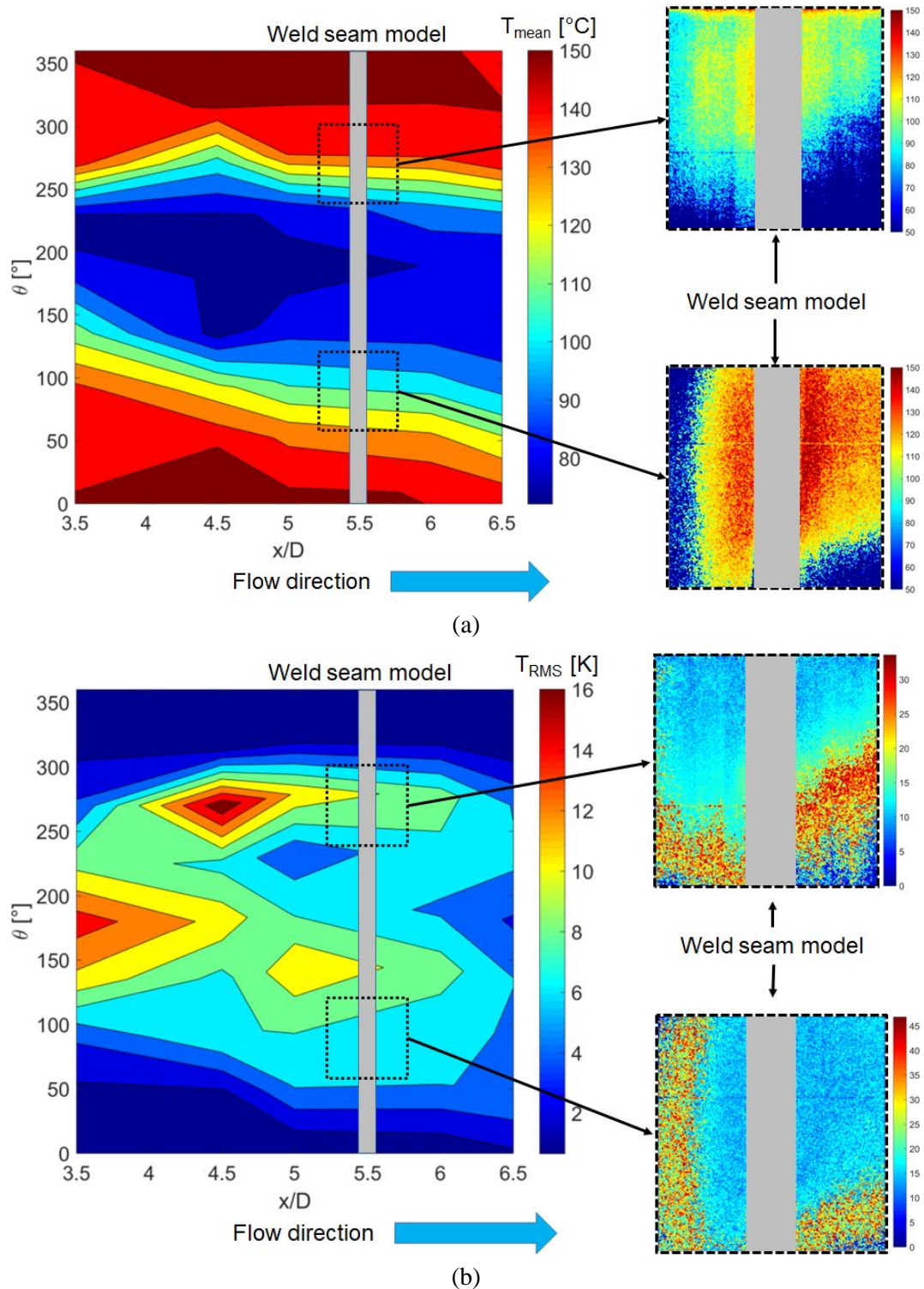


Figure 4-33: Results of NW-LED-IF measurements cases 10L and 10R in comparison with their correlated measurement areas in the thermocouple measurement: mean temperature (a), RMS temperature fluctuation (b)

To discuss the influence of the weld root on the nearby mixing flow, NW-LED-IF measurements have to be performed without weld seam model. Figure 4-34 shows the results of NW-LED-IF measurements without weld seam model in cases 10L and 10R. Compared to the measurements with weld seam model (see Figure 4-32), the shapes of the temperature distributions are all changed. In addition, the general values of temperature fluctuations have been reduced for about 10 K in comparison with the measurement with weld seam model. It indicates the weld root can increase temperature fluctuations in

the nearby mixing flow, so that the potential for material damage close to the weld seam due to thermal fatigue can be increased.

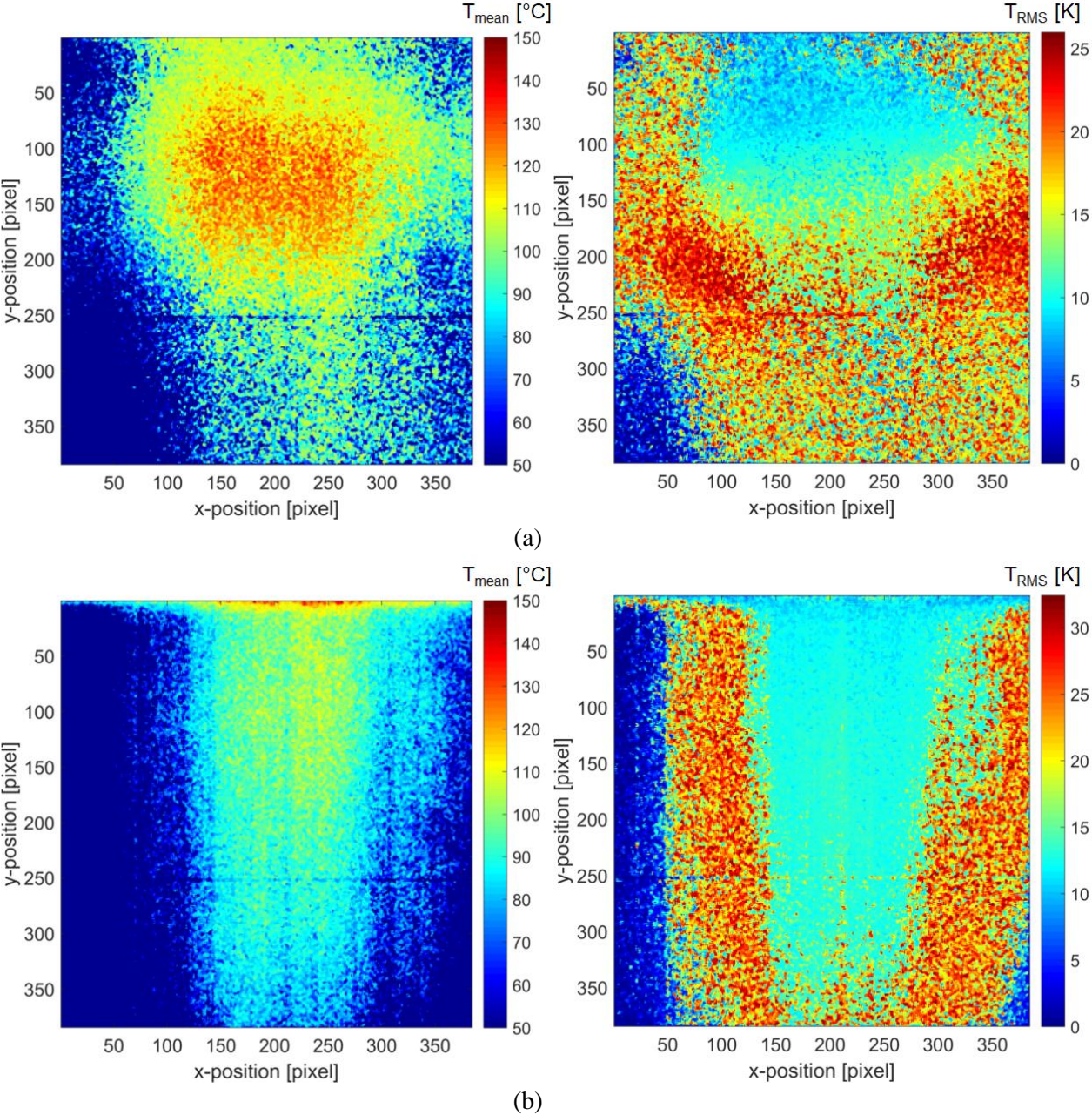


Figure 4-34: Distributions of mean temperature (left) and RMS temperature fluctuations (right) of the NW-LED-IF measurement without weld seam model in case 10L (a) and case 10R (b)

Frequency analysis is also needed for the fatigue assessment. With the advantage of high temporal resolution, the NW-LED-IF measurement can also provide temperature data for frequency analysis. In the minutes NW-LED-IF measurement, temperature data on every pixel in the measurement area has a length of 18,000. Temperature data of 64 monitor points (pixel) in the measurement field have been extracted from the 18,000 images for Fourier-Transformation. The positions of these temperature monitor point are shown in Figure 4-35. These temperature monitor point are referenced as IFTXY (X for the number of column, Y for the number of row).

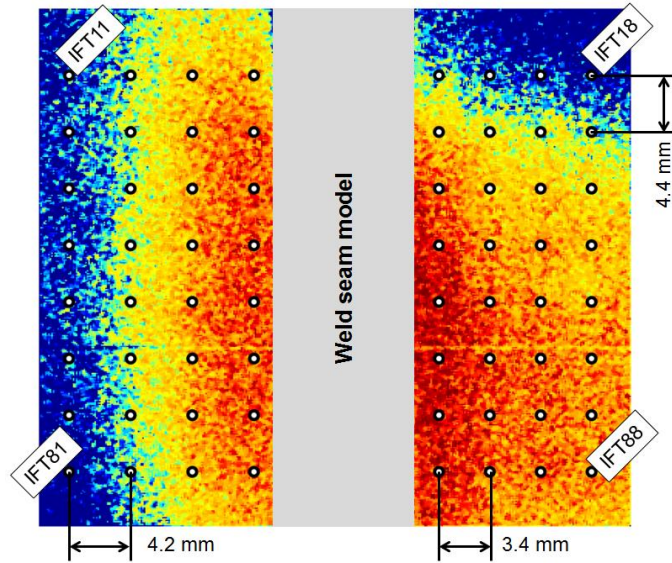


Figure 4-35: Temperature monitor points in the NW-LED-IF measurement area

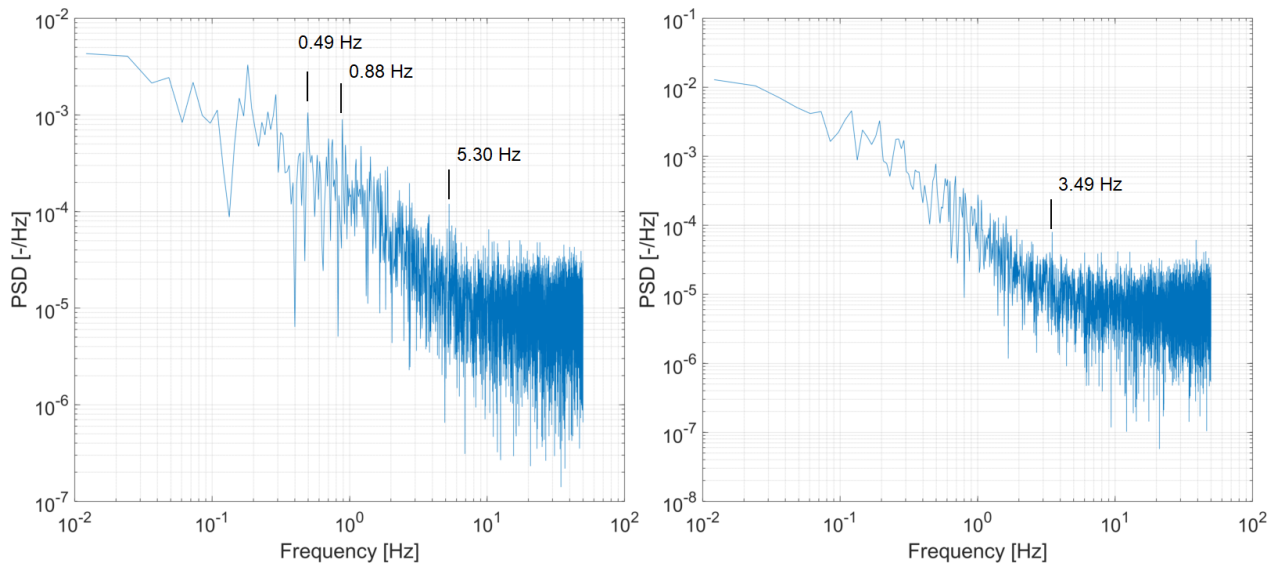


Figure 4-36: PSD diagram of normalized temperature data at IFT34 (left) and IFT67 (right) in case 10R with weld seam model

The extracted temperature data at these 64 monitor points are analyzed with Fourier-Transformation. At several temperature monitor points, regular temperature changes can be found in the spectra. The PSD diagrams of the monitor points IFT34 and IFT67, which are located respectively upstream and downstream of the weld seam model, are shown in Figure 4-36. In both of the spectra, frequency peaks are found in the range of 0.1 – 10 Hz, which is in relevance for thermal fatigue. However, the values of these frequencies and the positions of the monitor points with these frequencies have not shown any regularity. The cause of these frequencies can be the vortex structures in the mixing flow.

Summarize the results of frequency analysis in the measurement area, the monitor points with thermal fatigue relevant frequencies show a clear difference in the cases with and without the weld seam model (see Figure 4-37). In the measurement without weld seam model, several monitor points at the entrance show the frequencies in the thermal fatigue range (see Figure 4-37, left). Only one monitor point (IFT26), which is located far away from the entrance, has shown similar frequencies. It indicates the vortex structures in the mixing flow is breaking, while the mixing fluid flows through the measurement area. In the measurement with weld seam model (Figure 4-37, right), more monitor points downstream of the weld seam model have shown such frequencies for thermal fatigue. It means the weld root has created

more vortex structures in the nearby mixing flow. With this comparison, it is proved from the viewpoint of thermal hydraulics that the rimmed weld root can increase the possibility of material damage due to thermal fatigue. Hence, it is reasonable to grind down the weld root close the T-junction in the piping system to avoid the fatigue damage.

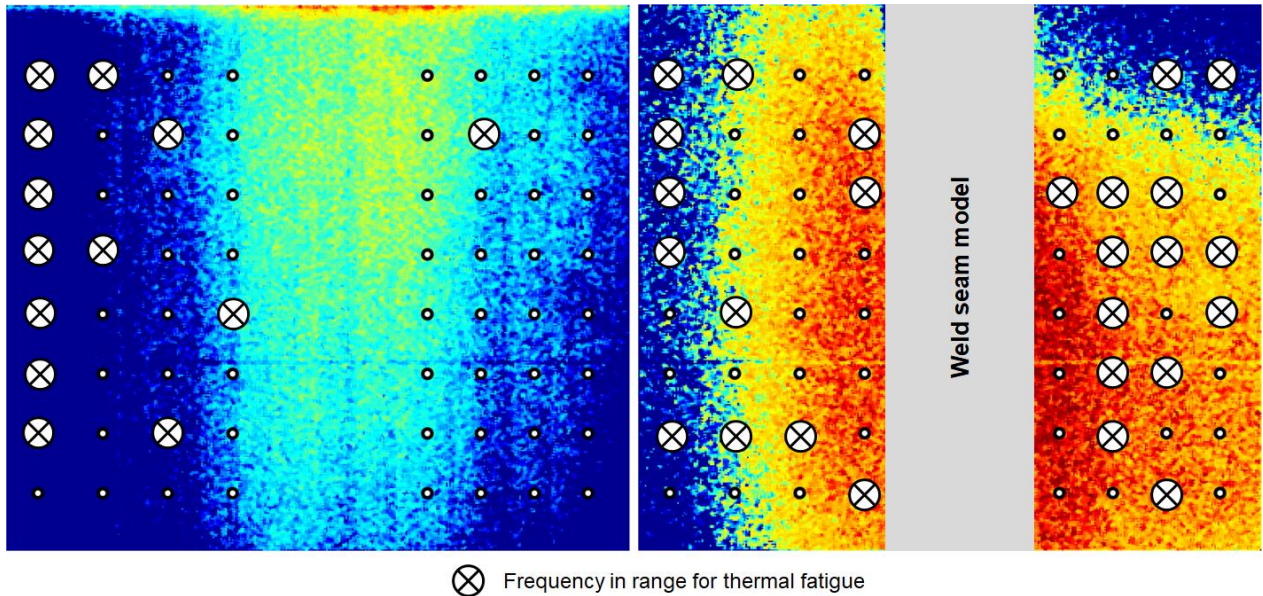


Figure 4-37: Summary of the frequency analysis results in the NW-LED-IF measurement in case 10R without (left) and with (right) weld seam model

The NW-LED-IF measurements have also performed with the case 8 and case 9 to check the influence of the varied temperature in the main pipeline. The results of these two cases can be found in appendix.

4.1.5 Velocity profiles in inlet flow streams

The velocity profiles in the inlet flow streams are investigated by using PIV technique. The optical modules are installed upstream the T-junction in the PIV measurements. The optical window for PIV measurement at the branch pipeline is located between $-8d$ and $-10d$ upstream the T-junction. Since neither the reversed hot flow reaches the optical measurement area (see Figure 4-31, right) nor thermal convection exists in the container of the optical module during the measurement, PIV measurement in the branch pipeline is not disturbed by temperature gradient. Therefore, it is not necessary to perform BOS for the PIV measurement in the branch pipeline. Figure 4-38 shows the velocity profiles at $-9d$ position in the PIV measurement at the branch pipeline. Since the PIV measurements are performed with continuous cold flow injection, the case numbers are also referenced with b. Generally, the velocity profiles indicate a low turbulent flow in the branch pipe, which can also be understood by the Re-number of the branch pipe flow (see Table 4-1). Among the vertical velocity profiles, case 10b has a more symmetrical profile than the other two cases. The horizontal velocity profiles in these three cases remain almost the same, and the shapes of the velocity profiles are quite symmetric. Thus, varied temperature in the main pipeline shows a minimum influence on the velocity profiles in the branch pipeline.

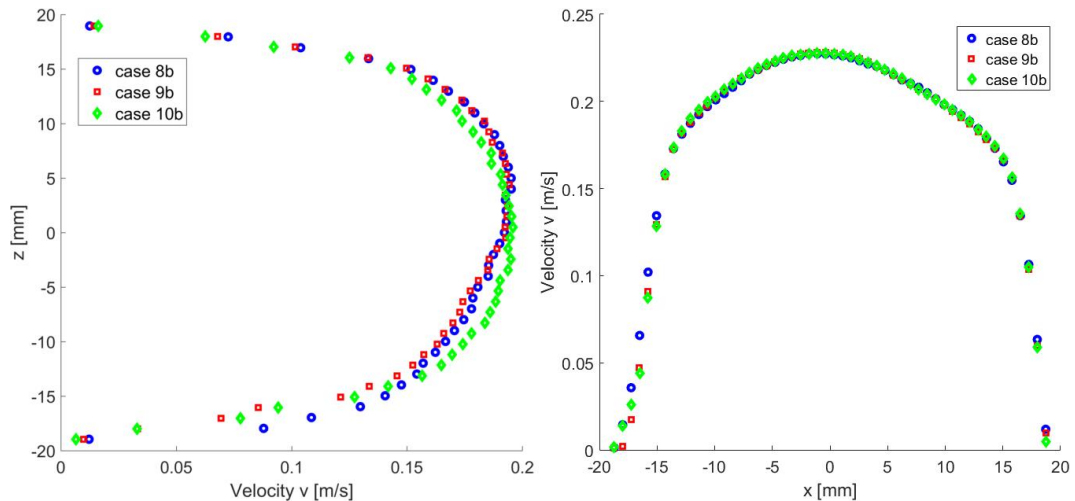


Figure 4-38: Vertical (left) and horizontal (right) velocity profiles at -9d position upstream the T-junction in the branch pipe flow

The optical measurement area of the PIV measurement in the main pipeline is located between -5D and -6D upstream the T-junction. Optical distortions exist in the PIV measurement on the main pipe flow. However, according to the thermocouple measurement results, the reversed cold flow in the main pipeline does not reach the optical window (see Figure 4-31, left). The optical distortion is only occurred by the thermal convection in the optical module, which can be reduced by using BOS technique.

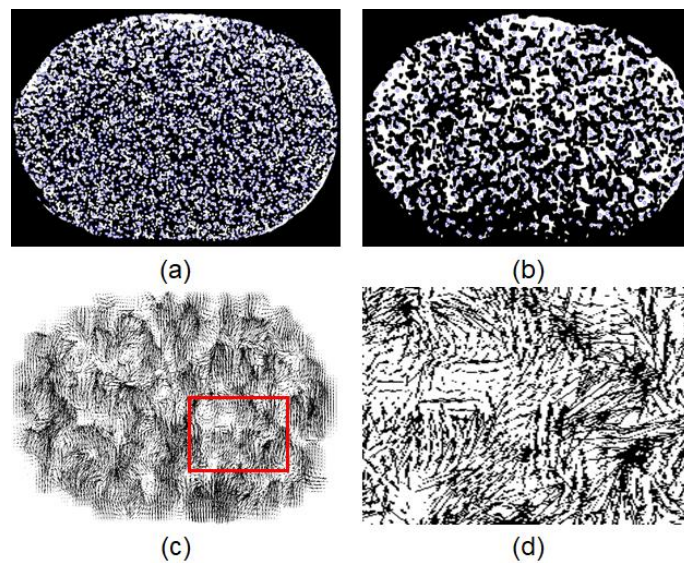


Figure 4-39: Enhanced images of the dot pattern without optical distortion (a), with optical distortion in case 10b with the flow temperature of 150° C (b), the correlated vectors of the dots shift (c) and its details (d)

In the first step of the BOS measurement, image of the dot pattern has been taken without optical distortion (cold condition at FSI test facility, see Figure 4-39a). In the second step, the FSI test facility is heat up to the measurement condition. Images of the dot pattern have been taken with optical distortion (see Figure 4-39b). The captured dots have been enhanced by digital image processing and compared with the image without optical distortion. The shifting vectors of the captured dots can be generated by cross-correlation process of the PIV software (see Figure 4-39c and d). With these shifting vectors, the optical distortions in the PIV measurements by the same measurement condition can be reduced. Moreover, no vector gap can be detected in the lower part of the vector field (Figure 4-39c), which

means no thermal interface in the measurement area. This is another proof that the reversed cold flow does not reach the measurement area.

Figure 4-40 shows the velocity profiles at the $-5.5D$ position in the vertical and horizontal cross-sections in PIV measurement in the main pipe flow. Firstly, the shapes of the velocity profiles indicate a turbulent pipe flow in the inlet of the main pipe, which can be proved by the associated Re-numbers in these cases (see Table 4-1). Secondly, the shapes of velocity profiles in these cases are all not symmetrical. In the vertical measurement cross-section, the velocity in the lower part of the flow is higher than the upper part. Among the horizontal velocity profiles, there is velocity reduction at the left side of the flow. In addition, the change of the flow temperature in the main pipeline has a small influence on the vertical velocity distribution and almost no influence on the horizontal velocity profiles.

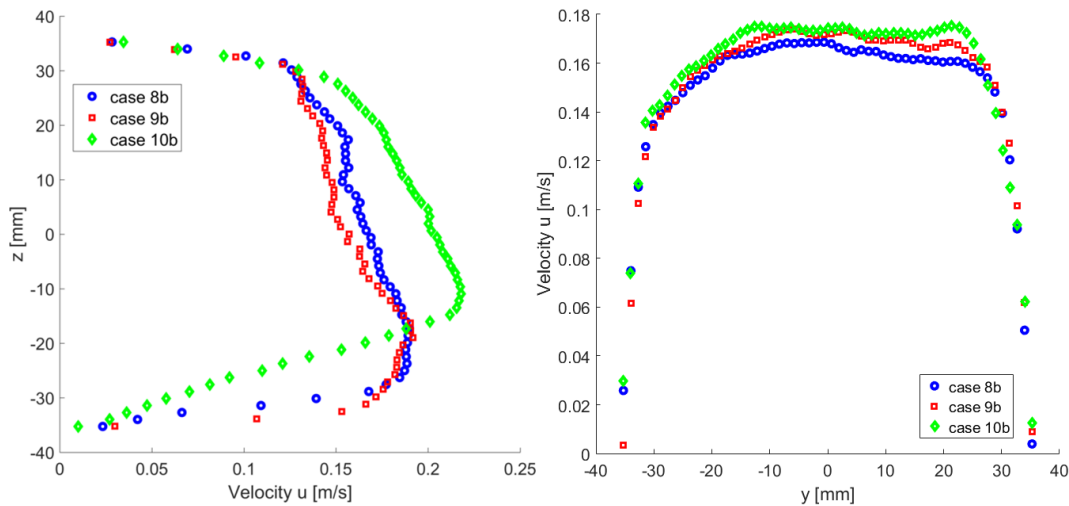


Figure 4-40: Vertical (left) and horizontal (right) velocity profiles at $-5.5D$ position upstream the T-junction in the main pipe flow

4.1.6 Harmonic oscillation of thermal stratification in pipe tangential direction

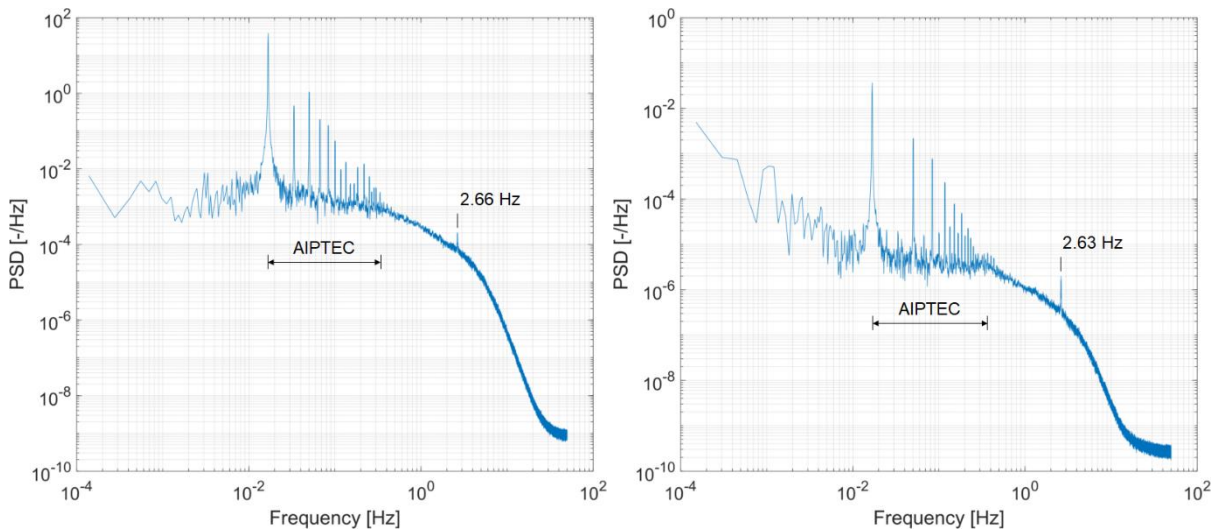


Figure 4-41: Power spectrum density (PSD) of the normalized temperature signals at measurement position FT30 ($6.5D$, $\theta = 225^\circ$, left) in case 2a and FT31 ($6.5D$, $\theta = 270^\circ$, right) in case 7a

Frequency analysis is an important step in the fatigue assessment based on the temperature measurement data. The PSD diagrams of normalized temperature at measurement positions FT30 in case 2a and FT31

in case 7a are shown in Figure 4-41 as example. The basic frequency of 0.0167 Hz is correlated to the period of the valve switching (60 s) in the experiments. The basic frequency and its related frequencies indicate the effect of AIPTEC. The peaks of the additional low frequency can also be found in these two PSD diagrams. Similar frequencies have also been found at several other positions and in the many of the other cases. However, there is a small deviation between the values of the additional low frequency among the cases. However, it can be believed that this small deviation does not appear due to any kinds of contingency. For an overview of the additional low frequencies in the experimental results, the experimental parameters and the values of the additional frequencies are summarized in Table 4-10 [118].

Table 4-10: Values of the addition low frequency in the measurement cases

Case No.	Pressure [bar]	T_m [°C]	\dot{M}_m [kg/s]	T_b [°C]	\dot{M}_b [kg/s]	Value of add. low frequency [Hz]
F/G	75	265	0.56	20	0.2	2.66
S	75	265	0.56	20	0.2	2.56
1	75	160	0.6	20	0.2	2.66
2	75	200	0.6	20	0.2	2.66
3	75	240	0.6	20	0.2	2.66
4	75	200	0.6	20	0.1	-
5	75	200	0.5	20	0.2	2.66
6	75	200	0.4	20	0.2	2.64
7	75	200	0.3	20	0.2	2.63
8	30	150	0.6	20	0.2	-
9	30	120	0.6	20	0.2	-
10	30	90	0.6	20	0.2	-

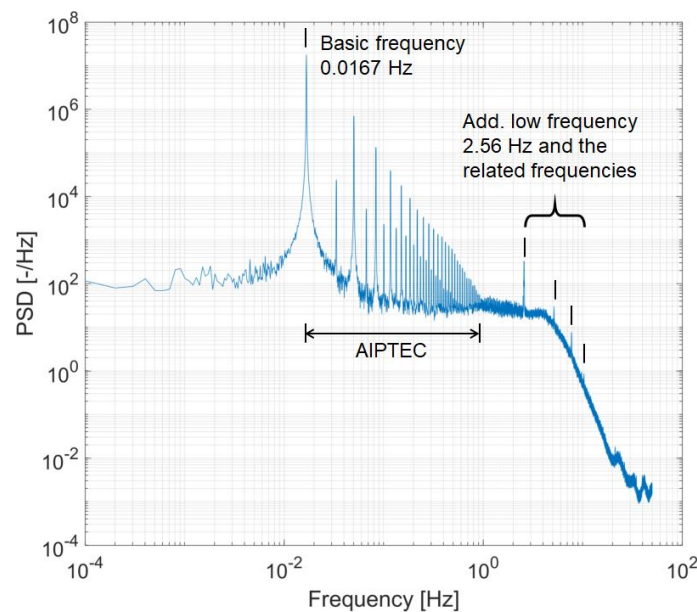


Figure 4-42: PSD diagram of the normalized temperature data at FT5 (1.7D, 180°) in the measurement downstream of shock module with 30 s/30 s AIPTEC (case S)

Firstly, the additional low frequency can be found only at the measurement positions in the mixing region downstream of the T-junction (or 25° shock module) but not the measurement positions in the inlet flow upstream the mixing tees. It means that the additional low frequency is a property only of thermal mixing flow. Secondly, the additional low frequency is a property of a periodical motion in the mixing flow. Similar with AIPTEC in the frequency spectrum, a periodical temperature change should show its related frequencies ($\times 2, \times 3, \times 4, \dots$ of the additional low frequency) in the spectrum. However, the related frequencies can be clearly recognized only with long enough temperature data for frequency analysis. The measurements downstream the T-junction have mostly 200000 – 300000 temperature data points, which are not long enough to show the related frequencies in the spectra. However, with 2 million of the temperature data points, such related frequencies can be clearly seen in the spectra of the measurements with shock module (case S, see Figure 4-42).

In the third, the values of the additional low frequencies match the calculation with the principle of the mathematic pendulum. For a simple pendulum swinging within $\pm 5^\circ$, the period of the oscillation can be calculated with the equation (E4-4).

$$T_0 = 2\pi \sqrt{\frac{l}{g}} \tag{E4-4}$$

If the swing motion is the tangential direction of the main pipe cross-section and captured by the micro-thermocouples, the length of the pendulum is equal to the main pipe radius ($R = 35.9 \text{ mm}$) minus the distance of the thermocouple measurement point from the pipe inner wall, which is about one millimeter at the FSI test facility. Thus, the frequency of this harmonic oscillation within $\pm 5^\circ$ can be calculated as 2.6667 Hz, which matches the values of the additional low frequency in most of the cases (see Table 4-10).

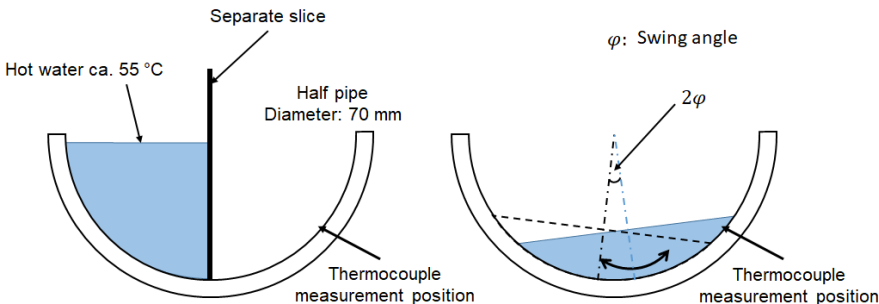


Figure 4-43: Principle of the test setup for tangential oscillation in a pipe

For proving the frequency caused by tangential oscillation in a pipe, an experiment is conducted with a small-scale test setup (see Figure 4-43). It is a half-pipe with radius of 35 mm and length of about 300 mm. For preparing the test, a separate slice is put in the middle of the half-pipe. One side of the half-pipe is filled with hot water about 55 °C – 65° C. In the other side of the half-pipe, micro-thermocouples are installed on the inner surface of the pipe. The distance of the thermocouple measurement point to the pipe inner surface can be neglected. After the temperature recording is started, the separate slice is moved up very fast. The hot water oscillates in the half-pipe in the tangential direction for a few seconds. The micro-thermocouples capture the water temperature with 100 Hz. Figure 4-44 shows the results of this small-scale swing test. Two micro-thermocouples are installed at different positions on the half-pipe. Periodical temperature change can be seen in the temperature signals. In the PSD diagram of the temperature data, a frequency peak of 2.667 Hz can be found and matches the calculation with equation (E4-4). This agreement proves the additional low frequency is created by tangential oscillation in the

mixing flow. The only possibility for such oscillation in the mixing flow must be the thermal stratification.

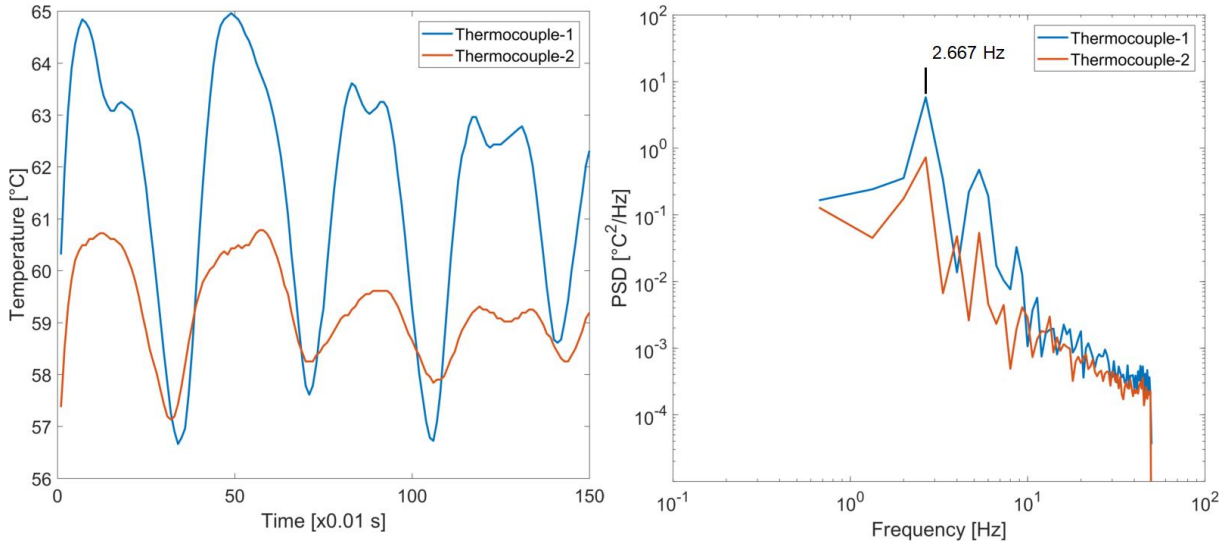


Figure 4-44: A segment of the temperature signals in the swing test (left) and the PSD diagram of these temperature signals (right)

According to the results of the swing test, the additional low frequency can be found only with stable enough stratified flow in the mixing region. Oppositely in cases 8, 9 and 10, Ri-numbers of the mixing flow are very low (see Table 4-9), which indicates the thermal stratification are very unstable. The effect of heat exchange (convection) takes the leading role in the mixing region. The heat exchange in the mixing flow is so strong, that the tangential motion of the thermal stratification are broken up. Therefore, no additional frequency has been observed in these three cases.

However, the values of additional low frequency in several cases have deviations with the calculated frequency. To explain this deviation, the initiation of the tangential oscillation must be discussed. Thermal stratification in the mixing flow is created due to the density difference of the hot and cold flow in main respectively branch pipeline. The initiation of its tangential oscillation leads back to the trace of the cold flow in the T-junction YZ-cross-section. At horizontal oriented T-junction, the trace of the cold flow can be simplified and separated into the motion in y- respectively z-directions. If the cold flow hits the inner wall of the main pipe in the T-junction, the cold flow will start to oscillate in the pipe tangential direction due to the pipe geometry and gravity. Otherwise, if the cold flow does not reach the main-pipe wall, the oscillation cannot be initiated. In case 4, the stratified flow is stable in the mixing region. However, the flow rate in the branch pipe is only 100 g/s (see Table 4-10). With such low kinetic energy, the cold flow in the branch pipe cannot hit the inner wall of the main pipe, so that the tangential oscillation has not been initiated. Thus, no additional low frequency has been observed in case 4.

Figure 4-45 shows the simplified trace of the cold flow in the main pipe cross-section. The angular position of the hit point of the branch pipe flow on the main pipe inner wall, which is defined as initial angle α , has the impact on the tangential oscillation and the value of the additional low frequencies. The movement of the cold flow in the main pipe cross-section at T-junction can be calculated with equations (E4-5) and (E4-6). It can be understood that the initial angle depends on the cold flow velocity v_{b_y} in combination with the local fluid density at the T-junction ρ_T .

$$Y: y = D/2 - v_{b_y} \cdot t \quad (\text{E4-5})$$

$$Z: z = (\rho_T - \rho_b) / \rho_b \cdot t^2 \quad (\text{E4-6})$$

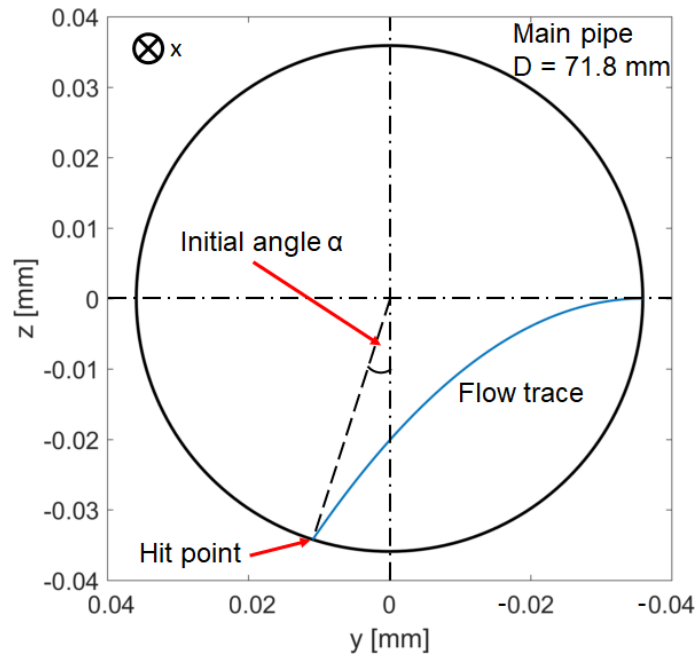


Figure 4-45: Initial angle of the tangential oscillation

The initial angle is however not the swing angle φ of the oscillating stratification. But with higher initial angle, the swing angle φ will be larger. For the oscillation higher than $\pm 5^\circ$, the expanded equation (E4-7) for oscillation period of simple pendulum can be applied [119].

$$T(\varphi) / T_0 = \sum_{n=0}^{\infty} \left[\frac{(2n)!}{(2^n \cdot n!)^2} \right]^2 \sin^{2n}(\varphi/2) \quad (\text{E4-7})$$

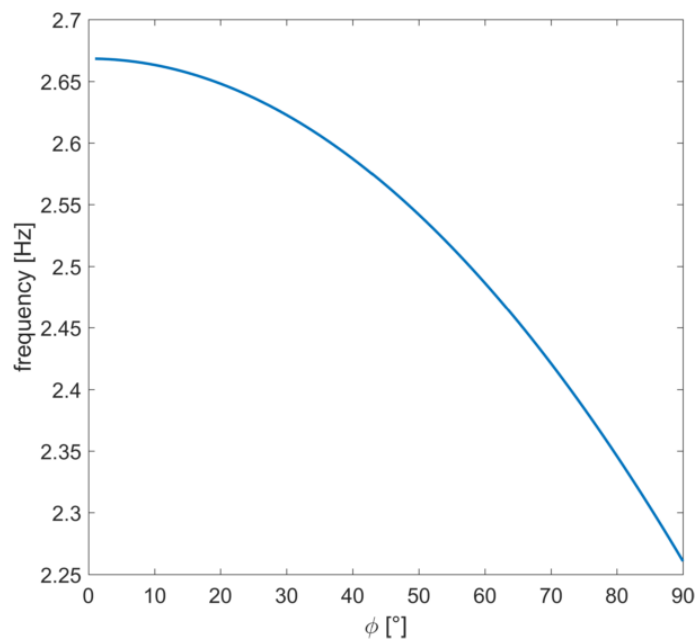


Figure 4-46: Frequency of tangential oscillation in the main pipeline as function of swing angle φ

For swing motion higher than $\pm 5^\circ$, equation (E4-7) shows that the duration of the swing period only depends on the swing angle φ . With the geometry of the TC-module at FSI test facility, the frequency of the tangential oscillation as function of the swing angle in range $1^\circ - 90^\circ$ is shown in Figure 4-46. As can be seen, the value of the additional low frequency decreases with increased swing angle.

From case 5 to case 7, the flow rate in the main pipeline is decreased (see Table 4-10). An increased reverse flow is observed with the decreased flow rate in the main pipe upstream the T-junction (see Figure 4-29 and 4-30). It indicates that the temperature in the T-junction is decreased and flow density is increased. With constant flow velocity and temperature in the branch pipe in these cases, the initial angle can be calculated as function of local fluid density in the T-junction ρ_T . And the initial angle increases with increased fluid density in the T-junction. Since the swing angle φ is proportional to the initial angle, the swing angle increases with the reduced fluid temperature in the T-junction. Therefore, with the chain of this relation, it can be understood that swing angle is increased with the reduced flow rate in the main pipe in cases 5 – 7. Hence, the value of the additional low frequency is decreased in these three cases, which matches the experimental results in Table 4-10.

In case S, the experiment is performed with 25° shock module. The cold flow velocity in y-direction is calculated as $v_{by} = v_b \cdot \sin(25^\circ)$. However, the temperature in the shock module can be as high as the temperature in the main pipe flow in this case (265°C). With equations (E4-5) and (E4-6), the hit point of the cold flow is located at the same side of the branch pipe with a very high initial angle (approximately 40°). Hence, the additional low frequency in the case S is much lower than the cases with 90° T-junction. An additional jet test has been performed on the half-pipe setup to compare the swing angle in the cases with different hit point of the cold flow on the pipe wall. Results of the jet test, which can be found in appendix A5, can help to understand the high swing angle in the case S.

Moreover, due to the tangential oscillation in the mixing flow, a S-shaped (snake path) path can be created in the lower part of the mixing flow. A segment of the snake path can be identified in the reconstructed circumferential temperature distributions in the thermocouple measurement (see chapter 4.1.1 and 4.1.2). This spatial temperature distribution in the mixing flow have also been observed in the previous CFD simulations [79]. The snake path is also one of the typical mixing characteristics in the horizontal T-junction. All the cases with additional low frequencies must have the snake path in the lower part of the mixing flow. But some cases with snake path in the mixing region may not show additional low frequency.

Furthermore, the tangential oscillation of the thermal stratification can create a regular temperature change at both edges of the thermal interface. The pipe wall area, which has direct contact with the thermal interface, will encounter the regular temperature change due to the tangential oscillation. The frequency of this regular temperature change due to the tangential oscillation is the additional low frequency, which is in the frequency range for thermal fatigue. Therefore, this pipe wall area has a high potential for material damage due to thermal fatigue. For the safety of the piping system, the tangential oscillation of thermal stratification must be avoided. In the current experimental work, the pipe wall area, which has the regular temperature change due to the tangential oscillation, cannot be determined with discretely installed thermocouples. However, it is illustrated with the results of the numerical simulation and presented in the next chapter.

4.2 Results of numerical simulations

4.2.1 Maximum operation condition at FSI test facility

4.1.1.1 AIPTEC (case F)

The maximum operation condition is the most representative experiment at the FSI test facility. On one hand, the experiments with this condition are conducted with the highest temperature difference between the inlet flow streams, and therefore can create the highest temperature fluctuation in the mixing flow. On the other hand, the typical mixing phenomena like turbulent penetration and harmonic oscillation of thermal stratification in pipe tangential direction have been observed in these experiments. Hence, the simulations on the experiments with the maximum operation condition are performed with the first priority. The simulations are conducted by using LES method on the experiment with AIPTEC (case F) and continuous cold flow injection (case G) respectively. A numerical grid with 17 million nodes is applied in these calculations. Each calculation has been performed with 1680 processors. The results of the simulation are compared with the experiments and presented in this chapter.

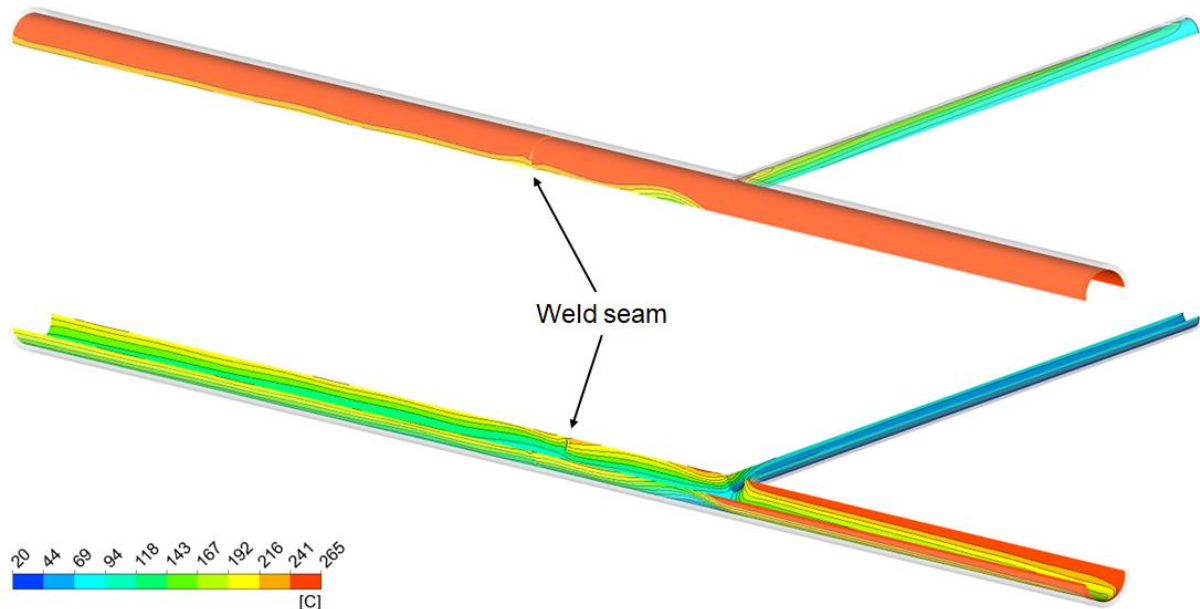


Figure 4-47: Time-averaged temperature distribution in the fluid-structure interface in the LES results of case F

The LES calculation on case F has been performed with a physical time of 250 s. The simulation results of the last 220 s have been taken for analysis (see Figure 3-6). The time-averaged temperature distribution in the fluid-structure interface in case F is shown in Figure 4-46. As can be seen, the temperature in the upper part of the main pipeline remains as high as the maximum temperature of 265 °C. In the lower part of the main pipeline, low temperature about 100 °C can be seen downstream of the T-junction and indicates that the flow streams are not mixed completely. In the main pipeline upstream of the T-junction, the reverse cold flow reaches almost the entrance of the hot flow in the domain of the simulation. In the branch pipeline, temperature difference can be seen between the upper and lower part, which indicates the increased temperature in the branch pipeline due to turbulent penetration, during the time the cold flow flows through the bypass.

Cross-sectional views of the time-averaged temperature are carried out within the simulation domain and presented in Figure 4-48. The cross-sectional views consist the simulation domain about $-5D$ to $7D$ in the main pipeline and $-8d$ in the branch pipeline upstream the T-junction. The temperature distribution

in the pipeline is set 30% transparent. In the XZ-plane, vertical temperature gradient can easily be recognized. It indicates the thermal stratification downstream and the reverse flow upstream of the T-junction. In the XY-plane, a spatial periodical temperature distribution, which is created by the harmonic oscillation of thermal stratification in pipe-tangential direction, can be found downstream of the T-junction. In this spatial periodical temperature distribution, the regions with high temperature (over 240 °C) and low temperature (about 190 °C) are located oppositely in the horizontal (XY-) plane. And these two regions exchange the side in every section with a length of 2D. Compared to the circumferential temperature distribution, such kind of periodical temperature distribution matches the S-shaped cold flow path (snake path), which is also created by the tangential oscillation of thermal stratification. The turnings of the snake path is located in the low temperature region of the XY-plane. In this Figure, three snake-path turnings can be found in the mixing flow downstream of the T-junction. According to the construction of the FSI test facility, the first turning is located at position about 1.5D, which is located in the T-junction and has no thermocouple measurement position. The second turning is located at position barely enough to 3.5D and can be captured by the thermocouples at 3.5D. The third turning is located close to the weld seam at 5.5D, where no thermocouple is installed. Therefore, the snake path of the cold flow in case F cannot be recognized in the reconstructed circumferential temperature distribution of the experimental results (see Figure 4-14, right). In the YZ-plane, vertical temperature gradient can be seen in the branch pipeline. Generally, the temperature distribution matches the experimental results. It proves the turbulent penetration of the hot flow in the branch pipe during the time of bypass. The flow in the lower part of the branch pipeline remains cold at 20 °C, which is about 11 K lower than the result in the experiment (compare to Figure 4-27, right).

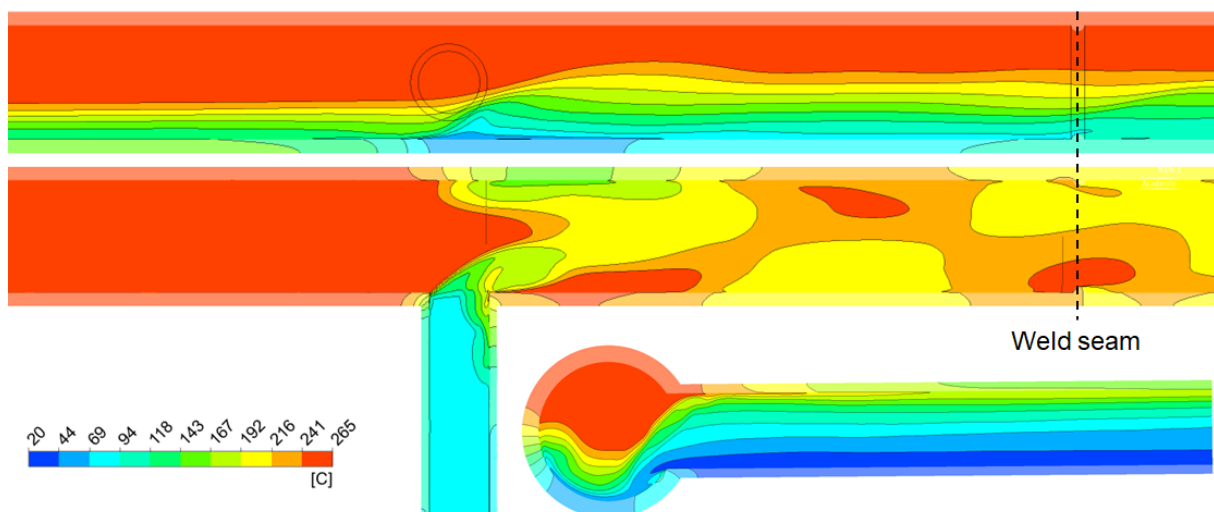


Figure 4-48: Cross-sectional views of the time-averaged temperature in the XZ- (top), XY- (middle) and YZ- (bottom) planes in the LES result of case F

The cross-sectional views of the RMS temperature fluctuation in the fluid domain of the LES results are shown in the Figure 4-49. In the complete mixing region at T-junction, the temperature fluctuation can reach the maximum of about 115 K in the position, where the main and branch pipeline are connected. Except this area, high temperature fluctuation (approximately 90 K) can also be found in the upper part of the flow region in the branch pipeline. It is created by periodical switching of the cold flow injection and the turbulent penetration of the hot fluid in the branch pipeline during the bypass time. Generally in the main pipeline, temperature fluctuation about 35 K can be found in the lower part of the flow upstream of the T-junction, which is created due to the reverse flow phenomenon. In the mixing region downstream of T-junction, an area with high temperature fluctuation (about 100 K) is located oppositely to the branch pipeline. Downstream of this area, the temperature fluctuation decreases along the flow direction in the main pipe. Heat exchange within the mixing flow is stabilized by the thermal stratification. Moreover, a flow region with temperature fluctuation of about 50 K can be seen close to

the weld seam in the XY-plane at the left side of the flow direction. The possibility for thermal fatigue in the piping material close to this flow region can be very high.

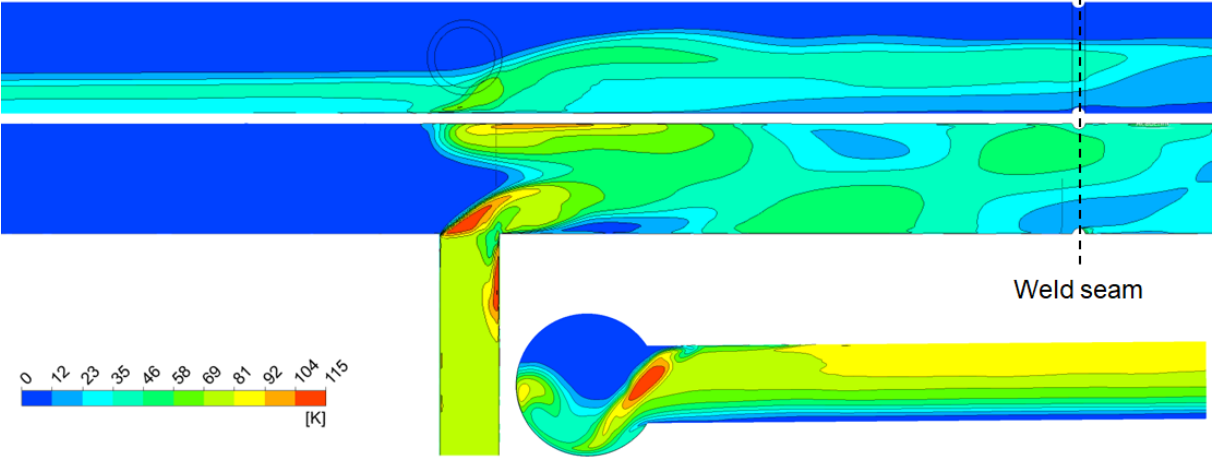
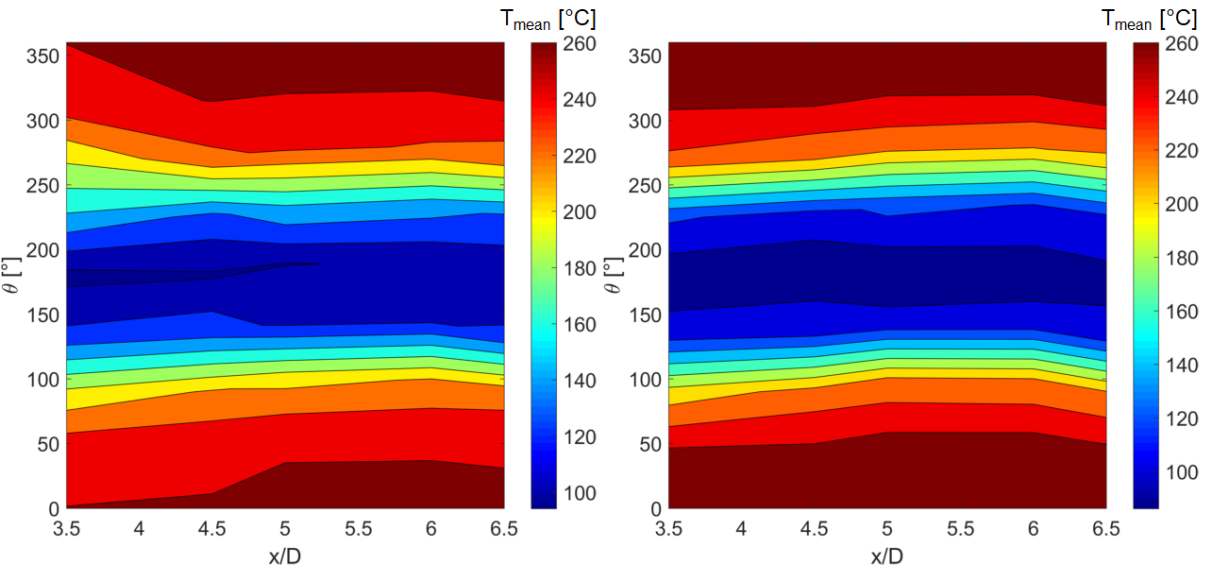
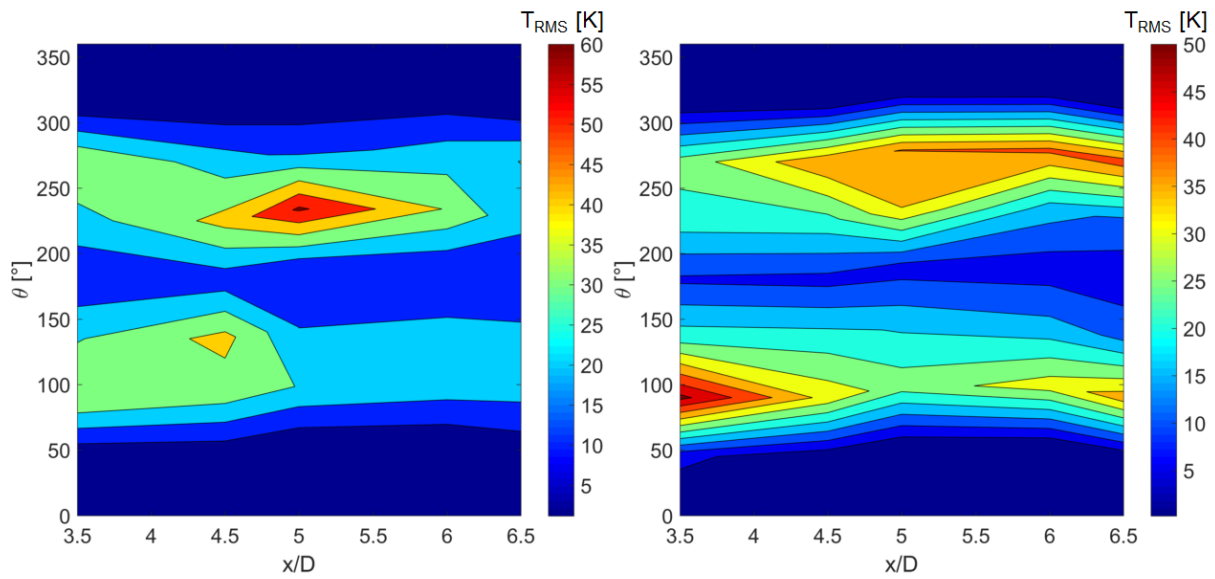


Figure 4-49: Cross-sectional views of the RMS temperature fluctuation in the XZ- (top), XY- (middle) and YZ- (bottom) planes in the LES result of case F

Temperature monitor points have been defined at measurement positions where micro-thermocouples have been installed in the experiment (see Figure 2-17). Temperature data have been recorded in the simulations to be compared with the experimental results. With the same analysis procedure for experimental data, the circumferential distributions of the mean temperature and the RMS temperature fluctuation have been reconstructed from the temperature monitor data of the LES calculation (see Figure 4-50). Compared to experimental results, the circumferential mean temperature distribution matches well with the experimental results (see Figure 4-50, a)). A thermal stratification of the mixing flow can be seen in the section 3.5D to 6.5D. The RMS temperature fluctuation is different (see Figure 4-50, b)) because the position of the maximum temperature fluctuation differs from the experimental results, and the value of the maximum temperature fluctuation is about 10 K lower than the experiment. However, the areas with high temperature fluctuation are all located on both horizontal edges of the thermal interface in the stratified mixing flow, which indicates a stable thermal stratification in the mixing region. In addition, at the position of the weld seam (5.5D), the temperature fluctuation at the left side is higher than the right side of the flow direction, which matches the experimental result and the distribution of temperature fluctuation in the XY-cross-section (see Figure 4-49).



(a)
91



(b)

Figure 4-50: Reconstructed circumferential distribution of mean temperature (a) and RMS temperature fluctuation (b) of LES (right) in comparison with experiments (left)

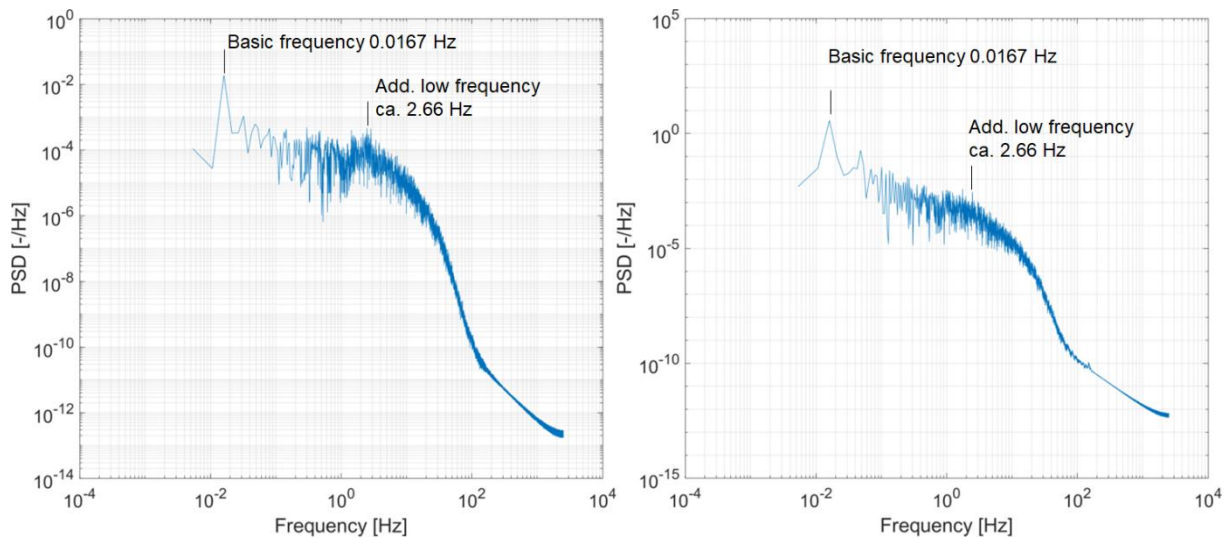


Figure 4-51: PSD diagrams of the normalized temperature at temperature monitor point FT2 (left, position: 3.5D, $\theta = 45^\circ$) and FT15 (right, position: 4.5D, $\theta = 270^\circ$)

Frequency analyses have been performed also with the temperature data from monitor points. The PSD diagrams of the normalized temperature data at monitor points, FT2 and FT15, are shown in Figure 4-51 as examples. The PSD diagrams are generated with 150 data sets from the original temperature data by using of average method [52]. The basic frequency of AIPTEC 0.0167 Hz can be identified in the PSD diagrams. However, related frequencies to the basic frequency, which indicate the periodical temperature changes in the mixing flow, cannot be recognized in the PSD diagram. Since the physical time of the simulation has a length less than four periods, the temperature data is not long enough to create significant peaks of the periodical temperature change in the frequency spectrum. The additional low frequency about 2.66 Hz identifies the harmonic oscillation of thermal stratification in pipe-tangential direction in the mixing flow. In the simulation results, this frequency cannot be easily found in the PSD diagrams (see Figure 4-51). The peaks of the additional low frequency are not so clear as those in the experimental results. And the values of those peaks have deviations (about 0.01 Hz – 0.03 Hz) to the calculated value of the additional low frequency. Moreover, the positions, where the additional low frequency can be seen, are also different to the experiment. However, the additional low

frequency is located in the frequency range for thermal fatigue, which indicates these positions have a high potential for material damage due to thermal fatigue.

4.1.1.2 Continuous cold flow injection (case G)

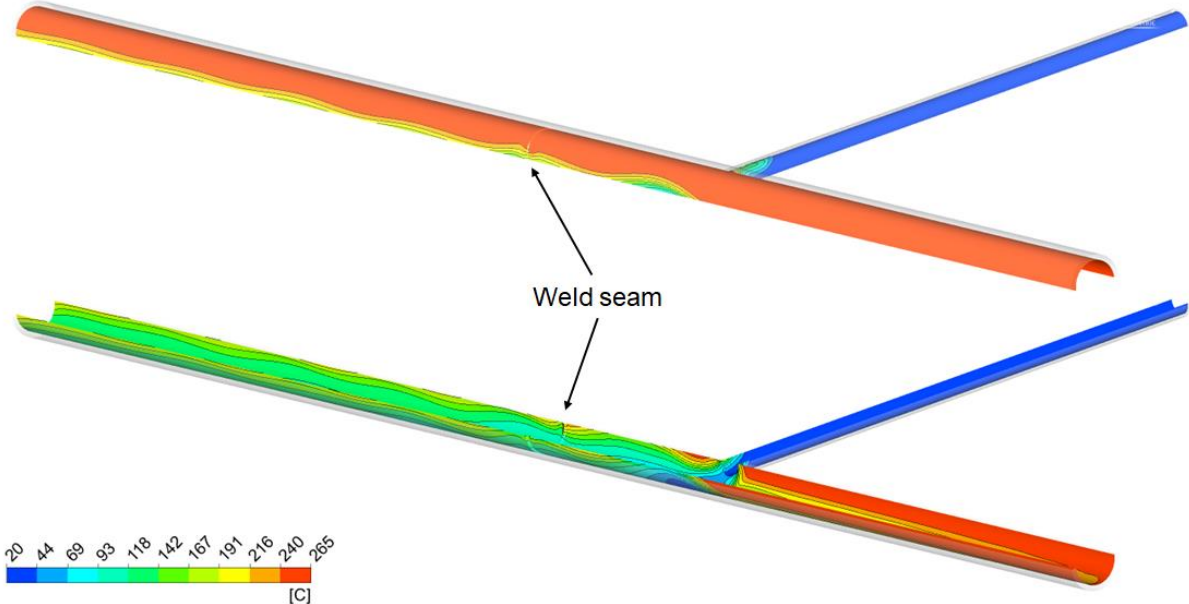


Figure 4-52: Time-averaged temperature distribution in the fluid-structure interface in the LES results of case G

The time-averaged temperature distribution in the fluid-structure interface of case G is shown in Figure 4-52. A significant difference to the case with AIPTEC (case F) is that the temperature in the branch pipe remains at the inlet temperature of 20 °C (compare to Figure 4-47). The hot flow penetrates only a small distance in the branch pipeline. The temperature distribution in the main pipeline is almost the same with case F. Thermal stratification can be seen downstream of the T-junction and reverse flow can be seen upstream of the T-junction.

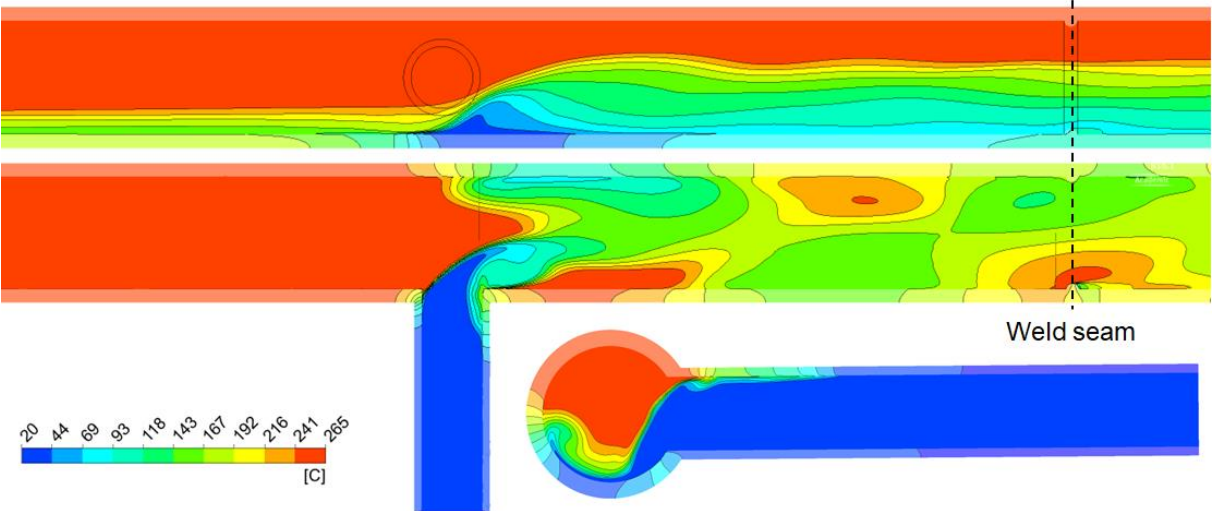


Figure 4-53: Cross-sectional views of the time-averaged temperature in the XZ- (top), XY- (middle) and YZ- (bottom) planes in the LES result of case G

The cross-sectional views of the time-averaged temperature within the simulation domain in case G are shown in Figure 4-53. The temperature distribution in the pipeline is set 30% transparent. In the YZ-cross-section, the phenomenon of turbulent penetration in the branch pipe is very small. The flow stream in the branch pipe remains mostly at 20 °C. Due to thermal conductivity, the pipe wall is warmed up in a specific range. In addition, the cold flow from the branch pipeline falls down, hits the main pipe wall and initiates the tangential oscillation. In the main pipeline, vertical temperature gradient in the XZ-cross-section confirms the thermal stratification in the mixing flow. And reverse flow can be seen upstream the T-junction. In the XY-cross-section, the spatial periodical temperature distribution downstream of the T-junction is similar with the case F, which indicates the snake path of the cold flow in the mixing region.

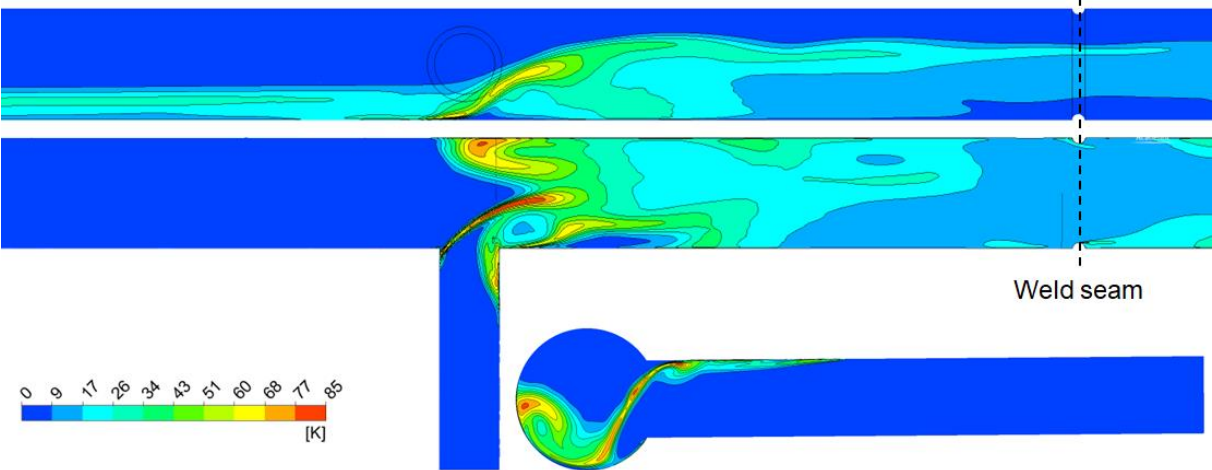
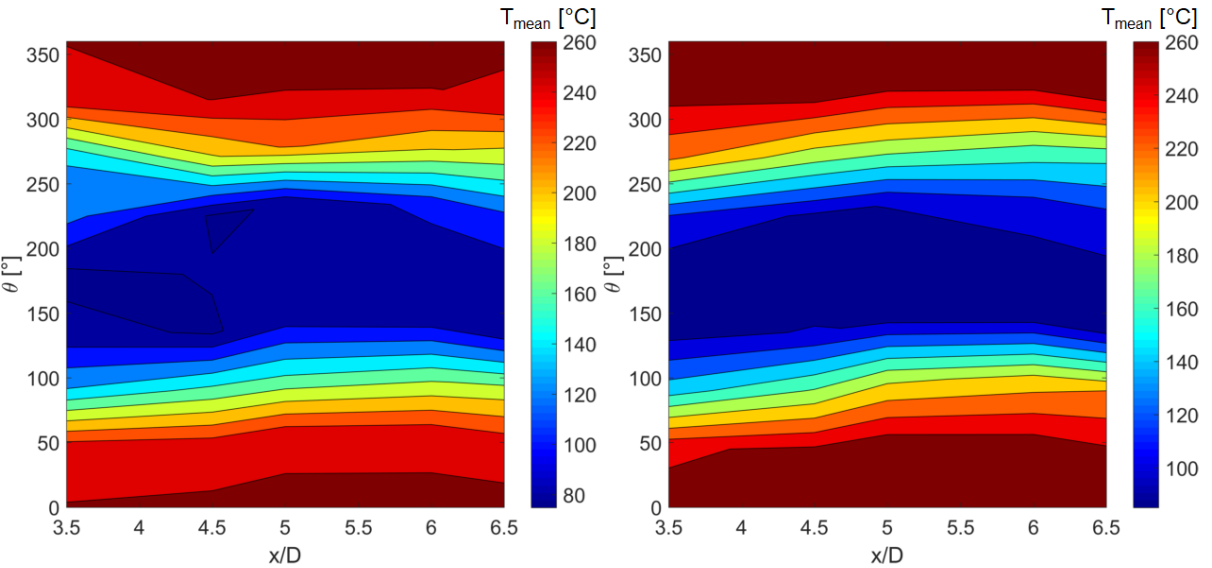
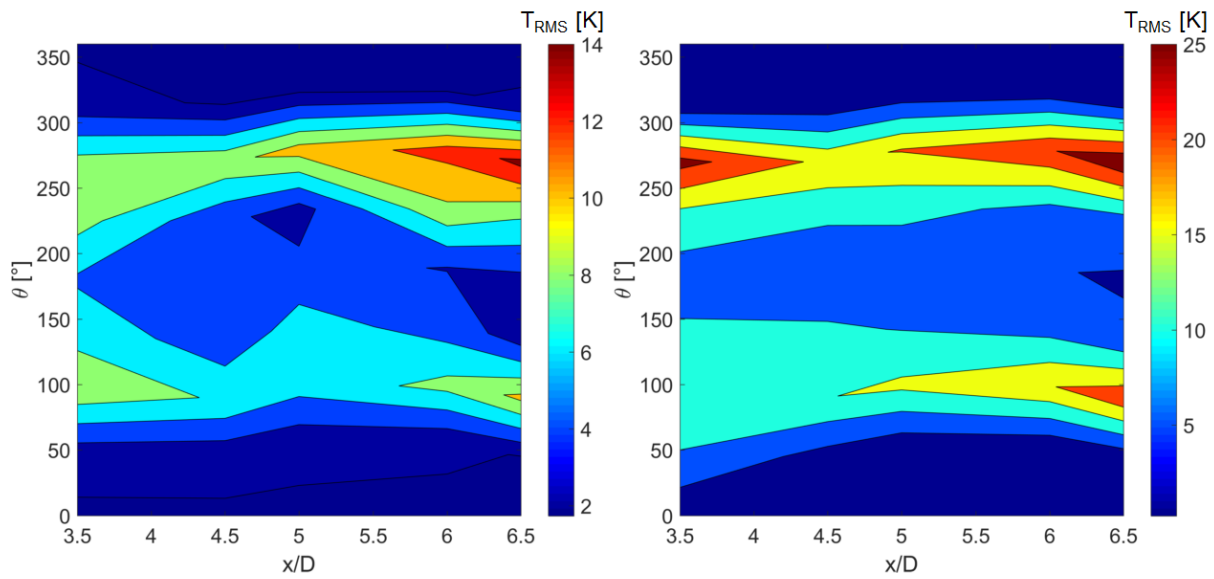


Figure 4-54: Cross-sectional views of the RMS temperature fluctuation in the XZ- (top), XY- (middle) and YZ- (bottom) planes in the LES result of case G

The cross-sectional views of the RMS temperature fluctuation in the fluid domain in the case G is shown in Figure 4-54. As can be seen, the maximum temperature fluctuation reduces to 85 K in comparison with the case F. However, the maximum temperature fluctuation is located close to the joint position of the main and branch pipe. Except this, the reverse flow in the main pipe upstream the T-junction creates a region with temperature fluctuation of about 30 K. Without the artificial temperature change due to AIPTEC, the temperature fluctuation in the main pipe downstream of the T-junction is much lower than case F.





(b)

Figure 4-55: Reconstructed circumferential distribution of mean temperature (a) and RMS temperature fluctuation (b) of LES (right) in comparison with experiments (left)

The circumferential distributions of the mean temperature and the RMS temperature fluctuation have been reconstructed from the LES temperature monitor data, and compared with the experimental results in Figure 4-55. The mean temperature distribution of the simulation matches very well with the experiment (see Figure 4-55a). Also the shape of the RMS temperature fluctuation distribution of the simulation is almost identical with the experimental results and indicates a stable thermal stratification in the mixing region. However, the maximum values of the temperature fluctuation of the simulation are about 11 K higher than in the experiment. The reason for this difference leads back to the inlet flow temperature in the branch pipe. Generally, the flow temperature in the branch pipe is 20 °C, and is captured by a thermocouple about 2.5 m upstream the T-junction in the branch pipe. In the simulation work, the inlet profile is set at -0.885 m in the y-direction in the branch pipe (see Figure 3-2). Due to thermal conduction in the piping material, the cold flow has been warmed in this range close to the T-junction. In the experiments, the thermocouples at position -7d (-0.272 m in y-direction) have captured an average temperature of about 31 °C while the temperature monitor points in the simulation have 20 °C at the same position. This temperature difference matches the increased RMS temperature fluctuation in the mixing region of the simulation results. Moreover, the heat exchange has been employed in the simulation between the fluid and solid domain. However, within such short range of the branch pipeline, the cold water cannot be heated up as much as in the experiment.

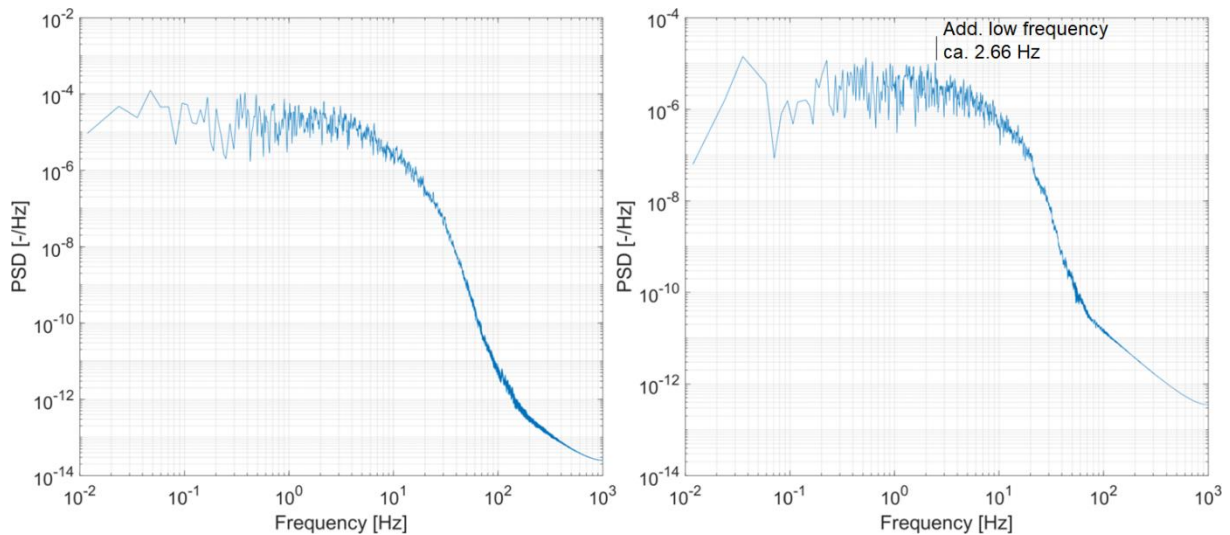


Figure 4-56: PSD diagrams of the normalized temperature at temperature monitor point FT10 (left, position: 4.5D, $\theta = 45^\circ$) and FT24 (right, position: 5D, $\theta = 315^\circ$)

Frequency analyses have been performed with the temperature monitor data. The PSD diagrams of normalized temperature at monitor points FT10 and FT24 are shown in Figure 4-56. Most of the examined monitor points in the mixing region show similar frequency spectra as at monitor point FT10. No clear frequency peak can be seen in the spectra. The additional low frequency can be found in the PSD diagram of monitor point FT24. However, the peak of the additional low frequency is not so distinct as in the experiment.

4.1.1.1 Harmonic oscillation of thermal stratification in pipe-tangential direction

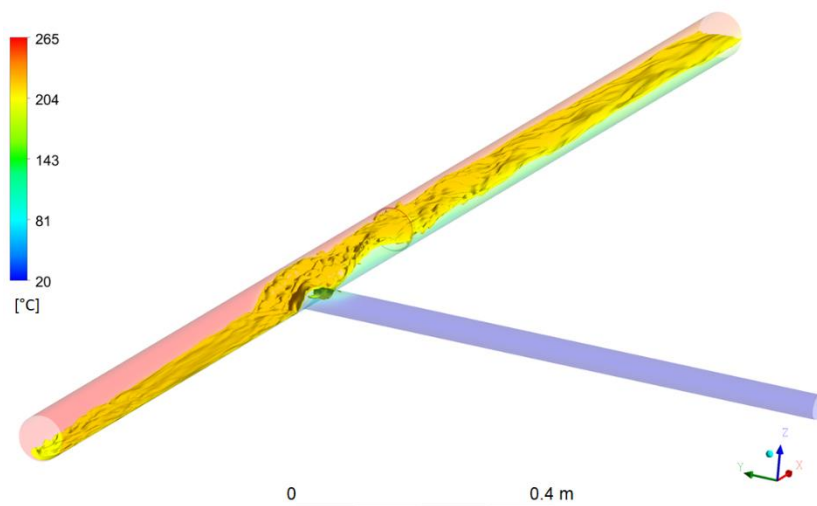


Figure 4-57: Instantaneous illustration of the temperature iso-surface 200.5 °C at simulated physical time 118.2 s of case G

The harmonic oscillation of thermal stratification in pipe-tangential direction is an unique thermal mixing characteristics at horizontal T-junction. The additional low frequency, which is found in the frequency spectra of some measurement positions in the mixing region, is as well as the identification of the tangential flows oscillation. However, the additional low frequency in the frequency spectra of the LES temperature monitor data is not so clear as in the experimental results. Figure 4-57 shows a snapshot in time of the temperature iso-surface 200.5 °C in the mixing flow at simulated physical time

of 118.2 s for the case continuous cold flow injection (case G). The temperature iso-surface is smooth in the mixing flow downstream of the T-junction, which indicates no significant heat exchange through the iso-surface. Therefore, the thermal stratification in this case is stable. Comparing the iso-surface at this temperature within a time interval, a tangential oscillation of the iso-surface can be seen in the mixing region downstream of the T-junction.

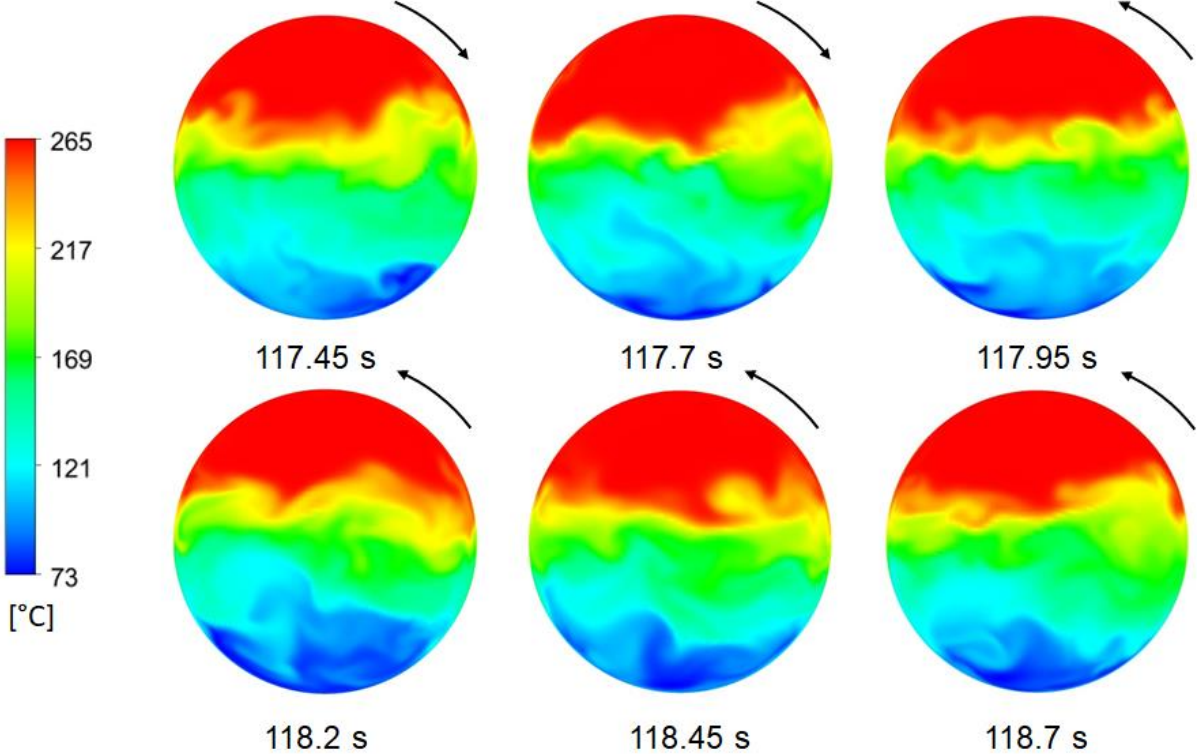


Figure 4-58: Temperature distributions in the cross-section F2 (4.5D) downstream of the T-junction within 1.25 s in the LES results of case G

The temperature distributions in the cross-section F2 (4.5D) at six time points within 1.25 s are shown in Figure 4-58. As can be seen, there is a temperature gradient in vertical direction in this cross-section, which indicates a thermal stratification. The thermal interface (yellow-green area in the cross-sections) do not remain in a constant horizontal level but changes with the time, and the movement of the thermal stratification can be recognized in the pipe tangential direction. Therefore, the tangential flow oscillation can create a temperature change with the additional low frequency on the pipe inner wall close to the thermal interface, which may increase the potential for material damage due to thermal fatigue in the mixing region.

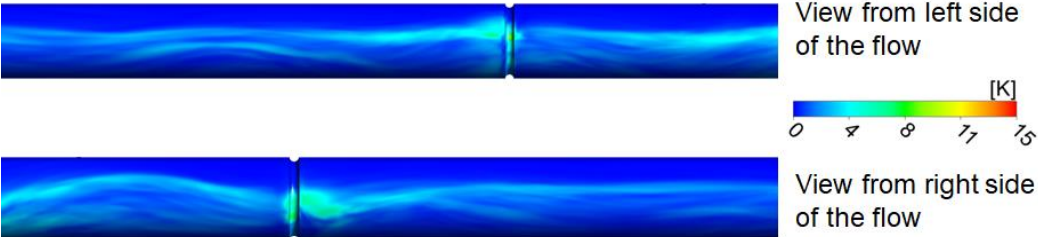


Figure 4-59: RMS Temperature fluctuations in the fluid-structure interface in the simulation result of case G

For the safety of the piping system in nuclear power plants, the tangential oscillation of thermal stratification is definitely a high potential risk for the piping materials due to thermal fatigue. Figure 4-59 shows the temperature fluctuation in the fluid-structure interface in the results of LES-calculation on case G (continuous cold flow injection). Along the flow direction, a band with high temperature fluctuation can be found close to the thermal interface from both horizontal sides, which is created by the tangential oscillation of thermal stratification. These temperature fluctuations have a periodic temperature change with the additional low frequency, which is in the frequency range for thermal fatigue [81]. Therefore, these areas close to the thermal interface have a high potential for material damage due to thermal fatigue. For the safety of the piping system, the tangential oscillation of thermal stratification must be avoided.

4.2.2 Flow patterns at horizontal T-junction

By initiation of the tangential oscillation, the flow trace calculation shows the cold flow has a two-dimensional movement in the YZ-cross-section at the T-junction (see chapter 4.1.6). This is one of the most important properties for the mixing flow in the horizontal T-junction. And it is different with the one-dimensional movement of the branch flow in the vertical T-junctions. The mixing phenomenon, tangential oscillation of thermal stratification, therefore cannot be initiated in the mixing flow at vertical T-junction nor described by the flow patterns of Kamide [34]. New flow patterns shall be summarized for the mixing behaviors at horizontal T-junctions.

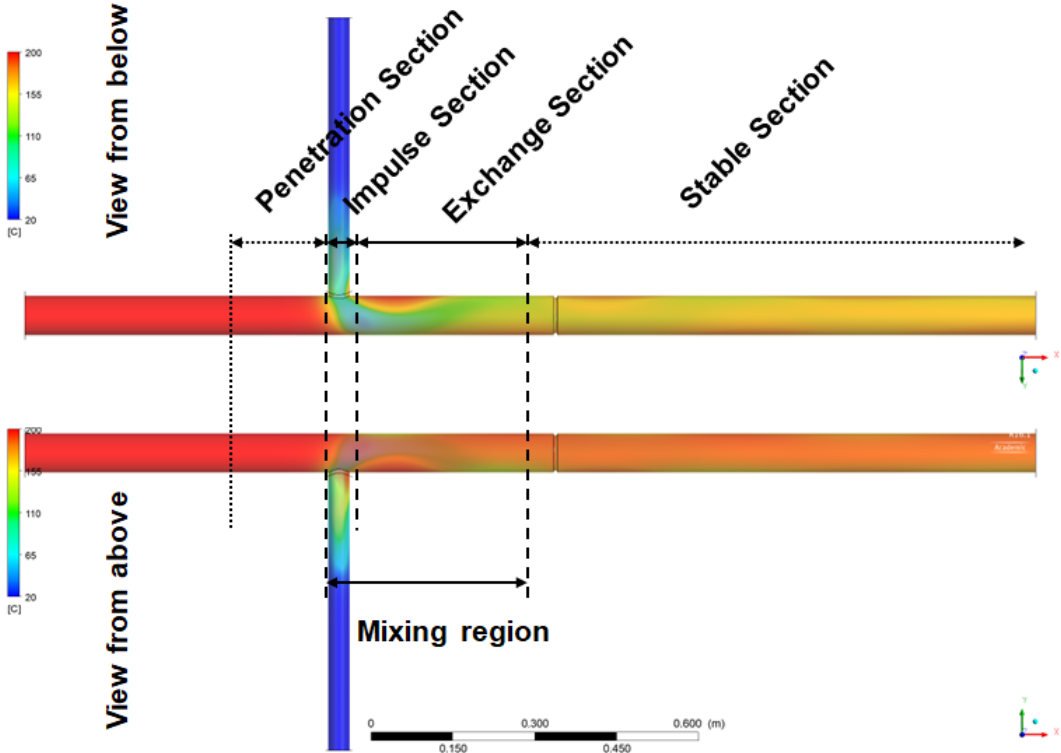


Figure 4-60: Flow sections in the mixing process at horizontal T-junction

For summarizing the mixing behaviors, the flow field close to the T-junction is needed to be visualized. However, it is not possible to perform flow field visualization to the complete flow region close to the T-junction in the experiment at the FSI test facility. LES calculations can provide results with good agreement to the experiments, but request a very long computational time. As compromise between the accuracy and efficiency in the numerical simulation, the results of the steady-state simulations, which

are used as initial condition for the LES calculation, are applied for summarizing the thermal mixing behaviors.

Figure 4-60 shows the temperature distribution in the fluid-structure interface in the result of steady-state simulation on case 4b. The illustration of the temperature distribution is made about 30% transparent, so that one can see the cold flow from above. For new categorizing of the flow patterns, the flow region close to the T-junction is separated into different flow section. Following the cold flow in the branch pipe, the mixing flow in the main pipeline is separated into impulse section, exchange section and stable section. If reverse flow exists in the main pipeline upstream the T-junction, an additional penetration section is defined upstream the T-junction. In the impulse section, the impulse energy of the cold flow takes the lead in this section. The cold flow in the impulse section still has the same property as well as in the branch pipeline. In the case 4b, the impulse section begins at the connecting position of the branch pipe, ends at the first turning of the cold flow path in the main pipe downstream of the T-junction. Then, the cold flow comes into the exchange section, in which most of the heat exchange in the mixing processes take place. Snake path shall be observed in this section, if it exists. Generally, the summary of the impulse section and exchange section is the mixing region. After the mixing flow is stabilized, the snake path will fade away. Two outcomes can be seen in the stable section. For total mixing, the temperature distribution in this section shall be homogenous. For non-total mixing, thermal stratification shall be seen in this section. According to the definition of the flow sections, the flow patterns at horizontal T-junction have been categorized and summarized in Figure 4-61.

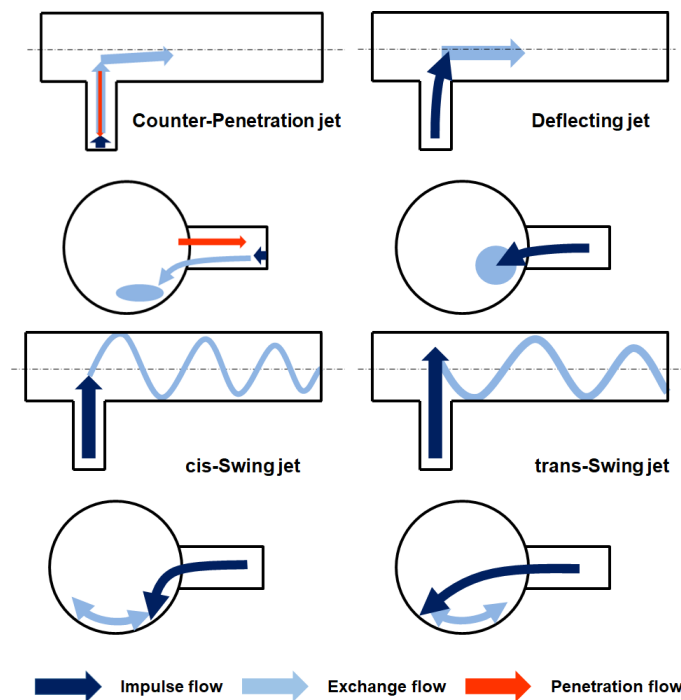


Figure 4-61: Flow patterns of thermal-mixing pipe flow in horizontal T-junction

Counter-penetration jet, which can be created with very low or even zero flow rate in the branch pipeline, has a very short mixing region as long as the diameter of the branch pipeline (see Figure 4-61). With the counter-penetration jet, the cold flow can already be warmed up in the branch pipe. The impulse section coincides with the exchange section in the branch pipe. Tangential oscillation cannot be observed in the main pipeline, because flow stream out of the branch pipe is already warmed up and has a very low velocity in y-direction. The outcome of counter-penetration jet will be total mixing in the stable section. No reverse flow will be observed in the main pipeline upstream the T-junction. The penetrated hot flow and the cold flow can create a velocity shear in the branch pipe. Such kind of velocity shear can be seen in the experiments of Downing et al. [66]. Due to Kelvin-Helmholtz instability, vortex structure can be

created at the interface of the velocity shear. Hence, temperature fluctuations can be generated because of the vortex structure. Therefore, counter-penetration jet has a high potential for material damage due to thermal fatigue in the branch pipeline.

Deflecting jet, which can be created by high flow rate difference or low temperature difference, may have a short impulse section but a long exchange section. The cold flow from the branch pipe has a low velocity and cannot touch any side of the main-pipe wall, so that the tangential oscillation cannot be initiated. However, after the cold flow direction turns to the main pipe direction (x-direction), it will land somewhere in the lower part of the pipe and create the snake path (see Figure 4-60). In the experimental work at the FSI test facility, cases 4, 8, 9 and 10 have the flow pattern of deflecting jet. Case 4 has high flow rate difference and high temperature difference (see Table 4-10). The thermal stratification in the mixing flow in case 4 is stable and can be seen in the stable section. Cases 8 – 10 have low temperature difference (see Table 4-10). The thermal stratification in these three cases are all very unstable. In case 4, the hot flow penetrates into the branch pipe. But the penetrated hot flow occupies only a small part of the branch pipe, and is already cooled down in the branch pipe. As the outcome of the mixing processes, the flow streams in cases 8 – 10 will be totally mixed, but not in case 4. The cold flow in these four cases touches the main pipe wall downstream of the turning point (end of the impulse section). Snake path is created in these four cases. However, the cold flow does not have any more velocity in y-direction, and the tangential oscillation cannot be initiated.

Swing jet, which consists two different configurations, has tangential oscillation of thermal stratification observed in the mixing region. For initiation of the tangential oscillation, the impulse flow must hit on the main-pipe wall. If the impulse flow hit the main-pipe wall at the same side of the branch pipe, the flow from is defined as *cis*-swing jet. If the hit point is located at the opposite side of the branch pipe, the flow from is defined as *trans*-swing jet. In this work, cases G, S, 2 and 3 have the flow pattern of *cis*-swing jet, while cases 1, 5, 6 and 7 have the flow pattern of *trans*-swing jet. Additional low frequencies have been detected in all these cases due to the tangential oscillation (see Table 4-10). Snake path of the cold flow can be found in the lower part of the mixing flow (see Figure 4-52). Thermal stratification in the cases with swing jet are all stable. Furthermore, reversed cold flow can be found in the penetration section upstream the T-junction in some of these cases. As the outcome of the swing jet, the flow streams will not be totally mixed. With the additional low frequency, the pipe-wall areas close to the thermal interface of the thermal stratification in the mixing region have a high potential for material damage due to thermal fatigue (see Figure 4-59).

Among the flow patterns, the deflecting jet cannot create periodical temperature change in the main pipe like swing jet, nor strong penetration flow in the branch pipe. The temperature fluctuation in the deflecting jets can be created only by the vortex in the mixing flow, and therefore is not a regular temperature change. The values of the temperature fluctuation is much lower than those in swing jet or counter-penetration jet. Hence, the potential for material damage due to thermal fatigue in deflecting jet is at the lowest among all the flow patterns.

In addition, the fact of AIPTEC is a periodical change between counter-penetration jet and one of the other flow patterns. Different AIPTEC durations cannot change the flow pattern in the mixing processes. Therefore, AIPTEC cannot change the mixing behavior in the mixing processes. At a specific horizontal oriented T-junction, the crucial factors on the flow pattern are temperature and flow rates of the inlet flow streams.

4.3 Mixing envelope

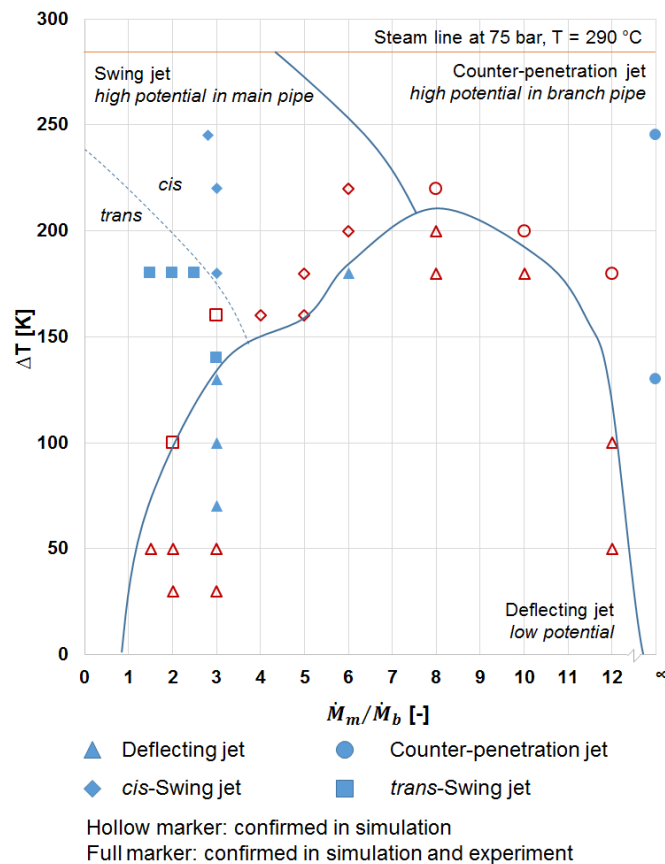


Figure 4-62: Mixing envelope of the DN80/40 horizontal T-junction at FSI test facility

So far, it can be understood that the mixing characteristics is the property of a specific horizontal mixing tee and can be influenced only by the temperature and flow rates of the inlet flow streams. With an inspiration of flight envelope in the aircraft design [120], a new diagram called mixing envelope is created to summarize the mixing characteristics (flow patterns) with the dependence on the crucial factors. Figure 4-61 shows the mixing envelope of the horizontal T-junction at the FSI test facility based on the results of the experimental and numerical investigations in this work. As can be seen, the region of deflecting jet is located inside of the envelope curve. If the operation condition is located inside of the envelope curve, thermal fatigue effect can be strongly reduce or even avoided in the thermal mixing processes. It also needs to be explained that this mixing envelope (Figure 4-62) is generated with the operation points at the FSI test facility, which has some limitations in the experiments. Firstly, there is no heater in the branch pipe, so that the flow temperature in the branch pipe remains constant at 20 °C. Secondly, the flow rate is limited at 0.6 kg/s in the main pipe and 0.2 kg/s in the branch pipe due to the power of the pumps. However, the mixing envelope points out a solution to reduce or avoid thermal fatigue in the thermal mixing processes. In addition, it is the first time a summary of all the three thermal fatigue related mixing phenomena together for a single specific T-junction. Moreover, the mixing envelope is a property of the specific T-junction. It can be changed, only when the configuration of the T-junction is changed (e.g. turn to vertical) or another flow property influenced pipe segment (e.g. elbow) is installed upstream of the T-junction. Furthermore, the mixing envelope is very meaningful for the design of piping system in the reality. Once the mixing envelope is generated for the mixing tee, it can be used as operation guideline to reduce or avoid thermal fatigue damage in the thermal mixing processes. In the comparison between different mixing tees, the one with larger envelope has the more possibility to reduce or avoid material damage due to thermal fatigue.

5 Conclusions

This work presents the turbulent-flow mechanisms in thermal-mixing pipe flow, which can cause thermal fatigue damage in the piping materials. The investigations for understanding these mechanisms have been performed in combination of experimental and numerical methods. The flow conditions have been chosen similar with the reality in nuclear power plants (pressure 75 bar, temperature up to 265 °C). The thermal-mixing investigations has been performed in a horizontal 90° T-junction. In particular, thermal fatigue damage close to weld connections has been investigated in this work. A pipeline with dissimilar weld seams has been applied in the experiment. Accelerated with the **Artificially Induced Periodical TE**mperature **C**hange (AIPTEC) and the 25° shock module, fatigue damages have been created in the piping materials close to the dissimilar weld seam and confirmed with the metallographic investigations. High-performance micro-thermocouples have been applied in the experiments for temperature measurement in the near-wall flow. Results of the fatigue assessment based on the temperature data matches the metallographic investigation. A standard data analysis procedure has been concluded for locating the thermal fatigue damage according to the temperature measurement data.

The experiments with the 90° T-junction have been performed with variations of inlet flow temperature and flow rate, respectively. Influence of the inlet boundary conditions on the mixing characteristics has been discussed with the temperature measurement. Pipe-wall locations with high potential for material damage due to thermal fatigue have estimated by using the standard data analysis procedure on the temperature data. The three thermal-fatigue related mixing phenomena, turbulent mixing, thermal stratification and turbulent penetration in the mixing flow have also been discussed with their relevance for thermal fatigue. Possibility of thermal fatigue damage due to these three phenomena has been discussed with different boundary conditions.

With the NW-LED-IF technique, the temporal and spatial temperature distribution in the near-wall flow close to the weld seam model has been captured for analysis. The results show the rimmed weld root can induce vortex structures in the nearby flow field, and therefore increase the possibility for thermal fatigue in the piping materials close to the weld seam.

An additional low frequency about 2.66 Hz has been found in the frequency analysis temperature data in the mixing region. With a small-scale half-pipe experiment and the model of mathematical pendulum, the additional low frequency is identified as the frequency of the harmonic oscillation of the thermal stratification in the pipe-tangential direction. It is a unique phenomenon in the thermal mixing pipe flow at a horizontal oriented mixing tee. The additional low frequency indicates a different mixing characteristics in comparison with the vertical T-junctions.

LES simulations provide a possibility to observe the mixing process, which cannot be completely visualized in the experiments. The temperature distribution in the LES calculations have shown a good agreement with the experimental results. Moreover, the mixing characteristics in the experiments can be better understood from the simulation results. Furthermore, the time-dependend temperature distributions can illustrate the tangential oscillation of thermal stratification in the mixing region.

Moreover, fatigue assessment is a method of statistics. An important experience has been summarized in this work: the large the data set is, the more significant are the results. No matter temperature data is occurred from experiments or simulations, the temperature recording shall be long enough to generate enough data for a significant result.

With the help of simulation results, new flow patterns have been concluded for categorizing the mixing characteristics at the horizontal T-junction. The *cis/trans*-swing jet, in which the tangential oscillation is initiated, has a high potential for thermal fatigue in the mixing region of the main pipeline. The

counter-penetration jet, in which heat exchange is started in the branch pipeline, has a high potential for thermal fatigue in the branch pipeline. The deflecting jet, in which the impulse flow from the branch pipe cannot reach the pipe wall of the main pipe, has the lowest potential for thermal fatigue in the thermal mixing processes among all the flow patterns.

Summarizing the flow patterns with the impact of the temperature and flow rate in the inlet flow streams, the mixing envelop diagram is drawn for categorizing the flow patterns at a horizontal T-junction. The mixing envelop diagram is a mixing-tee specific property, and provides a solution to reduce or avoid thermal fatigue effect in the specific mixing tee. Once the mixing envelop has been drawn for a specific mixing tee, it can be used as operation guideline for reducing or avoiding thermal fatigue. By controlling the two crucial factors in the inlet flow, the flow-mixing condition can be kept in the region of deflecting jet, in which the possibility for thermal fatigue is much lower than the others.

References

1. P. Chadeyron, "Communication Report Regarding the Incident on the Residual Heat Removal System at the Nuclear Power Plant of Civaux May12, 1998", *11th International Workshop on Nuclear Public Information in Practice*, Avignon, France, February 7-10, 1999.
2. S. Chapliot, "Thermal Fatigue in Mixing Areas: Overview of the Industrial Problem", Keynote lecture, NEA Headquarters, May 20, 2009.
3. S. Chapliot, C. Gourdin, T. Payen, J.P. Magnaud, A. Monavon, "Hydro-Thermal-Mechanical Analysis of Thermal Fatigue in a Mixing Tee," *Nuclear Engineering and Design*, **235**, pp. 575-596 (2005).
4. K.-J. Metzner, U. Wilke, "European THERFAT Project – Thermal Fatigue Evaluation of Piping System "Tee" – Connections", *Nuclear Engineering and Design*, **235**, pp. 473-484 (2005).
5. S. Courtin, J.A. Le Duff, B. Tacchini, A. Fissolo, L. Vincent, J.M. Stephan, R. Tampigny, High Cycle Thermal Fatigue FATHER Experiment: Non Destructive and Metallographic Examinations, *Structural Mechanics in Reactor Technology (SMiRT 21)*, New Delhi, India, November 6-11, 2011.
6. S. Courtin, "High Cycle Thermal Fatigue Damage Prediction in Mixing Zones of Nuclear Power Plants: Engineering Issues Illustrated on the FATHER Case," *Procedia Engineering*, **66**, pp. 240-249 (2013).
7. J.M. Stephan, Numerical Interpretation of the Endurance Test of FATHER Mixing Zone Mock-up, *Proceedings of the ASME 2011 Pressure Vessels & Piping Division Conference (PVP2011)*, Baltimore, Maryland, USA, July 17-21, 2011.
8. S. Taheri, E. Julan, X.-V. Tran, N. Robert, "Impacts of Weld Residual Stresses and Fatigue Crack Growth Threshold on Crack Arrest under High-Cycle Thermal Fluctuations," *Nuclear Engineering and Design*, **311**, pp. 16–27, (2017).
9. S. Taheri, A. Fatemi, "Fatigue Cracking Behavior in Power Plant Residual Heat Removal System Piping Including Weld Residual Stress Effects," *International Journal of Fatigue*, **101**, pp. 244–252 (2017).
10. S. Kuhn, O. Braillard, B. Niceno, H.-M. Prasser, "Computational study of conjugate heat transfer in T-junctions," *Nuclear Engineering and Design*, **240**, pp. 1548-1557 (2010).
11. A. Shams, N. Edh, K. Angele, P.I Veber, R. Howard, O. Braillard, S. Chapliot, E. Severac, E. Karabaki, J. Seichter, B. Niceno, "Synthesis of a CFD benchmarking exercise for a T-junction with wall," *Nuclear Engineering and Design*, **330**, pp. 199-216 (2018).
12. O. Braillard, R. Howard, K. Angele, A. Shams, N. Edh, "Thermal mixing in a T-junction: Novel CFD-grade measurements of the fluctuating temperature in the solid wall," *Nuclear Engineering and Design*, **330**, pp. 377-390 (2018).
13. NUGENIA MOTHER Project, http://nugenia.org/portfolio_item/mother-project/
14. Brian Smith, et al., "OECD/NEA–VATTENFALL T-junction benchmark specifications OECD/NEA Report", (2009).
15. B.L. Smith, J.H. Mahaffy, K. Angele, "A CFD benchmarking exercise based on flow mixing in a T-junction", *Nuclear Engineering and Design*, **264**, pp. 80-88 (2013).
16. Y. Odemark, T.M. Green, K. Angele, J. Westin, F. Alavyoon, S. Lundström, High-Cycle Thermal Fatigue in Mixing Tees New Large-Eddy Simulations Validated Against New Data Obtained by PIV in the VATTENFALL Experiment, *Proceedings of the 17th International Conference on Nuclear Engineering (ICONE17)*, Brussels, Belgium, July 12-16, 2009.
17. T. Höhne, Scale resolved simulations of the OECDNEA-Vattenfall T-junction Benchmark, *Structural Mechanics in Reactor Technology (SMiRT 21)*, New Delhi, India, November 6-11, 2011.
18. T. Höhne, "Scale Resolved Simulations of the OECD&NEA/Vattenfall T-Junction Benchmark," *Nuclear Engineering and Design*, **269**, pp. 149–154, (2014).
19. K. Das, M. Hasan, D. Basu, Spectral Analysis of Unsteady Turbulent Flow and Thermal Mixing in T-Junctions in the Coolant Loop of Pressurized Water Reactors, *Proceedings of the 2nd Thermal*

- and Fluid Engineering Conference (TFEC2017), 4th International Workshop on Heat Transfer, Las Vegas, USA, April 2-5, 2017.
20. A. Timperi, “Conjugate Heat Transfer LES of Thermal Mixing in a T-Junction,” *Nuclear Engineering and Design*, **273**, pp. 483-496 (2014).
 21. A. Timperi, “Development of a spectrum method for modelling fatigue due to thermal mixing,” *Nuclear Engineering and Design*, **331**, pp. 136-146 (2018).
 22. O.C. Garrido, A. Timperi, S. El Shawish, L. Cizelj, Comparison of Spectral Methods with CFD Simulation of Turbulent Fluid Mixing, *Structural Mechanics in Reactor Technology (SMiRT 24)*, Busan, Korea, August 20-25, 2017.
 23. O.C. Garrido, S. El Shawish, L. Cizelj, “Assessment of Thermal Fatigue Predictions of Pipes with Spectral Methods,” *ASME Journal of Nuclear Engineering and Radiation Science*, **Vol. 3 / 041001-1** (2017).
 24. O.C. Garrido, A. Timperi, S. El Shawish, L. Cizelj, Thermal fatigue assessment of nuclear piping under random loading, *ECCOMAS MSF 2017 Thematic Conference*, Ljubljana, Slovenia, September 20-22, 2017.
 25. O.C. Garrido, S. El Shawish, L. Cizelj, “Stress assessment in piping under synthetic thermal loads emulating turbulent fluid mixing,” *Nuclear Engineering and Design*, **283**, pp. 114–130, (2015).
 26. Y. Zhang, T. Lu, “Study of the Quantitative assessment Method for High-Cycle Thermal Fatigue of a T-Pipe under Turbulent Fluid Mixing Based on the Coupled CFD-FEM Method and the Rainflow Counting Method,” *Nuclear Engineering and Design*, **269**, pp. 149–154, (2014).
 27. O.C. Garrido, S. El Shawish, L. Cizelj, “Comments on “Study of the quantitative assessment method for high-cycle thermal fatigue of a T-pipe under turbulent fluid mixing based on the coupled CFD-FEM method and the rainflow counting method”,” *Nuclear Engineering and Design*, **318**, pp. 274-275 (2016).
 28. H. Ayhan, C.N. Sökmen, “CFD modeling of thermal mixing in a T-junction geometry using LES model,” *Nuclear Engineering and Design*, **253**, pp. 183-191 (2012).
 29. H.M.C. Hannik, F.J. Blom, “Numerical methods for the prediction of thermal fatigue due to turbulent mixing,” *Nuclear Engineering and Design*, **241**, pp. 681–687, (2011).
 30. J.-M. Ndombo, R.J.A. Howard, “Large Eddy Simulation and the Effect of the Turbulent Inlet Conditions in the Mixing Tee,” *Nuclear Engineering and Design*, **241**, pp. 2172-2183 (2011).
 31. J. Westin, F. Alavyoon, L. Andersson, P. Veber, M. Henriksson, C. Andersson, Experiments and unsteady CFD-calculations of thermal mixing in a T-junction, *CFD for Nuclear Reactor Safety (CFD4NRS)*, Munich, Germany, September 05-07, 2006.
 32. J. Westin, P. Veber, L. Andersson, C. Mannetje, U. Andersson, J. Eriksson, M. Henriksson, F. Alavyoon, C. Andersson, High-Cycle Thermal Fatigue in Mixing Tees. Large-Eddy Simulations compared to a new Validation Experiment, *Proceedings of the 16th International Conference on Nuclear Engineering (ICONE16)*, Orlando, Florida, USA, May 11-05, 2008.
 33. N. Kimura, J. Kobayashi, Y. Kameyama, K. Nagasawa, T. Ezure, A. Ono, H. Kamide, Study on High Cycle Thermal Fatigue in Mixing Tee – Evaluation of Transfer Characteristics of Temperature Fluctuation from Fluid to Structure, JAEA project report, 2014-009, 2014. (in Japanese)
 34. H. Kamide, M. Igarashi, S. Kawashima, N. Kimura, K. Hayshi, “Study on Mixing Behavior in a Tee Piping and Numerical Analyses for Evaluation of Thermal Stripping,” *Nuclear Engineering and Design*, **239**, pp. 58-67 (2009).
 35. S. Qian, S. Kanamaru, N. Kasahara, “High-accuracy CFD prediction methods for fluid and structure temperature fluctuations at T-junction for thermal fatigue evaluation,” *Nuclear Engineering and Design*, **239**, pp. 58-67 (2009).
 36. Isaev, R. Kulenovic, E. Laurien, “Experimental Investigation on isothermal Stratified Flow Mixing in a Horizontal T-Junction”, *ATW International Journal for Nuclear Power*, Vol. 61, Issue 10, pp. 621-624, 2016.

37. M. Tanaka, H. Ohshima, H. Monji, "Numerical Simulation of Thermal Stripping Phenomena in a T-Junction Piping System Using Large Eddy Simulation," *Journal of Power and Energy Systems*, **3**, pp. 237-248 (2009).
38. M. Tanaka, H. Ohshima, H. Monji, "Thermal Mixing in T-Junction Piping System Related to High-Cycle Thermal Fatigue in Structure," *Journal of Nuclear Science and Technology*, **47**, pp. 790-801 (2010).
39. S. Qian, N. Kasahara, LES Analysis of Temperature Fluctuations at T-Junctions for Prediction of Thermal Loading, *Proceedings of ASME 2011 Pressure Vessels & Piping Division Conference PVP2011*, Baltimore, Maryland, USA, July 17-21, 2011.
40. A. Nakamura, T. Oumaya, N. Takenaka, Numerical Investigation of Thermal Striping at a Mixing Tee Using Detached Eddy Simulation, *13th International Topical Meeting on Nuclear Reactor Thermal Hydraulics (NURETH-13)*, Kanazawa City, Ishikawa Prefecture, Japan, September 27-October 2, 2013.
41. Y. Utanohara, A. Nakamura, K. Miyoshi, N. Kasahara, "Numerical Simulation of Long-period Fluid Temperature Fluctuation at Mixing Tee for the Thermal Fatigue Problem," *Nuclear Engineering and Design*, **305**, pp. 639-652 (2016).
42. K. Miyoshi, A. Nakamura, N. Takenaka, "Numerical Evaluation of Wall Temperature Measurement Method Developed to Estimate Thermal Stress at T-Junction Pipe", *JSME Mechanical Engineering Journal*, **Vol. 1**, No. 2 (2014).
43. M. Kamaya, Y. Utanohara, A. Nakamura, Thermal Fatigue Analysis at a Mixing Tee by a Fluid-Structural Simulation, *Pressure Vessels & Piping Division Conference (PVP2011)*, Baltimore, USA, July 17-21, 2011.
44. M. Kamaya, A. Nakamura, "Thermal stress analysis for fatigue damage evaluation at a mixing tee," *Nuclear Engineering and Design*, **241**, pp. 2674-2687 (2011).
45. H. Ogawa, M. Igarashi, N. Kimura, H. Kamide, Experimental Study of Fluid Mixing Phenomena in T-Pipe Junction with Upstream Elbow, *11th International Topical Meeting on Nuclear Reactor Thermal-Hydraulics (NURETH-11)*, Avignon, France, October 2-6, 2005.
46. N. Kimura, H. Ogawa, H. Kamide, "Experimental study on fluid mixing phenomena in T-pipe junction with upstream elbow", *Nuclear Engineering and Design*, **240**, pp. 3055-3066 (2010).
47. P. Coste, P. Quemere, P. Roubin, P. Emonot, M. Tanaka, H. Kamide, Large Eddy Simulation of a Mixing-T Experiment, *Proceedings of International Congress on Advances in Nuclear Power Plants (ICAPP2006)*, Reno, USA, June 4-8, 2006.
48. S.M. Hosseini, K. Yuki, H. Hashizume, "Classification of turbulent jets in a T-junction area with a 90-deg bend upstream," *International Journal of Heat and Mass Transfer*, **51**, pp. 2444-2454, (2008).
49. S.M. Hosseini, K. Yuki, H. Hashizume, "Experimental Investigation of Flow Field Structure in Mixing Tee," *ASME Journal of Fluids Engineering*, **131**, 051103, (2009).
50. K. Miyoshi, M. Kamaya, Y. Utanohara, A. Nakamura, "An Investigation of Thermal Stress Characteristics by Wall Temperature Measurements at Mixing Tee," *JSME Mechanical Engineering Journal*, **Vol. 1**, No. 2 (2014).
51. K. Miyoshi, M. Kamaya, Monitoring Procedure for Wall Temperature Fluctuation by Temperature Measurement of Pipe Outer Surface at a Mixing Tee, *2017 International Congress on Advances in Nuclear Power Plants (ICAPP 2017)*, Fukui, Kyoto, Japan, April 24-28, 2017.
52. K. Miyoshi, M. Kamaya, Y. Utanohara, A. Nakamura, "An Investigation of Thermal Stress Characteristics by Wall Temperature Measurements at Mixing Tee," *Nuclear Engineering and Design*, **298**, pp. 109-120 (2016).
53. Y. Utanohara, A. Nakamura, K. Miyoshi, Numerical Simulation of Fluid and Wall Temperature Fluctuation Downstream from a Mixing Tee, *11th International Topical Meeting on Nuclear Thermal-Hydraulics, Operation and Safety (NUTHOS-11)*, Gyeongju, Korea, October 09-13, 2016.
54. Y. Utanohara, K. Miyoshi, A. Nakamura, "Conjugate Numerical Simulation of Wall Temperature Fluctuation at a T-junction Pipe," *JSME Mechanical Engineering Journal*, **Vol. 5**, No. 3 (2018).

55. M. Kamaya, K. Miyoshi “Thermal fatigue damage assessment at mixing tees (elastic-plastic deformation effect on stress and strain fluctuations),” *Nuclear Engineering and Design*, **317**, pp. 202-212 (2017).
56. M.-S. Chen, H.-E. Hsieh, Y.-M. Ferng, B.-S. Pei, “Experimental observations of thermal mixing characteristics in T-junction piping,” *Nuclear Engineering and Design*, **276**, pp. 107-114 (2014).
57. C.H. Lin, M.S. Chen, Y.M. Ferng, “Investigating Thermal Mixing and Reverse Flow Characteristics in a T-Junction by the Way of Experiments”, *Applied Thermal Engineering*, **99**, pp. 1171-1182 (2016).
58. C.H. Lin, Y.M. Ferng, “Investigating Thermal Mixing and Reverse Flow Characteristics in a T-Junction using CFD Methodology”, *Applied Thermal Engineering*, **102**, pp. 733-741 (2016).
59. G.Y. Chuang, Y.M. Ferng, “Experimentally investigating the thermal mixing and thermal stripping characteristics in a T-junction”, *Applied Thermal Engineering*, **113**, pp. 1585-1595 (2017).
60. G.Y. Chuang, Y.M. Ferng, “Investigating effects of injection angles and velocity ratios on thermal-hydraulic behavior and thermal stripping in a T-junction”, *International Journal of Thermal Sciences*, **126**, pp. 74-81 (2018).
61. Z.C. Guo, J.Q. Zou, Y.Q. Chen, K.L. Xu, T. Lu, “Online monitoring of wall temperature fluctuations of horizontal mixing T-junction pipe”, *Applied Thermal Engineering*, **127**, pp. 580-591 (2017).
62. Z.C. Guo, J.Q. Zou, Y.Q. Chen, K.L. Xu, T. Lu, B. Liu, “Monitoring of wall temperature fluctuations for thermal fatigue in a horizontal mixing T-junction pipe,” *Progress in Nuclear Energy*, **104**, pp. 298–305, (2018).
63. A. Nakamura, K. Miyoshi, T. Oumaya, N. Takenaka, S. Hosokawa, D. Hamatani, M. Hase, D. Onojima, Y. Yamamoto, A. Saito, “Temperature fluctuation phenomena in a normally stagnant pipe connected downward to a high velocity and high temperature main pipe,” *Nuclear Engineering and Design*, **269**, pp. 360-373 (2014).
64. T. Iguchi, A. Saito, N. Takenaka, K. Miyoshi, A. Nakamura, Experimental Study on Penetration Length in a Small Size Branch Pipe in a Nuclear Power Plant, *14th International Topical Meeting on Nuclear Reactor Thermal Hydraulics (NURETH-14)*, Toronto, Ontario, Canada, September 23 - 25, 2011.
65. B. Lafleur, V. Petrov, A. Menera, CFD Analysis of Main Flow Penetration Depth in Isolated Branch lines, *16th International Topical Meeting on Nuclear Reactor Thermal Hydraulics (NURETH-16)*, Chicago, USA, August 30 - September 4, 2015.
66. J.R. Downing, V. Petrov, A. Manera, Experiments Addressing Thermal Fatigue in Nuclear Reactor Branch Lines for CFD Predictive Model Validation and Enhancement, *17th International Topical Meeting on Nuclear Reactor Thermal-Hydraulics (NURETH-17)*, Xi’an, China, September 3-8, 2017.
67. X. Schuler, K.-H. Herter, S. Moogk, E. Laurien, D. Klören, R. Kulenovic, M. Kuschewski, “Thermal fatigue: Fluid-structure interaction at thermal mixing events”, *38th MPA-Seminar*, Stuttgart, Germany, October 1-2, 2012.
68. M. Kuschewski, R. Kulenovic, E. Laurien, Experimental Investigation of Stratified Pipe Flow Mixing in a Horizontal T-Junction, *CFD4NRS-5*, Zurich, Switzerland, September 9-11, 2014.
69. M. Kuschewski, R. Kulenovic, E. Laurien, “Experimental Setup for the Investigation of Fluid-Structure Interaction in a T-Junction”, *Nuclear Engineering and Design*, **264**, pp. 223-230 (2013).
70. M. Kuschewski, R. Kulenovic, E. Laurien, Experimental Setup for the Investigation of Fluid-Structure Interaction in a T-Junction, *14th International Topical Meeting on Nuclear Reactor Thermal Hydraulics (NURETH-14)*, Toronto, Ontario, Canada, September 25-30, 2011.
71. M. Kuschewski, Development and Application of a flow measurement method for investigating near-wall temperature field, dissertation, 2015. (in German)
72. J. Kickhofel, H.-M. Prasser, P.K. Selvam, E. Laurien, R. Kulenovic, “T-junction cross-flow mixing with thermally driven density stratification,” *Nuclear Engineering and Design*, **309**, pp. 23-39 (2016).

73. D. Klören, E. Laurien, Coupled Large-Eddy Simulation of Thermal Mixing in a T-Junction, *14th International Topical Meeting on Nuclear Reactor Thermal Hydraulics (NURETH-14)*, Toronto, Ontario, Canada, September 25-30, 2011.
74. D. Klören, M. Kuschewski, E. Laurien, Large-eddy simulations of stratified flows in pipe configurations influenced by a weld seam, *CFD4NRS-4*, Daejeon, Korea, September 10-12, 2012.
75. P.K. Selvam, Thermal Mixing Characteristics of Flows in Horizontal T-junctions, dissertation, 2015.
76. P.K. Selvam, R. Kulenovic, E. Laurien, "Large eddy simulation on thermal mixing of fluids in a T-junction with conjugate heat transfer," *Nuclear Engineering and Design*, **284**, pp. 238-246 (2015).
77. P.K. Selvam, R. Kulenovic, E. Laurien, Numerical analysis of Influence of branch flow on thermal mixing in a T-junction piping system, *16th International Topical Meeting on Nuclear Reactor Thermal Hydraulics (NURETH-16)*, Chicago, USA, August 30 - September 4, 2015.
78. P. Gauder, P.K. Selvam, E. Laurien, R. Kulenovic, "Large Eddy Simulation Studies on the Influence of Turbulent Inlet Conditions on the Flow Behavior in a mixing tee," *Nuclear Engineering and Design*, **298**, pp. 51-63 (2016).
79. P.K. Selvam, E. Laurien, R. Kulenovic, "Experimental and numerical analyses on the effect of increasing inflow temperatures on the flow mixing behavior in a T-junction," *International Journal of Heat and Fluid Flow*, **61**, pp. 323-342 (2016).
80. P.K. Selvam, R. Kulenovic, E. Laurien, J. Kickhofel, H.-M. Prasser, "Thermal mixing of flows in horizontal T-junctions with low branch velocities," *Nuclear Engineering and Design*, **322**, pp. 32-54 (2017).
81. J. Galpin, J.P. Simoneau, "Large Eddy Simulation of a thermal mixing tee in order to assess the thermal fatigue," *International Journal of Heat and Fluid Flow*, **32**, pp. 539-545 (2011).
82. J.I. Lee, L.-W. Hu, P. Saha, M.S. Kazimi, "Numerical analysis of thermal striping induced high cycle thermal fatigue in a mixing tee", *Nuclear Engineering and Design*, **239**, pp. 833-839 (2009).
83. M. Kammerer, X. Schuler, S. Weihe, M. Zhou, R. Kulenovic, E. Laurien, Thermo-mechanical loading of full-scale welded piping components in high temperature water environment, *Proceedings of the ASME 2017 Pressure Vessels & Piping Division Conference (PVP2011)*, Hawaii, USA, July 16-20, 2017.
84. M. Zhou, R. Kulenovic, E. Laurien, Experimental Investigation on Different Static Mixers for the IKE/MPA Fluid-Structure-Interaction Facility, *47th Annual Meeting on Nuclear Technology*, Hamburg, Germany, May 10-12, 2016.
85. DIN IEC 60584-2: 1992-06, "Thermocouples; tolerances; identical with IEC 60584-2 (status of 1989)," 1990.
86. ELECTRONIC SENSOR GmbH. Common technical data of sheathing thermocouple: <http://www.electronic-sensor.com/en/sheathing-thermocouple>
87. J.P. Crimaldi, "Planar Laser Induced Fluorescence in Aqueous Flows," *Experiments in Fluids*, **44**, pp. 851-863 (2008).
88. M. Yoda, H. E. Fiedler, "The Round Jet in a Uniform Counterflow: Flow Visualization and Mean Concentration Measurements," *Experiments in Fluids*, **21**, pp. 427-436 (1996).
89. F. Guillard, R. Fritzon, J. Revstedt, C. Tragardh, M. Alden, L. Fuchs, "Mixing in a Confined Turbulent Impinging Jet Using Planar Laser-Induced Fluorescence," *Experiments in Fluids*, **25**, pp. 143-150 (1998).
90. R.J. Adrian, "Image shifting technique to resolve directional ambiguity in double-pulsed velocimetry," *Applied Optics*, **25**, pp. 3855-3858 (1986).
91. M. Raffel, C. Willert, S. Werely, J. Kompenhans, "Particle Image Velocimetry: a Practical Guide," Second edition, Springer Berlin Heidelberg New York, 2007, ISBN 978-3-540-72307-3.
92. R.J. Adrian, J. Westerweel, "Particle Image Velocimetry," Cambridge, 2011, ISBN 978-0-521-44008-0.
93. C. Poelma, P. Vennemann, R. Lindken, J. Westerweel, "In vivo blood flow and wall shear stress measurements in the vitelline network," *Experiments in Fluids*, **45**, pp. 703-713 (2008).

94. G.S. Settles, "Schlieren and Shadowgraph Techniques: Visualizing Phenomena in Transparent Media," Springer Berlin Heidelberg New York, 2001, ISBN 978-3-540-66155-9.
95. F. Klinge, Vermessung von Wirbeln mit der Hintergrundschlieren-Methode, dissertation, University Hannover, 2003. (in German)
96. G.E. Elsinga, Tomographic Particle Image Velocimetry and its Application to turbulent boundary Layers, dissertation, Delft University of Technology, 2008.
97. M. Raffel, "Background-oriented Schlieren (BOS) Techniques," *Experiments in Fluids*, **3**, pp. 56-60 (2015).
98. V.M. Dulin, L.M. Chikishev, M.P. Tokarev, D.M. Markovich, Study of Helical Vortices in Swirling Jets and Flames by Tomographic PIV, *17th International Symposium on Applications of Laser Techniques to Fluid Mechanics*, Lisbon, Portugal, July 07-10, 2014.
99. L. Venkatakrishnan, G. E. A. Meier, "Density Measurements Using the Background Oriented Schlieren Technique," *Experiments in Fluids*, **37**, pp 237-247 (2004).
100. S.B. Pope, "Turbulent Flows," Cambridge University Press, 2000.
101. ANSYS model hand book.
102. U. Piomelli, 2001. An introduction to direct and large-eddy simulations. In: CFD2001, 9th Annual Conference of the CFD Society of Canada, Kitchener, Canada.
103. Y. Addad, U. Gaitonde, D. Laurence, S. Rolfo, "Optimal unstructured meshing for large eddy simulations, ERCOFTAC Series, Quality and Reliability of Large-Eddy Simulations," vol. 12, Springer, pp. 93-103 (2008).
104. ANSYS, Best Practice: Scale-Resolving Simulations in ANSYS CFD (2015).
105. G.T.D. Kalegam, CFD Simulation of Thermal Mixing Process in a Pipe line, master thesis, University of Stuttgart, IKE 8D-103, 2017. (in German)
106. M. Zhou, R. Kulenovic, E. Laurien, M. Kammerer, X. Schuler, Investigation on temperature fluctuations in thermal mixing pipe flows by micro-thermocouple measurements, *11th International Topical Meeting on Nuclear Thermal-Hydraulics, Operation and Safety (NUTHOS-10)*, Gyeongju, Korea, 09.-13. Oktober, 2016.
107. M. Zhou, R. Kulenovic, E. Laurien, M. Kammerer, X. Schuler, "Thermocouple Measurements to Investigate the Thermal Fatigue of a Cyclical Thermal Mixing Process on a Dissimilar Weld Seam," *Nuclear Engineering and Design*, **320**, pp. 77-87 (2017).
108. W. Schneider, "Mathematic methods for fluid dynamics," Braunschweig, 1978, ISBN 3-528-03573-0, (in German).
109. X. Jiang, Y. Andreopoulos, T. Lee, Z. Wang, "Numerical Investigations on the Vortex-Induced Vibration of Moving Square Cylinder by Using Incompressible Lattice Boltzmann Method," *Computers and Fluids*, **124**, pp. 270-277 (2016).
110. J. Lighthill, "Waves in Fluids," Cambridge University Press, 1978.
111. M. Kammerer, X. Schuler, S. Weihe, "Synergy of Experiments and Numerical Analysis for Thermo-mechanically Loaded Dissimilar Metal Welds Experiencing Corrosion Fatigue," *43. Tagung DVM Arbeitskreis Betriebsfestigkeit*, Steyr, Austria, October 10-12, 2016.
112. M. Zhou, R. Kulenovic, E. Laurien, Investigation on Temperature Fluctuations near a Geometric Weld-Seam Model Downstream of a 90° T-Junction in a Thermal Mixing Process, *17th International Topical Meeting on Nuclear Reactor Thermal-Hydraulics (NURETH-17)*, Xi'an, China, September 3-8, 2017.
113. M. Zhou, R. Kulenovic, E. Laurien, Flow Rate Influence on Temperature Fluctuations in Thermal-Mixing Pipe-Flow Experiments at a 90° T-Junction, *2017 International Congress on Advances in Nuclear Power Plants (ICAPP 2017)*, Fukui, Kyoto, Japan, April 24-28, 2017.
114. M. Zhou, R. Kulenovic, E. Laurien, "T-junction experiment with high temperature and high pressure to investigate flow rate influence on mixing characteristics", *International Journal of Heat and Fluid Flow*, **71**, pp. 451-459 (2018).

115. M. Zhou, R. Kulenovic, E. Laurien, "Experimental Investigation on the Thermal Mixing Characteristics at a 90° T-junction with Varied Temperature Differences", *Applied Thermal Engineering*, **128**, pp. 1359-1371 (2018).
116. M. Zhou, R. Kulenovic, E. Laurien, "T-Junction Experiments to Investigate Thermal-Mixing Pipe flow with Combined Measurement Techniques", *Applied Thermal Engineering*, **150**, pp. 237-249 (2019).
117. V. Armenio, "Stratified Turbulent Flows", *Non-homogeneous Fluids and Flows Summer School and Workshop*, Prague, August 27-31, 2012.
118. M. Zhou, R. Kulenovic, E. Laurien, "Advanced flow pattern for describing tangential flow oscillation in thermal-mixing pipe flow at a horizontal T-Junction", *International Journal of Thermal Sciences*, **136**, pp. 328-336 (2019).
119. G.L. Baker, J.A. Blackburn, "The Pendulum: a Case Study in Physics," Oxford University Press, 2005.
120. Z. Jing, "Legend of Energy Combat, History of the Generation III Fighter, Part II", *Weapon*, **61**, pp. 34-37 (2004). (in Chinese)

Acknowledgment

Firstly, I want to thank my supervisor Prof. E. Laurien for his guidance in this path to the world of fluid-dynamics, his support on the theoretical and practical work and his patience, when I had trouble in the works. Also, I want to thank Dr. R. Kulenovic for his help and encouragement during my time at IKE.

I would like to thank our MPA colleagues, Mr. M.C. Kammerer, Mr. F. Silber, Mr. H. Huber, Mr. T. Pfeiffer and Dr. X. Schuler for the cooperative work in the research project and the support in the experimental works.

I want to thank the IKE CFD team, Dr. K. Sevlam, Dr A. Mansour, Dr C. Kaltenbach for the helps in the simulation works.

Moreover, I want to thank the INSS Thermal Hydraulics and Mechanics Group, Dr. M. Kamaya, Dr. Y. Utanohara and Dr. K. Miyoshi for the hospitality by my visiting at INSS and the helpful advices on the analysis of the measurement data.

In addition, I want to thank Prof. T. Lu and his team at the Beijing University of Chemical Technology for the hospitality by my visiting and the information exchange in this working area.

Furthermore, I would like to thank the IKE staff, especially the IKE director, Prof. Staflinger for creating an wonderful environment for research work. Also, I want to thank the IKE secretary team, Ms. M. Vencia, Ms. J. Edwards, Ms. A. Schmidt and Ms. F. Mauscherling for the supporting work at IKE and solving the problems outside of the lab; the IKE mechanical workshop team, Mr. T. Öztürk, Mr. U. Pein and Mr. J.-P. Teixeira-Marques for manufacturing the components for the experiments; the KE-GmbH colleagues, Dr. H.-J. Menz, Dr. Marschall, Mr. Reiss for the supporting work on the electronics; the other IKE colleagues, Dr. R. Mertz, Mr. S. Schmid, Mr. A. Isaev, Mr. T. Boldt, Mr. C. d'Alessandro, Mr. M. Strätz, Mr. C. Nigbur, Mr. G. Pohlner, Ms. Ö. Yilmaz, Ms. C. Graß, Ms. M.F. López and the former IKE colleagues: Dr. M. Linder, Dr. M. Kuschewski, Dr. J. Zhang, Dr. X. Chu, Mr. N. Kaufmann and Mr. A. Lurk for all kinds of support in my work.

I also want to thank my skillful Students, F. Wiltschko, P. Zimmerman, T. Ott, M. Frey, M. Pflieger, D. Neusser, E. Rodriguez, S. Eck, D. Kalegam, M. Kachel, S. Hagi and C. Weber for the excellent jobs in context of this work.

Finally, I want to thank my family, my father P. Zhou, my mother C. Wang and my wife Y. Zhang for the understanding and support during my study in Germany.

Appendix

A1. PSD diagrams of temperature data in the Case E, F and G as example

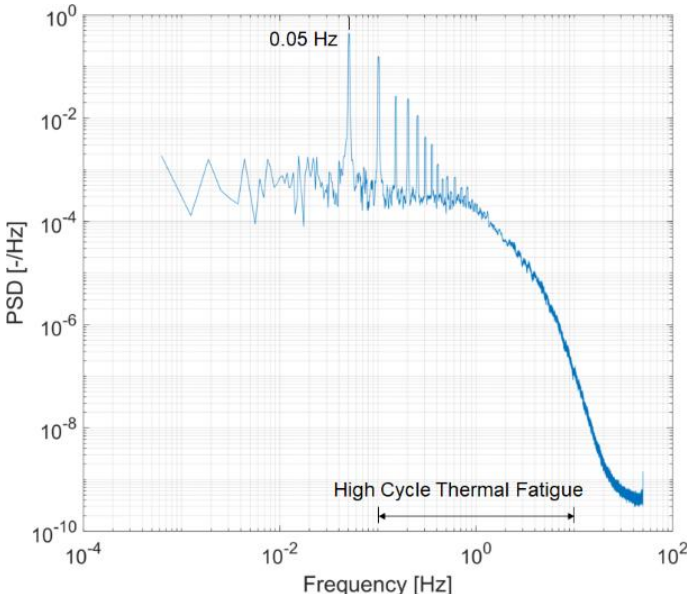


Figure A1-1: PSD diagram of the normalized temperature data at FT13 (4.5D, $\theta = 180^\circ$) in case E

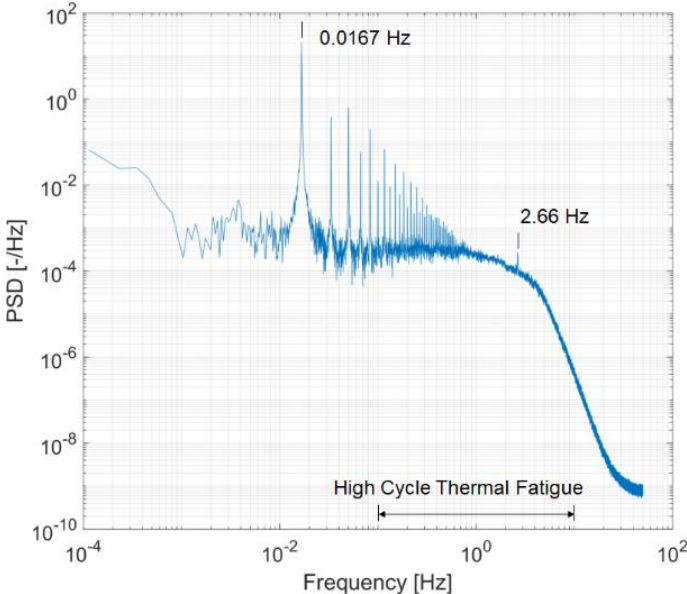


Figure A1-2: PSD diagram of the normalized temperature data at FT23 (5D, $\theta = 279^\circ$) in Case F

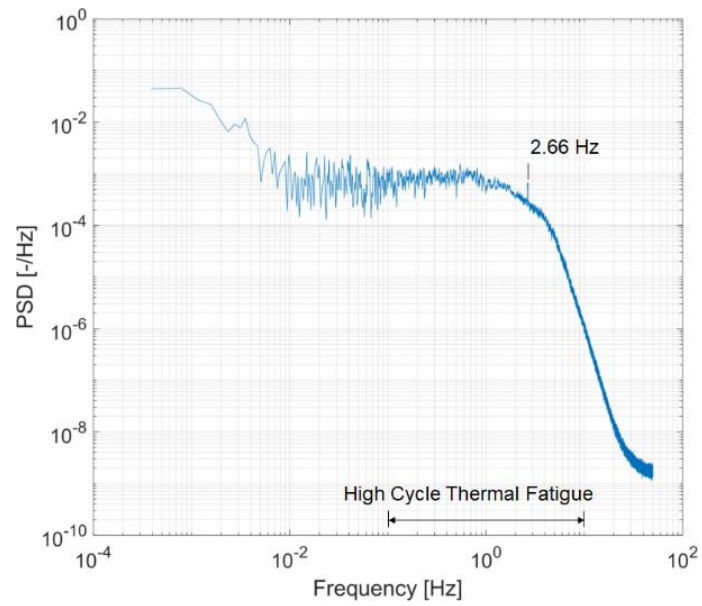
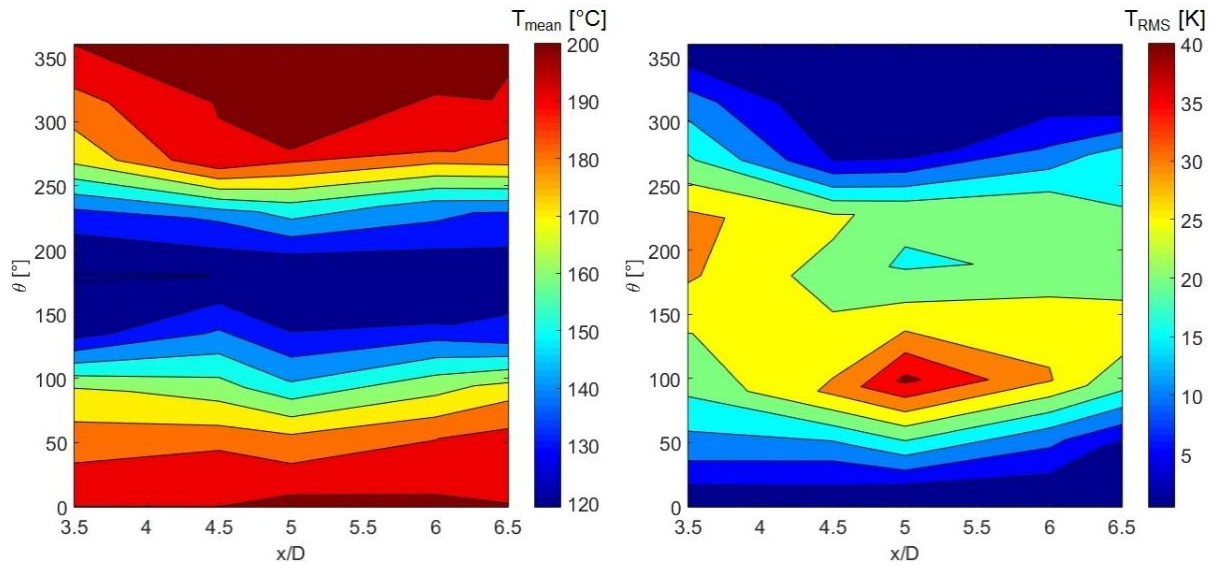


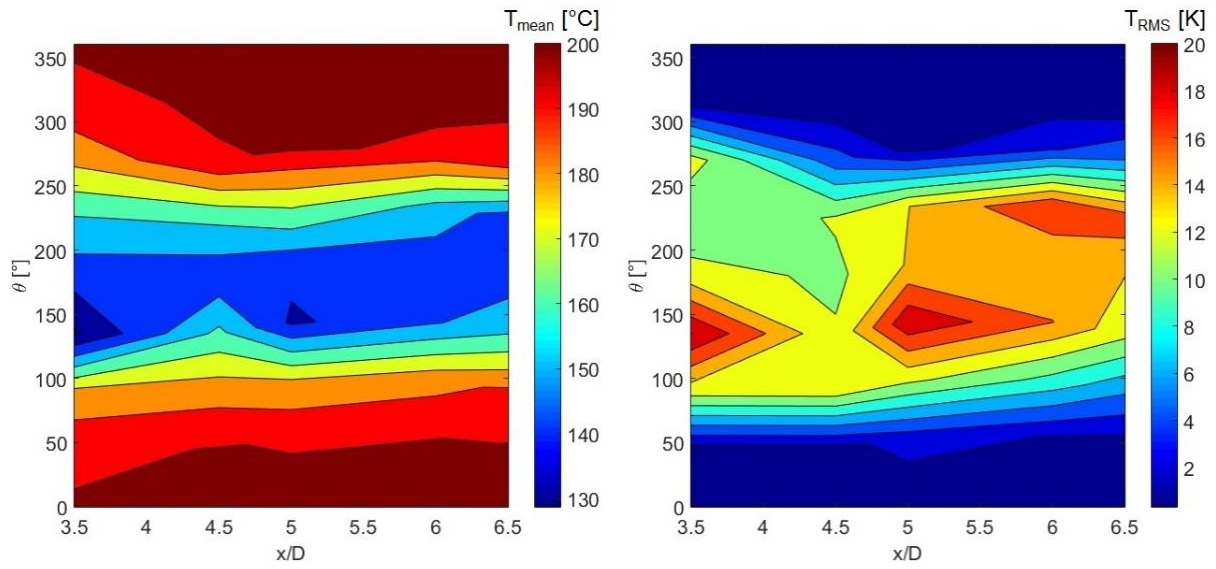
Figure A1-2: PSD diagram of the normalized temperature data at FT23 (5D, $\theta = 279^\circ$) in Case G

In these three cases, the basic frequency is changed with the duration of AIPTEC. However, frequency peaks due to AIPTEC can always be found in the range for thermal fatigue. Also, clear peak of the additional low frequency (2.66 Hz) can be recognized in the spectra.

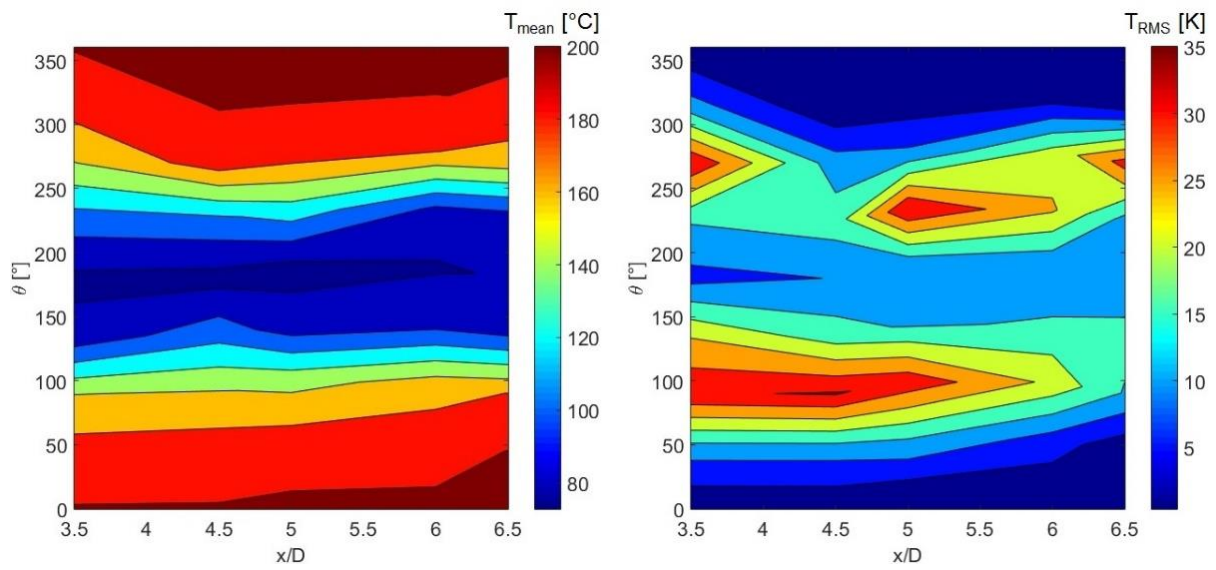
A2. Results of the experiments with varied flow rate (Phase III) and AIPTEC



(a)



(b)



(c)

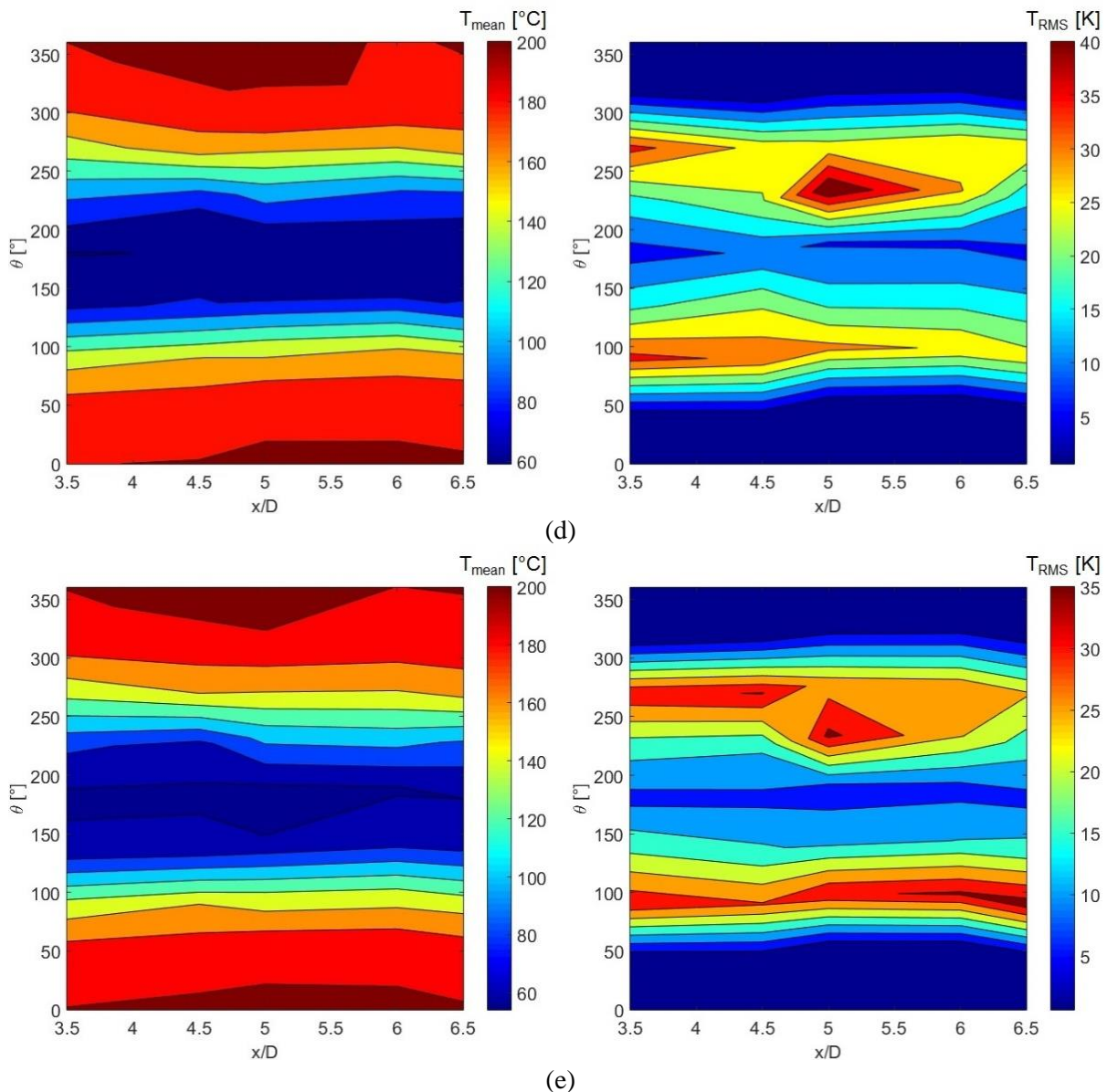


Figure A2-1: Reconstructed circumferential distribution of mean temperature (left) and RMS temperature fluctuations (right) in the mixing flow of the measurement case 2a (a), case 4a (b), case 5a (c), case 6 (d) and case 7a (e)

In the investigation cases with AIPTEC, the mixing process is not continuous. The stability of the stratified mixing flow cannot be quantitatively estimated with the calculation of the Richardson-number. However, the results of the temperature measurements provide a qualitative estimation for the stability of the thermal stratification. For case 2a, the temperature fluctuations in the cold layer of the stratified mixing flow ($\theta = 90^\circ - 250^\circ$) are higher than 20 K. Compared with the mean temperature distribution, the lower part of the flow is generally cold but contains a high temperature fluctuation (about 20 K). It indicates that the mixing process is still taking place in the lower part of the flow during the measurement. For the stratified flow with a high temperature fluctuation in the lower part (not only at the edges, but also in the middle of the lower part of the stratified flow), the thermal stratification in this case is unstable. The stratified mixing flow of case 4a is similar to case 2a. The temperature fluctuations in the lower part of the flow ($\theta = 90^\circ - 250^\circ$) are generally above 8 K and even higher than 10 K in the middle of the cold flow path ($\theta = 130^\circ - 180^\circ$). It indicates that the stratified mixing flow through the TC-module is unstable. The distributions of temperature fluctuations in cases 5a – 7a are similar to each other, but different to the cases 2a and 4a. The areas with high temperature fluctuation are located on the both

horizontal sides of the interface in the stratified flow ($\theta = 90^\circ$ and 270°). It indicates that the heat exchange takes place only at the thermal interface in the stratified flow. Therefore, the thermal stratifications in these three cases are stable. The temperature fluctuations in the cold fluid of the stratified flow ($\theta = 135^\circ - 225^\circ$) are $T_{RMS} = 20 - 25$ K for case 2a, $T_{RMS} = 10 - 15$ K for case 5a, $T_{RMS} < 10$ K for case 6a and $T_{RMS} < 5$ K for case 7a. The decreased temperature fluctuations in the lower part of the flow indicate the increase of the stability of the thermal stratification.

Weld seam model (5.5D)

θ	F1 (3.5D)	F2 (4.5D)	F3 (5D)	F4 (6.5D)
0	FT1	FT9	FT17	FT25
45	FT2	FT10	FT18	FT26
90	FT3	FT11 31.1	FT19 41.2	FT27
135	FT4	FT12	FT20 28.0	FT28 28.3
180	FT5 30.7	FT13	FT21	FT29
225	FT6 31.2	FT14	FT22	FT30
270	FT7	FT15	FT23	FT31
315	FT8	FT16	FT24	FT32

(a)

Weld seam model (5.5D)

θ	F1 (3.5D)	F2 (4.5D)	F3 (5D)	F4 (6.5D)
0	FT1	FT9	FT17	FT25
45	FT2	FT10	FT18	FT26
90	FT3	FT11	FT19	FT27
135	FT4 20.1	FT12	FT20 19.6	FT28
180	FT5	FT13	FT21	FT29
225	FT6	FT14	FT22	FT30 17.1
270	FT7	FT15	FT23	FT31
315	FT8	FT16	FT24	FT32

(b)

Weld seam model (5.5D)

θ	F1 (3.5D)	F2 (4.5D)	F3 (5D)	F4 (6.5D)
0	FT1	FT9	FT17	FT25
45	FT2	FT10	FT18	FT26
90	FT3 34.4	FT11 35.5	FT19 33.2	FT27
135	FT4	FT12	FT20	FT28
180	FT5	FT13	FT21	FT29
225	FT6	FT14	FT22 34.9	FT30
270	FT7 34.3	FT15	FT23	FT31 32.0
315	FT8	FT16	FT24	FT32

(c)

Weld seam model (5.5D)

θ	F1 (3.5D)	F2 (4.5D)	F3 (5D)	F4 (6.5D)
0	FT1	FT9	FT17	FT25
45	FT2	FT10	FT18	FT26
90	FT3 36.6	FT11 33.8	FT19 31.4	FT27 27.3
135	FT4	FT12	FT20	FT28
180	FT5	FT13	FT21	FT29
225	FT6	FT14	FT22 44.9	FT30
270	FT7 36.3	FT15 28.3	FT23	FT31 29.1
315	FT8	FT16	FT24	FT32

(d)

Weld seam model (5.5D)				
θ	F1 (3.5D)	F2 (4.5D)	F3 (5D)	F4 (6.5D)
0	FT1	FT9	FT17	FT25 ○
45	FT2	FT10	FT18	FT26
90	FT3 33.7	FT11 30.4	FT19 34.2	FT27 37.3
135	FT4	FT12	FT20	FT28
180	FT5	FT13	FT21	FT29
225	FT6	FT14	FT22 36.1	FT30
270	FT7 33.1	FT15 35.3	FT23 27.4	FT31 25.6 ○
315	FT8	FT16	FT24	FT32

(e)

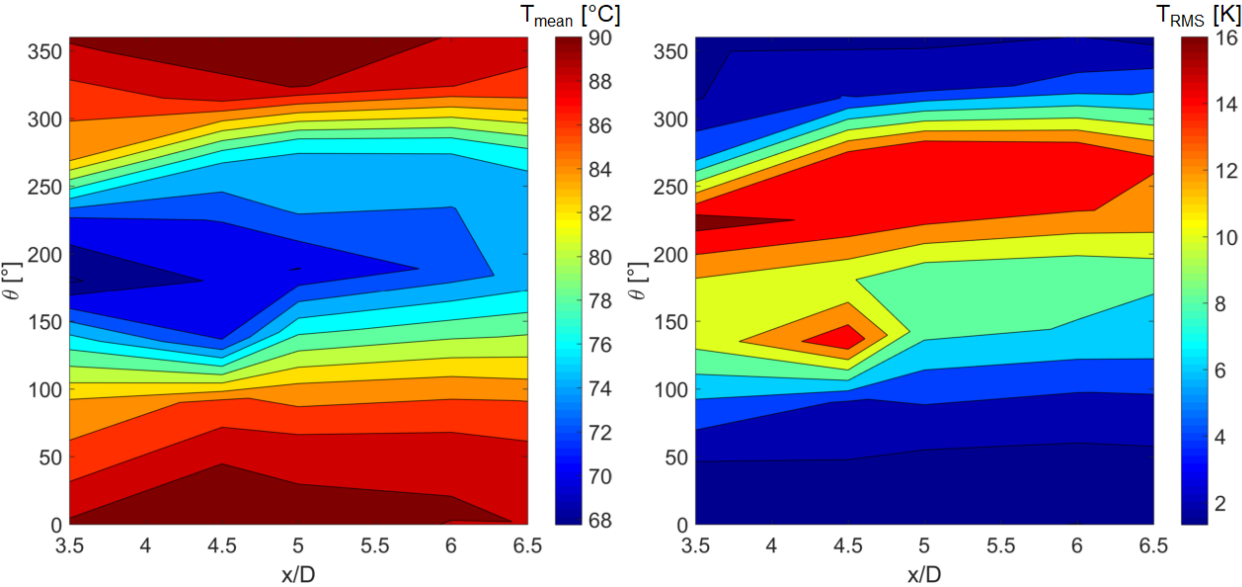
	Effect of AIPTEC (strong)	Value in K	RMS temp. fluctuation
	Effect of AIPTEC (weak)	○	additional low frequency

Figure A2-2: Spectrum pattern of measurement case 2a (a), case 4a (b), case 5a (c), case 6a (d) and case 7a (e)

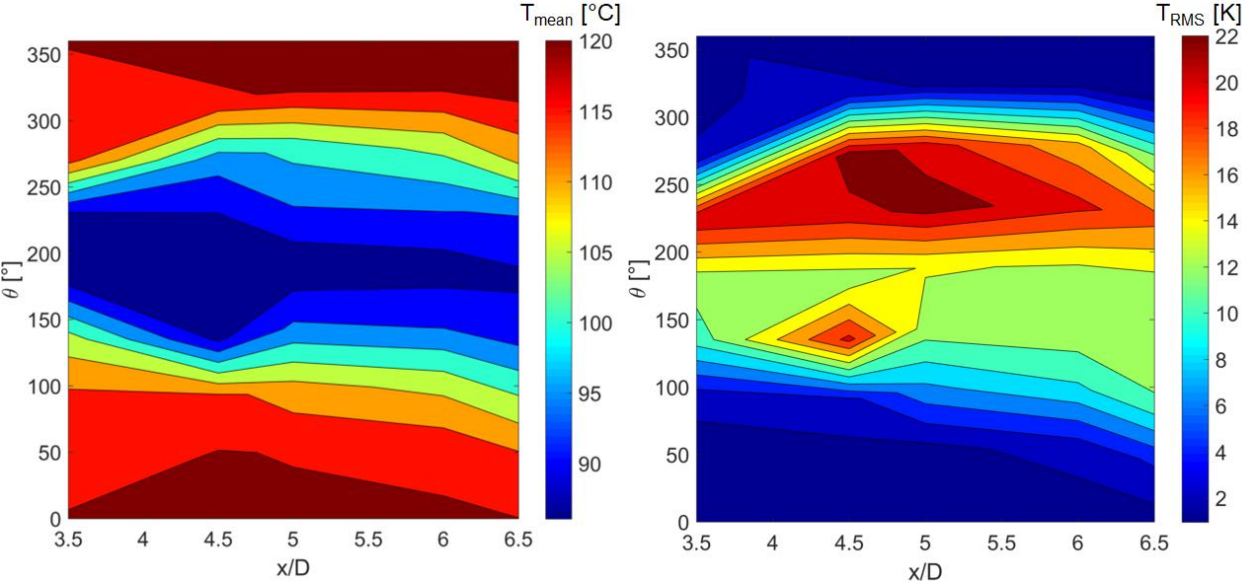
In the comparison between case 2a and 4a, the area indicating the effect of AIPTEC is clearly reduced with reduced flow rate in the branch pipe. Moreover, the maximum temperature fluctuation of case 2a is higher than case 4a. The location with the maximum temperature fluctuation in both cases are close to the weld seam model. Summarizing all the information, the possibility for thermal fatigue in the mixing zone is increased with increased flow rate in the branch pipeline. These results confirm the numerical analysis of the numerical work of Selvam et al. [79].

In the cases with different flow rates in the main pipeline, the AIPTEC effect appears in a larger area of the pipe inner wall with a lower flow rate in the main pipeline. But the area with strong AIPTEC effect remains almost the same. The high temperature fluctuations are located at the edge of the area with strong AIPTEC effect. These are the both horizontal sides of the pipe module. The areas with high temperature fluctuations are increased with decreasing flow rate in the main pipeline. For high flow rates in case 2a or 5a, only a small area of the pipe module has the possibility for thermal fatigue. With the low flow rate in case 6a and 7a, both sides in the whole module have this possibility. Thermal fatigue can be initiated in a larger inner wall area of the TC-module with the decreased flow rate in the main pipeline. Considering the position of the weld seam, the inner wall area with high potential for material damage due to thermal fatigue are all located near the position FT19 respectively FT22.

A3. Results of the experiments with reduced boundary conditions (Phase IV) and AIPTEC



(a)



(b)

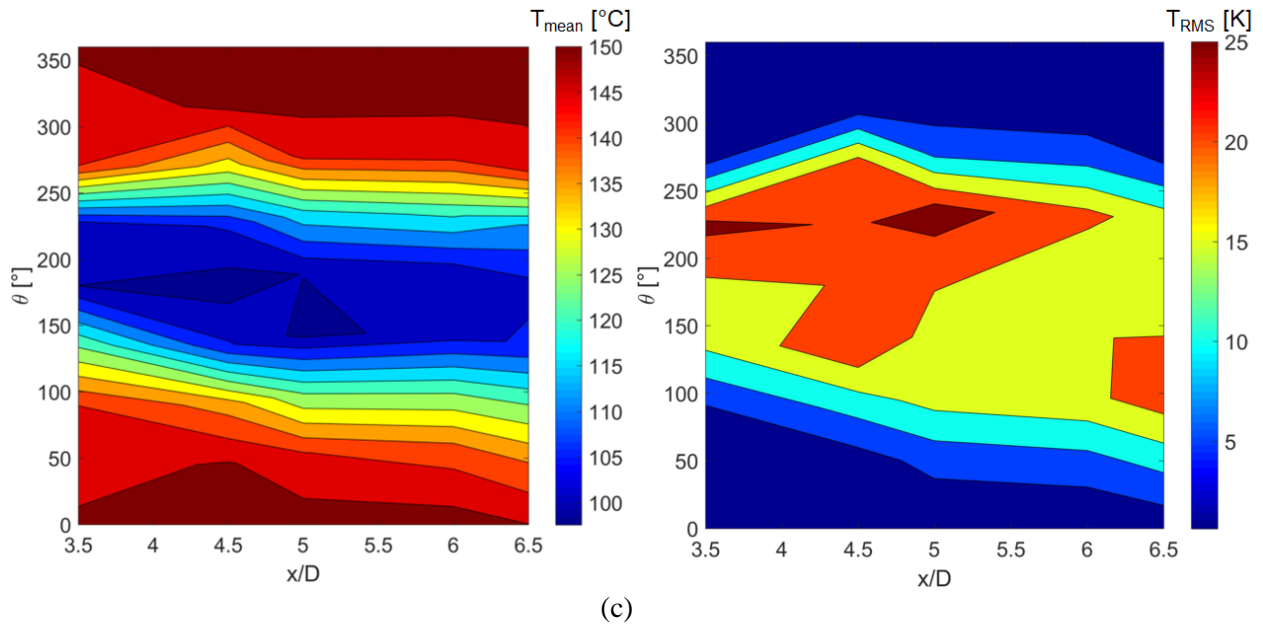


Figure A3-1: Reconstructed circumferential distributions of mean temperature (left) and effective temperature fluctuations (right) for case 8a (a), case 9a (b) and case 10a (c)

The temperature gradient in the stratified flow is increased from case 8a to 10a with increased temperature difference. The shapes of the mean temperature in these three cases are different to each other. This differs from the cases 1 – 3 at high temperature, in which the shapes of mean temperature were similar. It indicates a mixing behavior change in this temperature range. The temperature fluctuations in the mixing flow is generally increased with the increased flow temperature in the main pipeline. The maximum temperature fluctuation in case 8a is located at measurement position FT6 (3.5D, $\theta = 225^\circ$) with the value of 16.9 K, in case 9a at FT15 (4.5D, $\theta = 270^\circ$) with 23.8 K and in case 10a at FT22 (5D, $\theta = 234^\circ$) with 27.8 K. In these three cases, an area with high temperature fluctuation can be seen on the left side of the flow direction ($\theta = 225^\circ \sim 270^\circ$). Compared to their correlated mean temperature distributions, the temperature fluctuation in the middle of the cold flow ($\theta \approx 180^\circ$) has a small difference (6 ~ 10 K) to the both side of the thermal interface ($\theta \approx 135^\circ$ or 225°). Considering that the temperature fluctuations in the mixing flow in these three cases are generally low, the thermal stratifications in these three cases are all unstable.

Weld seam model (5.5D)

θ	F1 (3.5D)	F2 (4.5D)	F3 (5D)	F4 (6.5D)
0	FT1	FT9	FT17	FT25
45	FT2	FT10	FT18	FT26
90	FT3	FT11	FT19	FT27
135	FT4	FT12	FT20	FT28
180	FT5	FT13	FT21	FT29
225	FT6 16.9	FT14 15.5	FT22 15.8	FT30
270	FT7	FT15	FT23	FT31
315	FT8	FT16	FT24	FT32

(a)

Weld seam model (5.5D)

θ	F1 (3.5D)	F2 (4.5D)	F3 (5D)	F4 (6.5D)
0	FT1	FT9	FT17	FT25
45	FT2	FT10	FT18	FT26
90	FT3	FT11	FT19	FT27
135	FT4	FT12	FT20	FT28
180	FT5	FT13	FT21	FT29
225	FT6 21.7	FT14 20.8	FT22 23.2	FT30
270	FT7	FT15 23.8	FT23	FT31
315	FT8	FT16	FT24	FT32

(b)

Weld seam model (5.5D)

θ	F1 (3.5D)	F2 (4.5D)	F3 (5D)	F4 (6.5D)
0	FT1	FT9	FT17	FT25
45	FT2	FT10	FT18	FT26
90	FT3	FT11	FT19	FT27
135	FT4	FT12	FT20	FT28
180	FT5	FT13	FT21	FT29
225	FT6 26.4	FT14 24.4	FT22 27.8	FT30
270	FT7	FT15	FT23	FT31
315	FT8	FT16	FT24	FT32

(c)

Effect of AIPTEC (strong)	Value in K	RMS temp. fluctuation
Effect of AIPTEC (weak)	○	additional low frequency

Figure A3-2: Spectrum patterns of the case 8a (a), case 9a (b) and case 10 (c)

In these cases, AIPTEC effect can be found in a large area of the mixing region. But the additional low frequency cannot be found in these cases. High temperature fluctuations can be found in several measurement positions. However, measurement position FT22, which has a high temperature fluctuation, strong AIPTEC effect and is located close to the weld seam model, has the highest potential for material damage due to thermal fatigue. Moreover, this potential is increased with increased flow temperature in the main pipeline.

A4. Results of NW-LED-IF measurements with variation of inlet flow temperature

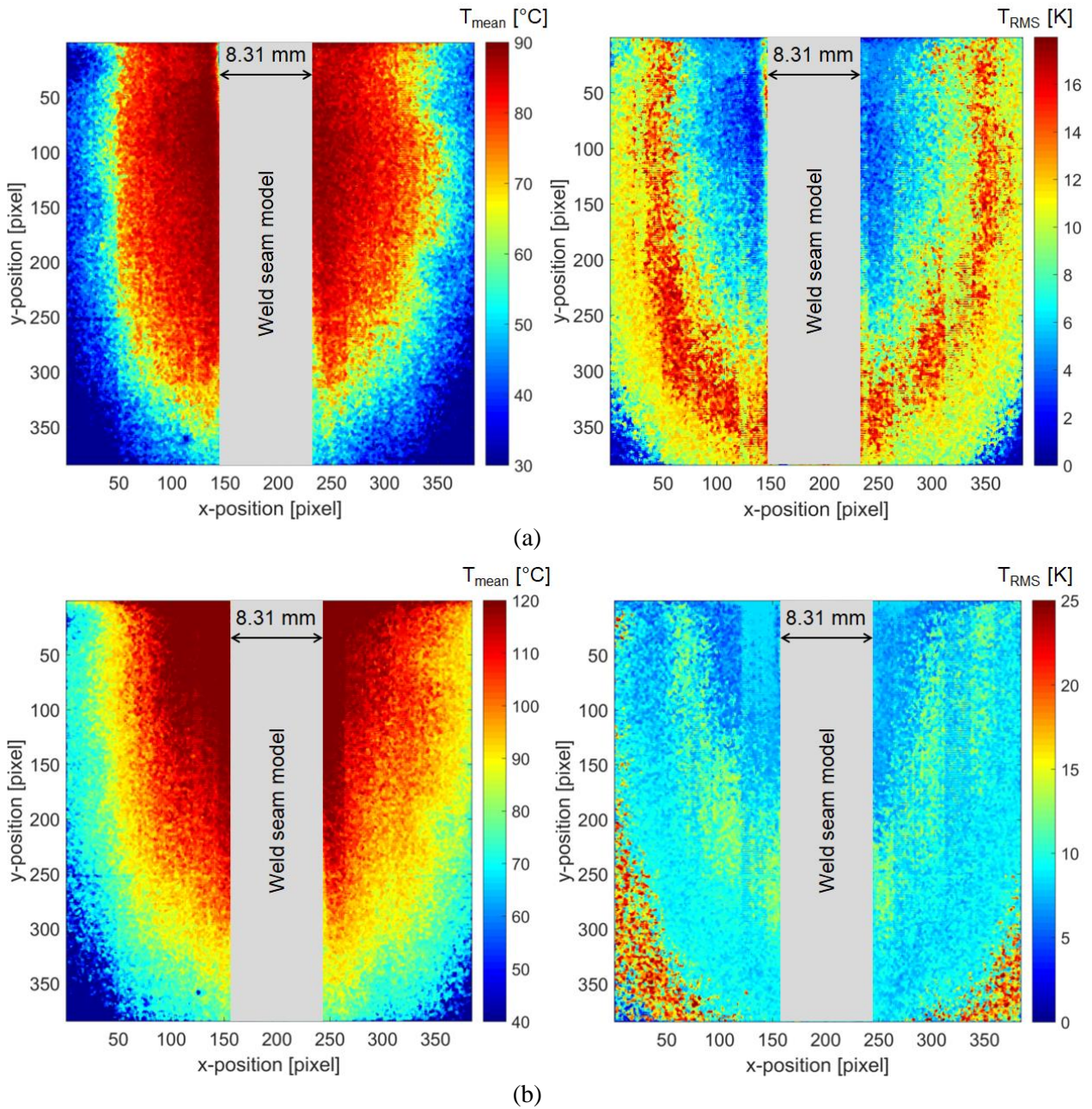
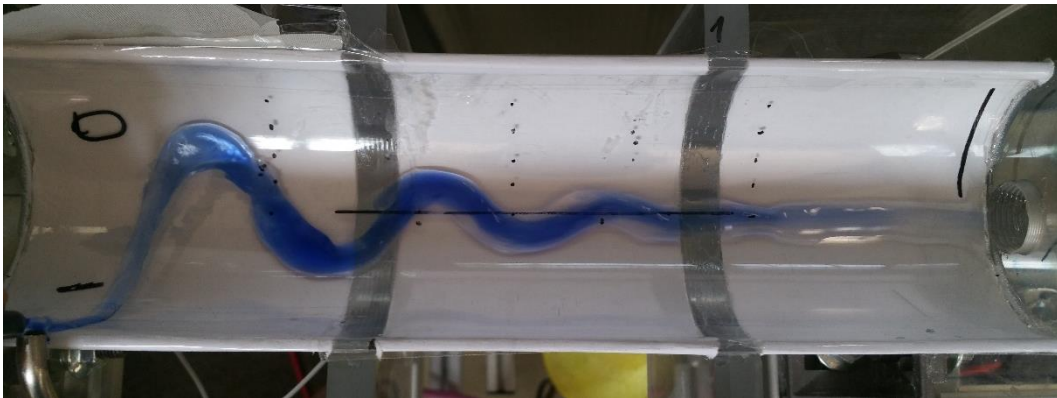


Figure A4-1: Distributions of mean temperature (left) and RMS temperature fluctuations (right) in NW-LED-IF measurements with weld seam model in case 8R (a) and case 9R (b)

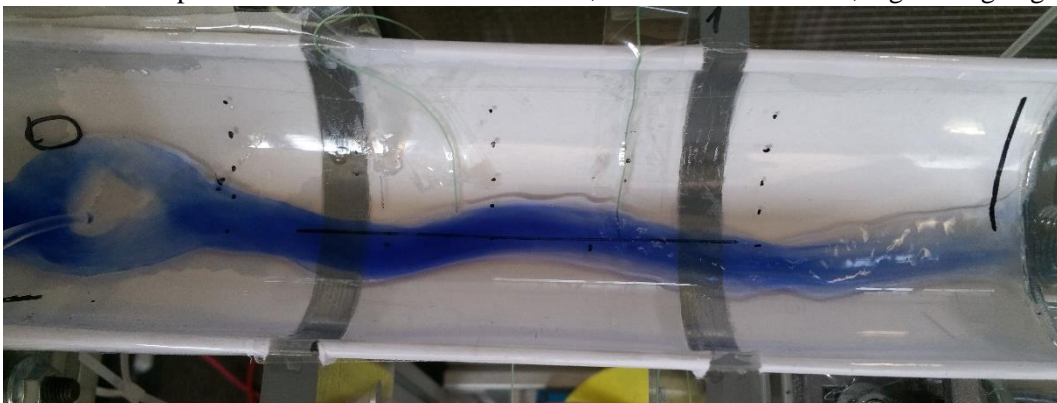
In comparison with the results of case 10R with weld seam model, it can be understood, that the temperature fluctuations in the mixing region can be increased by increased temperature difference between the inlet flow streams, which matches the results of the thermocouple measurements.

A5. Results jet test on the small-scale half-pipe setup

The jet test is an additional experiment to find out the impact of the branch flow hit point on the swing angle of the tangential oscillation. The test setup is modified form the half-pipe setup of the swing test. The half pipe is made 5° to the horizontal level. The lower side of the half pipe has been opened for the water flow. A nozzle is installed on the higher side of the half pipe and normally to the axis of the half pipe. By controlling of the flow rate from the nozzle, the hit point can be changed in the half pipe, so that the initial angle can be varied for the swing jet. For visualization of the flow path, the water flow is mixed with ink.



Run a: hit point at the same side of the nozzle, flow rate ca. 1 L/min, high swing angle



Run b: hit point at the middle of the half pipe, flow rate ca. 3 L/min, low swing angle



Run c: hit point at opposite side of the nozzle, flow rate ca. 7 L/min, low swing angle

Figure A5-1: Photographs of the flow path in the jet test

The different flow rate for the hit point locations have been chosen for the test. As can be seen, run a has a very high swing angle but a very low flow rate (velocity) in comparison with run c. It can explain

why the add. low frequency is lower than the other cases at T-junction. In case G, the experiment has been performed with 25° shock module. The velocity in y-direction is equal to branch flow velocity times $\sin(25^\circ)$, which is much lower than the other cases at T-junction. Just like run a, the velocity is very low, but the swing angle is very high. According to the relation of the swing angle and the add. low frequency (see Figure 9 in paper), the add. low frequency in case G is lower than the cases at T-junction. Run b shows also a weak snake path, although the hit point is located in the middle of the pipe. It can explain the snake path in the deflecting jet (e.g. case 4). In case 4, the branch flow cannot reach any side of the main pipe wall, but has a soft landing in the middle of the main pipe. It cannot initiate the tangential oscillation. However, just like run b, a weak snake path can be found in the mixing flow.

